2003

Strengthening of reinforced concrete beams using innovative ductile composite fiber-reinforced polymer systems.

Wael Fathy. Ragheb
University of Windsor

STRENGTHENING OF REINFORCED CONCRETE BEAMS USING INNOVATIVE DUCTILE COMPOSITE FIBER-REINFORCED POLYMER SYSTEMS

by

WAEL FATHY RAGHEB

A Dissertation
Submitted to the Faculty of Graduate Studies and Research
through Civil and Environmental Engineering Department
in Partial Fulfillment of the Requirement for
the Degree of Doctor of Philosophy at the
University of Windsor

Windsor, Ontario, Canada

2003

ABSTRACT

Although the technique of external strengthening of reinforced concrete beams using externally bonded Fiber Reinforced Polymer (FRP) materials has been established as an effective tool for rehabilitating and strengthening reinforced concrete beams, it is still suffering from some drawbacks. A significant part of these drawbacks is attributed to the characteristics of currently available FRP strengthening systems. This study deals with the development and evaluation of the effectiveness of two innovative ductile FRP systems for flexural/shear strengthening of reinforced concrete beams. The systems are fabrics that are hybrid of glass and carbon fibers and designed to have the potential to avoid most of the drawbacks experienced by currently available FRP strengthening systems. The new systems are unique as they can provide yield plateaus similar to that provided by steel in tension. The ideal characteristics of a strengthening material for both flexure and shear were investigated. A parametric study was conducted on the loading behavior of triaxially braided fabrics. Based on these investigations, the systems were designed and manufactured. An experimental investigation was conducted to evaluate the behavior of reinforced concrete beams strengthened in flexure/shear using the new systems. Reinforced concrete simple and continuous beams were strengthened in flexural/shear using the new systems applying different strengthening schemes. Identical beams were strengthened using some commercially available carbon fiber sheets, fabrics, and plates, as well as steel plates, in order to compare their behavior with those strengthened with the developed systems. The beams were loaded until failure and their responses were investigated for ductility, FRP exploitability, and failure modes. The beams strengthened in flexure with the new systems exhibited greater ductility than those strengthened with the carbon fiber strengthening systems and produced yield plateaus similar to those of the unstrengthened beams and also to those strengthened using steel plates. The test results showed that the strengths of the new systems were fully exploited. Guidelines for the design of the developed systems for flexural and shear strengthening of reinforced concrete beams were presented. Numerical examples of reinforced concrete beams strengthened in flexure or shear were also presented in order to clarify the design procedures.

To My Parents

With Gratitude

ACKNOWLEDGEMENTS

Thanks to God, the greatest creator that the heavens declare His glory and the firmament shows His handiwork, for giving me strength and patience to complete this work.

I would like to express my deep thanks to my co-advisor Prof. George Abdel-Sayed for his supervision, continuous encouragement, and valuable suggestions throughout this work. Also, I wish to express my appreciation to my co-advisor Prof. Nabil Grace for his financial support, helpful suggestions, encouragement, and his sincere efforts to provide all necessary research facilities for this work.

I wish to express my grateful thanks to Mr. John Doyle, President of Diversified Composites Inc., Kentucky, USA, for manufacturing the fabrics, Mr. Habib El-Jezi, Shelby Precast Concrete, Michigan, USA, for contributing most of the test beams, and Mr. Matt Boone, Vice President of Baker Concrete Technology Inc., Ohio, USA, for contributing some of the test beams and some of the carbon fiber sheets used.

This research has been conducted at the Structural Testing Center at Lawrence Technological University, Southfield, Michigan, USA, and was funded by the US-National Science Foundation under grant No. CMS-9906404 awarded to Prof. Grace.

I would like to express my grateful thanks to the faculty members of the Department of the Civil and Environmental Engineering, University of Windsor for their continuous encouragement. I would like to thank the University of Windsor for the tuition scholarship awarded to me in 2001 and 2002.

Finally, I would like to express my grateful thanks to my parents without whom this work would not have been completed.

TABLE OF CONTENTS

LIST OF TABLES

LIST OF FIGURES

LIST OF SYMBOLS

The following symbols are used in this dissertation:

A_s = Area of tension steel reinforcement;

A_f = Area of fabric;

B = Section width;

b_f = Fabric width;

c_1 = Distance from the neutral axis to the extreme compression fiber;

c_2 = Distance from the neutral axis to the fabric bonded surface;

C = Total compression force in concrete;

d = Effective beam depth;

d_f = Effective depth of the fabric;

E_{2fa} = Modulus of elasticity of fabric in the axial direction after yield;

E_{2fd} = Modulus of elasticity of fabric in the diagonal direction after yield;

E_c = Modulus of elasticity of concrete;

E_f = Modulus of elasticity of FRP;

E_{fa} = Modulus of elasticity of fabric in the axial direction;

E_{fd} = Modulus of elasticity of fabric in the diagonal direction;

E_s = Modulus of elasticity of steel;

f_c = Stress in fabric;

$f_c^{'}$ = Compressive strength of concrete;

f_{ct} = Tensile strength of concrete;

f_f = Stress in FRP;

f_{fa} = Stress in fabric in its axial direction;

f_{fam} = Maximum anchorable fabric stress;

f_{fd} = Stress in fabric in its diagonal direction;

f_{fua} = Ultimate strength of fabric in its axial direction;

f_{ud} = Ultimate strength of fabric in its diagonal direction;

f_{fya} = Yield strength of fabric in its axial direction;

f_{fyd} = Yield strength of fabric in its diagonal direction;

f_s = Stress in steel;

f_y = Yield strength of steel;

F_{fe} = Effective FRP force per unit width;

h = Total section height;

I_{cr} = Moment of inertia of the cracked concrete section;

k = Ratio of the depth to the elastic neutral axis to the effective depth, d;

k_1, k_2 = Reduction factors;

k_b = Geometry factor;

k_c = Compaction factor;

K_v = Bond reduction factor;

L_e = Effective bond length;

M_{add} = Additional bending moment;

M_n = Nominal bending moment;

M_o = Bending moment at the time of installation of fabric;

$M_{service}$ = Service load moment;

M_u = Factored bending moment;

n = Number of fabric layers;

n_f = Fabric modular ratio;

n_s = Steel modular ratio;

s = Axial yarn spacing;

s_f = Spacing of fabric strips;

s_s = Spacing of steel stirrups;

t_f = Fabric thickness;

T = Estimated additional tension force;

T_f = Tension force in fabric;

T_m = Maximum anchorable force;

T_s = Tension force in steel reinforcement;

V = Shear strength of the beam;

V_c = Nominal shear strength provided by concrete;

V_{cal} = Calculated beam shear strength;

V_{exp} = Experimental beam shear strength;

V_f = Composite fiber volume fraction;

$V_{factored}$ = Factored shear force;

V_{frp} = Nominal shear strength provided by FRP;

V_s = Nominal shear strength provided by steel shear reinforcement;

w_f = Width of fabric strip;

β = Angle between principal fiber orientation and longitudinal axis of the beam;

β_1 = Ratio between the average compressive stress to the maximum stress;

ε_b = Strain in fabric corresponding to maximum anchorable strength;

ε_c = Concrete strain;

ε_f = FRP strain;

ε_{fa} = Strain of fabric in the axial direction;

ε_{fau} = Rupture strain of fabric in the axial direction;

ε_{fd} = Strain of fabric in the diagonal direction;

ε_{fdu} = Rupture strain of fabric in the diagonal direction;

ε_{fe} = Effective FRP strain;

ε_m = Maximum usable strain of fabric;

ε_o = Initial strain in the concrete substrate at the time of fabric installation;

ε_s = Strain in steel reinforcement;

ε_{sy} = Yield strain of steel;

ε_{fya} = Yield strain of fabric in the axial direction;

ε_{fyd} = Yield strain of fabric in the diagonal direction;

ϕ = Strength reduction factor;

η_1, η_1 = Bond factors;

θ = Braider angle;

ρ = Steel reinforcement ratio;

ρ_{frp} = FRP reinforcement ratio; and

ψ = Reduction factor for the material.

CHAPTER 1

INTRODUCTION

1.1 General

Fiber Reinforced Polymers (FRP) have been attractive new materials for structural engineers in the concrete construction field, especially for use as strengthening materials for reinforced concrete beams. Several FRP systems are now commercially available for external strengthening of concrete structures. Fibers commonly used in these systems include glass, aramid, and carbon, and are available in many forms such as pultruded plates, uniaxial fabrics, woven fabrics, and sheets (Fig. 1.1).

1.2 Statement of the Problem

Although the technique of external strengthening of reinforced concrete beams using epoxy bonded FRP materials has been established as an effective tool for increasing the flexural and/or shear strength of reinforced concrete beams, it is still suffering from some drawbacks. A significant part of these drawbacks is attributed to the characteristics of currently available FRP strengthening materials.

Currently available FRP strengthening systems have a behavior that is not similar to steel. Although these materials have high strengths, they are very brittle. When loaded in tension, they exhibit a linear stress-strain behavior up to failure without exhibiting yield plateaus or any indication of an impending failure. Their strain response is also different from that of conventional steel, which yields after elastically deforming to relatively small values of strain (0.2% for Grade 60 and 0.14% for Grade 40), while FRP materials exhibit elastic deformation to relatively large strain values (compared to the

yield strain of steel) before rupture (Fig. 1.2). As a result, when they are used for flexural strengthening of concrete beams reinforced with conventional steel, the steel reinforcement may yield before the FRP strengthening material provides any measurable contribution to the load of the beam. Therefore, there is no significant improvement in beam yield load or stiffness. When an increase in beam yield load or stiffness is required, larger cross sections of these materials must be used in order to contribute to the beam load when deformations are limited (before steel yields), which generally increases the cost of strengthening. Using some special low strain fibers such as ultra-high modulus carbon fibers may appear to be a solution; it however results in brittle failures due to failure of fibers.

More important, flexural strengthening of reinforced concrete beams using currently available FRP materials is always accompanied by a significant loss in ductility. Brittle failures without significant yield plateaus are experienced by the strengthened beams. Despite the high strength of these materials, taking advantage of such high strength is limited by the bond capacity between the FRP and the concrete surface. In many cases, brittle failures are experienced as a result of debonding that occurs at FRP stress levels that are small fractions of their strengths.

In beam shear strengthening applications, FRP materials usually stretch to strain values that are usually small fractions of their ultimate strains when the beam reaches its shear capacity. Therefore, the benefits of the strengthening material are not fully realized. FRP materials are also highly orthotropic (see Table 1.1). They strengthen only if loaded in the fiber direction. Strengthening the beam in shear requires orienting the fibers perpendicular to the beam longitudinal axis, or for better effectiveness, at 45^{o}. Therefore,

for simultaneous flexural and shear strengthening of beams, more than one layer of these materials must be used.

Accordingly, the drawbacks experienced when using commercially available FRP materials in strengthening reinforced concrete beams can be summarized in the following:

1- No significant gain in beam yield load or beam stiffness is experienced compared to the gain in ultimate load.
2- A Significant loss in beam ductility is experienced after strengthening.
3- Brittle debonding failures are experienced in many cases due to the limited bond capacity between the FRP and the concrete surface.
4- The strength of the FRP is not fully exploited in most cases.
5- For simultaneous flexural and shear strengthening of beams, more than one layer of these materials must be used.

1.3 Objectives

The main objectives of this research work are summarized as follows:

1- Developing new FRP strengthening systems for reinforced concrete beams that have a similar tensile behavior to steel, i.e., a linear stress-strain behavior up to a certain yield point and then exhibit a yield plateau.
2- Designing these systems with the capability to carry load in more than one direction, namely the 0^{o}, $+45^{o}$, -45^{o} directions, in order to be able to be simultaneously utilized for flexural and shear strengthening.

3- Verifying the effectiveness of the developed systems in flexural strengthening of reinforced concrete beams without sacrificing much of the beam ductility.

4- Investigating the exploitability of the developed systems in shear strengthening of reinforced concrete beams.

5- Comparing the behavior of the developed systems with the behavior of currently available FRP systems in strengthening reinforced concrete beams.

6- Providing design guidelines for using these systems for flexural/shear strengthening of reinforced concrete beams.

1.4 Research Procedure

The ideal characteristics of a strengthening material for flexure and shear were investigated. In view of this investigation, two pseudo-ductile FRP strengthening systems were designed and manufactured. The first system is a uniaxial fabric, while the second system is a triaxially braided fabric. An analytical parametric study was conducted on the behavior of triaxially braided composite fabrics. Based on this study, the fabric geometry was selected. A special micromechanic analytical modeling technique developed by NASA was used to conduct this study and to design the systems. The systems were manufactured and their tensile mechanical properties were evaluated by tensile testing samples according to ASTM D 3039 specifications.

An experimental investigation was conducted to study the effectiveness of the first system, the uniaxial fabric, in flexural strengthening of reinforced concrete beams. Reinforced concrete simple beams were strengthened in flexure using the developed fabric. Similar beams were strengthened using currently available uniaxial carbon fiber sheets, fabrics, and plates in order to compare their behaviors with those strengthened

with the developed fabric. The beams were loaded until failure and their loading behavior, ductility, strength, and failure modes were investigated.

Similarly, the effectiveness of the second system, the triaxially braided fabric for flexural strengthening of beams was experimentally investigated. Reinforced concrete simple beams of different steel reinforcement ratios were strengthened in flexure using the new fabric. Similar beams were strengthened using a commercially available carbon fiber sheet in order to compare their behavior with those strengthened with the developed fabric. The beams were loaded until failure and their behavior was investigated for ductility, strength, and failure modes.

Thereafter, the use of the developed triaxially braided fabric in shear strengthening of beams was investigated. Reinforced concrete simple beams were strengthened in shear using the developed fabric. A commercially available carbon fiber sheet was used to strengthen similar beams in shear in order to compare their behavior with those strengthened with the triaxial fabric. The beams were loaded until failure and their behavior was investigated for FRP exploitability and failure modes. The applicability of the approach of ACI committee 440 for estimating the fabric contribution to the shear strength of the tested beams was also examined.

The experimental program was then extended to evaluate the effectiveness of the new triaxially braided fabric in flexural strengthening of cantilever and continuous reinforced concrete beams. Two series of beams were experimentally investigated. The first series included beams with one overhanging cantilever strengthened in flexure and loaded with one concentrated load at the end of the cantilever. The second series included continuous beams with two spans strengthened in flexure along their positive and negative moment regions and loaded with a concentrated load at the middle of each span. The behavior of the beams strengthened with the new fabric were investigated and

compared with the behavior of similar beams strengthened using a commercially available carbon fiber sheet. The responses of the beams were examined for deflections, strains, and failure modes with emphasis on the capability of fabric to provide adequate ductility at the regions of the plastic hinges.

Finally, guidelines for the design of the developed triaxial fabric for flexural and shear strengthening of reinforced concrete beams were presented. Numerical examples for reinforced concrete beams strengthened in flexure or shear were also presented in order to clarify the design procedure

1.5 Organization of the Study

The study is organized in nine chapters:

Chapter 2 reviews the reported experimental investigations on the behavior of reinforced concrete beams strengthened in flexure or shear and the development of hybrid composites.

Chapter 3 discusses the development of two new FRP strengthening systems.

Chapter 4 presents an experimental investigation on flexural strengthening of reinforced concrete beams using the developed uniaxial fabric.

Chapter 5 presents an experimental investigation on flexural strengthening of reinforced concrete beams using the developed triaxially braided fabric.

Chapter 6 presents an experimental investigation on shear strengthening of reinforced concrete beams using the developed triaxially braided fabric.

Chapter 7 presents an experimental investigation on flexural strengthening of reinforced concrete cantilever and continuous beams using the developed triaxially braided fabric.

Chapter 8 presents guidelines and numerical examples for the design of flexural and shear strengthening of reinforced concrete beams using the developed triaxially braided fabric.

Chapter 9 presents conclusions of the study and recommendations for future studies.

Table 1.1 Typical FRP Properties* [ACI Committee 440 (2002)]

FRP System	Modulus of Elasticity		Ultimate Strength		Rupture Strain at (0°)
	At (0°) GPa (Msi)	At (90°) MPa (Msi)	At (0°) MPa (ksi)	At (90°) MPa (ksi)	(%)
High strength carbon/epoxy	117-145 (17-21)	2-7 (0.3-1)	1380-2070 (200-300)	35-70 (5-10)	1.0-1.5
E-glass/epoxy	34-48 (5-7)	(2-7) (0.3-1)	690-1380 (100-200)	35-70 (5-10)	1.5-3.0
High-performance aramid/epoxy	55-68 (8-10)	(2-7) (0.3-1)	1035-1725 (150-250)	35-70 (5-10)	2.0-3.0

*Based on 50% composite fiber volume fraction

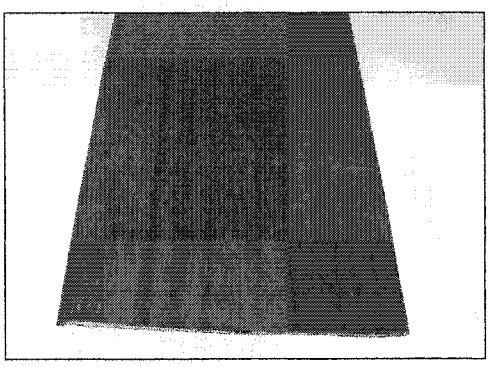

(a) Pultruded plates

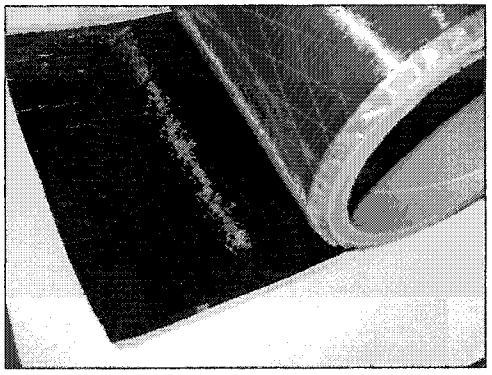

(b) Sheets

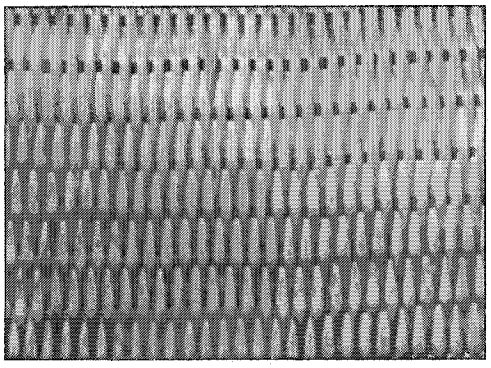

(c) Fabrics

Fig. 1.1 Forms of FRP strengthening systems

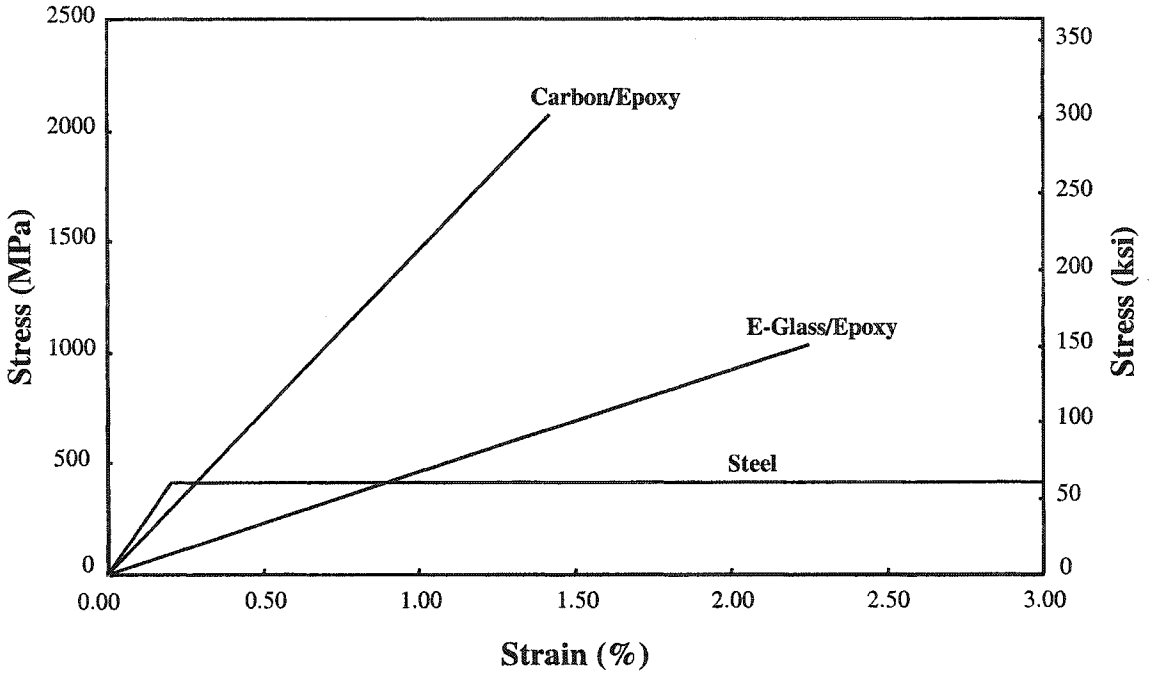

Fig. 1.2 Typical stress-strain diagrams of some FRP systems and steel

CHAPTER 2

BACKGROUND AND LITERATURE REVIEW

2.1 General

Several experimental investigations have been reported on the behavior of reinforced concrete beams strengthened in flexure or shear using Fiber Reinforced Polymers (FRP). In this chapter, these investigations are briefly reviewed with the highlight on the points related to the current investigation. In case of flexural strengthening, the review is focused on ductility of the beam, failure modes, and gain in yield load, while in case of shear strengthening, the review is focused on the useable strength of the FRP (degree of FRP exploitation) and the effect of fiber orientation. The guidelines of ACI 440 committee regarding the ductility of the strengthened beams are also reviewed.

Hybrid composites were the subject of several investigations. Hybridization of different types of fibers was found a good tool to enhance the mechanical properties of fibers acting alone, as well as, to reduce cost. Some of these investigations are reviewed with the highlight on ductility enhancement.

2.2 Flexural Strengthening

2.2.1 Strengthening using glass FRP

Saadatmanesh and Ehsani (1991) experimentally investigated the behavior of reinforced concrete beams strengthened in flexure using Glass Fiber Reinforced Polymer (GFRP) plates epoxy bonded to their tension faces. Considerable increase in beam strength was experienced. However, similar increase in beam yield load or stiffness was not experienced. Different failure modes were experienced such as plate debonding from

the concrete surface, shear-tension failure at plate end, and crushing of the concrete. The strengthened beams experienced a significant loss in ductility.

Ritchie et al. (1991) reported experimental investigation of reinforced concrete beams strengthened using GFRP plates of different rigidities. Generally, the strengthened beams showed higher ultimate loads compared to the non-strengthened ones. Increases in beam stiffness were reported but with less percentages than those of the ultimate loads. Beams strengthened with GFRP sections of high rigidities showed high increases in stiffness; however, that was accompanied by a great loss in beam ductility. The strengthened beams exhibited brittle failures such as shear-tension failure at plate ends or FRP rupture.

2.2.2 Strengthening using carbon FRP

Ritchie et al. (1991) tested two beams strengthened in flexure using CFRP plates. Since CFRP has higher elastic modulus than GFRP, the beams strengthened with the CFRP plates showed similar gain in stiffness to those strengthened with GFRP plates of larger cross sections. Beams strengthened with CFRP exhibited increases in ultimate loads but with a considerable loss in ductility. The experienced modes of failure were plate rupture or shear-tension failure at plate end. In addition, they reported test results of similar beams strengthened using steel plates. Some of the beams strengthened with the steel plate exhibited significant ductility in comparison with those strengthened with CFRP plates.

Triantafillou and Plevris (1992) reported experimental investigations of reinforced concrete beams strengthened in flexure using CFRP plates of different cross sectional areas. The load-deflection relations of the tested beams showed that the increase in yield load was not as significant as that of the ultimate load. All the strengthened beams

showed considerable decrease in ductility. The strengthened beams failed either by CFRP rupture or by CFRP peeling off. They concluded that the FRP peeling-off debonding mechanism gives a limitation on the FRP thickness beyond which brittle failure occurs without achieving the full flexural strength and ensuring ductility.

Arduini et al. (1997) reported test results of four reinforced concrete beams strengthened with pultruded CFRP plates. All the strengthened beams showed very brittle response and failed by shear-tension failure at plate ends without showing any significant yield plateaus. The reported CFRP strain values at failure were less than 50% of its ultimate strain, which indicated that less than half the strength of CFRP was utilized.

Norris et al. (1997) experimentally examined the behavior of reinforced concrete beams strengthened in flexure using CFRP sheets. Various orientations of the CFRP sheets with respect to the beam longitudinal axis were applied. Their test results showed that when the CFRP sheet was installed so that its fiber direction was parallel to the beam longitudinal axis, a large increase in stiffness and strength was experienced; however, brittle failures were experienced due concrete rupture as a result of stress concentration near the end of the CFRP. When the CFRP fibers were placed obliquely to the beam longitudinal axis, the increase in strength and stiffness was not considerable; however, the failure was more ductile. Generally, the increase in beam yield loads was not as high as that of the ultimate loads

Takahashi et al. (1997) experimentally investigated the flexural behavior of reinforced concrete beams with externally bonded CFRP sheets. The effect of wrapping the beam as U-jackets using CFRP sheets was studied. U-jacket wrapped beam did not exhibit any increase in flexural strength than the non-wrapped one. However, wrapping the beam was able to control the progress of peeling. The failure mode shifted from peeling of the CFRP sheet to rupture of the sheet FRP, which was more ductile.

Spadea et al. (1997) tested reinforced concrete beams strengthened in flexure using CFRP plates. The plates of some of the beams were provided with additional external anchorages. Their test results indicated that although the CFRP plates increased the ultimate capacity of the beam as high as 60%, it transformed a ductile flexural behavior of the beam before strengthening into a brittle failure caused by plate debonding. The capacity of the CFRP plate was underutilized as it exhibited strains at failure that were less than its ultimate strain by 50%. Using additional anchorage for the CFRP slightly increased the utilization of the CFRP plates. Decreases in beam ductility of 20 to 25% of that of the non-strengthened beam were reported.

Grace et al. (1999) reported experimental investigations of reinforced concrete beams strengthened using various types of carbon and glass FRP. Their investigations showed that strengthening the beams using FRP laminates reduces deflections and increases the load carrying capacity. However, the strengthened beams experienced losses in ductility. Brittle failures such as FRP debonding, shear-tension failure at plate ends, and FRP tensile rupture were reported.

Bencardino et al. (2002) tested reinforced concrete beams strengthened in flexure using a carbon fiber woven fabric. They recognized the fact that wrapping the beam with a bidirectional fabric around the tension face and up the vertical sides is able to provide local anchorage all along the span unlike unidirectional laminates that can only cover the tension face without any local anchorage. Their test results showed that beams with bidirectional fabrics were able to develop their full theoretical flexural strength, which contrasts with the behavior of similar beams strengthened with unidirectional laminates. However, their strengthened beams exhibited significant losses in structural ductility. The increases in beam yield loads were not as significant as that of the ultimate loads.

2.2.3 Ductility considerations in ACI committee 440 guidelines

ACI 440 Committee guidelines (2002) for the design of externally bonded FRP systems for strengthening concrete structures suggests a strength reduction factor (ϕ) to account for the loss of ductility as a result of strengthening. This reduction factor followed the philosophy of ACI 318, where a section with low ductility should compensate with a higher reserve of strength. The higher reserve of strength is achieved by applying a strength reduction factor of 0.70 for brittle sections, as opposed to 0.9 for ductile sections. This reduction factor is related to the strain level in the steel at the ultimate load. The strain level in the steel at the ultimate load should be checked and ductility is considered adequate if the strain value is at least 0.5%. This strength reduction factor (ϕ) was given by the following equation:

$$\phi = \begin{cases} 0.9 & \text{for } \varepsilon_s \geq 0.5\% \\ 0.7 + \dfrac{0.2(\varepsilon_s + \varepsilon_{sy})}{0.005 - \varepsilon_{sy}} & \text{for } \varepsilon_{sy} < \varepsilon_s < 0.5\% \\ 0.7 & \text{for } \varepsilon_s \leq \varepsilon_{sy} \end{cases} \qquad (2.1)$$

where

ε_s = Strain in steel reinforcement at ultimate load

ε_{sy} = Yield strain of steel

A graphical representation of this equation is shown in Fig. 2.1. Note that the equation sets the reduction factor at 0.9 for ductile sections and 0.7 for brittle sections where the steel does not yield and provides a linear transition for the reduction factor between these two extremes.

2.3 Shear Strengthening

2.3.1 Experimental investigations

Chajes et al. (1995) tested reinforced concrete T-beams externally strengthened on their sides and bottoms using glass, carbon, and aramid FRP woven fabrics. The weave directions were oriented along and perpendicular to the beams' longitudinal axis (i.e., fibers at 0/90°) in some beams, and rotated 45° from the beams' longitudinal axis (i.e., fibers at 45/135°) in other beams. Increases in ultimate strength of 60 to 150 percent were achieved. Generally, failures occurred by fracture of the FRP along the lines of diagonal cracks. However, the maximum recorded FRP strains prior to failure were much below their ultimate values and were less than 0.6%, which indicates that the FRP was not fully utilized. Beams with fibers at 45/135° achieved higher strengths than those with fibers at 0/90°.

Sato et al. (1996) tested reinforced concrete beams strengthened in shear using a unidirectional carbon fiber sheet. They applied two strengthening schemes: (i) bonding the sheet around the beam bottom face and sides and (ii) bonding the sheet at beam sides only. All the shear failures experienced were by peeling of the carbon fiber sheet from the surface of the concrete along the shear crack. The carbon fiber sheet significantly increased the shear strength of the beams. The carbon fiber sheet, attached to three sides of the beam as a U-wrap, was more effective than that attached only at the sides.

Taerwe et al. (1997) reported test results of reinforced concrete beams strengthened in shear using a carbon fiber sheet. The beams were wrapped around their bottom faces and sides along the shear span in a form of either a continuous sheet or strips of a given spacing. Failures occurred mainly by peeling of the sheet from the beam surface. However, the carbon fiber sheet increased the shear capacity of the beams. The recorded CFRP stains before beam failure were less than 1.0%.

Umezu et al. (1997) experimentally investigated the shear behavior of reinforced concrete beams strengthened using an aramid fiber sheet. The sheet was wrapped around the upper, bottom, and side surfaces of the beams. Most of the strengthened beams experienced shear failure of the concrete followed by rupture of the sheet. They concluded that in test beams with larger quantities of aramid fiber sheets applied, the rupture strain of the sheet was not reached when the shear failure of the concrete occurred, thus the full tensile capacity of the sheet was not experienced.

Sato et al. (1997) tested reinforced concrete T-beams strengthened in shear using carbon fiber sheet bonded around beam bottom face and sides. Mechanical anchorage of the carbon fiber sheet was applied in one of the beams. The strengthened beams failed by debonding of the carbon fiber sheet from the concrete surface with considerable increase in beam shear strength. Carbon fiber sheet with mechanical anchorage was more effective than that without mechanical anchorage.

Araki et al. (1997) tested reinforced concrete specimens strengthened in shear using carbon or aramid sheets. The beams had rectangular cross sections and were all wrapped around by the sheet. The strengthened beams failed by shear failure of the concrete followed by rupture of the sheet. The recorded strain in the sheet of some of the tested specimens at the maximum load was about two third of its ultimate strain, which indicated that the full strength of the sheet was not utilized.

Chaallal et al. (1998) experimentally investigated the response of reinforced concrete beams strengthened in shear using externally applied epoxy bonded unidirectional carbon fiber plastic strips. The beams were strengthened in their sides and the strips were placed either perpendicularly or diagonally at 45^{o} to the beam longitudinal axis. Generally, failures were experienced by debonding of the strips from the concrete surface. However, the beams strengthened by diagonal strips outperformed

those strengthened with vertical strips in terms of crack propagation, stiffness, and shear strength.

Triantafillou (1998) reported experimental results of beams strengthened in shear using carbon fiber fabrics. The beams were strengthened on their sides only and the fabric was applied with its fiber direction perpendicular or 45° diagonally to the beam longitudinal axis. All the beams experienced a shear failure mode by development of diagonal shear cracks followed by fabric debonding. Beams installed with diagonally at 45° fabrics exhibited higher ultimate load than those strengthened with fabric with fiber direction perpendicular to the beam longitudinal axis. Therefore, it was concluded that the effectiveness of the FRP increases as the fibers' direction becomes closer to the direction perpendicular to the diagonal crack.

2.3.2 Analytical investigations

Some investigators were interested in analytically predicting the contribution of externally boded FRP to the shear capacity of the reinforced concrete beams. Some of the systematic investigations reported in this subject are reviewed below. Generally, most researchers idealized FRP materials in an analogy with internal steel stirrups, assuming that the contribution of FRP to shear capacity emanates from the capacity of fibers to carry tensile stresses as the case of internal steel stirrups. However unlike steel stirrups, experimental investigations showed that the FRP stress levels before failure of the strengthened beams are always lower than the strength of the FRP material. The key element in this investigation was to predict the strain in the FRP at shear failure of the beam, known as the effective strain (ε_{fe}).

Triantafillou (1998) derived a polynomial function to predict the effective strain (ε_{fe}). This polynomial was derived through curve fitting on about 40 test data published by various researchers. The polynomial showed that the effective strain (ε_{fe}) decreases with increasing FRP axial rigidity. The contribution of the FRP is calculated in analogy with steel stirrups and the polynomial was used to calculate the effective strain (ε_{fe}) and then calculate the stress level in the FRP.

Khalifa et al. (1998) used the bond model of Maeda et al. (1997) to develop an approach to describe the shear failure combined with FRP debonding. They also slightly modified Triantafillou's polynomial (1998) and used it as an approach to describe shear failure combined with FRP fracture. The two approaches were combined together to calculate the effective stress level in the FRP.

Triantafillou and Antonopoulos (2000) improved the model reported in Triantafillou (1998). The effective strain was taken as the minimum of three values: maximum strain to control crack opening, strain corresponding to premature shear failure due to FRP debonding, and strain corresponding to shear failure combined with or followed by FRP rupture.

2.4 Development of Hybrid Composites

Hayashi (1972) is believed to be the first to study hybrid composites. He recognized the fact that it is possible to obtain pseudo-ductile composites that have high initial modulus and high elongations at failure by hybridization of different fibers. He experimentally tested the tensile behavior of sandwich composites of glass and carbon fibers. Although his test results confirmed the possibility to obtain pseudo-ductile

composites, a significant drop in stress accompanied the stress-strain behavior of his samples during load transfer from the carbon fibers to the glass fibers.

Bunsell and Harris (1974) studied the behavior of hybrid laminated samples of glass and carbon fibers. Two types of hybrids were made, with the alternate layers either unbonded or bonded together. Their test results showed that bonded sandwich hybrids had better transfer of load from the carbon fibers to the glass fibers than the unbonded ones. No significant drop in stress was experienced in the stress-strain diagrams of the bonded hybrids when compared with those of the unbonded hybrids.

Manders and Bader (1981) evaluated the tensile mechanical properties of hybrid composites fabricated from glass and carbon fibers. Different mix ratios of glass and carbon fibers and different states of dispersion were studied. They concluded that a higher failure strain is observed in the carbon fibers when they are more finely dispersed and occupied a lower proportion of the volume of the hybrid.

More recently, hybridization of fibers interested structural engineers as a tool to overcome the problem of lack of ductility of FRP reinforcing bars.

Nanni et al. (1994) developed reinforcing bars using epoxy impregnated braided fibers as a skin around a steel core. The braided FRP skin was made of aramid or vinylon fibers. Bars with different skin thickness, steel core diameters, and steel core yield strength were tested. Although the bars exhibited a bilinear stress-strain behavior, they are still vulnerable to corrosion because of the existence of steel core.

Somboonsong et al. (1998) developed hybrid FRP reinforcing rebar using braided aramid fibers around a carbon fiber core. The bar was fabricated using an in-line braiding and pultrusion process. Tensile specimens were tested in tension and found to have pseudo-ductile behaviors.

Harris et al. (1998) used the bar developed by Somboonsong et al. (1998) in reinforcing concrete beams. The beams exhibited a load-deflection behavior similar to that experienced by concrete beams reinforced with conventional steel.

Belarbi et al. (1999) introduced a hybrid FRP bar consisting of different types of carbon fibers. The rebar was manufactured using pultrusion and filament winding techniques. A pseudo-ductile response was experienced through testing of coupon rebar as well as RC beams. Testing of large scale beams reinforced with the hybrid rebar exhibited remarkable ductile behavior.

2.5 Conclusions

2.5.1 Flexural strengthening

The reported investigations of reinforced concrete beams strengthened in flexure using currently available FRP materials showed that the beams exhibited higher ultimate loads in comparison to the non-strengthened ones. However, similar increases in beam yield loads were not noted (see Fig. 2.2). A loss in beam ductility is always observed, especially when the beam is strengthened with large FRP sections The results of these investigations showed that for a beam strengthened with an epoxy bonded FRP sheet on its tension face, four modes of failure could be expected (see Fig. 2.3):

(i) concrete crushing,

(ii) FRP tensile rupture,

(iii) debonding at the concrete adhesive interface, and

(iv) shear-tension failure at the sheet end.

The fact that the FRP material is linearly elastic up to failure partially explains the loss of ductility of the strengthened beam. In the case of the first mode of failure, concrete crushing, the loss in ductility is similar to that experienced when increasing the

reinforcement ratio of a beam. However, because the FRP is linearly elastic up to failure and does not yield, compression failures would take place at less deformation than is the case when strengthening with a steel plate of the same rigidity. The loss of ductility experienced during the second mode of failure, FRP tensile rupture, takes place when the ultimate strain of the FRP is not large enough to enable the beam to exhibit large deformations before FRP rupture. The last two modes of failure are rather complicated; however, the properties of the FRP material are involved in the loss in beam ductility in two parts. First, as the deformation of the beam increases, the tension in the FRP increases (because the FRP is linearly elastic and does not yield), requiring further anchorage. This is difficult to obtain because the maximum anchorable FRP force is always limited. This is even more difficult when the required cross section of the FRP is large. In this case, brittle failures are likely due to the loss of the composite action between the FRP and the beam either by FRP debonding or by shear-tension failure at sheet end. The second part concerns the orthotropic nature of FRP materials. These materials can provide their high strength if only loaded in the fiber direction. Therefore, when U-wrapped around the bottom face and the sides of the beam, no significant improvement in anchorage would be expected unless the wrapping was perpendicular to the layer(s) at the bottom, which would complicate the strengthening process.

2.5.2 Shear strengthening

The reported investigations of reinforced concrete beams strengthened in shear showed that bonding FRP strips, fabrics, or sheets to the sides of beams improves their shear strength. These investigations showed that when the strengthened concrete beam reaches its shear capacity, the FRP stretches to a certain strain value known as the effective strain (ε_{fe}). This strain is usually a small fraction of the FRP ultimate strain and

hence the full strength of the FRP is not fully exploited, and their use is not economical. The effectiveness of the FRP was found to increase as the fibers' direction becomes perpendicular to the diagonal crack. Therefore, installing the FRP with the fiber direction at 45° angle to the longitudinal axis of the beam increases the FRP effectiveness in increasing the beam shear strength.

2.5.3 Hybrid composites

Hybridization of different types maybe used to provide a pseudo-ductile behavior to fiber reinforced polymer materials. Some hybrid FRP bars have been used in reinforcing concrete beams. The beams exhibited a load-deflection behavior similar to that experienced by concrete beams reinforced with conventional steel.

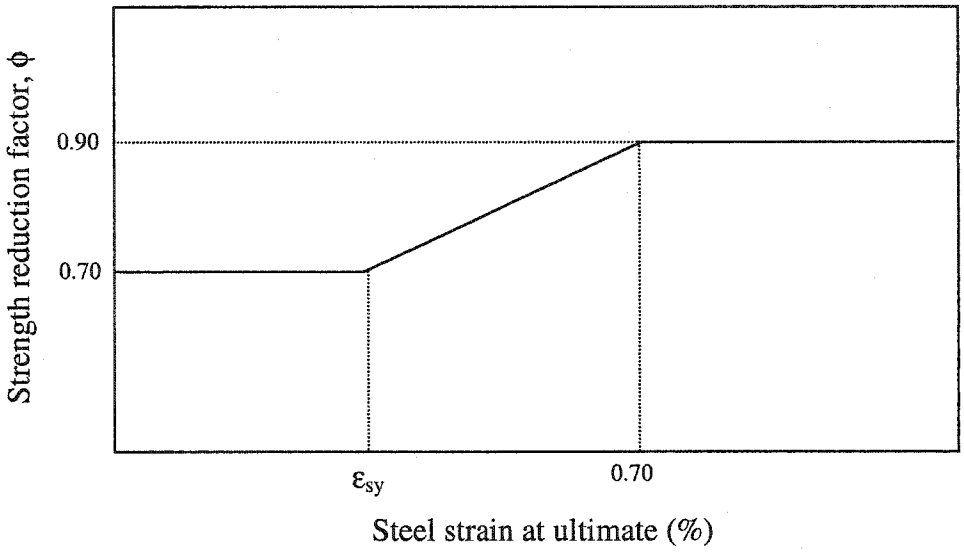

Fig. 2.1 Strength reduction factor according to ACI 440 committee (2002) guidelines

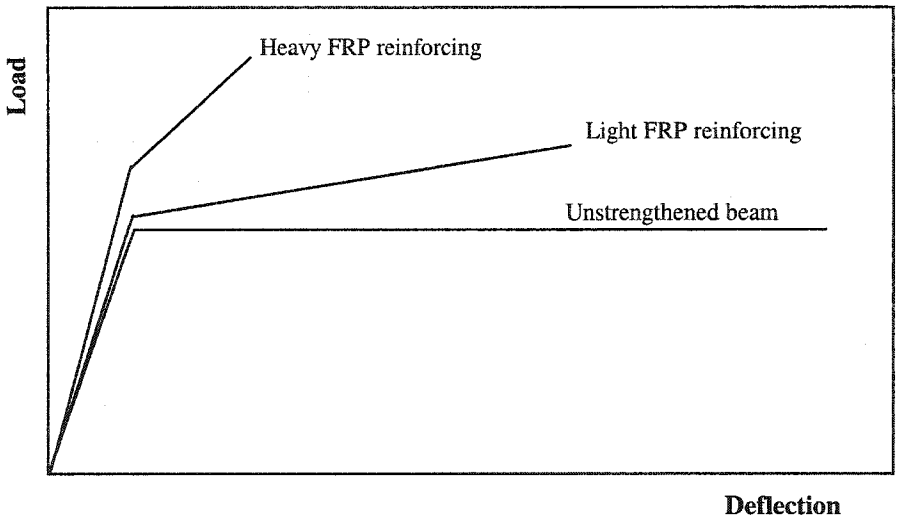

Fig. 2.2 Schematic diagrams of load-deflection relationships experienced by strengthened RC beams using FRP

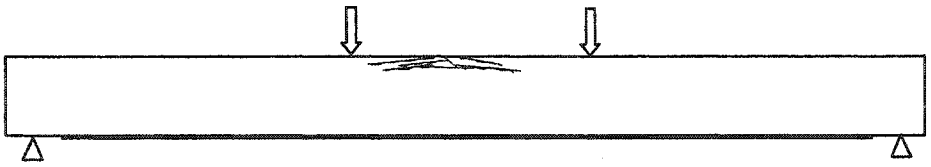

(a) Concrete compression failure

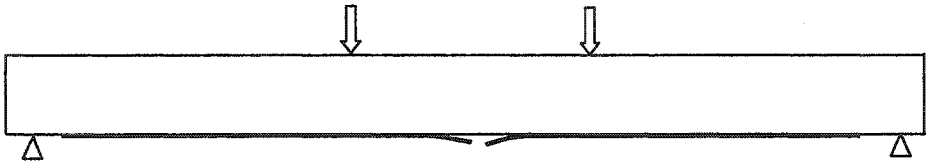

(b) FRP rupture

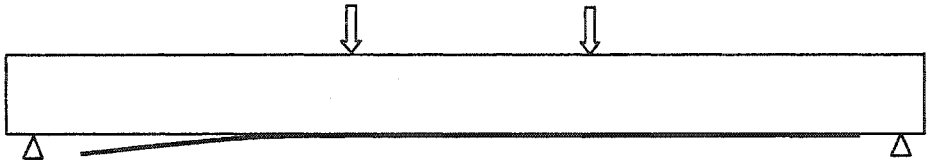

(c) FRP debonding

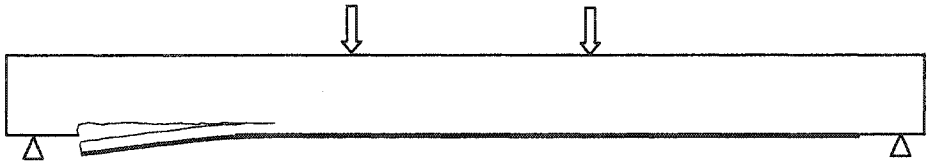

(d) Shear-tension failure at FRP end

Fig. 2.3 Failure modes of reinforced concrete beams strengthened in flexure with FRP

CHAPTER 3

DEVELOPMENT OF NEW DUCTILE FRP SYSTEMS FOR STRENGTHENING CONCRETE BEAMS

3.1 General

In this chapter, the development of two new pseudo-ductile FRP strengthening systems is discussed. The systems are fabrics that are hybrids of carbon and glass fibers. The first fabric has uniaxial fibers and designed to be used for beam strengthening for flexure. The second fabric has triaxially braided bundles of fibers braided in three directions (+45°, 0°, -45°) and designed to be used for beam strengthening for flexure and/or shear. The ideal characteristics of a strengthening material for both flexure and shear were investigated. A parametric study was conducted on the loading behavior of triaxially braided fabrics. Based on these investigations, the fabric geometry was selected. A special micromechanic analytical modeling technique developed by NASA was used to analyze and design the fabric. Both fabrics were manufactured and their tensile mechanical properties were evaluated by testing samples according to ASTM D 3039 specifications.

3.2 Ideal Characteristics of a Strengthening System

3.2.1 Flexure strengthening

The review of the reported experimental investigations of the behavior of concrete beams strengthened in flexure using FRP indicated that the strengthened beams showed higher ultimate loads in comparison to the non-strengthened ones. However, similar increases in beam yield loads were not noted. This is attributed to the fact that steel has a yield strain value that is significantly less than the ultimate strain of the FRP. Therefore,

it yields before the FRP shows any significant contribution to beam load or stiffness. Accordingly, the strengthening material should exhibit its full strength at small strain values, preferably slightly more than the yield strain of the reinforcing steel, in order to contribute its full strength simultaneously with the steel (being installed on the outer surface of the beam, the strengthening material undergoes slightly larger strain than the inner reinforcing steel). On the other hand, the strengthening material should not rupture after reaching this strain value; otherwise a brittle failure will take place due to rupture of the FRP. Therefore, the strengthening material should have enough ultimate strain to guarantee that the beam will exhibit large deformations before failure, and hence enough ductility. In order to achieve these requirements, the strengthening material must initially exhibit a linear stress-strain response up to a certain strain value. This strain value should be slightly greater than the yield strain of steel. Then, the strengthening material should exhibit an increase in strain without a corresponding increase in stress, similar to the yield phenomenon experienced by steel, up to a reasonable ultimate strain.

Furthermore, offering a yield plateau will indirectly help to avoid brittle beam failures that occur by either debonding of the FRP from the concrete surface or by shear-tension at the FRP end. Although these two modes of failures are rather complicated, the fact that FRP behaves in a linear elastic manner until failure is involved, in part, in causing these two failures. As the deformation of the beam increases, the tension in the FRP increases (because the FRP is linearly elastic and does not yield), requiring further anchorage. This is difficult to obtain, as the maximum anchorable FRP force is always limited. Therefore, by offering a yield plateau, the increase in the FRP tension force will be limited after yield and hence these two modes of failure might be avoided.

In view of these observations, the characteristics of an ideal FRP strengthening material for flexure can be summarized as follows:

1- It should initially exhibit a linear stress-strain response up to a certain strain value, then experience an increase in strain without a corresponding increase in stress, similar to the yield phenomenon experienced by steel.

2- The "yield strain" or "the yield-equivalent strain" should be slightly greater than the yield strain of steel.

3- The ultimate strain should be large enough to guarantee sufficient beam deformation before FRP rupture (more than 2%) and hence adequate ductility.

3.2.2 Shear strengthening

In Chapter 2, the review of the recent experimental investigations of the behavior of concrete beams strengthened in shear using FRP showed that bonding FRP strips, fabrics, or sheets on sides of beams improves their shear capacity. These investigations showed that when the strengthened concrete beam reaches its shear capacity, the FRP stretches to a certain strain value known as the effective strain (ε_{fe}). This strain is usually a small fraction of the FRP ultimate strain and hence the strength of the FRP is not fully exploited, which is not economical. Based on the results of several reported experimental investigations, Triantafillou (1998) expressed the effective FRP strain ε_{fe} in terms of $\rho_{frp}E_f$ as follows:

$$\varepsilon_{fe} = 0.0119 - 0.0205(\rho_{frp}E_f) + 0.0104(\rho_{frp}E_f)^2 \quad \text{for} \quad 0 \le \rho_{frp}E_f \le 1\text{GPa} \qquad (3.1)$$

$$\varepsilon_{fe} = 0.00245 - 0.00065(\rho_{frp}E_f) \quad \text{for} \quad \rho_{frp}E_f > 1\text{GPa} \qquad (3.2)$$

where ρ_{frp} is an FRP area fraction factor equal to 2 t_f /b, t_f is the FRP thickness, b is the beam width, and E_f is the FRP elastic modulus. By expressing E_f in terms of ε_{fe} and F_{fe}, where F_{fe} is the FRP load per unit width corresponding to the effective strain ε_{fe}, as $E_f = F_{fe}/(t_f \times \varepsilon_{fe})$, the term $\rho_{frp}E_f$ can be rewritten as $2F_{fe}/(b \times \varepsilon_{fe})$. Substituting in (3.1) and (3.2), the two equations can be rewritten as follows:

$$\varepsilon_{fe} = 0.0119 - 0.0205\left(\frac{2F_{fe}}{b.\varepsilon_{fe}}\right) + 0.0104\left(\frac{2F_{fe}}{b.\varepsilon_{fe}}\right)^2 \quad \text{for} \quad 0 \le \left(\frac{2F_{fe}}{b.\varepsilon_{fe}}\right) \le 1\text{GPa} \qquad (3.3)$$

$$\varepsilon_{fe} = 0.00245 - 0.00065\left(\frac{2F_{fe}}{b.\varepsilon_{fe}}\right) \quad \text{for} \quad \left(\frac{2F_{fe}}{b.\varepsilon_{fe}}\right) > 1\text{GPa} \qquad (3.4)$$

Based on equations (3.3) and (3.4), the relationship between the effective strain ε_{fe} and the corresponding FRP load per unit width F_{fe} is calculated for different values of beam widths (b=125, 200, 300, 400 mm). This is shown in Fig. 3.1. Note from the figure that the contribution of the FRP to beam shear capacity can be optimized if it can provide a certain value of load at a strain of 0.5%.

In view of this, the shear strengthening material should exhibit its maximum strength at a strain value of 0.5%, with its corresponding load to be equal to the optimum load discussed above. Since it is possible to install more than one layer of strengthening material on a beam, to get multiples of the load provided by one, it is better to have this load equal to the peak load of the smallest practical beam width (125 mm for example).

The literature review showed that the effectiveness of the FRP increases as the fibers' direction becomes perpendicular to the diagonal crack. Accordingly, the strengthening system should have fibers at 45° to the longitudinal axis of the beam. The system would be ideal if it contained fibers at 0° for flexural strengthening and fibers in

the +45°, -45° directions for shear strengthening, all in the same layer. In this case, the orthotropic characteristics involved with using FRP materials would be no longer a problem for beam strengthening applications.

3.3 Development of Uniaxial Ductile Fabric

3.3.1 Fabric design

A uniaxial ductile fabric has been developed for applications that require strengthening/stiffening for flexure only. To generate a yield plateau, a hybridization technique of different types of fibers was used. Three fibers were selected with different elongations to failure. By combining these fibers and controlling their mix ratio, the fibers with the lowest elongation (LE) fail first when loaded in tension, allowing a strain relaxation (that is, an increase in strain without an increase in load). The remaining high elongation (HE) fibers then sustain the total load up to failure. The LE fiber strain at failure represents the value of the "yield-equivalent" strain of the hybrid, while the HE fiber strain at failure represents the ultimate strain. The load corresponding to failure of LE fibers represents the "yield-equivalent" load, and the maximum load carried by the HE fibers is the ultimate load. Ultra-high modulus carbon fibers (Carbon #1) were used as the LE fibers, in order to have the lowest yield equivalent strain possible, which was not less than the yield strain of steel (about 0.2% for Grade 60 steel). On the other hand, E-glass fibers were used as the HE fibers to provide the highest possible strain at failure, in order to produce a high ductility index (the ratio between deformation at failure and deformation at yield). High modulus carbon fibers (Carbon #2) were selected as medium elongation (ME) fibers in order to minimize the load drop that could occur after failure of

the LE fibers during the strain relaxation, and also to provide a gradual load transition from the LE fibers to the HE fibers. Based on these concepts, the fabric was manufactured by combining these fibers together as adjacent yarns in repeated cells. The fabric was designed to be impregnated by an epoxy resin before installing it on the beam surface. The epoxy works as a matrix for the fibers and as an adhesive to attach the fabric to the concrete surface. Table 3.1 shows the mechanical properties of the fibers used and Fig. 3.2 shows their stress-strain behavior.

3.3.2 Fabric testing

Samples of fabric 2 mm thick were tested according to ASTM D 3039 specifications in order to compare its behavior in tension with the theoretical predicted loading behavior. The theoretical behavior is based on the "rule of mixtures" in which the axial stiffness of the hybrid is calculated by summation of the relative stiffness of each of its components. Fig. 3.3a shows the average tensile load-strain curve of four samples. Note that the behavior was linear up to a strain of 0.35%, when the LE fibers started to fail. At this point, the slope of the load-strain curve decreased significantly. When the strain reached 0.90%, the ME fibers started to fail, resulting in an additional increase in strain without significant increase in load up to total failure of the coupons by failure of the HE fibers. A "yield-equivalent" load (the first point on the load-strain curve where the behavior becomes non-linear) of 0.46 kN/mm (2.6 kips/in.) and an average ultimate load of 0.78 kN/mm (4.4 kips/in.) was observed. Fig. 3.4 shows a photo and details of the fabric. The yarn sizes in the figure are measured in thousands of filaments (k).

The fabric is capable of absorbing energy before total failure due to failure of the LE and ME fibers. To investigate the amount of energy absorbed, a fabric sample was unloaded just before failure and the elastic and inelastic energies were calculated from the loading diagram. This is shown in Fig. 3.3b. The sample showed an energy ratio (the ratio between the inelastic energy and the total energy) of 32%.

3.4 Development of Triaxially Braided Ductile Fabric

A triaxially braided ductile fabric has been developed. In this fabric, bundles of fibers were oriented in three different directions. These directions are 0°, $+45^{\circ}$, and -45°. The 0° direction (referred to as the axial direction) acts mainly for flexural strengthening, while the $+45^{\circ}$ and -45° directions (referred to as the diagonal directions) act mainly for shear strengthening, in order to have fibers perpendicular to any potential shear cracks. A 2x2 triaxial braid pattern was used to combine the fiber bundles (yarns) in the three directions (Fig. 3.5). The 0° yarns are known as the "axial yarns", while the $\pm\theta$ yarns are known as the "braider yarns". The term "2x2" refers to the way diagonal yarns are intertwined; a $+\theta$ braider yarn continuously passes over two $-\theta$ braider yarns and then under two $-\theta$ braider yarns and vice versa, as shown in Fig. 3.5.

3.4.1 Method of analysis

NASA developed a general purpose analytical micromechanic technique to analyze textile composites [Naik (1994a), Naik (1994b)]. This technique utilizes the periodicity of the textile composite to isolate a Repeating Unit Cell (RUC) and then discretely modeling each yarn within the RUC. First, a three dimensional description of

the textile composite is performed, then the three dimensional effective stiffness of the composite are computed by discretizing each yarn in the RUC into yarn slices and using the material properties, spatial orientation, and volume fraction of each slice in a volume average technique that assumes an iso-strain state within the RUC. This analytical technique was implemented by Naik (1994c) in an analysis package called TEXCAD (TEXtile Composite Analysis for Design). TEXCAD has the ability to analyze different types of textile composites. TEXCAD was used to analyze and design the new fabric with the permission of NASA.

3.4.2 Parametric study

Interactions occur between the yarns in the triaxially braided fabrics. Therefore, it was necessary to understand the geometry and behavior of triaxially braided fabrics by addressing the following two points:

1- Although each group of fibers is orthotropic in nature, with the highest stiffness and strength in the fiber direction, each group still has some stiffness and load contribution when loaded in the other directions. As a result, if the triaxial fabric is loaded in the direction of any particular group of fibers, the contributions of the other two groups should also be taken into account.

2- In 2X2 triaxially braided fabrics (Fig. 3.5), the axial yarns are mainly straight, without any undulations; the diagonal yarns however, are always undulating as they pass over and under the axial yarns. The undulation angle is known as the "crimp angle". These undulations are expected to affect the diagonal loading behavior of

these yarns. The main factors affecting the undulation geometry are the diagonal yarn size, axial yarn spacing, and axial yarn size.

A parametric study has been conducted to address the above two points. The study was conducted for three fiber types: (1) ultra high modulus carbon fibers (carbon #1), (2) high modulus carbon fibers (carbon #3), and (3) E-glass fibers. The composite mechanical properties of these fibers are listed in Table 3.1.

3.4.2.1 Diagonal yarn contribution

TEXCAD was used to study the contribution of the diagonal yarns to the axial load carrying capacity of the fabric for three cases of fibers. In each case, models with a 45° braiding angle and different yarn sizes were analyzed. The study was performed on fabrics with a 45% fiber volume fraction (V_f) and an axial yarn spacing (s) of 6.3 mm (0.25 in.). In each case, the contributions of the axial and diagonal yarns to the fabric axial load carrying capacity were calculated. Fig. 3.6 shows the results of this study. The study indicates that the axial yarns generally have the greatest contribution to the total axial load.

3.4.2.2 Diagonal yarn size

The effect of diagonal yarn size on the diagonal loading behavior was studied. TEXCAD was used to analyze three models of triaxially braided fabrics with 45% fiber volume fraction, one for each type of fiber. In each case, the axial yarn size and spacing were kept constant as the diagonal yarn size changed. The failure strain, ultimate load per unit width, and the unit rigidity (E_f t_f) were calculated for the diagonal direction. The

relation between diagonal yarn size and failure strain is plotted in Fig. 3.7. The relation between diagonal yarn size and yarn crimp angle is plotted in the same figure using a secondary axis. Clearly, as the diagonal yarn size increases the failure strain decreases. This is attributed to the increase in yarn crimp angle with the increase of yarn size. Note that Carbon #1 is very sensitive to this effect (Fig. 3.7a). The failure strains are very small compared to the ultimate strain of this type of fiber. Therefore, diagonal yarn sizes should not be increased to the extent that the failure strain of the fabric becomes compromised. Fig. 3.8 shows the effect of diagonal yarn size on diagonal ultimate load and unit rigidity. For the case of carbon #1, as diagonal yarn size increases, the ultimate load deceases and the unit rigidity increases. However, for the carbon #3 and glass cases, the ultimate load increases with the increase in diagonal yarn size due to the increase in its area. However after a certain size, it starts to decrease. This decease in ultimate load is attributed to the increase in yarn crimp angle as the yarn size increases. In all cases, the unit rigidity ($E_f t_f$) increases as the size of the diagonal yarn increases.

3.4.2.3 Axial yarn spacing

TEXCAD was used to study the effect of axial yarn size on the behavior of three diagonally loaded models, one for each fiber type. In each case, the axial and diagonal yarn sizes were kept constant and the axial yarn spacing was changed. The study was done for fabrics with 45% fiber volume fraction. The failure strain, ultimate load per unit width, and unit rigidity ($E_f t_f$) were calculated for each model. The effect of axial yarn spacing on failure strain and crimp angle is shown in Fig. 3.9. Clearly, failure strain increases with the increase of axial yarn spacing, while the crimp angle decreases with

increasing axial yarn spacing. This is attributed to the increase in undulation length as the axial yarn spacing increases. The relations between axial yarn size and ultimate load and unit rigidity (E_f t_f) are plotted in Fig. 3.10. The figure indicates that unit rigidity decreases with increasing axial yarn spacing, while ultimate load increases with increasing axial yarn spacing. However, after a certain point, the ultimate load starts to decrease with increasing axial yarn spacing (in the cases of carbon #3 and glass) or becomes constant (in the case of carbon #1). In cases of very small spacing, the diagonal strength of the fabric is almost lost.

3.4.2.4 Axial yarn size

The effect of axial yarn size on diagonal loading behavior was studied. Three models of diagonally loaded fabrics with a 45% fiber volume fraction were studied, one for each type of fiber. In each case, axial yarn spacing and diagonal yarn size were kept constant as the axial yarn size was changed. TEXCAD was used to calculate the failure strain, ultimate load per unit width, and unit rigidity (E_f t_f) for each model. The effect of axial yarn size on failure strain and crimp angle is shown in Fig. 3.11. Clearly, the failure strain decreases with increasing axial yarn size, while the crimp angle increases with increasing axial yarn size. This is attributed to the increase in the undulation vertical shift when the axial yarn size increases. The relations between axial yarn size and both ultimate load and unit rigidity (E_f t_f) are plotted in Fig. 3.12. No significant change in unit rigidity is noted when changing axial yarn size. However, as axial yarn size increases, the ultimate load decreases.

3.4.3 Fabric geometry

In view of the parametric study discussed above and the design requirements, the geometry shown in Fig. 3.13 was selected and the fabric was manufactured. A photo of the fabric is shown in Fig. 3.14. In order to generate ductility, a hybridization technique was implemented in each direction. For the axial group of fibers (the 0^{o} group), three different types of fibers were used. The first type was ultra high modulus carbon fiber (Carbon #1), used as the LE fiber. The second type was high modulus carbon fiber (Carbon #3), used as the ME fiber. The third type was E-glass fiber, used as the HE fiber. The yarn sizes and configurations were selected so that the ductility generation technique, used in the case of the uniaxial fabric, would still be successful. For the two diagonal groups ($+45^{o}$ and -45^{o}), only two types of fibers were used. The first type was high modulus carbon fiber (Carbon #3), used as the ME fiber. The second type was E-glass fiber, used as the HE fiber. With respect to diagonal loading, the ductility generation technique was similar to that used for the case of the uniaxial fabric, but with only one strain relaxation. The fabric was designed so that when it is loaded in the axial direction (0^{o}), it exhibits a linear load-strain behavior up to 0.35% strain, and then exhibits an increase in strain without a corresponding increase in load up to failure. If loaded in a diagonal direction ($+45^{o}$ or -45^{o}), the fabric was designed to have an almost linear load-strain relation up to a strain of 0.5% and a corresponding load close to 0.12 MN/m, then exhibit a significant reduction in the slope of the load-strain relationship. The selected fabric geometry was checked by using TEXCAD to predict the tensile loading behavior of the fabric. The predicted load-strain behaviors of the fabric in both the axial and diagonal directions are plotted in Fig. 3.17.

3.4.4 Fabric testing

Epoxy impregnated samples of this fabric were tested according to ASTM D 3039. Two groups of samples were prepared. The first group was used to investigate the load-strain response of the fabric in the axial direction. In this group, samples were prepared so that the axial yarns were parallel to the direction of loading. The second group was used to investigate the load-strain response of the fabric in the diagonal directions. Fig. 3.15 shows a photo of the test samples and Fig. 3.16 shows a photo of the tensile testing machine used for testing. The samples were prepared so that one set of diagonal yarns was parallel to the direction of loading. Fig. 3.17 shows the experimental tensile load-strain response of the fabric in both the axial and diagonal directions together with the theoretical prediction. The experimental results shown in figure are the average results of three samples tested in each direction. Note that for axial loading, the fabric exhibited a linear load-strain behavior up to a strain of 0.38%, when the axial LE yarns failed. After this point, the strain started to increase at a faster rate than the load until failure occurred. For diagonal loading, the load-strain curve was almost linear up to a strain of 0.50%, when the diagonal LE yarns failed. At this point, an increase in strain occurred without a corresponding increase in load until total failure of the fabric occurred. The theoretical predication was in a good agreement with the experimental results. In order to investigate the energy absorption capability of the fabric in the axial direction, a sample was unloaded just before failure and the elastic and inelastic energies were calculated from the loading diagram. This is shown in Fig. 3.18. The sample showed an energy ratio (the ratio between the inelastic energy and the total energy) of 55%. Fig. 3.19 shows the test samples after failure.

3.5 Conclusions

Two pseudo-ductile FRP strengthening systems for concrete structures have been developed. The first is a uniaxial ductile fabric designed to be used mainly for flexural strengthening applications. The fabric is a hybrid of one type of glass fiber and two types of carbon fibers, and is designed to have the potential to yield simultaneously with the steel reinforcement of the strengthened beams. The fabric exhibits a ductile behavior with a low "yield equivalent" strain value in tension. The second system is a triaxially braided fabric. This fabric was developed mainly for applications that require shear and/or flexural strengthening. The fabric contains fibers braided in three different directions (0°, +45 °, and –45 °). It is designed to offer strength, stiffness, and ductility if loaded axially or diagonally. A parametric study was conducted on 2X2 triaxially braided fabric to study the contribution of the diagonal yarns to axial loading behavior and the effect of axial yarn size, axial yarn spacing, and diagonal yarn size on diagonal loading behavior. Diagonal yarns were found to contribute little to axial load carrying capacity. Diagonal failure strain was found to decrease with increasing diagonal and axial yarn sizes and increase with increasing axial yarn spacing. Ultimate diagonal load and unit rigidity were found to be affected by axial and diagonal yarn sizes and axial yarn spacing. The fabric exhibited ductile plateaus when loaded axially or diagonally.

Table 3.1 Mechanical Properties of the Materials

Material	Description	Manufacture	Type	Longitudinal Modulus of Elasticity GPa (Msi)	Longitudinal Tensile Strength MPa (ksi)	Failure Strain (%)	Transverse Modulus of Elasticity GPa (Msi)	Filament Diameter μm
Carbon #1*	Ultra-High Modulus Carbon Fibers	Mitsubishi Chemicals	K63712	379 (55)	1324(192)	0.35	5.5 (0.8)	11
Carbon #2*	High Modulus Carbon Fibers	Toray Carbon Fibers	M40J	231 (33.5)	2413 (350)	0.9-1.0	10.3 (1.5)	5
Carbon #3*	High Modulus Carbon Fibers	Toray Carbon Fibers	M46J	265 (38.5)	2200 (320)	0.8	10.3 (1.5)	5
Glass*	E-Glass Fibers	PPG Industries	Hybon 2022	48 (7)	1034 (150)	2.1	9.6 (1.4)	12.1
Epoxy	Resin	Dow Chemicals	DER 332 /DEH 32	-	66.3 (9.6)	4.4	-	-

* Composite properties based on 60 % fiber volume fraction

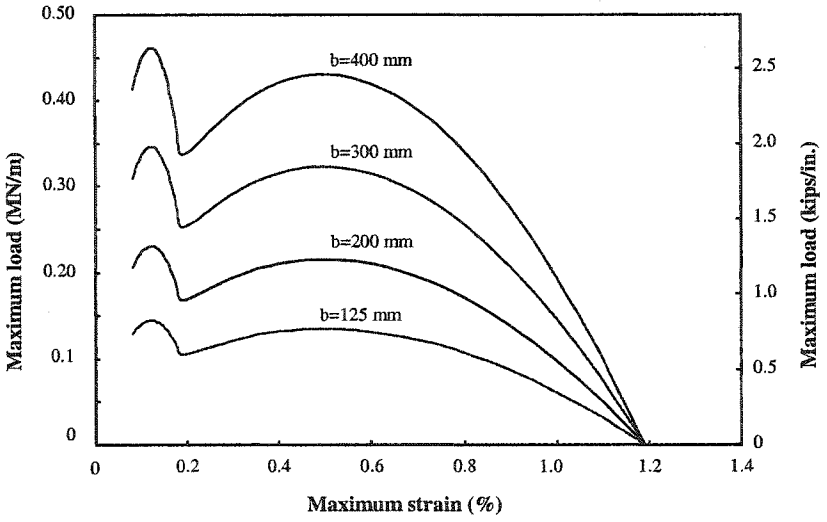

Fig. 3.1 Effective FRP strain and corresponding FRP load

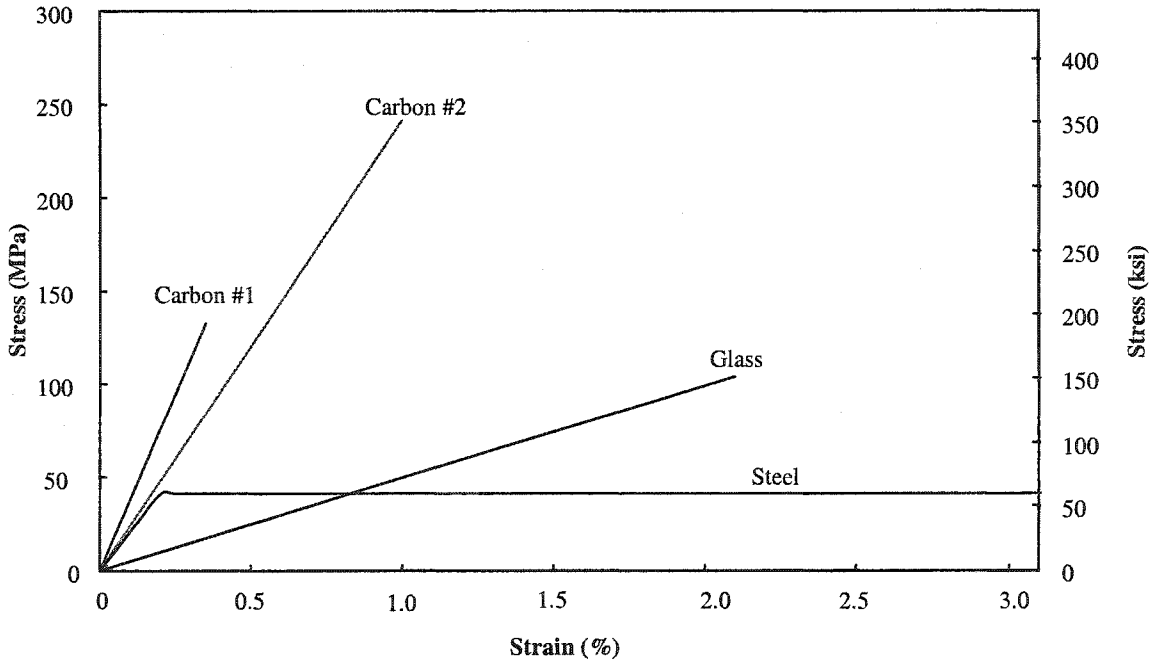

Fig. 3.2 Stress-strain behavior of fibers used and steel

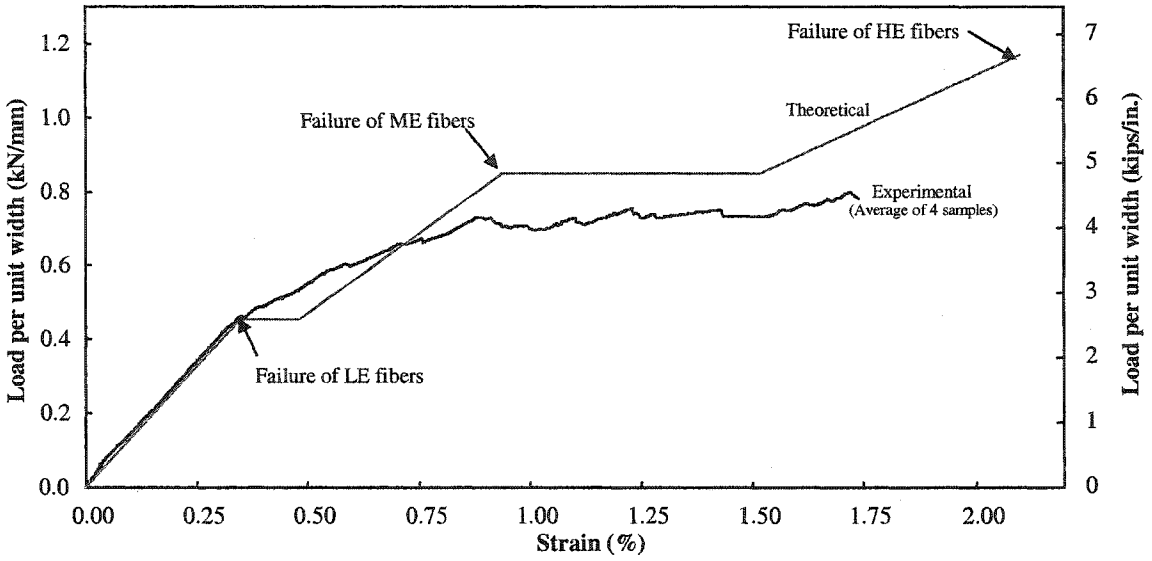

(a) Experimental tensile behavior

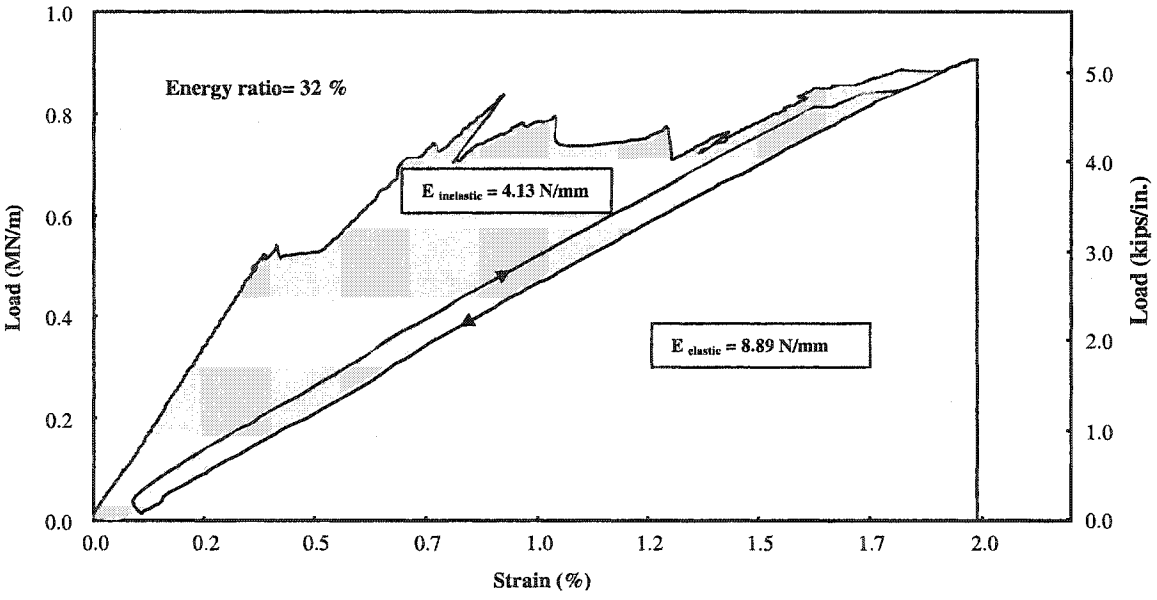

(b) Typical energy absorption

Fig. 3.3 Experimental tensile results for uniaxial hybrid fabric

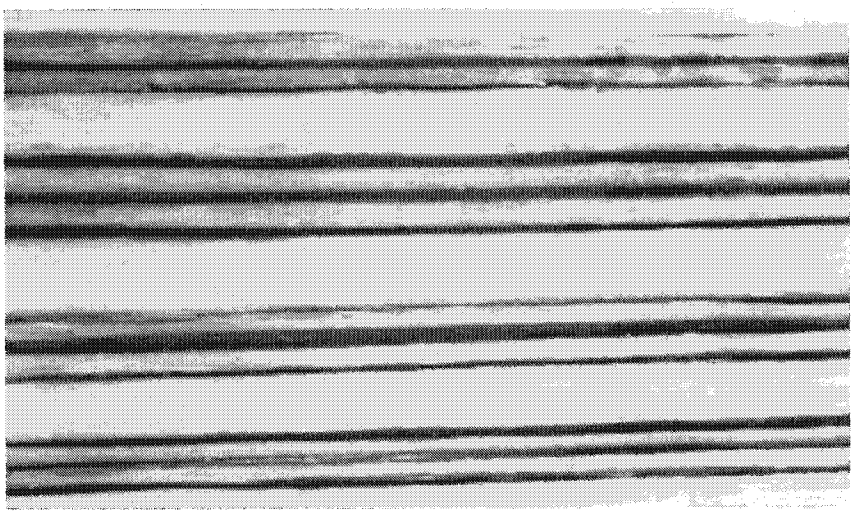

(a) Epoxy impregnated sample of the uniaxial fabric

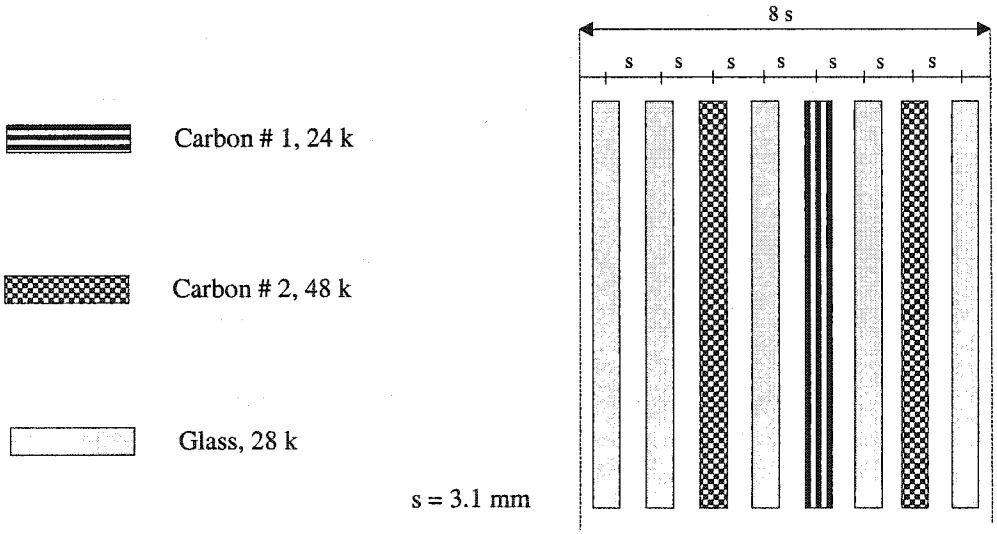

(b) Details of repeating unit cell

Fig. 3.4 Photo and details of the uniaxial fabric

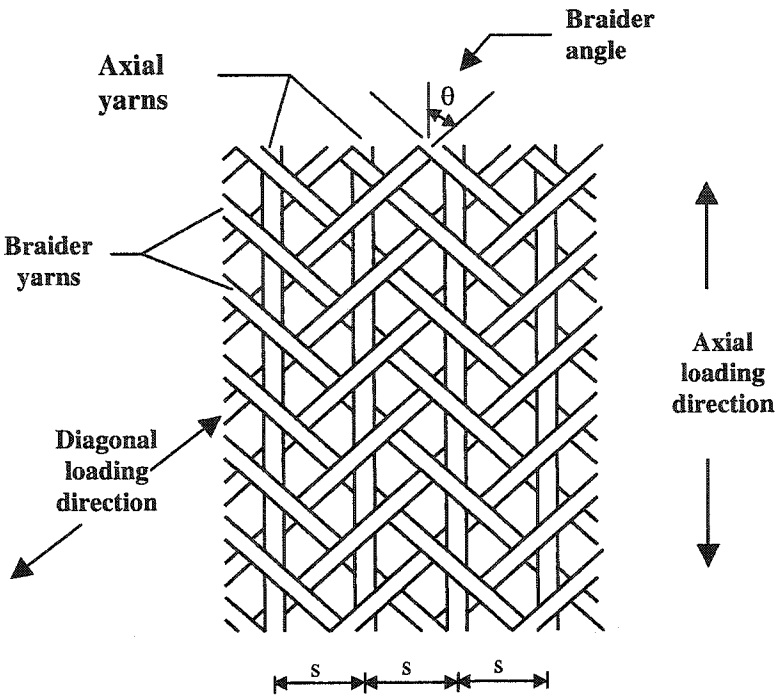

Fig. 3.5 2x2 Triaxial braid pattern

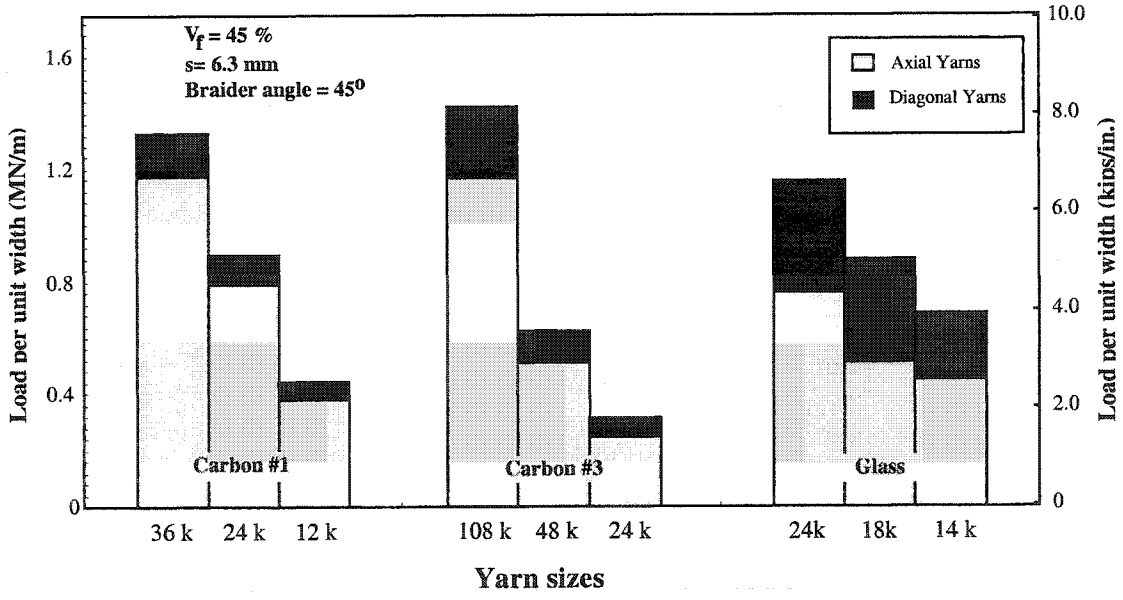

Fig. 3.6 Contribution of axial and diagonal yarns to axial load

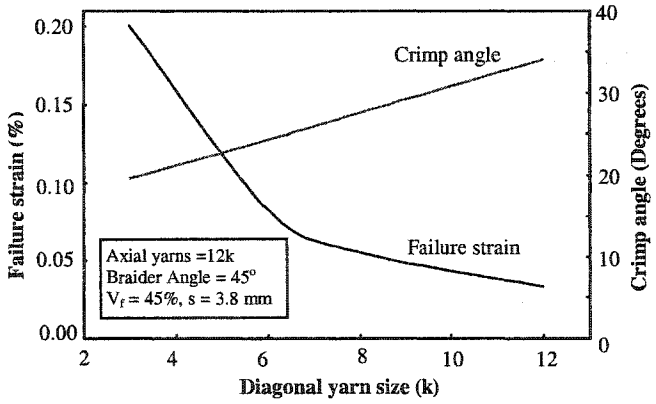

(a) Carbon #1

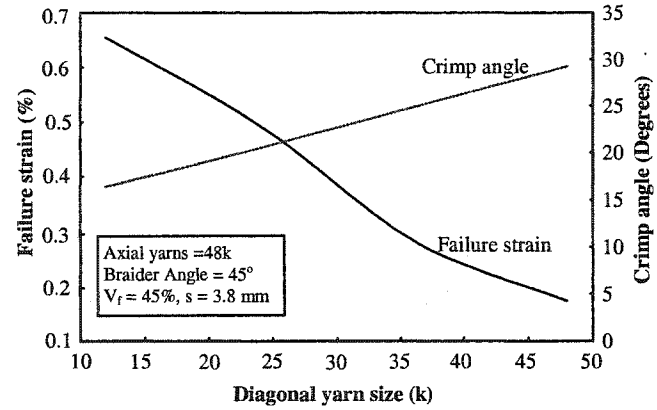

(b) Carbon #3

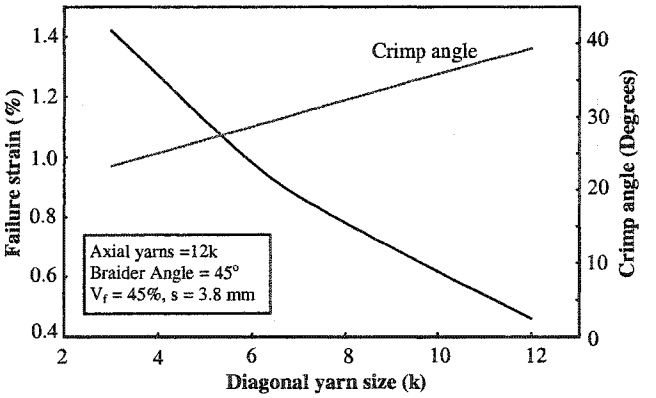

(c) Glass

Fig. 3.7 Effect of diagonal yarn size on diagonal loading failure strain and crimp angle

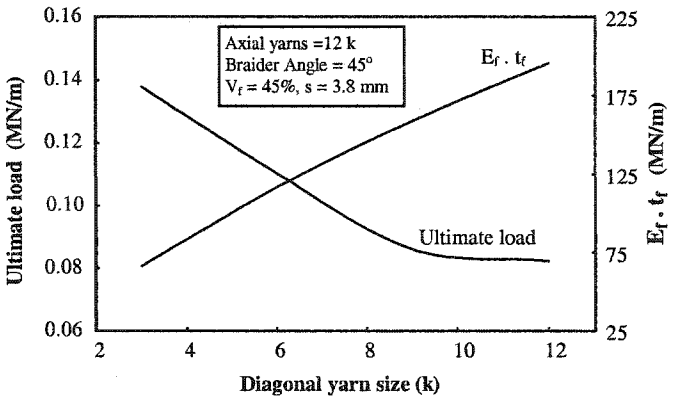

(a) Carbon #1

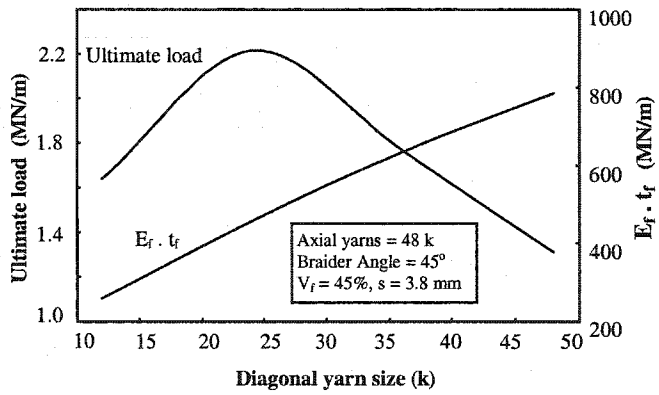

(b) Carbon #3

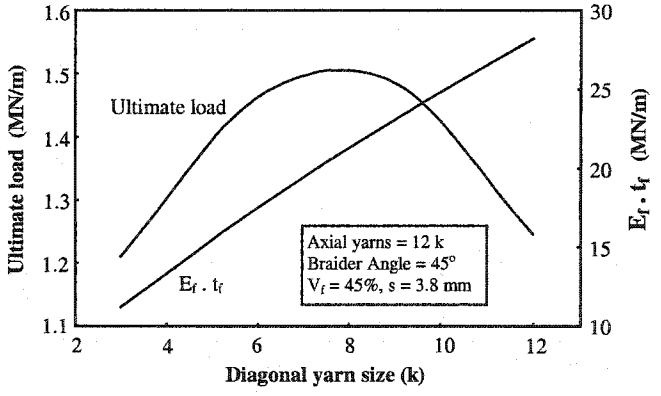

(c) Glass

Fig. 3.8 Effect of diagonal yarn size on diagonal ultimate load and rigidity

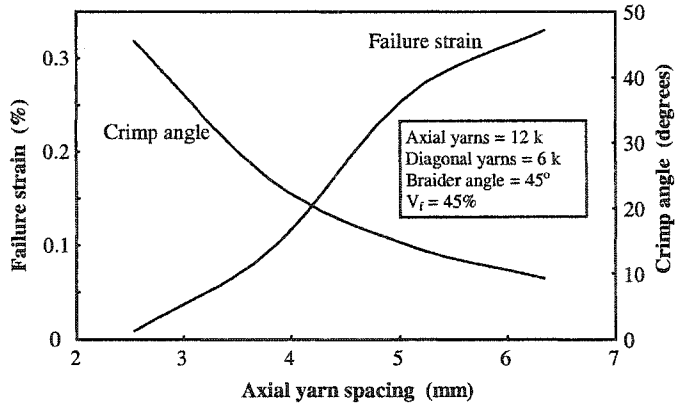

(a) Carbon #1

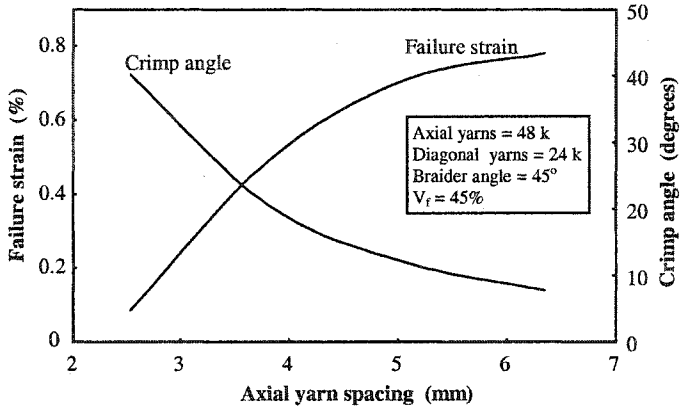

(b) Carbon #3

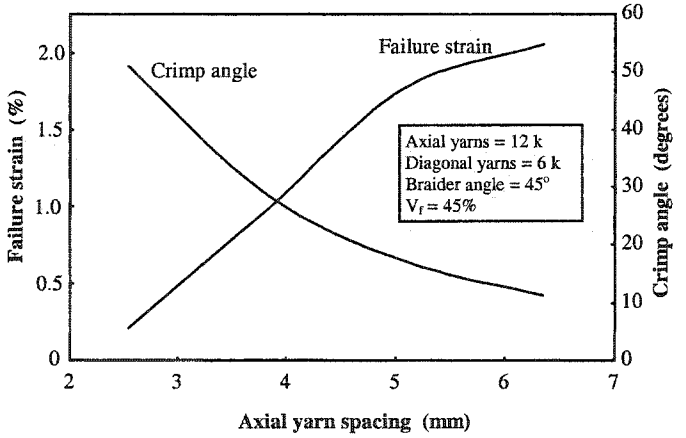

(c) Glass

Fig. 3.9 Effect of axial yarn spacing on diagonal loading failure strain and crimp angle

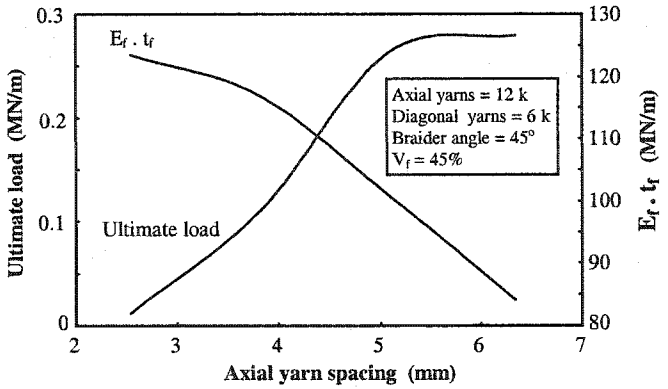

(a) Carbon #1

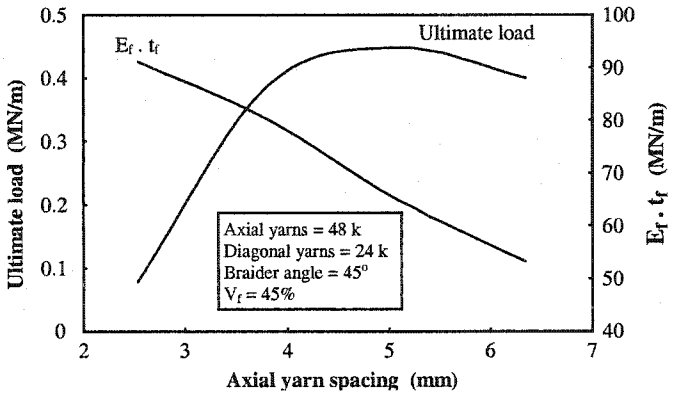

(b) Carbon #3

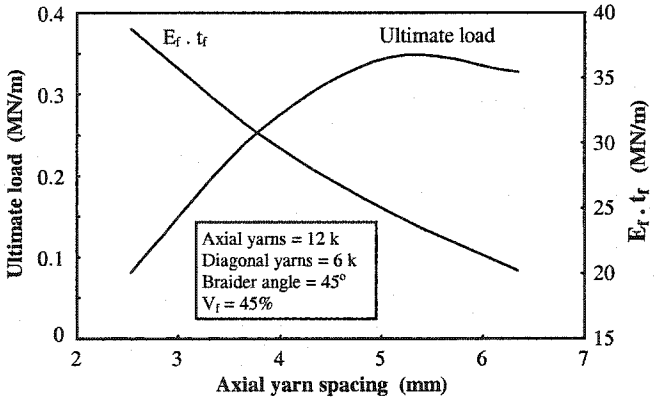

(c) Glass

Fig. 3.10 Effect of axial yarn spacing on diagonal ultimate load and rigidity

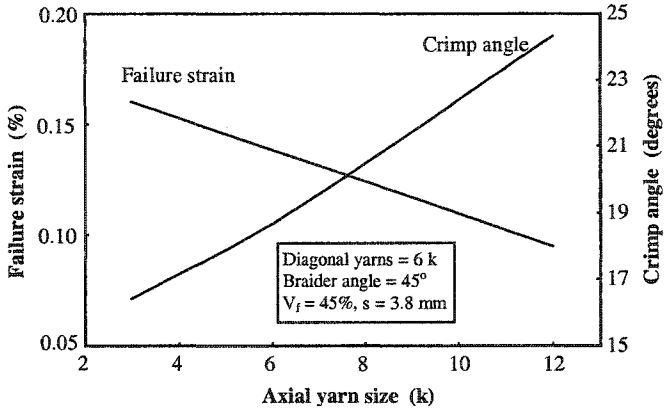

(a) Carbon #1

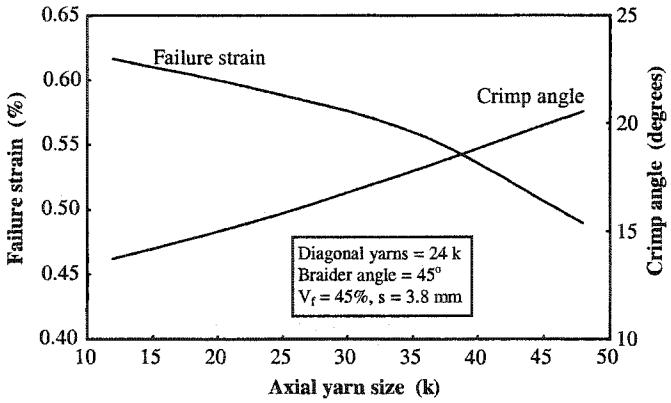

(b) Carbon #3

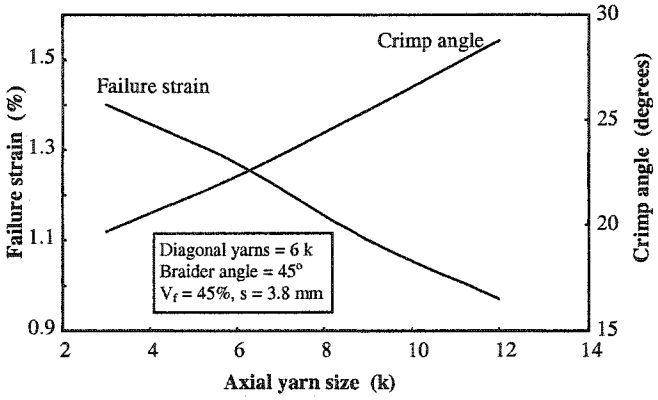

(c) Glass

Fig. 3.11 Effect of axial yarn size on diagonal loading failure strain and crimp angle

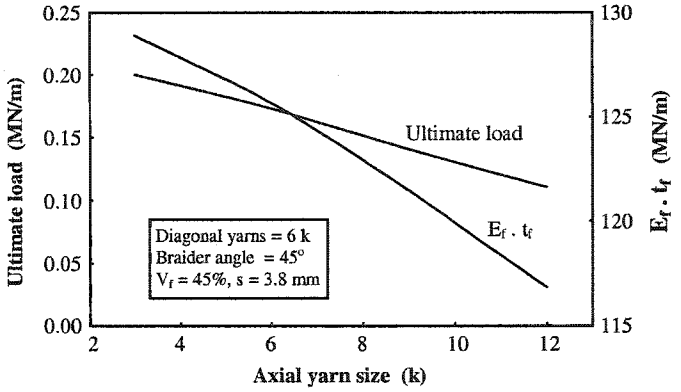

(a) Carbon #1

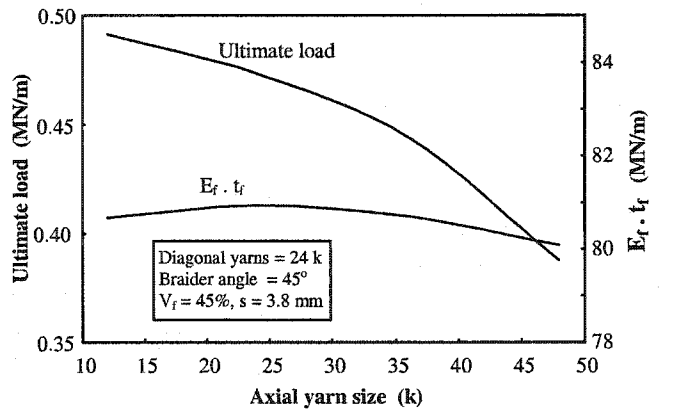

(b) Carbon #3

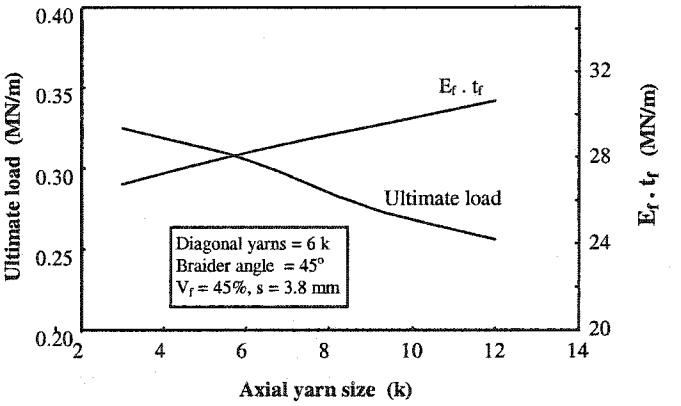

(c) Glass

Fig. 3.12 Effect of axial yarn spacing on diagonal ultimate load and rigidity

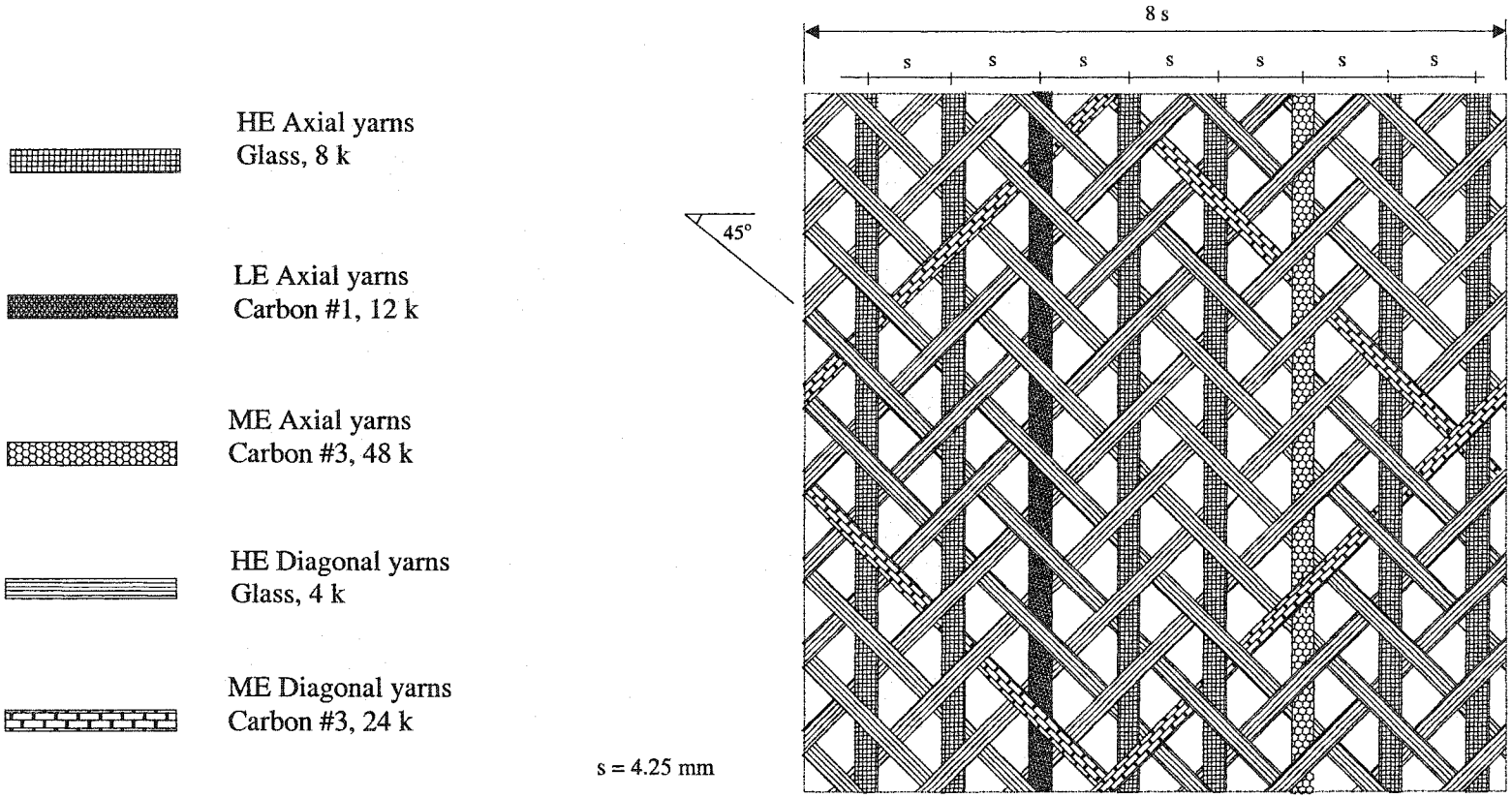

Fig. 3.13 Details of triaxial fabric geometry

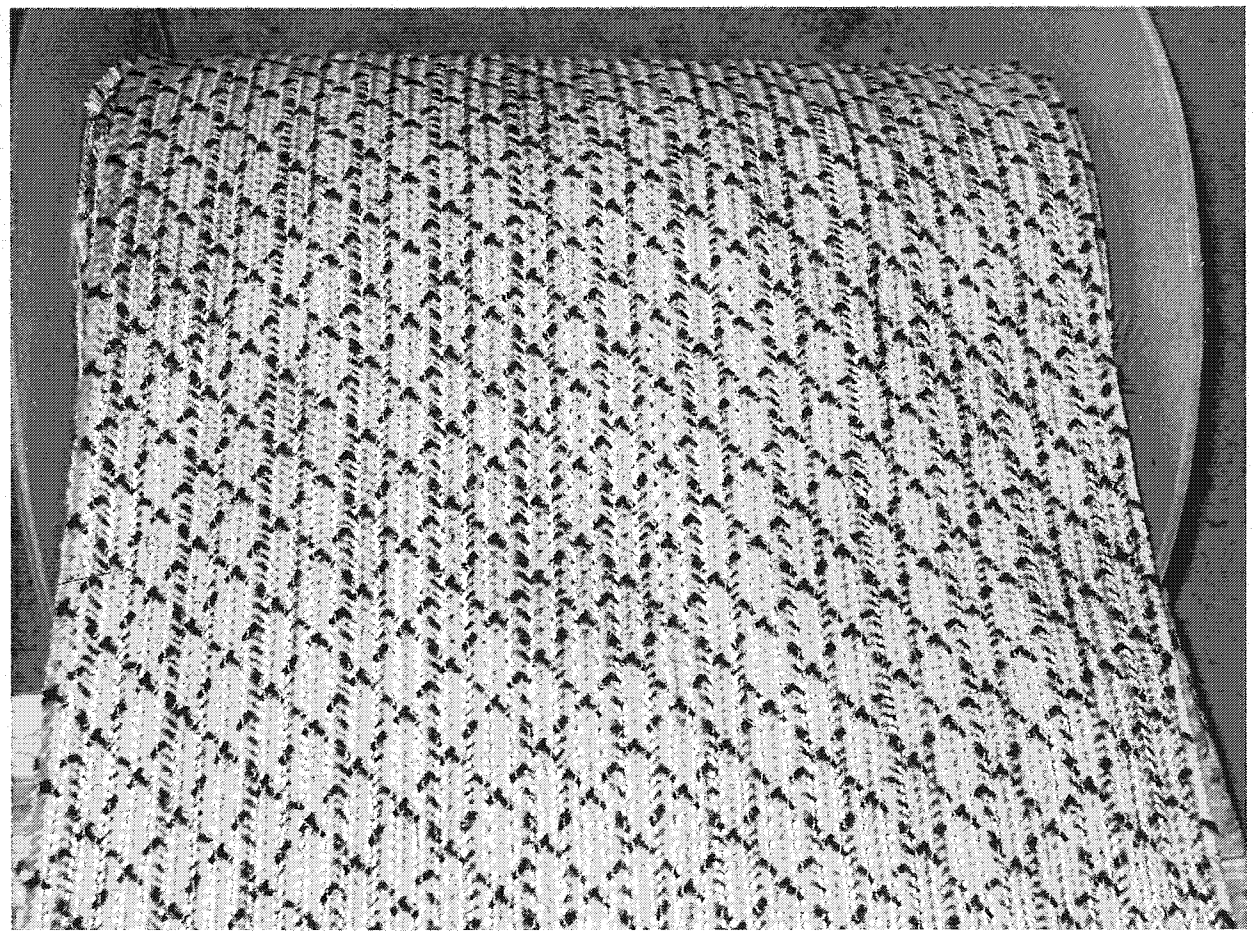

Fig. 3.14 Photo of the triaxial fabric

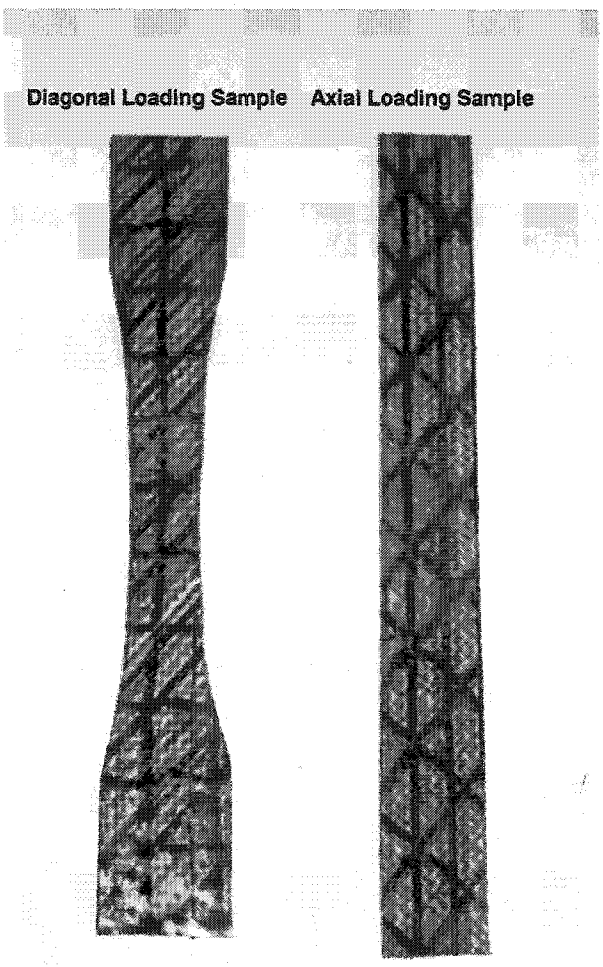

Fig. 3.15 Photo of test coupons

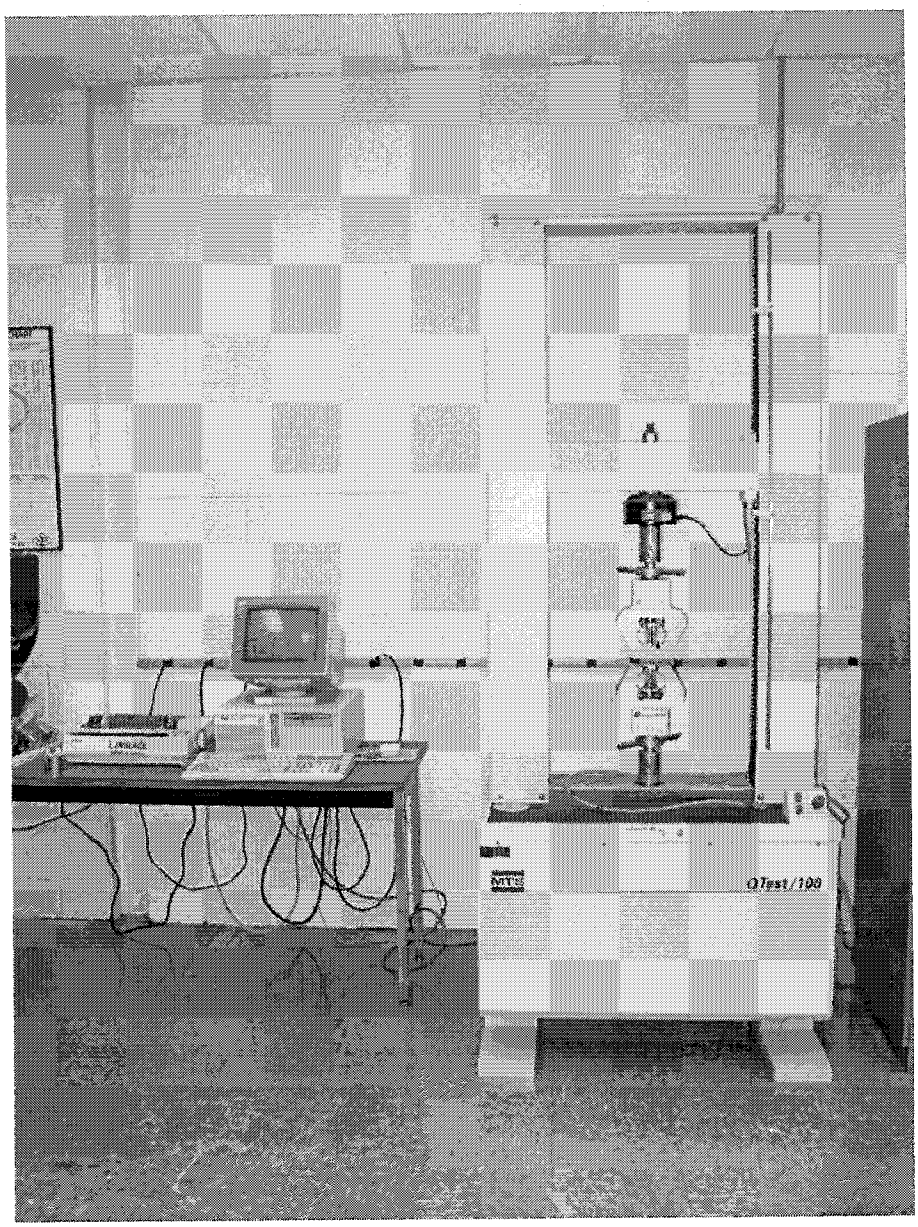

Fig. 3.16 Tensile testing machine

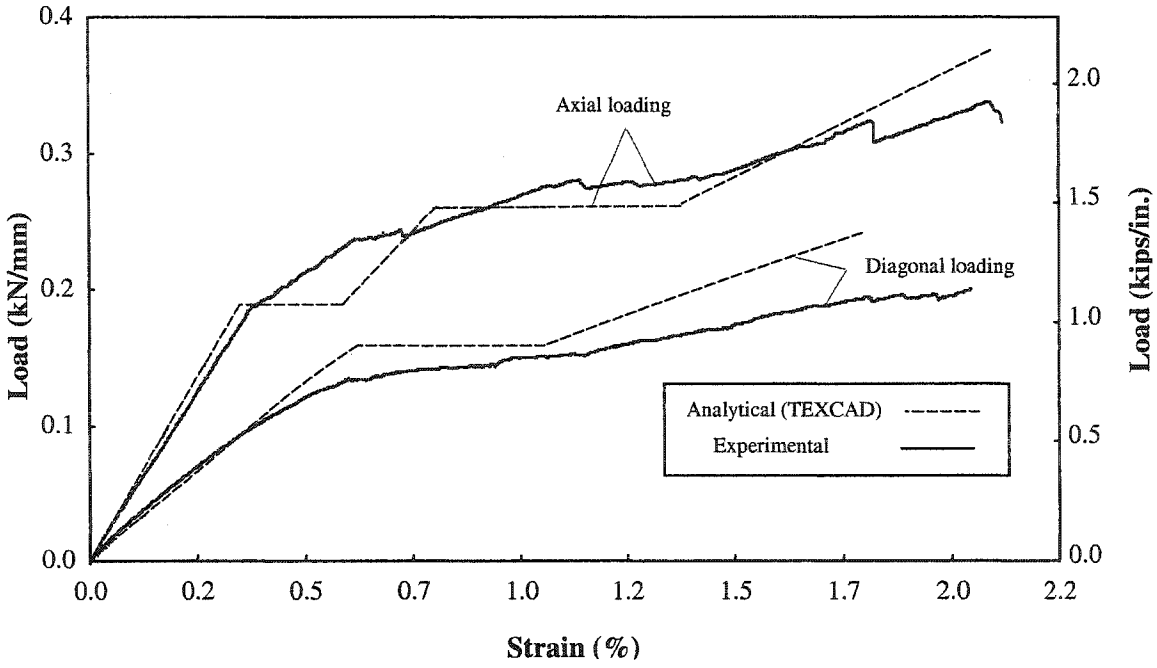

Fig. 3.17 Experimental and analytical tensile behavior of triaxially braided fabric

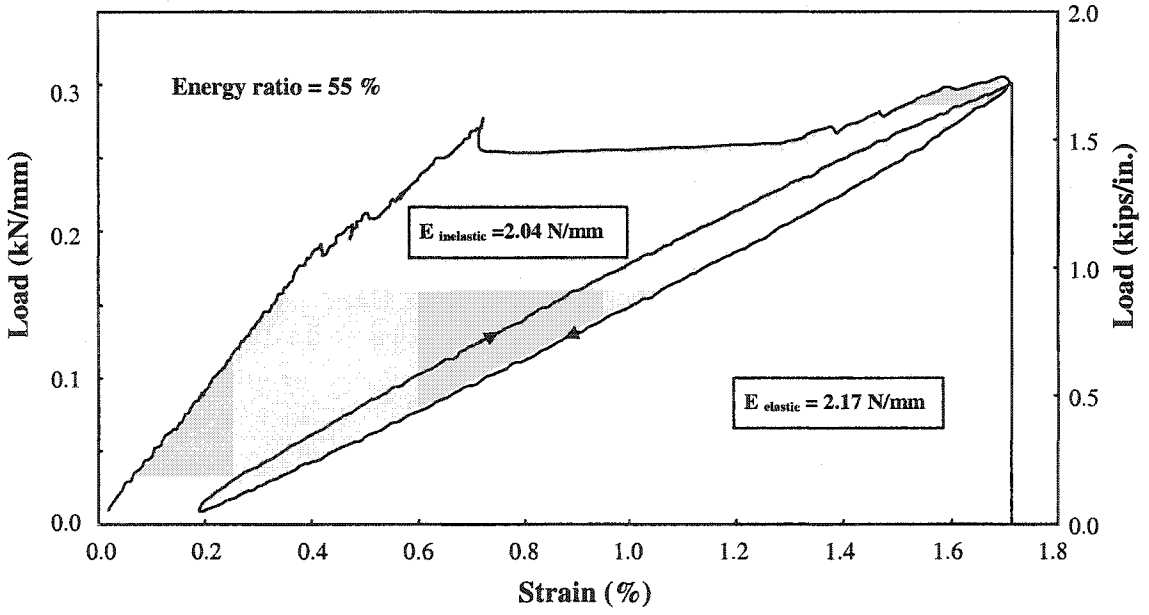

Fig. 3.18 Typical energy absorption of triaxial braided fabric in axial direction

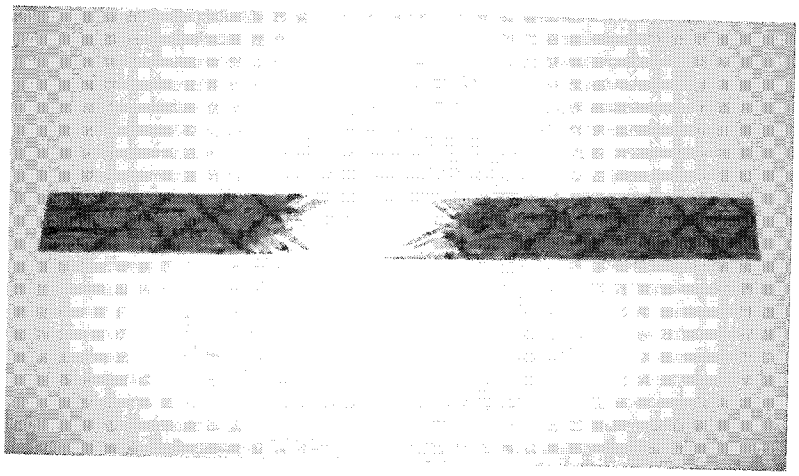

(a) Axial loading sample

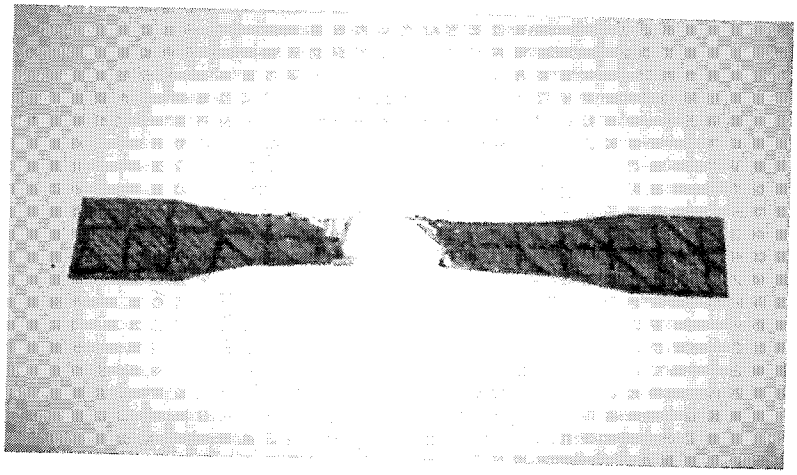

(b) Diagonal loading sample

Fig. 3.19 Failure of test samples

CHAPTER 4

FLEXURAL STRENGTHENING OF REINFORCED CONCRETE BEAMS USING THE DEVELOPED UNIAXIAL FABRIC

4.1 General

This chapter reports an experimental investigation to study the effectiveness and ductility of the developed uniaxial fabric for flexural strengthening of reinforced concrete beams. The developed uniaxial fabric was used to strengthen reinforced concrete simple beams in flexure. Similar beams were strengthened using some commercially available carbon fiber sheets, fabrics, and plates in order to compare their behavior with those strengthened with the developed fabric. The beams were loaded until failure and their responses were examined for deflections, strains, failure modes, and ductility.

4.2 Test Beams

Thirteen reinforced concrete beams with cross sectional dimensions of 152 mm × 254 mm (6 in. × 10 in.) and lengths of 2740 mm (108 in.) were cast. The flexure reinforcement of the beams consisted of two #5 (16 mm) tension bars near the bottom and two #3 (9.5 mm) compression bars near the top. To avoid shear failure, the beams were over-reinforced for shear with #3 (9.5 mm) closed stirrups spaced at 102 mm (4.0 in.). Five beams were formed with rounded corners of 25 mm (1 in.) radius, in order facilitate the installation of the strengthening material on their sides and bottom faces without stress concentrations. Fig. 4.1 shows the beam dimensions, reinforcement details, support locations, and location of loading points. The steel used was Grade 60 with a yield strength of 415 MPa (60,000 psi) while the concrete compressive strength at the time of testing the beams was 55.2 MPa (8,000 psi).

4.3 Strengthening Materials

The developed hybrid fabric was used to strengthen eight beams. Two different thicknesses of fabric were used. The first (H-system, t=1.0 mm) had a thickness of 1.0 mm (0.04 in.) and the second (H-system, t=1.5 mm) had a thickness of 1.5 mm (0.06 in.). Four other beams were strengthened with three currently available carbon fiber strengthening materials: (i) a uniaxial carbon fiber sheet with an ultimate load of 0.34 kN/mm (1.95 kips/in.), (ii) two layers of a uniaxial carbon fiber fabric with an ultimate load of 1.31 kN/mm (7.5 kips/in.) for the two layers combined, and (iii) a pultruded carbon fiber plate with an ultimate load of 2.8 kN/mm (16 kips/in.). The tested load-strain diagrams for all these materials are shown in Fig. 4.2. Table 4.1 shows the properties of the strengthening materials, including the developed fabric.

4.4 Adhesives

For the hybrid fabric, an epoxy resin (epoxy A) was used to impregnate the fibers and as an adhesive between the fabric and the concrete surface. This epoxy has an ultimate strain of 4.4%, to insure that it will not fail before the failure of the fibers. For the beams strengthened with carbon fiber sheet, plate, and fabric, an epoxy resin with an ultimate strain of 2.0% was used (epoxy B). The mechanical properties of the adhesives provided by their manufactures are shown in Table 4.2.

4.5 Strengthening

The beam bottom faces and sides were sandblasted to roughen the surface. The beams were then cleaned with acetone to remove dirt. Two strengthening configurations were used: (i) strengthening material on the bottom face of the beam only (beam group A) and (ii) strengthening material on the bottom face and extended up 152 mm (6 in.) on

both sides to cover approximately all the flexural tension portions of the beam (beam group B). The strengthening was installed for 2.24 m (88 in.) centered along the length of the beam (see Fig. 4.3). The epoxy was allowed to cure for at least two weeks before the beams were tested. For the beams strengthened with the developed hybrid fabric (H-system), two beams were fabricated and tested for each configuration to verify the results. Table 4.3 summarizes the test beams.

4.6 Instrumentation

The FRP strain at mid-span was measured by three strain gages located at the bottom face of the beam. The steel tensile strain was measured by monitoring the strain on the side surface of the beam at rebar level using a DEMEC (detachable mechanical gage) with gage points for beam group A, while strain gages were used for beam group B. The mid-span deflection was measured using a string potentiometer. The beams were loaded using a hydraulic actuator. The load was measured by means of a load cell. All the sensors were connected to a data acquisition system to scan and record the readings (see Fig. 4.4 and Fig. 4.5).

4.7 Test Results and Discussion

4.7.1 Control beam

The control beam had a yield load of 82.3 kN (18.5 kips) and an ultimate load of 95.7 kN (21.5 kips). The beam failed by the yielding of steel followed by compression failure of concrete at the mid-span. Test results for the control beam are shown in the figures of the test results of the strengthened beams (Fig. 4.6 through 4.10).

4.7.2 Beam group A

Beam group A contains the beams strengthened at the bottom face only. Figs. 4.6 to 4.10 show the test results for these beams. The results of beams H-50-1 and H-75-1 were very close to those of H-50-2 and H-75-2 respectively and hence, the discussions concerning these beams are focused on the last two to avoid repetition. The ductility of each beam is indicated by calculating the ductility index (the ratio between the deflection of the beam at failure and its deflection at yield).

4.7.2.1 Beam C-1

Fig. 4.6(a) shows the load versus mid-span deflection diagram for beam C-1 in which the carbon fiber sheet was used for strengthening. The beam yielded at a load of 85.9 kN (19.3 kips) and failed at a load of 101.9 kN (22.9 kips), due to rupture of the carbon fiber sheet. It is noticed from this figure that although ductile behavior is experienced, only a 4% increase in the yield load compared to that of the control beam was achieved. A ductility index of 2.15 was experienced. Fig. 4.6(b) shows the load versus carbon fiber strain at mid-span.

4.7.2.2 Beam C-2

Fig. 4.7(a) shows the load-deflection response for beam C-2. This beam was strengthened using the pultruded carbon fiber plate. The beam showed no yielding plateau (1.0 ductility index) and had a sudden failure at 132.6 kN (29.8 kips), due to shear-tension failure at the end of the plate. Although an increase in load of 61% was obtained, the failure was brittle. Fig 4.7(b) shows the load versus carbon fiber strain at mid span. The maximum recorded strain of carbon fiber plate at failure was 0.33%, which indicates that 24% of the capacity of the plate was utilized.

4.7.2.3 Beam C-3

The load deflection response of beam C-3 is shown in Fig. 4.8(a). Beam C-3 was strengthened by two layers of the carbon fiber fabric. The beam yielded at a load of 107.7 kN (24.2 kips) and failed by fabric debonding at a load of 134.4 kN (30.2 kips), before showing any significant yielding plateau similar to that of the control beam. A ductility index of 1.64 was experienced. It is noted from Fig. 4.8(b) that the maximum recorded carbon fiber strain at failure was 0.67%, which indicates that about 48 % of the fabric capacity was utilized.

4.7.2.4 Beam H-50-2

Fig. 4.9(a) shows the load deflection response of beam H-50-2. This beam was strengthened with 1 mm thick hybrid fabric developed. A yield load of 97.9 kN (22.0 kips) was experienced (a 19% increase in yield load over that of the control beam). It is noted from Fig. 4.9(b) that the fabric had a strain of 0.40% when the beam yielded. The beam experienced a ductility index of 2.33 and failed by total rupture of the fabric at an ultimate load of 114.8 kN (25.8 kips). Fig. 4.11 shows the beam at failure.

4.7.2.5 Beam H-75-2

Fig. 4.10(a) shows the load deflection response for beam H-75-2. The beam was strengthened with 1.5 mm thick hybrid fabric developed. The beam yielded at a load of 113.9 kN (25.6 kips) and exhibited a ductility index of 2.13 before total failure occurred by debonding of the fabric at an ultimate load of 130.8 kN (29.4 kips). It is noticed that although final failure was by debonding of the fabric, it happened after achieving a

reasonable ductility. Fig. 4.10(b) shows that fabric had a strain of 0.35% when the beam yielded. Fig. 4.12 shows the beam at failure.

4.7.2.6 Comparison

Fig. 4.13 and Table 4.4 compare the results from beam group A. The following are observed:

1- Beams C1 and H-50-2 exhibited relatively good ductile behavior. However, beam H-50-2 showed a higher yield load than beam C-1. This is because the developed hybrid fabric was designed so that it has a higher initial stiffness than the carbon fiber sheet; hence, it contributed to strengthening more effectively than the carbon fiber sheet before the yielding of steel.

2- Although the carbon fiber fabric has an ultimate load several times greater than the "yield- equivalent" load of the 1.5 mm thick hybrid fabric, beam H-75-2 showed a similar behavior to beam C-3 up to its yield. However, beam H-75-2 exhibited a reasonable yielding plateau, and beam C-3 did not.

3- Relative to current carbon fiber strengthening materials, the developed fabric has a "yield-equivalent" strain that is close to the yield strain of steel. Although it is still higher, hybrid fabric strain values were close to its yield value when the beam yielded, which indicated that it yielded simultaneously with the steel. This is attributed in part to the fabric being installed on the outer surface of the beam, which undergoes more tensile strain than inner steel. As a result, the designed yield strain value of the fabric seems to be acceptable.

4- While the use of a carbon fiber plate of a high load capacity (like the one used in beam C-2) provided a high failure load, it also produced a brittle failure.

4.7.3 Beam group B

The beams in this group were strengthened at the bottom face and also up 152 mm (6 in.) on both sides. The results of this group are shown in Table 4.4 and Figs. 4.14 to 4.18. The results of beams H-S50-1 and H-S75-1 were very close to those of H-S50-2 and H-S75-2 respectively and hence, the discussions concerning these beams are focused on the last two to avoid repetition.

4.7.3.1 Beam CS

Fig. 4.14(a) shows the load versus deflection response of beam CS. This beam was strengthened using the carbon fiber sheet system. The beam yielded at a load of 99.2 kN (22.3 kips), due to the yielding of the steel. The increase in yield load was 20%. The beam finally failed at an ultimate load of 123.3 kN (27.7 kips), due to compression failure of concrete at mid-span. Fig. 4.14(b) shows that the carbon fibers had a strain of 0.35% when the beam yielded, and hence contributed approximately 30% of its capacity at this stage of loading. The maximum recorded strain before beam failure was 1.0%. A ductility index of 2.04 was attained.

4.7.3.2 Beam H-S50-2

The results of beam H-S50-2 are shown in Fig. 4.15. This beam was strengthened by 1 mm thick hybrid fabric developed. Fig. 4.15(a) shows the load versus deflection curve of the beam. The beam yielded at a load of 113.9 kN (25.6 kips) due to the yielding of both the steel and the fabric. The increase in yield load gained was 38%. The beam failed at an ultimate load of 146.4 kN (32.9 kips), due to compression failure of concrete. A ductility index of 2.25 was experienced. Fig. 4.15(b) shows the load versus the fabric strain at mid-span. The recorded strain when the beam yielded was 0.35% and the

maximum recorded strain before beam failure was 1.2%. The beam at failure is shown in Fig. 4.17.

4.7.3.3 Beam H-S75-2

Fig. 4.16 shows the results of beam H-S75-2. This beam was also strengthened by the developed hybrid fabric but with 1.5 mm thickness. Fig. 4.16(a) shows that the beam yielded at a load of 127.3 kN (28.6 kips) with an increase in yield load of 55%, due to yielding of both the steel and the fabric. The beam finally failed at an ultimate load of 162.0 kN (36.4 kips) by compression failure of concrete at mid-span. The beam exhibited a ductility index of 1.89. Fig. 4.16(b) shows the load versus the fabric strain at mid-span. The maximum recorded strain before beam failure is 0.74%. The beam at failure is shown in Fig. 4.18.

4.7.3.4 Comparison

Fig. 4.19 shows a comparison between the results of beams of group B. The following are the observations from their test results;

1- Beam H-S50-2 showed a higher yield load than beam CS, although the hybrid fabric has a lower "yield-equivalent" load than the ultimate load of the carbon fiber sheet. This is because the hybrid sheet has a higher initial stiffness than that of the carbon fiber sheet.

2- The beams strengthened with the developed hybrid fabric showed high yield loads with reasonable yielding plateaus.

One of the advantages of the developed hybrid fabric is that it is easy to determine by visual inspection whether the fabric yielded or not, since any failed carbon fiber yarns

can be seen. Also, the hybrid fabric is less expensive than currently available carbon fiber materials as more than 75% of the fibers used are glass fibers that are less costly than carbon fibers.

4.8 Conclusions

Based on the research investigation presented in this chapter, the following can be concluded:

1- Currently available FRP materials used as flexural strengthening systems for concrete structures do not always provide yielding plateaus in the strengthened beams similar to those for unstrengthened beams. In some applications, the strengthening may result in a brittle failure and/or an insignificant increase in the yield load of the strengthened beam.

2- The hybridization of selected types of fibers is utilized to develop a pseudo-ductile fabric, which has a low strain value at yield (0.35%). The fabric is designed so that it has the potential to yield simultaneously with the reinforcing steel of the strengthened beam.

3- The beams strengthened using the developed hybrid fabric generally showed a higher increase in yield load than those strengthened with the carbon fiber strengthening systems. Some of the beams strengthened with the hybrid fabric showed a yield plateau similar to that of the unstrengthened beam. This is critically important to ensure adequate warning before structural failure.

4- The beams strengthened with the developed hybrid fabric system showed no significant loss in beam ductility. The beams strengthened with carbon fiber sheet showed also no significant loss in ductility but with relatively less yield loads.

Table 4.1 Properties of the Strengthening Materials

Type	Yield-Equivalent Load kN/mm (kips/in.)	Yield-equivalent Strain (%)	Ultimate Load kN/mm (kips/in.)	Ultimate Strain (%)	Thickness mm (in.)
Carbon Fiber Sheet**	-	-	0.34 (1.95)	1.2	0.13 (0.005)
Carbon Fiber Plate**	-	-	2.8 (16.0)	1.4	1.3 (0.05)
Carbon Fiber Fabric **	-	-	1.31 (7.50)	1.4	1.90 (0.075)
H-System† (t=1mm)	0.23 (1.30)	0.35	0.39 (2.24)	1.74	1.0 (0.04)
H-System† (t=1.5mm)	0.34 (1.95)	0.35	0.59 (3.36)	1.74	1.5 (0.06)

**Commercially available
† Developed ductile hybrid system

Table 4.2 Properties of Epoxy Adhesives

Epoxy Type	Tensile Strength MPa (ksi)	Ultimate Strain (%)	Compressive Strength MPa (ksi)
A	66.3 (9.62)	4.4	109.2 (15.84)
B	68.9 (10.0)	2.0	86.2 (12.50)

Table 4.3 Summary of Test Beams

Beam Group	Beam Designation	Strengthening Material
N/A	Control	N/A
Group A	C-1	Carbon Fiber Sheet
	C-2	Carbon Fiber Plate
	C-3	Carbon Fiber Fabric
	H-50-1	H- System (t = 1 mm)
	H-50-2	
	H-75-1	H- System (t = 1.5 mm)
	H-75-2	
Group B	CS	Carbon Fiber Sheet
	H-S50-1	H- System (t = 1 mm)
	H-S50-2	
	H-S75-1	H- System (t = 1.5 mm)
	H-S75-2	

Table 4.4 Summary of Test Results

Beam Designation (1)	Strengthening System (2)	Yield Load kN (kips) (3)	Deflection at Yield mm (in.) (4)	Failure Load kN (kips) (5)	Deflection at Failure mm (in.) (6)	Ductility Index (7) = Col. 6 / Col. 4	FRP Strain at Failure (%) (8)	Type of Final Failure (9)
Control	N/A	82.3 (18.5)	14.0 (0.55)	95.7 (21.5)	49.5 (1.95)	3.55	N/A	Steel yield followed by concrete failure
C-1	Carbon Fiber Sheet	85.9 (19.3)	13.2 (0.52)	101.9 (22.9)	28.4 (1.12)	2.15	1.10	Steel yield followed by FRP rupture
C-2	Carbon Fiber Plate	-	-	132.6 (29.8)	16.0 (0.63)	1.00	0.33	Shear tension failure
C-3	Carbon Fiber Fabric	107.7 (24.2)	13.5 (0.53)	134.4 (30.2)	22.1 (0.87)	1.64	0.67	Steel yield followed by FRP debonding
H-50-2	H- System (t=1.0 mm)	97.9 (22.0)	15.2 (0.6)	114.8 (25.8)	35.6 (1.40)	2.33	1.55	Steel & FRP yield followed by FRP rupture
H-75-2	H- System (t=1.5 mm)	113.9 (25.6)	13.7 (0.54)	130.8 (29.4)	29.2 (1.15)	2.13	0.74	Steel & FRP yield followed by FRP debonding
CS	Carbon Fiber Sheet	99.2 (22.3)	14.2 (0.56)	123.3 (27.7)	29.0 (1.14)	2.04	1.00	Steel yield followed by concrete failure
H-S50-2	H- System (t=1.0 mm)	113.9 (25.6)	14.2 (0.56)	146.4 (32.9)	32.0 (1.26)	2.25	1.20	Steel & FRP yield followed by concrete failure
H-S75-2	H- System (1.5 mm)	127.3 (28.6)	15.8 (0.62)	162.0 (36.4)	29.7 (1.17)	1.89	0.74	Steel & FRP yield followed by concrete failure

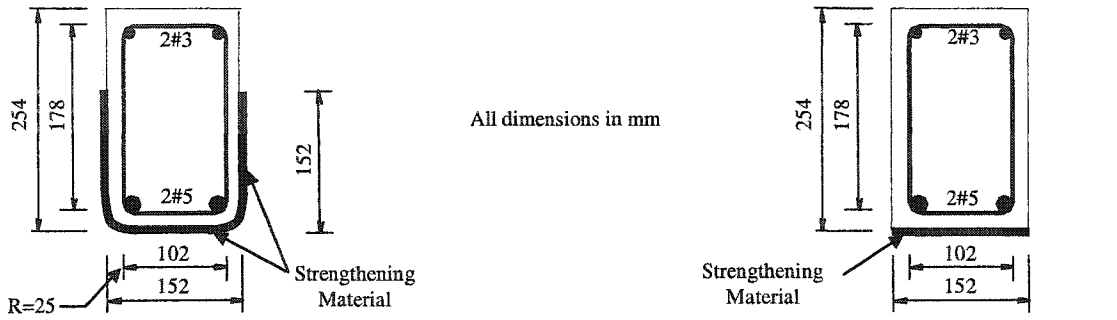

(a) Cross Section for Group B

(b) Cross Section for Group A

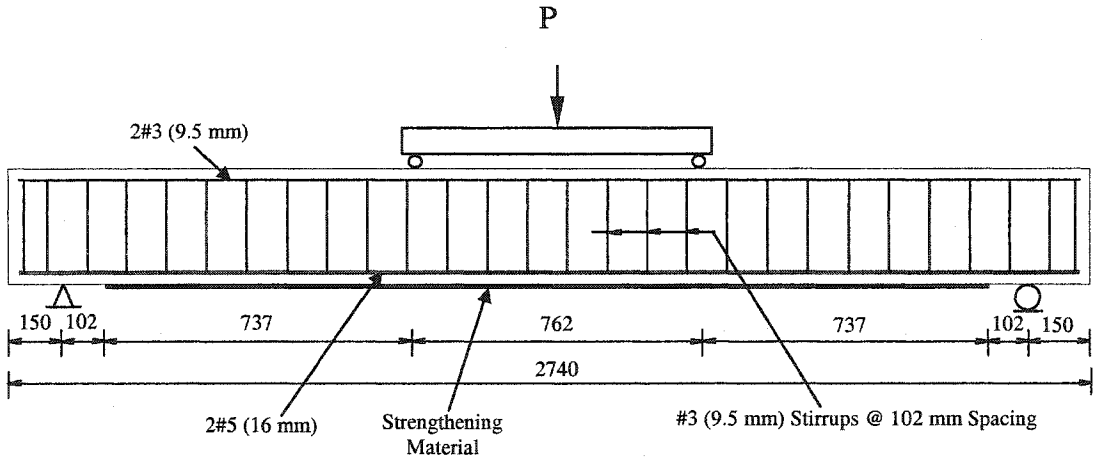

(c) Loading Set-up

Fig. 4.1 Details of test beams

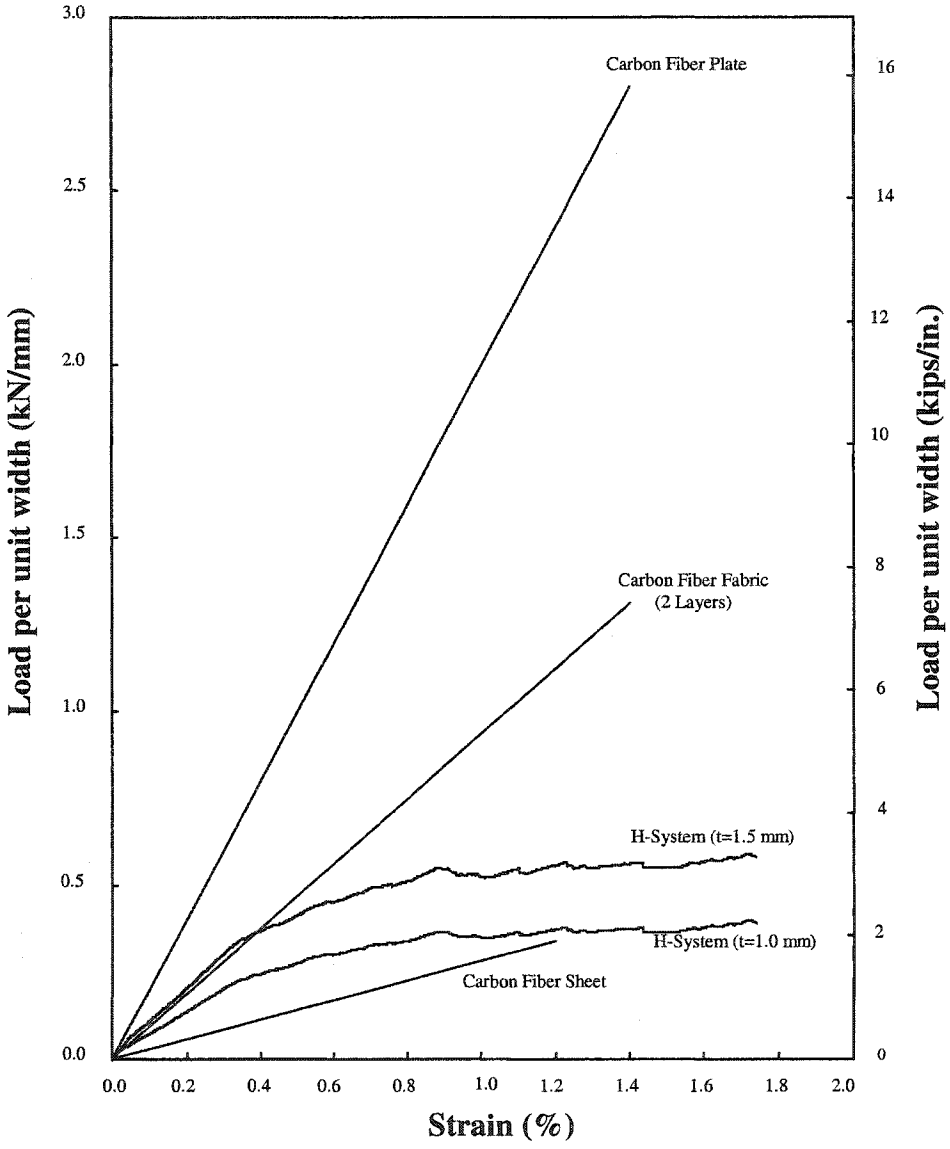

Fig. 4.2 Comparison between carbon fiber plate, fabric, sheet, and the developed uniaxial fabric (H-System)

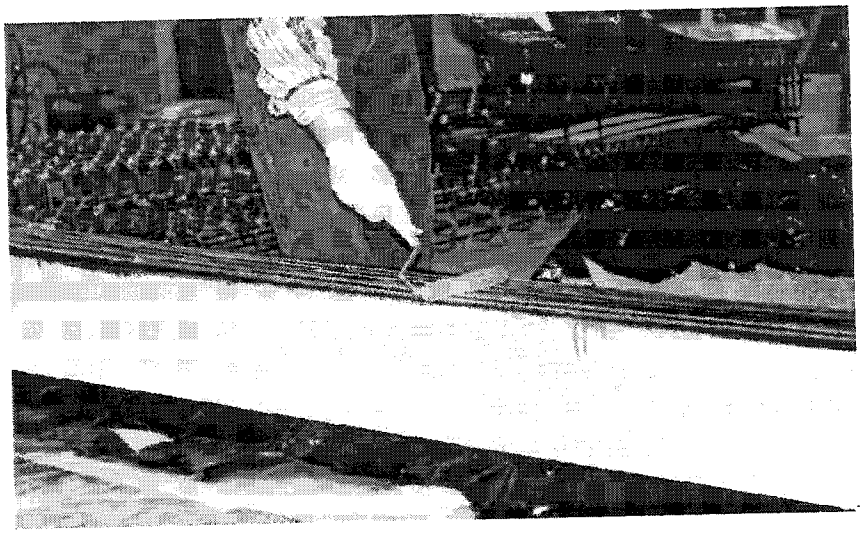

Fig. 4.3 Fabric installation

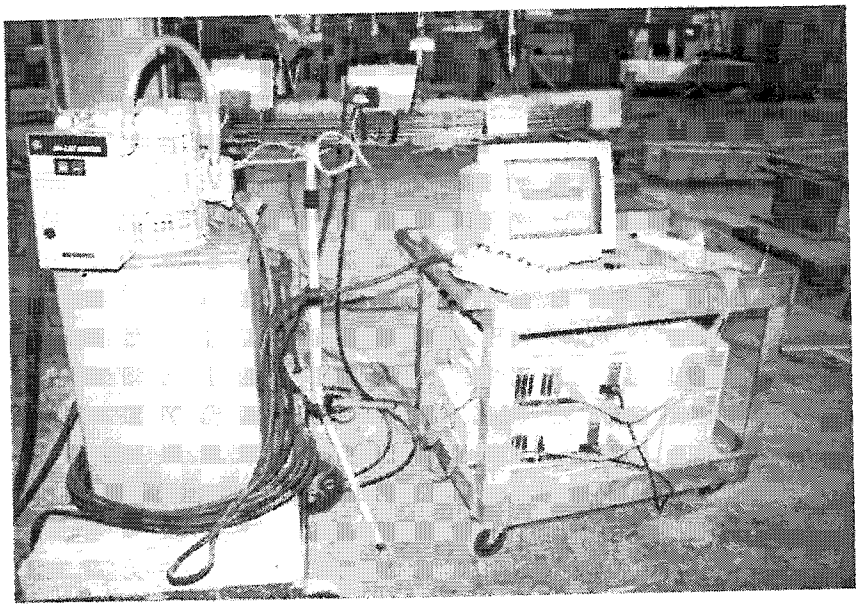

Fig. 4.4 Data acquisition system and hydraulic pump

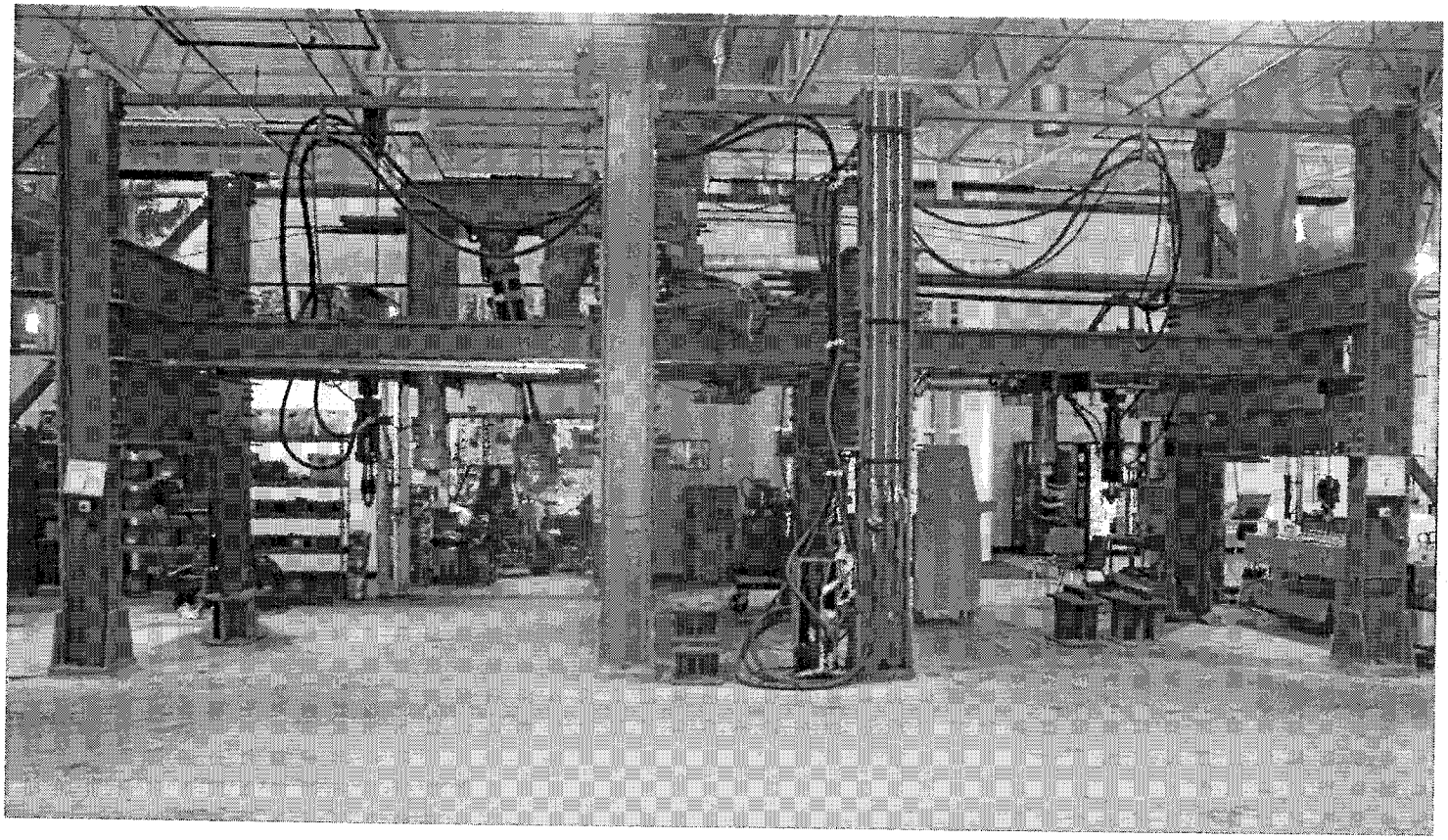

Fig. 4.5 Testing frame

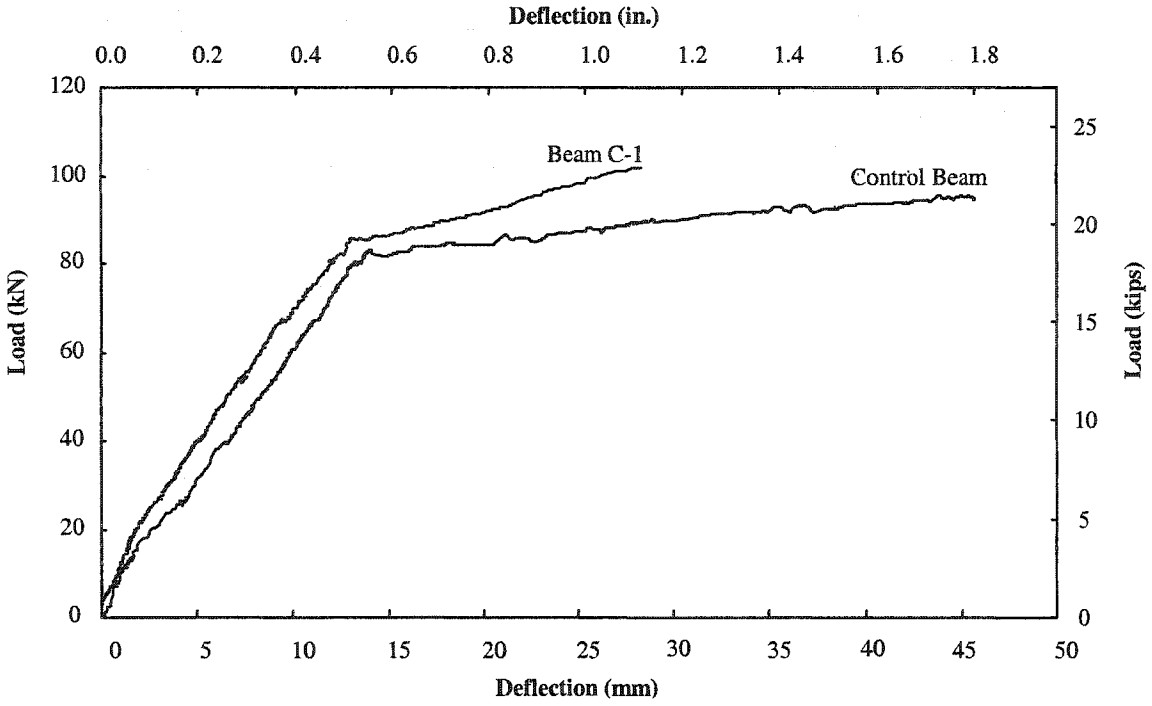

(a) Mid-Span Deflection

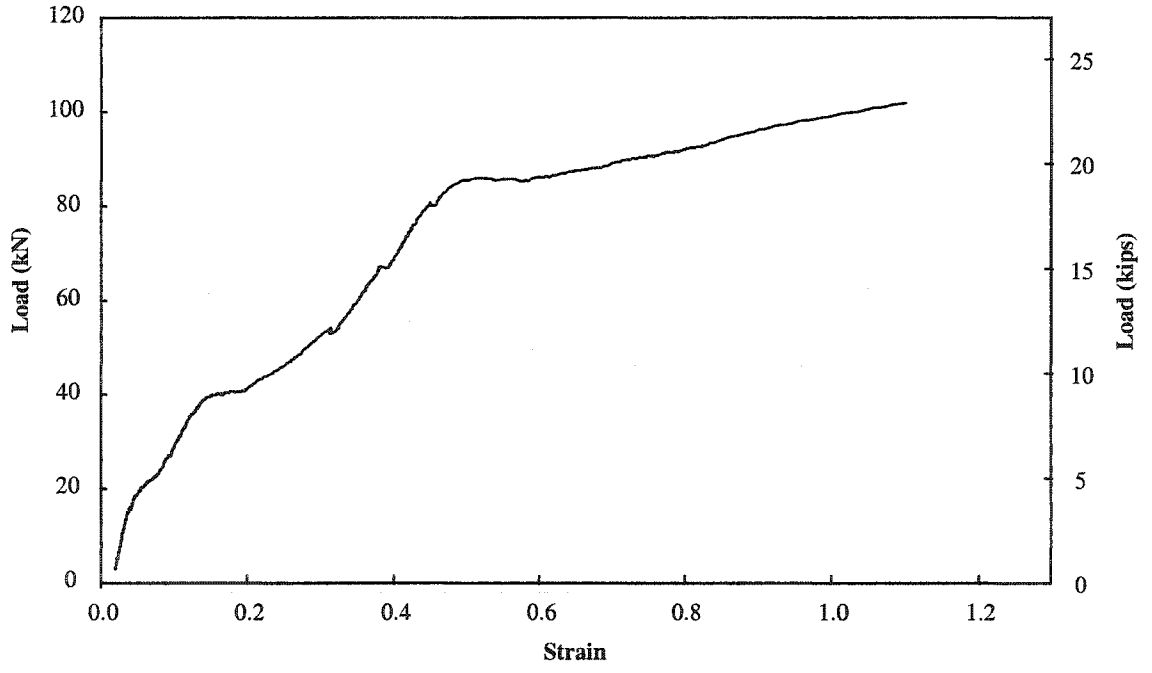

(b) FRP Strain at Mid-Span

Fig. 4.6 Behavior of beam C-1

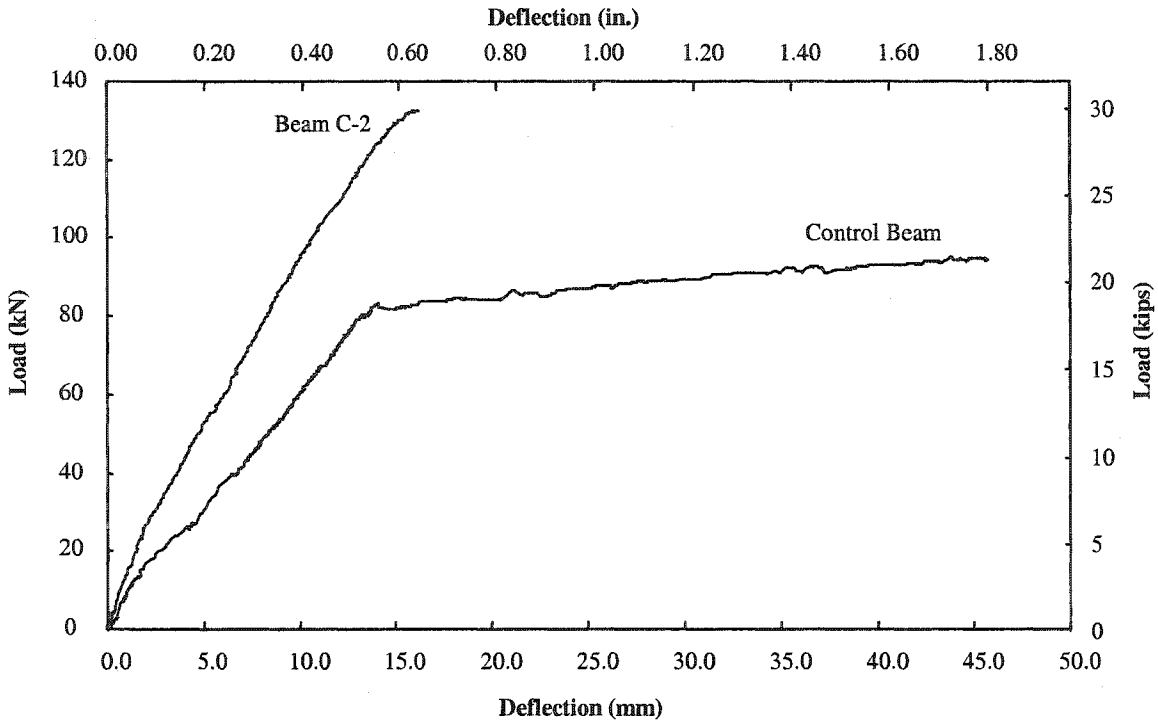

(a) Mid-Span Deflection

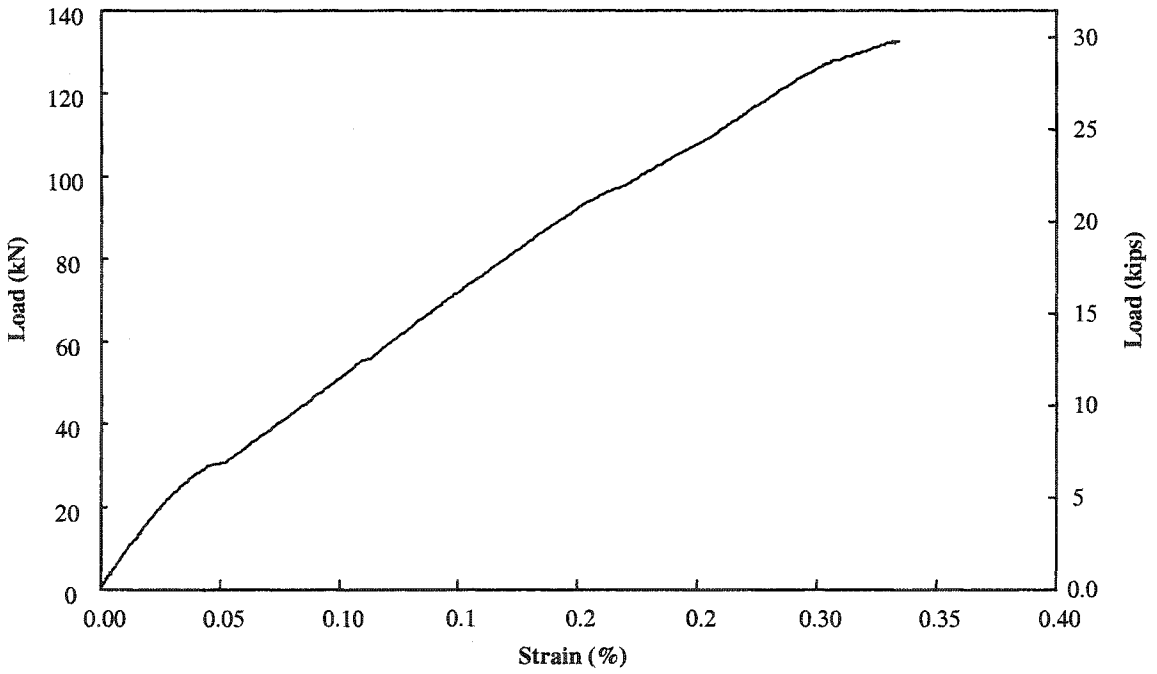

(b) FRP Strain at Mid-Span

Fig. 4.7 Behavior of beam C-2

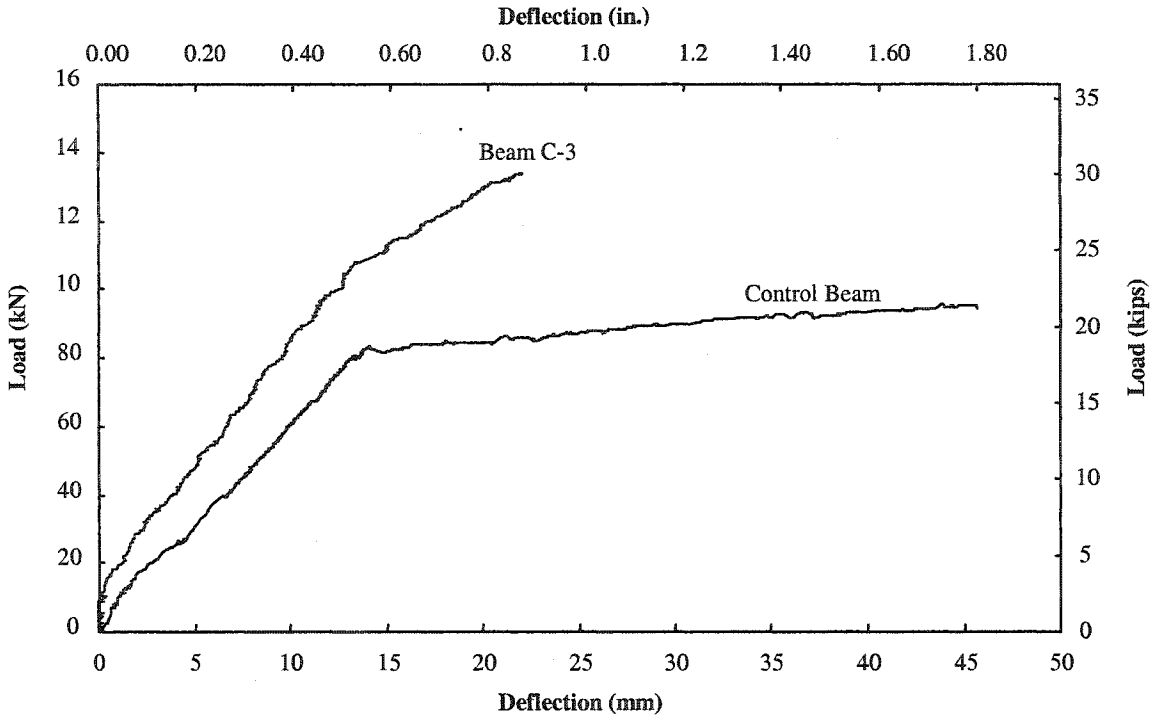

(a) Mid-Span Deflection

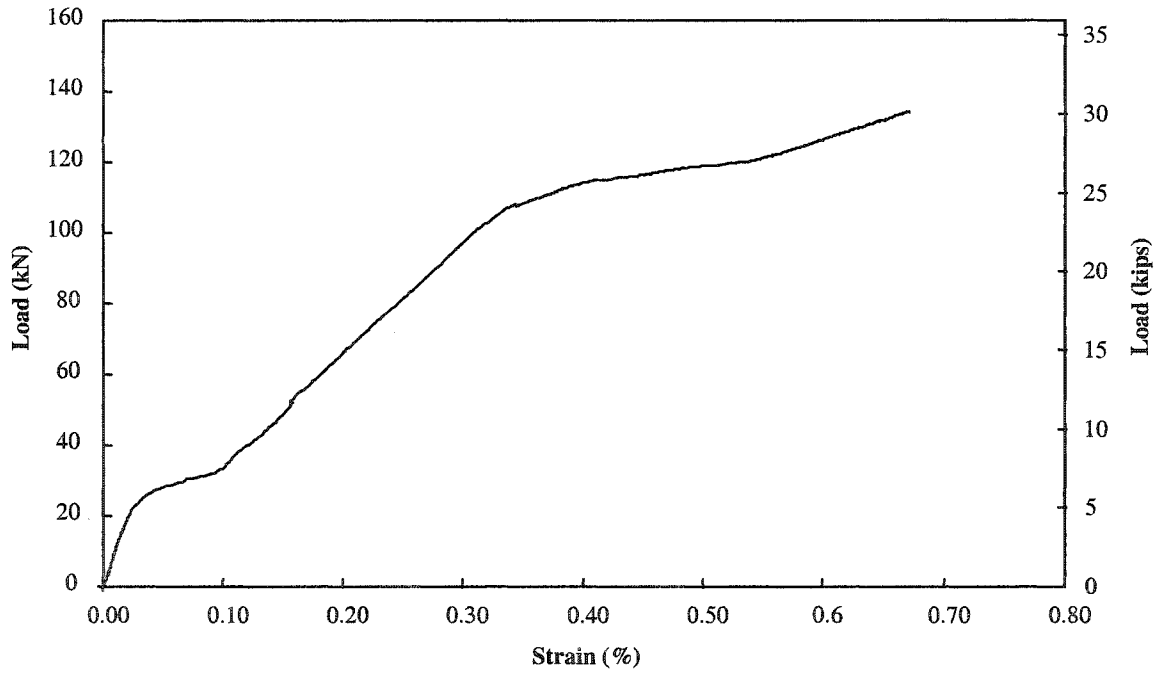

(b) FRP Strain at Mid-Span

Fig. 4.8 Behavior of beam C-3

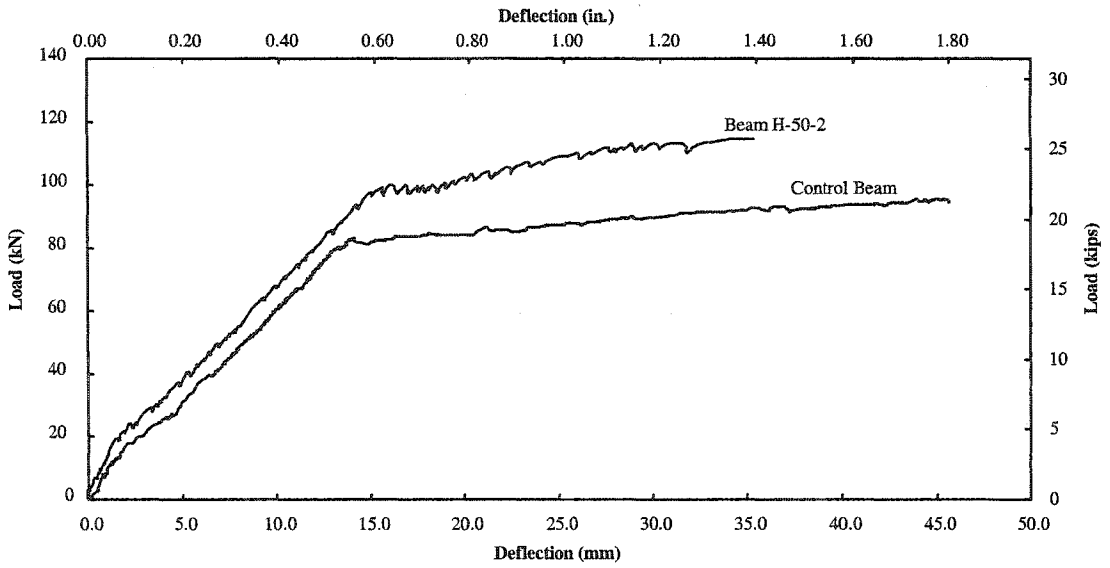

(a) Mid-Span Deflection

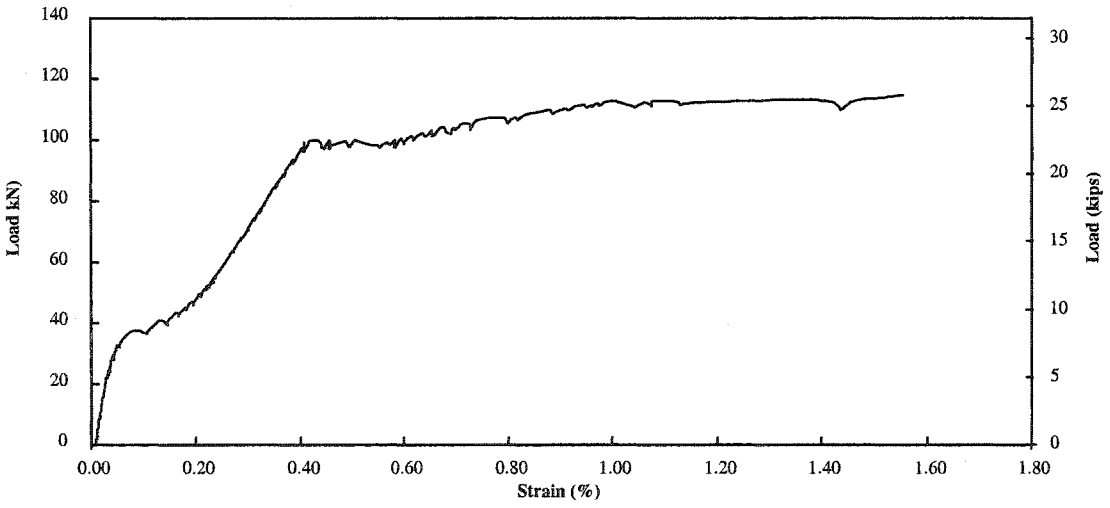

(b) Mid-Span FRP Strain

Fig. 4.9 Behavior of beam H-50-2

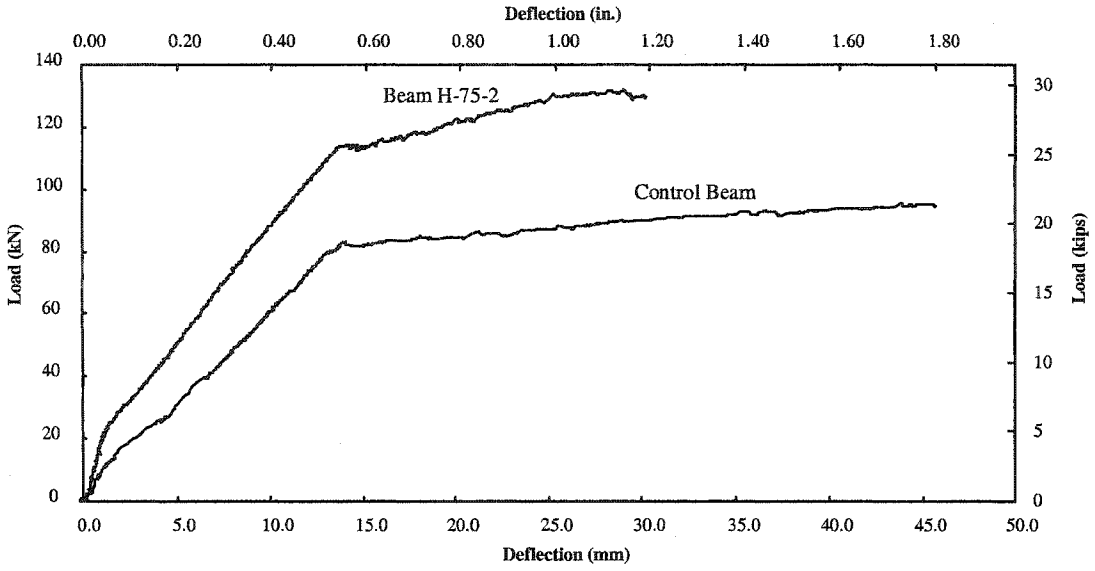

(a) Mid-Span Deflection

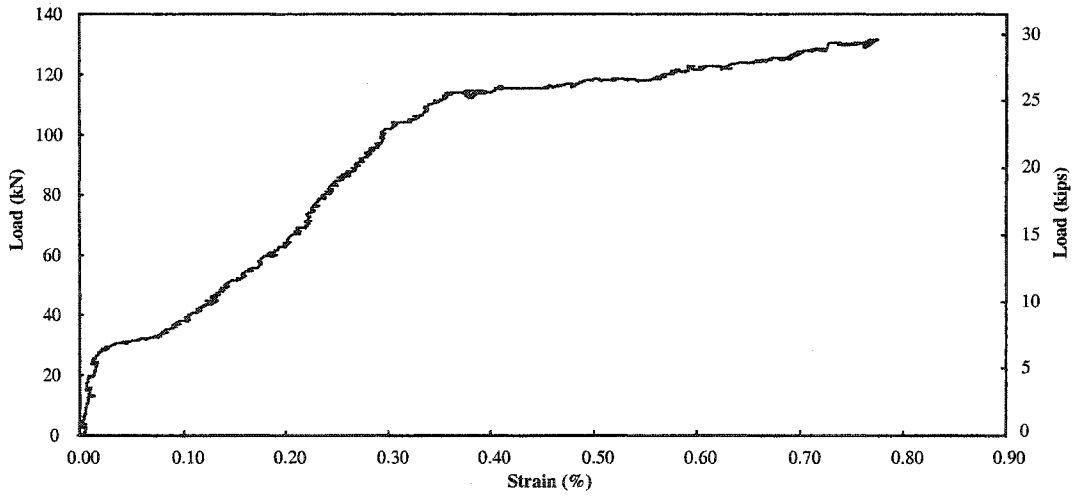

(b) FRP Strain at Mid-Span

Fig. 4.10 Behavior of beam H-75-2

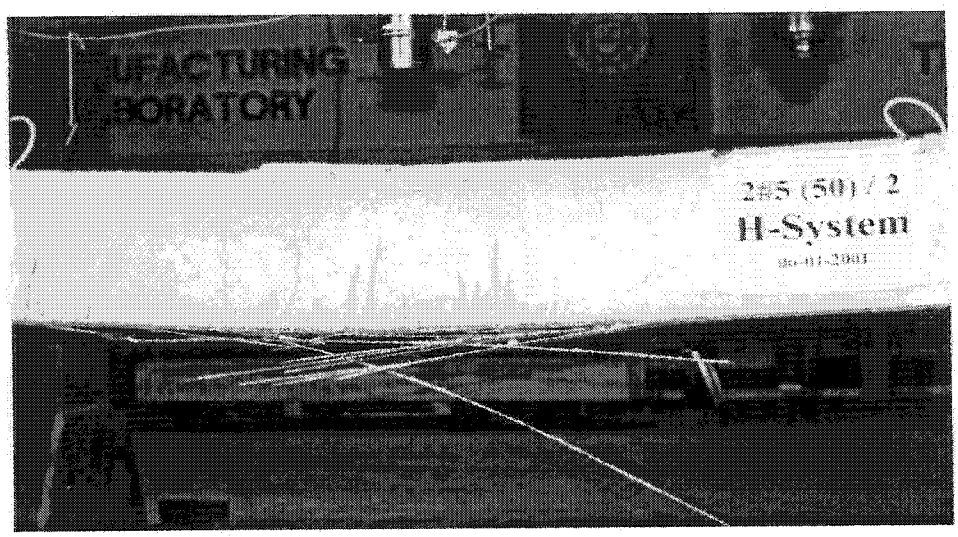

Fig. 4.11 Beam H-50-2 at failure

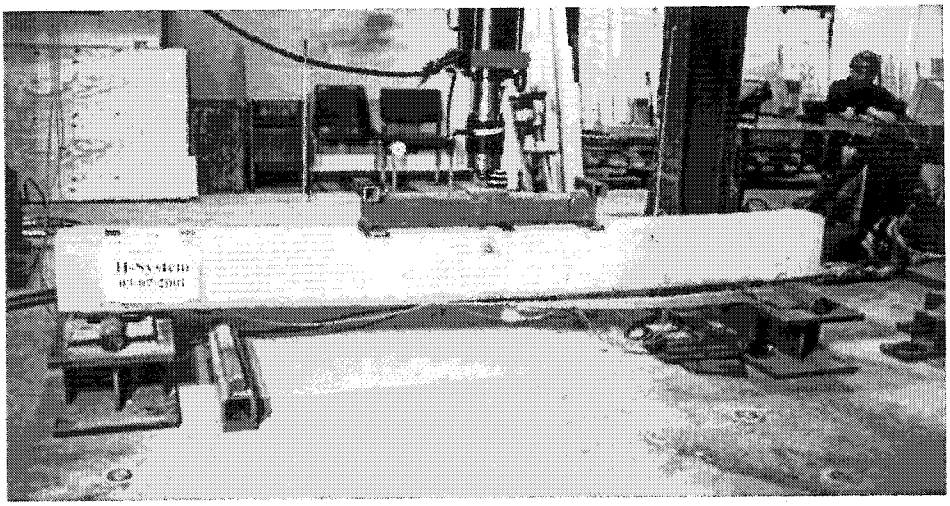

Fig. 4.12 Beam H-75-2 at failure

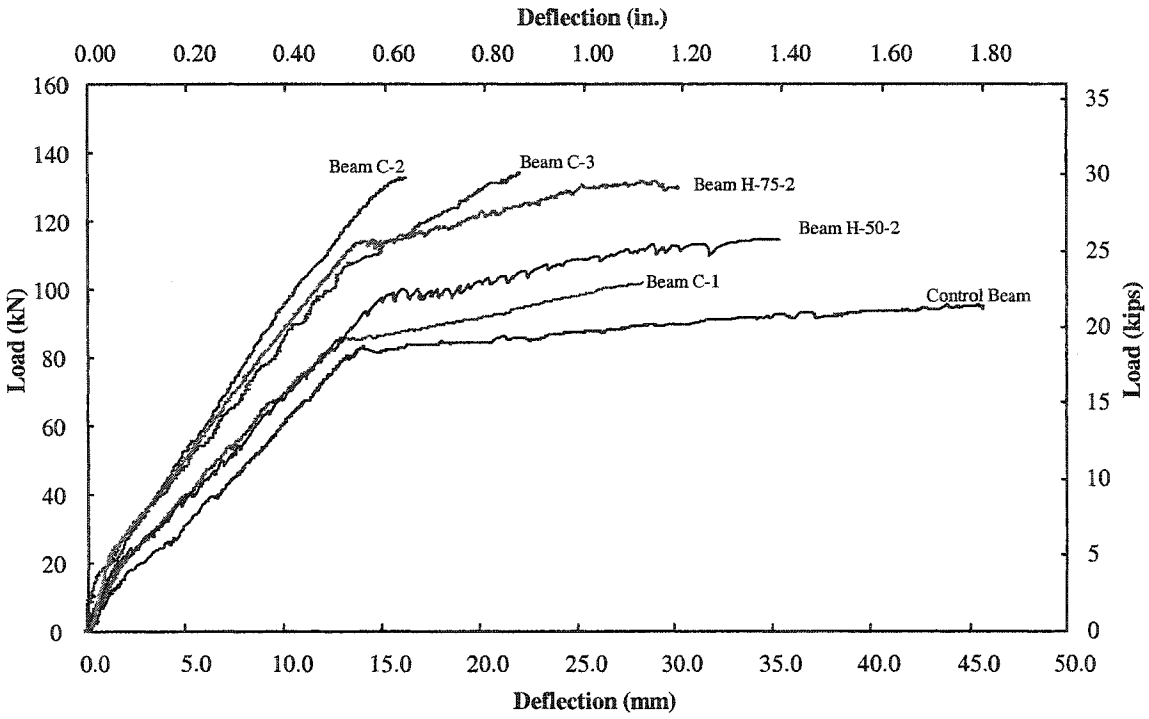

(a) Mid-Span Deflection

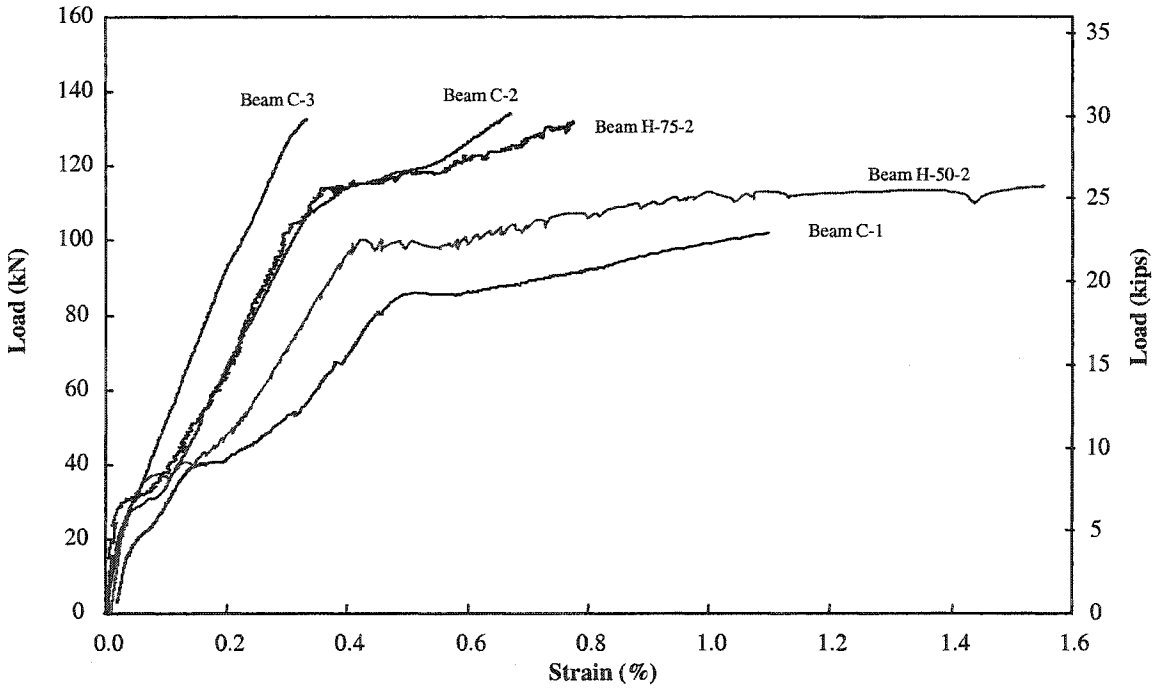

(b) FRP Strain at Mid-Span

Fig. 4.13 Comparison between group A beams

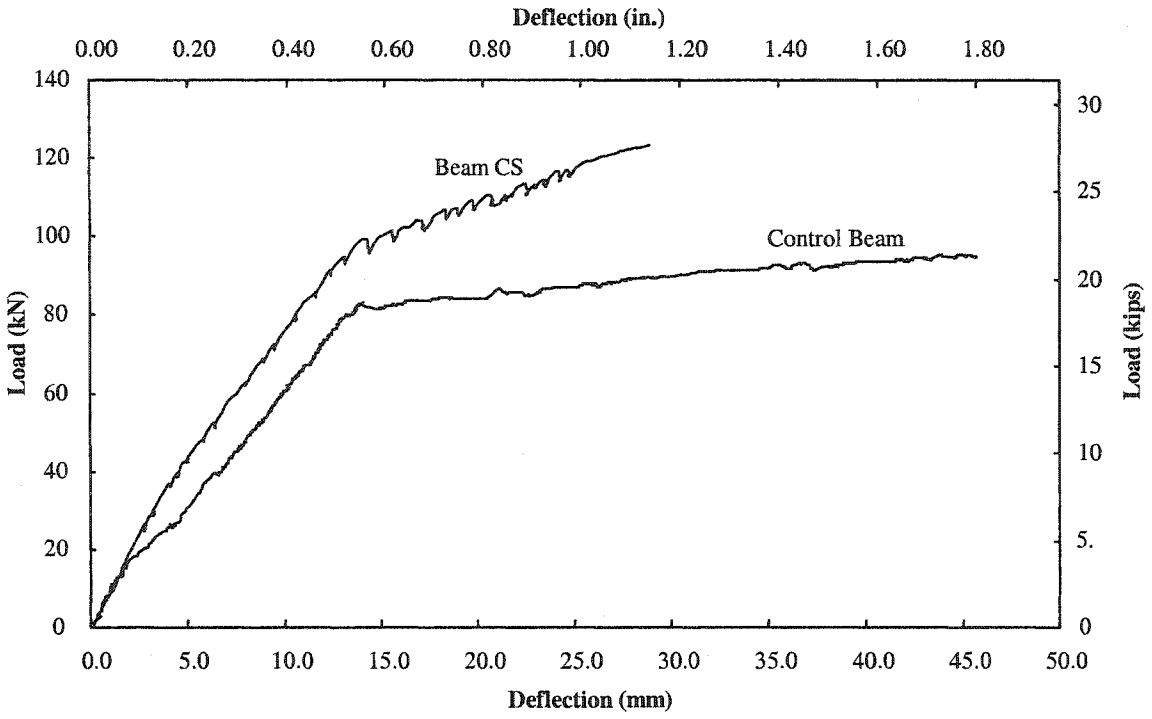

(a) Mid-Span Deflection

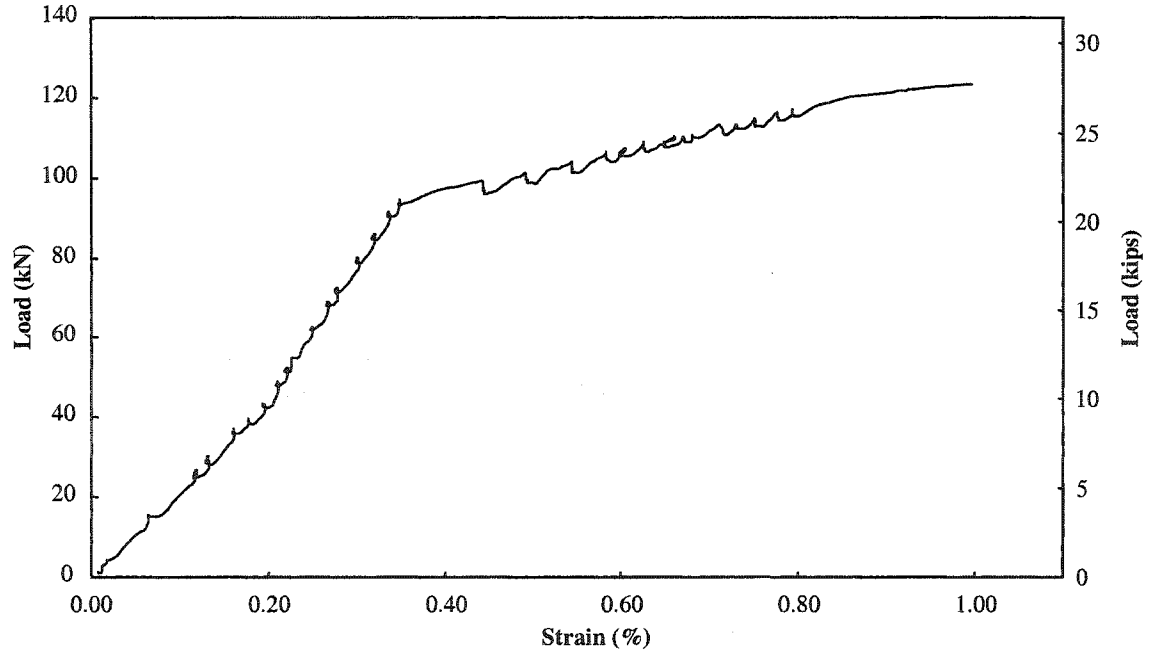

(b) FRP Strain at Mid-Span

Fig. 4.14 Behavior of beam CS

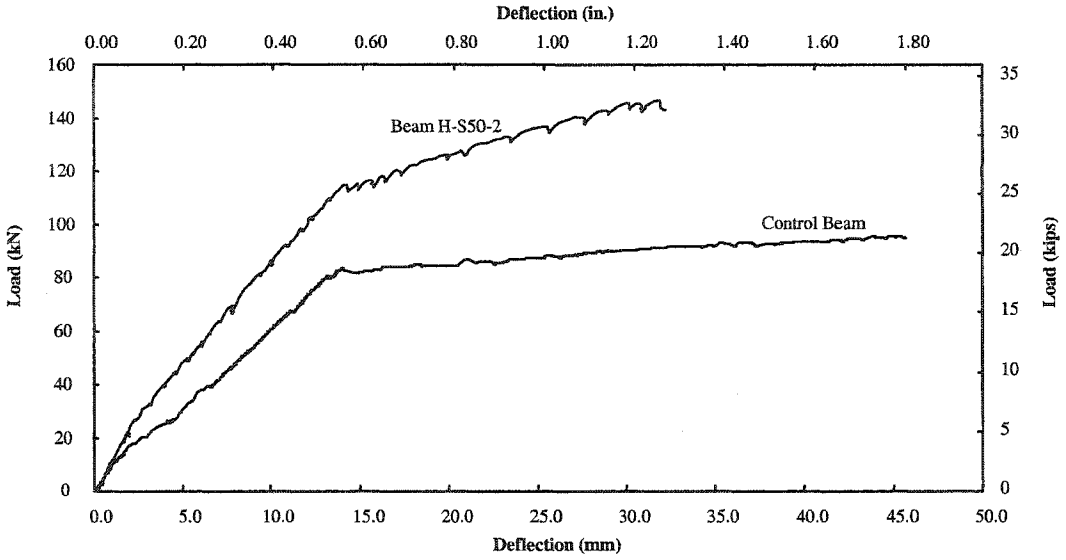

(a) Mid-Span Deflection

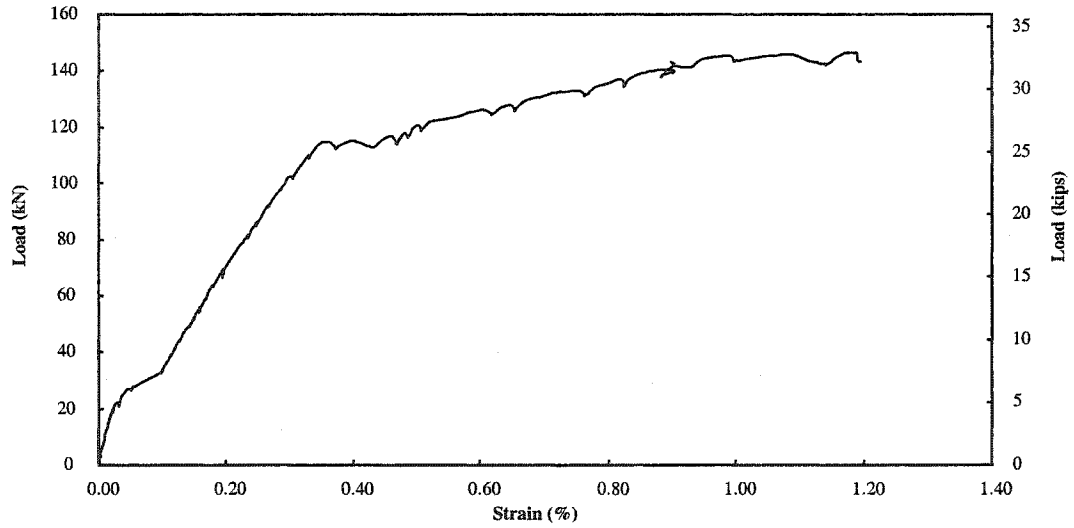

(b) FRP Strain at Mid-Span

Fig. 4.15 Behavior of beam H-S50-2

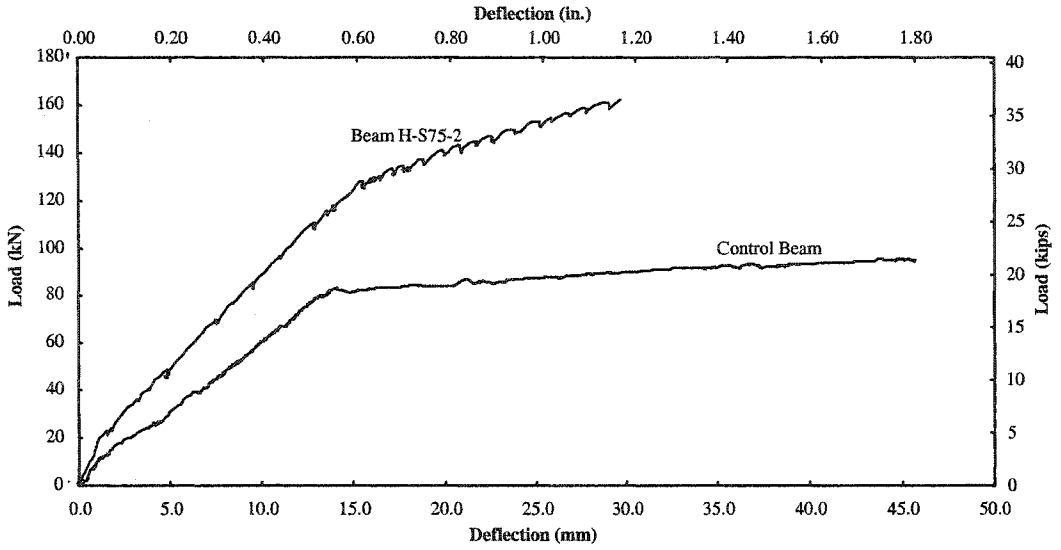

(a) Mid-Span Deflection

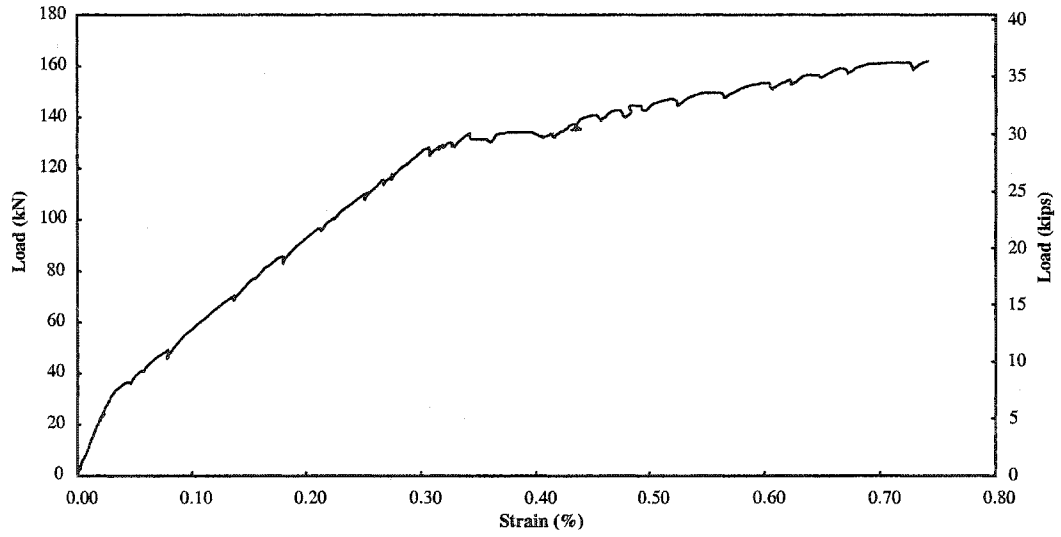

(b) FRP Strain at Mid-Span

Fig. 4.16 Behavior of beam H-S75-2

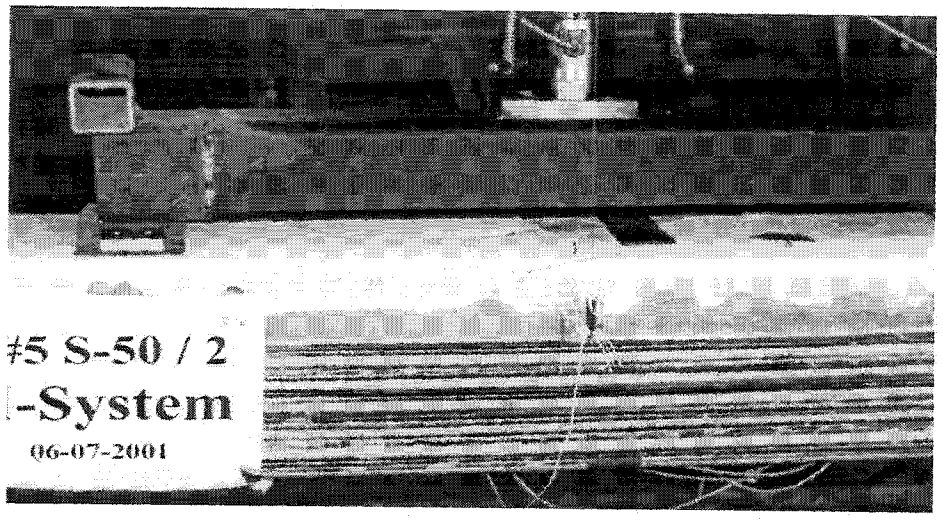

Fig. 4.17 Failure of beam H-S50-2

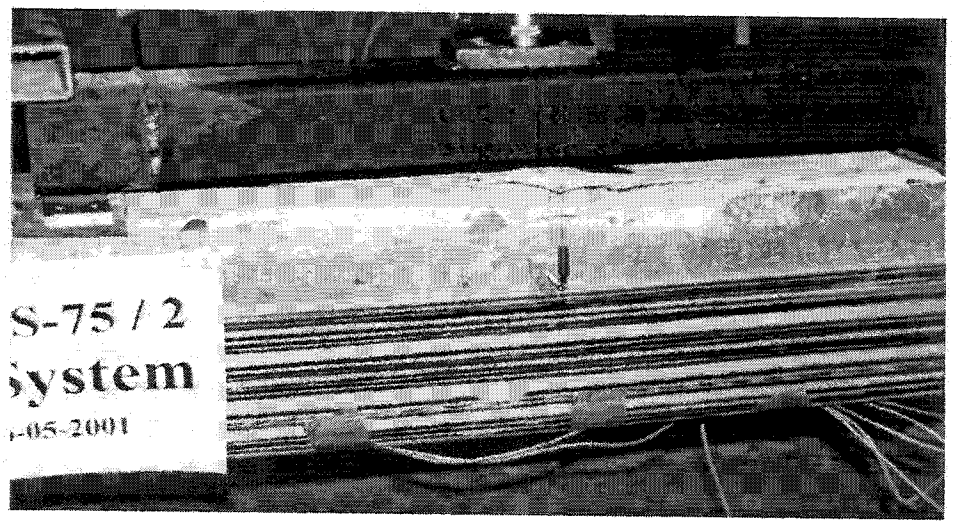

Fig. 4.18 Failure of beam H-S75-2

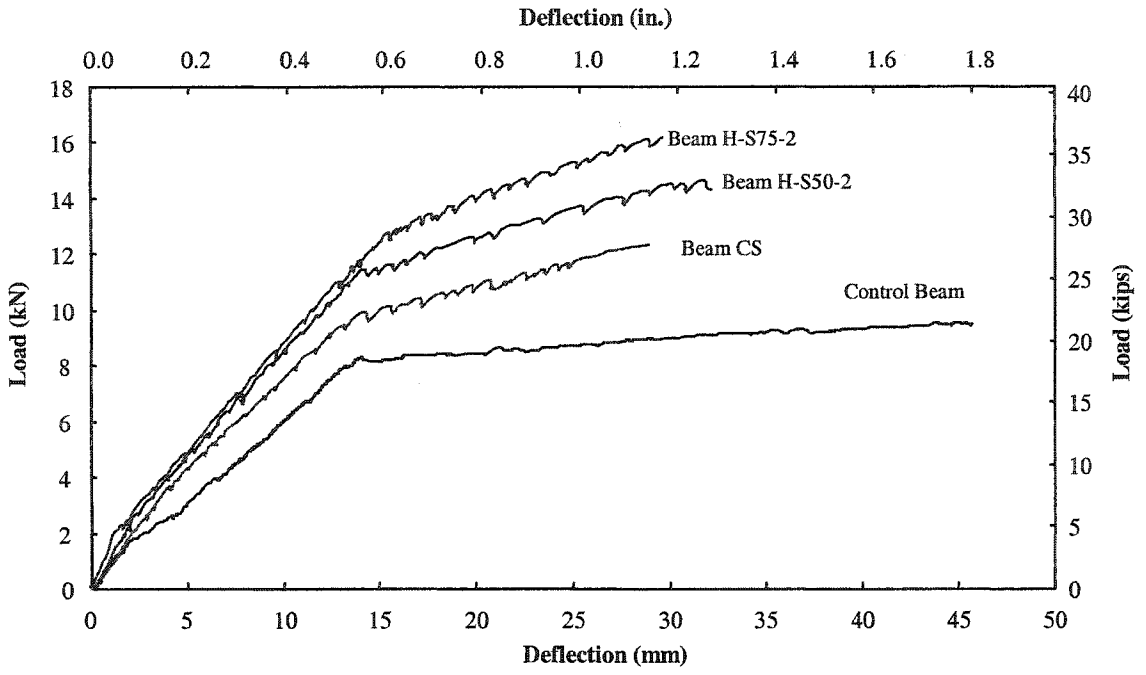

(a) Mid-Span Deflection

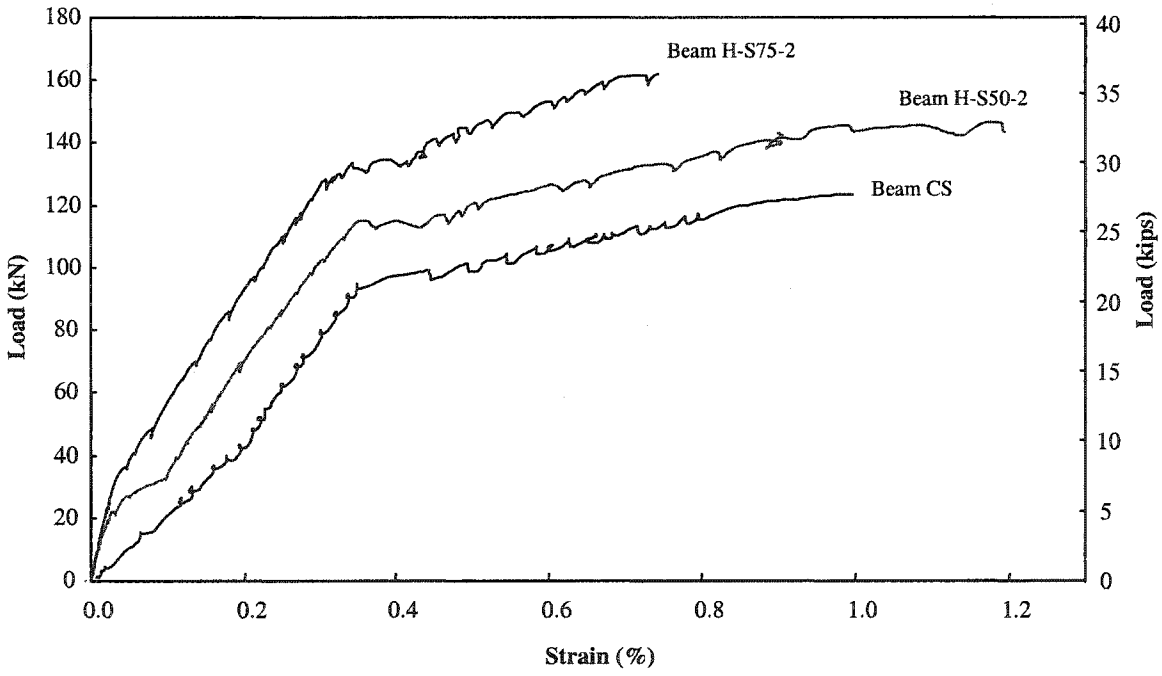

(b) FRP Strain at Mid-Span

Fig. 4.19 Comparison between group B beams

CHAPTER 5

FLEXURAL STRENGTHENING OF BEAMS USING THE DEVELOPED TRIAXIALLY BRAIDED DUCTILE FABRIC

5.1 General

In this chapter, an experimental investigation is reported to evaluate the effectiveness of the developed triaxially braided ductile fabric in flexural strengthening of reinforced concrete beams. The study is focused on the capability of the fabric to offer the required strengthening level without sacrificing a significant amount of beam ductility. The triaxial fabric was used to strengthen reinforced concrete simple beams of different steel reinforcement ratios using different strengthening schemes. Identical beams were strengthened with a commercially available carbon fiber sheet and a steel plate to compare their behavior with those strengthened with the triaxial fabric. The beams were loaded until failure and were investigated for deflections, strains, failure modes, and ductility.

5.2 Experimental Program

The experimental program consisted of strengthening and testing twenty-one beams divided into three groups. All the beams were tested as simple beams in four point bending until failure.

5.2.1 Test beams

Three groups of beams were cast. All beams had cross sectional dimensions of 152 mm × 254 mm (6 in. × 10 in.) and lengths of 2740 mm (108 in.). Group C and Group E beams had a flexural reinforcement of two #5 (16 mm) tension bars near the

bottom and two #3 (9.5 mm) compression bars near the top (ρ=1.25%). Group D beams had a flexural reinforcement of two #3 (9.5 mm) tension bars near the bottom and two #3 (9.5 mm) compression bars near the top (ρ=0.46%). In order to avoid shear failure, all beams were over-reinforced for shear with #3 (9.5 mm) closed stirrups spaced at 102 mm (4.0 in.). All beams except one were formed with rounded corners of 25 mm (1 in.) radius between the bottom face and the sides. Fig. 5.1 shows the beam dimensions, reinforcement details, and loading set up. Fig. 5.2 shows a photo of the form and the steel cages. The compressive strength of the concrete at the time the beams were tested was 41.5 MPa (6,000 psi) for Group C and Group E and 55.2 MPa (8,000 psi) for Group D. The steel reinforcement that was used had a yield stress of 490 MPa (71,000 psi).

5.2.2 Strengthening materials

The newly designed and developed triaxially braided ductile fabric (referred to as the triaxial fabric) was used to strengthen thirteen beams. A commercially available carbon fiber sheet was used to strengthen five beams in order to compare their behavior with those strengthened with the new fabric. Another beam was strengthened with a Grade 40 steel plate of 1.52 mm (0.0598 in.) thickness. The experimental load-strain diagrams of all these materials are shown in Fig. 5.3 and their properties are listed in Table 5.1. Herein, it can be noted that the triaxial fabric has a yield-equivalent load of 0.19 kN/mm (1.08 kips/in.), while the carbon fiber sheet has an ultimate load of 0.34 kN/mm (1.95 kips/in). The steel plate has a yield load of 0.44 kN/mm (2.5 kips/in.). In order to objectively compare the behavior of the fabric with that of the carbon fiber sheet, the number of carbon fiber layers was selected so that it would exhibit the same load-strain response as that initially (before it yields) exhibited by the triaxial fabric. Based on the tensile properties of the materials, it was determined that two layers of the carbon

fiber sheet would exhibit a load-strain response similar to that initially exhibited by one layer of the triaxial fabric. An epoxy resin was used to impregnate the fibers and as an adhesive between the strengthening material and the concrete surface. This epoxy has an ultimate tensile strength of 66.2 MPa (9.62 ksi) with an ultimate strain of 4.4% and a compressive strength of 109.2 MPa (15.84 ksi).

5.2.3 Strengthening and instrumentation

The beams were prepared by sandblasting the surfaces to roughen them, and cleaned with an air nozzle and finally wiped to remove any dust or loose particles (see Fig. 5.4). Two strengthening configurations were applied: (i) strengthening material on the bottom face of the beam only and (ii) strengthening material on the bottom face and extended up 152 mm (6 in.) on both sides to cover approximately all the flexural tensile zone of the beam. The strengthening material was installed for 2.24 m (88 in.) centered along the length of the beam (see installation procedures in Fig. 5.5). The epoxy was allowed to cure for at least two weeks before the beams were tested. Table 5.2 summarizes all the test beams.The FRP strain at midspan was measured by three strain gages located at the bottom face of the beam. The deflection was measured at the mid and quarter span using string potentiometers. The beams were loaded using a hydraulic actuator. The load was measured by means of a load cell. A data acquisition system was used to scan and record the readings of all sensors.

5.3 Test Results and Discussion

5.3.1 Group C

The beams of Group C had a steel reinforcement ratio of 1.25%, which is 42% of the balance steel ratio (ρ_b). The triaxial fabric was used to strengthen six beams, while

two other beams were strengthened with the carbon fiber sheet. One beam was strengthened with the steel plate and one other beam was a control beam. Test results for all these beams are shown in Fig. 5.6 through 5.14 and listed in Table 5.3. The ductility of each beam is determined by calculating its ductility index; that is the ratio between the ultimate deflection and the yield deflection.

5.3.1.1 Control Beam A

The control beam had a yield load of 77 kN (17.3 kips) and an ultimate load of 87 kN (19.6 kips). The beam failed by yielding of steel followed by compression failure of concrete at the midspan.

5.3.1.2 Beams F-B-1, 2 and Beam F-CB-1

Beams F-B-1 and F-B-2 were identically strengthened with the triaxial fabric to determine if the test results were repeatable. Two layers 135 mm (5.33 in.) wide were installed on the bottom face of the each beam. Beam F-CB-1 was strengthened with four layers of the carbon fiber sheet 146 mm (5.75 in.) wide installed on its bottom face. The test results of beams F-B-1 and F-B-2 were very similar. Hence, the discussion here will be focused on beam F-B-2 in order to avoid repetition. Fig. 5.6 shows the test results for beams F-B-2 and F-CB-1. Beam F-B-2 yielded at a load of 113 kN (25.4 kips) and failed at a load of 123 kN (27.6 kips) by compression failure of the concrete at the midspan, after exhibiting a considerable amount of ductility. Some debonded areas of fabric were noticed near the midspan just before failure, however this did not affect the behavior of the beam as the anchoring portions of the fabric away from the midspan were still attached. Beam F-CB-1 yielded at a load of 119 kN (26.7 kips) but failed suddenly by debonding of the carbon fiber sheet at a load of 141 kN (31.7 kips), after exhibiting less

ductility than beam F-B-2. The ductility index of beam F-B-2 was 1.95, while the ductility index of beam F-CB-1 was 1.61. The difference in failure modes between the two beams was due to the difference in the load-strain response between the triaxial fabric and the carbon fiber sheet. Both the fabric and the carbon fiber sheet carried almost the same amount of load up to yield of the beam. However, the tensile force in the carbon fiber sheet increased after the steel yielded. This increase in force appeared to be the reason for the debonding of the carbon fiber sheet. On the other hand, degradation of the stiffness of the triaxial fabric (as it yielded) in case of beam F-B-2 helped to limit the force increase in it and hence debonding was avoided, leading to a more ductile failure. Both beams showed considerable increases in beam yield load and stiffness; however, beam F-B-2 showed higher ductility and failed less catastrophically than beam F-CB-1. Beam F-B-2 yielded due to the yielding of both the steel reinforcement and the fabric, while beam F-CB-1 yielded due to the yielding of the steel only. The carbon fiber sheet had a midspan strain of 0.7%, which indicates that it reached only about half of its load capacity when it failed. In contrast, the triaxial fabric had a midspan strain of 1.06 %, which was more than the strain necessary to reach most of its load capacity (more than its yield strain). Fig. 5.7 and Fig. 5.8 show photos of the two beams after failure.

5.3.1.3 Beam F-ST-1

This beam was strengthened with a Grade 40 steel plate 1.52 mm (0.0598 in.) thick and 152 mm (6 in.) wide. The objective of including this test specimen in the program was to compare the behavior of a beam strengthened with a highly ductile material, such as steel, with the behavior of a beam strengthened with the triaxial fabric. To facilitate the installation of the plate, the beam had no rounded corners. To isolate the effect of debonding, the plate was well anchored to the concrete using steel screws (see

Fig. 5.9). Test results for this beam are shown in Fig. 5.6. Beam F-ST-1 exhibited a higher initial stiffness than beam F-B-2. The steel plate yielded at a load of 60 kN (13.5 kips) causing a decrease in beam stiffness. The inner steel rebar yielded at a load of 119 kN (26.7 kips) and the beam exhibited a yield plateau similar to that of beam F-B-2. Beam F-ST-1 failed by compression of the concrete at midspan at a load of 121 kN (26.7 kips). The test indicated that the beam strengthened with the triaxial fabric produced a similar yield plateau to that of a beam strengthened with a highly ductile material such as steel. The failed beam is shown in Fig. 5.10

5.3.1.4 Beams F-U-1,2 and Beam F-CU-1

Beams F-U-1 and F-U-2 were strengthened with one layer of the triaxial fabric as a U-wrap along the bottom face, which extended 152 mm (6 in.) on both sides. Beam F-CU-1 had the same U-wrap scheme but with two layers of the carbon fiber sheet. The results of beam F-U-1 and beam F-U-2 were very similar and hence the discussion below is focused on beam F-U-2 in order to avoid repetition. Test results from beam F-U-2 and beam F-CU-1 are shown in Fig. 5.11. Both beams showed similar initial stiffness. Beam F-U-2 yielded at a load of 108 kN (24.3 kips) and failed by compression failure of the concrete at midspan at a load of 130 kN (29.2 kips). Beam F-CU-1 yielded at a load of 111 kN (24.9 kips) and also failed by compression failure of the concrete at midspan at a load of 133 kN (29.9 kips). However, beam F-U-2 showed more ductility than beam F-CU-1. This is attributed to the degradation of the fabric stiffness after it yielded which in turn led to a compression failure at a higher FRP strain value than that of beam F-CU-2 in which the stiffness of the carbon fiber sheet did not decrease.

5.3.1.5 Beam F-BL3-1 and Beam F-UB1-1

To provide additional experimental data for the behavior of concrete beams strengthened with the triaxial fabric, the triaxial fabric was used to strengthen two beams, beam F-BL3-1 and beam F-UB1-1.

Beam F-BL3-1 was strengthened with three layers of the triaxial fabric 135 mm (5.33 in) wide installed at the bottom face of the beam. Test results for this beam are shown in Fig. 5.12. The beam yielded at a load of 130 kN (29.2 kips) and reached its ultimate strength at a load of 141 kN (31.7 kips) by compression failure of the concrete at midspan. Before failure of the beam, the fabric debonded from the concrete surface near the midspan. However, this did not affect the behavior of the beam as the anchoring portions of the fabric located away from the midspan were still attached. The beam experienced a reasonable ductility before failure (a ductility index of 1.89). The failed beam is shown in Fig. 5.13.

Beam F-UB1-1 was strengthened with one layer of the triaxial fabric 135 mm (5.33 in.) wide and also wrapped with another outer layer of the fabric 453 mm (18 in.) wide around the beam bottom face and the sides. Test results for this beam are included in Fig. 5.12. The beam showed similar initial deflection and strain behaviors to that of beam F-BL3-1.The beam yielded at a load of 123 kN (27.6 kips) due to yielding of the fabric and the steel, which was slightly less than that of beam F-BL3-1. Beam F-UB1-1 exhibited a reasonable yield plateau and failed at a load of 147 kN (33 kips) by compression failure of the concrete near the mid span (see Fig. 5.14). A ductility index of 1.94 was experienced. The fabric exhibited a strain value of 0.93 before beam failure.

Installing the fabric on the tension face of the beam only fully utilizes its resources. Beam F-B-2 and beam F-BL3-1 showed similar behavior to beam F-U-2 and beam F-UB1-1, respectively. However, less fabric was used in case of beam F-B-2 and

beam F-BL3-1. On the other hand, U-wrapping the beam makes it less vulnerable to experience anchorage failures, which will be addressed later by Group E. Similar to that applied in case of beam F-UB1-1, installing layers of the fabric on the beam tension side that are covered with an outer layer bonded around the beam tension face and sides as a U-wrap is a good way to utilize the fabric and at the same time provide better anchorage to these layers.

5.3.2 Group D

The beams of this group had a flexural reinforcement ratio of 0.44% (13% of ρ_b), which is close to minimum steel reinforcement ratio required by ACI code. Therefore, these beams were lightly reinforced. This group contained five beams. Two beams were strengthened with the triaxial fabric and two beams were strengthened using the carbon fiber sheet. One beam was a control beam. Test results for all these beams are shown Fig. 5.15 though 5.17 and listed in Table 5.4.

5.3.2.1 Control Beam B

The control beam had a yield load of 22 kN (4.9 kips) and an ultimate load of 42 kN (9.40 kips). The beam failed by yielding of steel followed by compression failure of the concrete at the midspan.

5.3.2.2 Beams F3-B-1 and F3-CB-1

Both beams were strengthened by bonding the FRP on their bottom faces only. Beam F3-B-1 was strengthened with two layers of the triaxial fabric, 135 mm (5.33 in.) wide. Beam F3-CB-1 was strengthened with four layers of the carbon fiber sheet, 145 mm (5.75 in.) wide. Test results for the two beams are shown in Fig. 5.15, along with the

test results for the control beam. Beam F3-B-1 yielded at a load of 53 kN (11.9 kips), while beam F3-CB-1 yielded at a load of 58 kN (13.0 kips). Beam F3-CB-1 showed a slightly greater stiffness and failed at a load of 67 kN (15.1 kips). Beam F3-CB-1 failed by debonding of the carbon fiber sheet from the concrete surface initiated by crack opening near the loading points and propagated towards the sheet ends. Beam F3-CB-1 had a ductility index of 1.5. Beam F3-B-1 also failed by debonding of the fabric from the concrete surface initiated by crack forming near the midspan and propagated towards the fabric ends at a load of 70 kN (15.7 kips). However, beam F3-B-1 exhibited a reasonable ductile plateau with a ductility index of 2.92.

5.3.2.3 Beams F3-U-1 and F3-CU-1

Beam F3-U-1 was U-wrapped with one layer of the triaxial fabric on the bottom face, which extended 152 mm (6 in.) up on both sides. Beam F3-CU-1 had a similar wrapping scheme but with two layers of the carbon fiber sheet. Test results for the two beams are shown in Fig. 5.16, along with the test results of the control beam. Beam F3-CU-1 showed a slightly higher stiffness than Beam F3-U-1. The two beams yielded at a load of 58 kN (13.0 kips). Beam F3-U-1 showed an increase in deflection and strain after yielding. Beam F3-U-1 failed by rupture of the fabric near the midspan at a load of 91 kN (20.5 kips), and after exhibiting considerable ductility with a ductility index of 3.75. However, beam F3-CU-1 did not show similar deflections and strains after yield. Beam F3-CU-1 failed suddenly at a load of 92 kN (20.70 kips) due to debonding of the sheet from the bottom face. The two failed beams are shown in Fig. 5.17. The triaxial fabric has an advantage over the carbon fiber sheet as it contains yarns in the (+45°, -45°) directions. These yarns worked to self anchor the fabric in beam F3-U-1 during wrapping; hence debonding failure was not experienced. On the other hand, the carbon

fiber sheet is uniaxial and hence wrapping the beam did not improve the anchoring of the fibers on the bottom face.

5.3.3 Group E

The objectives of the experimental investigation of the beams of this group were to address the effect of the used fabric length on the beam behavior, the benefits of U-wrapping the beam in offering better anchorage, and advantage of the triaxial fabric over the uniaxial sheets in self anchorage. The beams in this group had a steel reinforcement ratio of 1.25%. Test results for all these beams are shown Fig. 5.18 through 5.29 and are listed in Table 5.5.

5.3.3.1 Beam F-B82-1

Beam F-B82-1 was strengthened at its bottom face with two layers of the triaxial fabric 135 mm (5.33 in.) wide and 1980 mm (78 in.) long each, centered along the beam span. The beam was similar to beam F-B-1 and beam F-B-2 except that the fabric herein was 150 mm (6 in.) less in length than that used for those two beams. Fig. 5.18 shows test results for this beam. The beam yielded at a load of 111 kN (25 kips), which was very close to that of beam F-B-2 (see Table 5.3 and Table 5.5). The beam then exhibited a yield plateau until failure at a load of 123 kN (27.6 kips), which was similar to beam F-B-2 and at a deflection of 40 mm (1.57 in.), which was slightly more than that of beam F-B-2. The beam failed by compression failure of the concrete near the midspan, which was accompanied by debonding of the fabric form the concrete surface as shown in Fig. 5.19. The decrease in fabric length compared to beam F-B-2 almost did not affect the behavior of the beam.

5.3.3.2 Beam F-B75-1

The beam had the same strengthening scheme as beam F-B82-1 but the fabric herein had a length of 1830 mm (72 in.), which was 150 mm (6 in.) less that that of beam F-B82-1. Test results for this beam are shown in Fig. 5.20. The beam behaved similar to beam F-B82-1 until it yielded at a load of 113 kN (25.4 kips). The beam then exhibited a yield plateau until it failed suddenly at a load of 119 kN (26.7 kips) due to shear-tension failure at fabric end where the concrete cover cracked along the plane of the steel reinforcement as shown in Fig. 5.21.

It can be concluded that insufficient fabric lengths will results in debonding of the fabric from the concrete surface or shear-tension failure at plate end (if the length is much less). Such failures are catastrophic and therefore providing additional anchorage is important in these cases to maintain the beam ductility.

5.3.3.3 Beam F-U75-1

Beam F-U75-1 was U-wrapped with the triaxial fabric along its bottom face and extended 152 mm (6 in.) on both sides. The fabric was installed along 1830 mm (72 in.) centered along the beam span similar to that of beam F-B75-1 and less than that of beam F-U-2 by 406 mm (16 in.). Test results of this beam are shown in Fig. 5.22. The beam yielded at a load of 112 kN (25.2 kips) and failed at a load of 133 kN (29.9 kips) due to compression failure of the concrete near the midspan (see Fig. 5.24). The beam behavior was similar to that of beam F-U-2 however with slightly more deflection at failure (see Table 5.3 and Table 5.5). Therefore, decreasing the fabric length did not significantly affect the beam behavior.

5.3.3.4 Beam F-U65-1

Beam F-U65-1 had the same strengthening scheme as beam F-U75-1 but the fabric herein had a length of 1594 mm (62 in.), which was 254 mm (10 in.) less that that of beam F-U75-1. Test results of this beam are shown in Fig. 5.23. Again, decreasing the fabric length did not significantly affect the beam behavior. . The beam yielded at a load of 110 kN (24.7 kips) and failed at a load of 128 kN (28.8 kips) due to compression failure of the concrete near the midspan (see Fig. 5.25).

5.3.3.5 Beam F-CU65-1

Beam F-CU65-1 had the same strengthening scheme as beam F-U65-1. However, two layers of the carbon fiber sheet were used in this case. Test results for this beam are shown in Fig. 5.26. The beam yielded at a load 112 kN (25.2 kips), which was very similar to that of beam F-CU-1. The beam failed suddenly at a load of 126 kN (28.3 kips) with a ductility index of 1.33, which was less than that of beam F-U65-1 and beam F-CU-1 due to shear-tension failure at sheet end at the bottom face of the beam. The failed beam is shown in Fig. 5.27

The test results of beam F-CU65-1 and beam F-U65-1 indicate that when the triaxial fabric is bonded around the beam tension face and sides as a u-wrap makes it less vulnerable, in comparison to the uniaxial carbon fiber sheet, to exhibit shear-tension failures. That is attributed to the $\pm 45^{\circ}$ direction bundles of fibers that work to self anchor the fabric to the beam unlike the carbon fiber sheet that has fibers in only one direction.

5.3.3.6 Beam F-U57-1

In order to know the limit of fabric length decrease that would not affect the structural behavior of the beam, beam F-U57-1 was strengthened along only 1372 mm (54 in.) of its length with the same U-wrapping scheme as beam F-U65-1. Test results for this beam are shown in Fig. 5.28. Although the beam showed similar yield load to that of beam F-CU65-1 (see Table 5.5), the unstrengthened section just beside the fabric end started to yield at a load of 115 kN (25.8 kips) as it reached the its yield strength. A drop in load was then experienced and beam failed later by compression failure of the concrete near the loading point. See Fig. 5.29 for the failed beam.

Just after yielding of the beams strengthened with the triaxial fabric, distinguishable sounds were heard. These sounds were due to failure of the low and medium elongation fibers in the fabric. The fact that these sounds are audible means that they may be used to indicate any potential failure of the strengthened beam. That is in addition to the visual signs of a potential failure revealed by the ductile behavior of the beam (excessive increase in strains and deformation).

5.4 Conclusions

1- The beams strengthened with the triaxial fabric behaved in a more ductile manner than those strengthened with the carbon fiber sheet. The new fabric produced a yield plateau similar to that of the unstrengthened beam and also similar to that produced by a beam strengthened with a ductile material such as steel.

2- Most of the beams strengthened with the carbon fiber sheets exhibited brittle failures due debonding of the carbon fiber sheet from the concrete surface. The beams strengthened with the triaxial fabric were less vulnerable to exhibit such failures due to the different load-strain response of the fabric. Yielding of the

fabric limits the force increase in it and as a result it was less demanding for anchorage.

3- Although the beam strengthened with the steel plate exhibited considerable ductility, the steel plate yielded at a lower load than the inner reinforcing steel, since the plate has a lower yield strain than the steel bars and was installed on the outside surface of the beam that underwent more strains than the inner steel. In contrast, as the triaxial fabric has a yield strain value that is slightly more than the yield strain of steel, it has the potential to yield simultaneously with the inner steel reinforcement.

4- In case of U-wrapped beams, the triaxial fabric had an advantage over the carbon fiber sheet as it contains yarns in the $+45^{\circ}$, -45° directions. These yarns worked to self anchor the fabric when bonded around the tension face and sides of the beam and hence debonding failure was not experienced. On the other hand, the carbon fiber sheet is uniaxial; hence wrapping the beam did not improve the anchoring of the fibers on the bottom face.

5- When installed on the beam tension face only, insufficient fabric lengths may result in debonding of the fabric from the concrete surface or shear-tension failure at plate end (if the length is significantly less). Such failures are catastrophic and therefore providing additional anchorage by U-wrapping the beam is important in these cases to maintain the beam ductility.

6- In case of U-wrapped beams, anchorage failures due to shear-tension failures at the fabric end are less likely to happen when the triaxial fabric is used.

7- Yielding of the fabric was accompanied by distinctly audible sounds due to failure of the low and medium elongation fibers of the fabric.

Table 5.1 Properties of the Strengthening Materials

Type	Yield-Equivalent Load kN/mm (kips/in.)	Yield-equivalent Strain (%)	Ultimate Load kN/mm (kips/in.)	Ultimate Strain (%)	Thickness mm (in.)
Carbon Fiber Sheet	-	-	0.34 (1.95)	1.2	0.13 (0.005)
Triaxial Ductile Fabric	0.19 (1.08)	0.35	0.33 (1.89)	2.10	1.0 (0.039)
Steel Plate	0.44 (2.50)	0.14	0.58 (3.31)	> 3	1.52 (0.0598)

Table 5.2 Summary of Test Beams

Beam Group	Beam Designation	Steel Reinforcement Ratio	Strengthening Scheme	Strengthening Material	Strengthening Length (L)
Group C	Control A	1.25%	N/A	N/A	N/A
	F-B-1		Bottom face only	Triaxial fabric (2 layers)	2236 mm (88 in.)
	F-B-2				
	F-CB-1			Carbon fiber sheet (4 layers)	
	F-ST-1			Steel plate	
	F-BL3-1			Triaxial fabric (3 layers)	
	F-U-1		U-Wrap	Triaxial fabric (1 layer)	
	F-U-2				
	F-CU-1			Carbon fiber sheet (2 layers)	
	F-UB1-1		Bottom Face & U-wrap	Triaxial fabric (1 layers at bottom & 1 layer U-wrap)	
Group D	Control B	0.46%	N/A	N/A	N/A
	F3-B-1		Bottom face only	Triaxial fabric (2 layers)	2236 mm (88 in.)
	F3-CB-1			Carbon fiber sheet (4 layers)	
	F3-U-1		U-Wrap	Triaxial fabric (1 layer)	
	F3-CU-1			Carbon fiber sheet (2 layers)	
Group E	F-B82-1	1.25%	Bottom face only	Triaxial fabric (2 layers)	1980 mm (78 in.)
	F-B75-1			Triaxial fabric (2 layers)	1830 mm (72 in.)
	F-U75-1		U-Wrap	Triaxial fabric (1 layer)	
	F-U65-1			Triaxial fabric (1 layer)	1594 mm (62 in.)
	F-CU65-1			Carbon fiber sheet (2 layers)	
	F3-U57-1			Triaxial fabric (1 layer)	1372 mm (54 in.)

Table 5.3 Summary of Test Results for Group C Beams

Beam Designation (1)	Strengthening System (2)	Yield Load kN (kips) (3)	Deflection at Yield mm (in.) (4)	Failure Load kN (kips) (5)	Deflection at Failure mm (in.) (6)	Ductility Index (7) = Col. 6 / Col. 4	FRP Strain at Failure (%) (8)	Mode of Final Failure (9)
Control A	N/A	77 (17.3)	16 (0.63)	87 (19.6)	44 (1.73)	2.75	N/A	Steel yield followed by concrete failure
F-B-2	Triaxial fabric (2 layers)	113 (25.4)	19 (0.75)	123 (27.6)	37 (1.46)	1.95	1.06	Steel & fabric yield followed by concrete failure
F-CB-1	Carbon fiber sheet (4 layers)	119 (26.7)	18 (0.71)	141 (31.7)	29 (1.14)	1.61	0.70	Steel yield followed by sheet debonding
F-ST-1	Steel plate	119 (26.7)	16 (0.63)	121 (27.2)	34 (1.33)	2.13	1.10	Steel yield followed by concrete failure
F-BL3-1	Triaxial fabric (3 layers)	130 (29.2)	19 (0.75)	141 (31.7)	36 (1.41)	1.89	1.14	Steel & fabric yield followed by concrete failure
F-U-2	Triaxial fabric (1 layer)	108 (24.3)	17 (0.67)	130 (29.2)	37 (1.46)	2.18	1.23	Steel & fabric yield followed by concrete failure
F-CU-1	Carbon fiber sheet (2 layers)	111 (24.9)	18 (0.71)	133 (29.9)	29 (1.14)	1.61	0.78	Steel yield followed by concrete failure
F-UB1-1	Triaxial fabric (2 layers at bottom & 1 layer U –wrap)	123 (27.6)	18 (0.71)	147 (33.0)	35 (1.38)	1.94	0.93	Steel & fabric yield followed by concrete failure

Table 5.4 Summary of Test Results for Group D Beams

Beam Designation (1)	Strengthening System (2)	Yield Load kN (kips) (3)	Deflection at Yield mm (in.) (4)	Failure Load kN (kips) (5)	Deflection at Failure mm (in.) (6)	Ductility Index (7) = Col. 6 / Col. 4	FRP Strain at Failure (%) (8)	Type of Final Failure (9)
Control B	N/A	22 (4.9)	7 (0.28)	42 (9.4)	57 (2.24)	8.14	N/A	Steel yield followed by concrete failure
F3-B-1	Triaxial fabric (2 layers)	53 (11.9)	13 (0.51)	70 (15.7)	38 (1.50)	2.92	1.21	Steel & fabric yield followed by fabric debonding
F3-CB-1	Carbon fiber sheet (4 layers)	58 (13.0)	12 (0.47)	67 (15.1)	18 (0.71)	1.5	0.42	Steel yield followed by sheet debonding
F3-U-1	Triaxial fabric (1 layer)	58 (13.0)	12 (0.47)	91 (20.5)	45 (1.77)	3.75	1.68	Steel & fabric yield followed by fabric rupture
F3-CU-1	Carbon fiber sheet (2 layers)	58 (13.0)	11 (0.43)	92 (20.7)	25 (0.98)	2.27	0.80	Steel yield followed by sheet debonding

Table 5.5 Summary of Test Results for Group E Beams

Beam Designation (1)	Strengthening System (2)	Yield Load kN (kips) (3)	Deflection at Yield mm (in.) (4)	Failure Load kN (kips) (5)	Deflection at Failure mm (in.) (6)	Ductility Index (7) = Col. 6 / Col. 4	FRP Strain at Failure (%) (8)	Type of Final Failure (9)
F-B82-1	Triaxial fabric (2 layers)	111 (25.0)	19 (0.75)	123 (27.6)	40 (1.57)	2.1	1.25	Steel & fabric yield followed by concrete failure and fabric debonding
F-B75-1	Triaxial fabric (2 layers)	113 (25.4)	19 (0.75)	119 (26.7)	28 (1.10)	1.47	0.97	Steel & fabric yield followed by shear-tension failure at fabric end
F-U75-1	Triaxial fabric (1 layer)	112 (25.2)	18 (0.71)	133 (29.9)	42 (1.65)	2.33	1.37	Steel & fabric yield followed by concrete failure
F-U65-1	Triaxial fabric (1 layer)	110 (24.7)	19 (0.75)	128 (28.8)	37 (1.46)	1.95	1.33	Steel & fabric yield followed by concrete failure
F-CU65-1	Carbon fiber sheet (2 layers)	112 (25.2)	18 (0.71)	126 (28.3)	24 (0.94)	1.33	0.62	Steel yield followed by shear-tension failure at sheet end
F-U57-1	Triaxial fabric (1 layer)	111 25.0)	18 (0.71)	115 (25.8)	21 (0.83)	1.17	0.58	Steel & fabric yield followed by yielding of the unstrengthened section of the beam

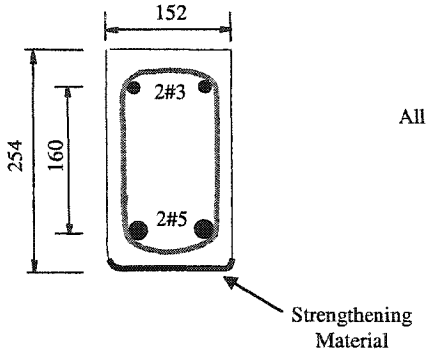

All dimensions in mm

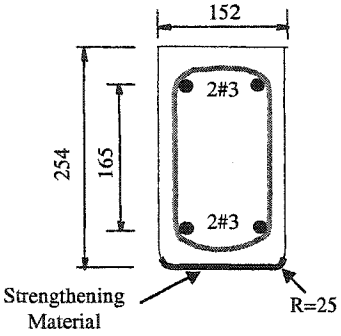

(a) Cross Section for Group C and Group E

(b) Cross Section for Group D

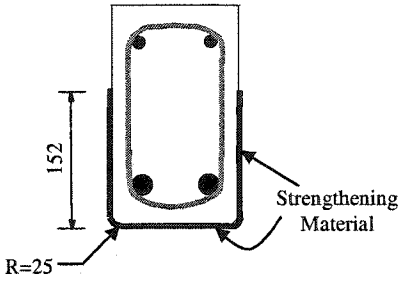

(c) U-Wrapping scheme

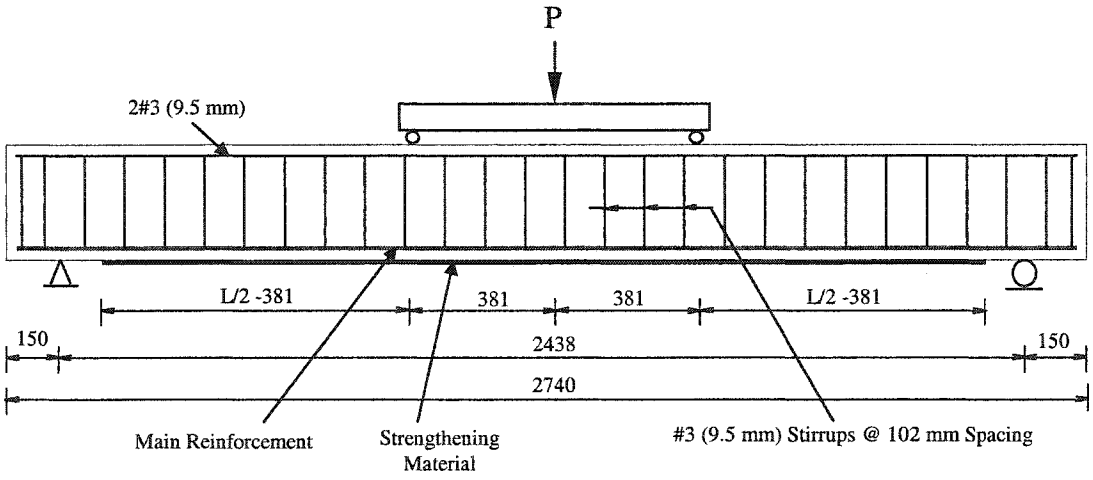

(d) Loading Set-up

Fig. 5.1 Details of test beams

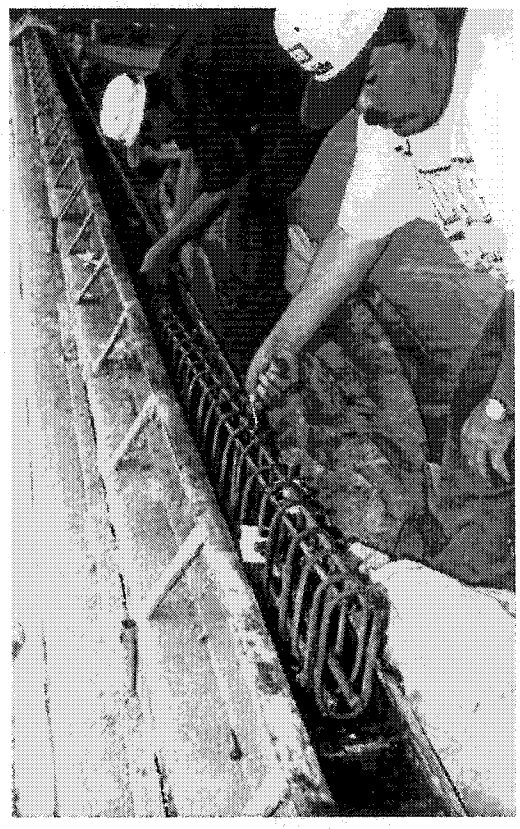

Fig. 5.2 Placing steel cages inside forms

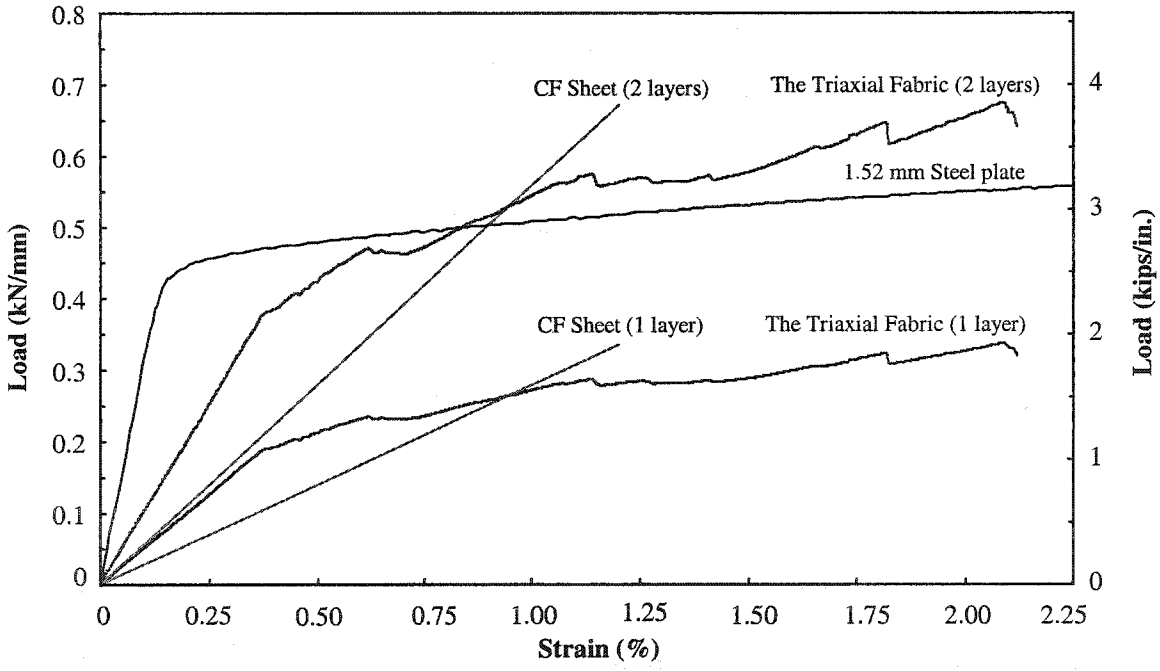

Fig. 5.3 Tensile properties of materials used

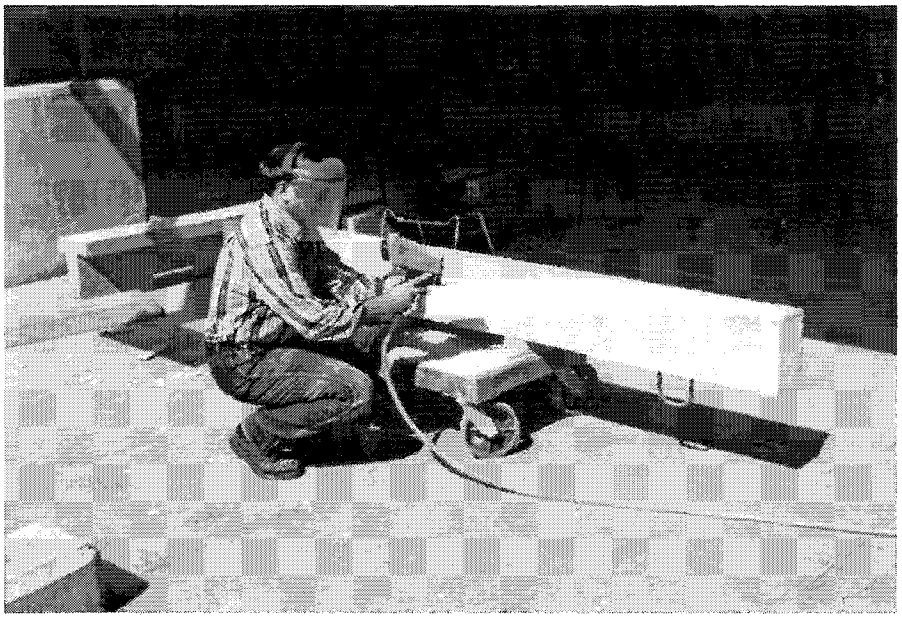

(a) Sand blasting

(b) Surface wiping

Fig. 5.4 Preparation of beam surface

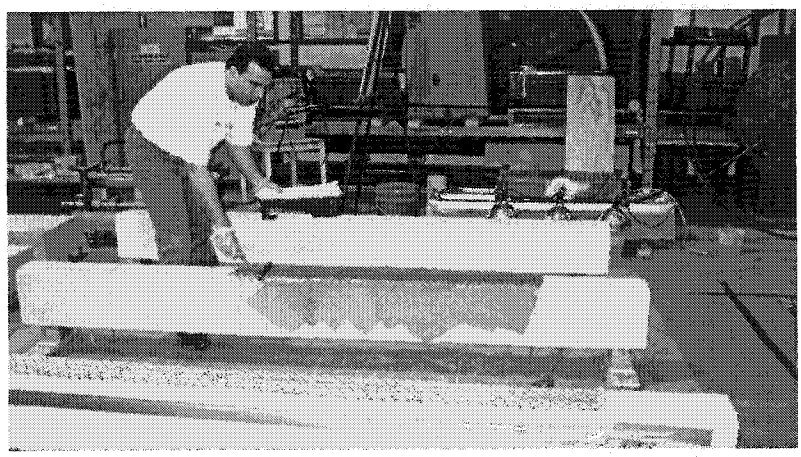

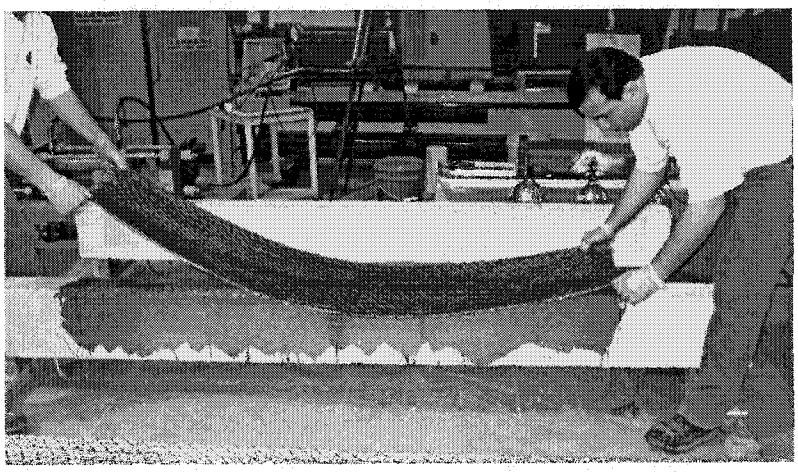

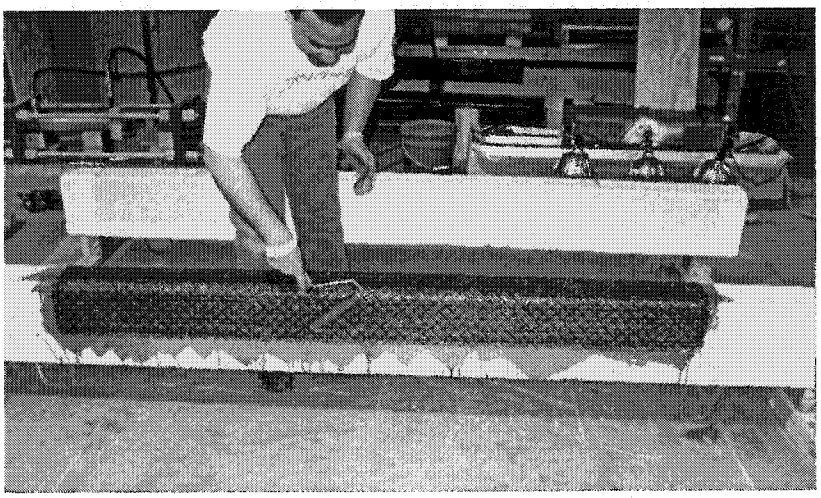

Fig. 5.5 Fabric installation procedures

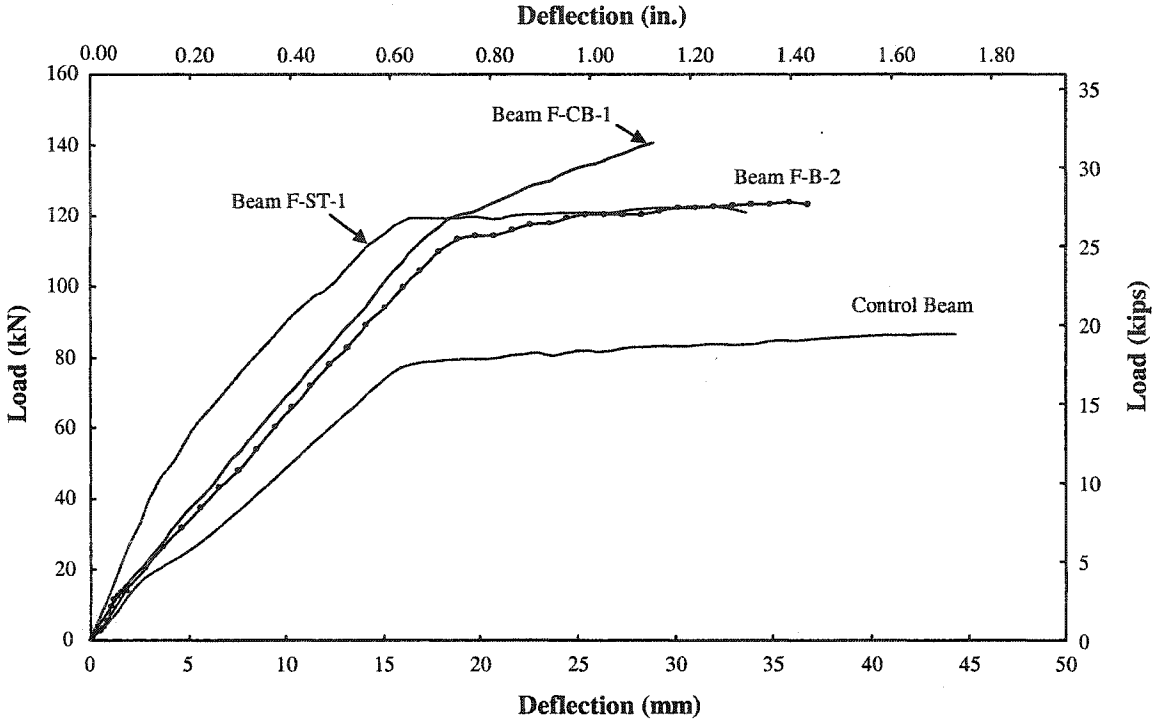

(a) Midspan deflection

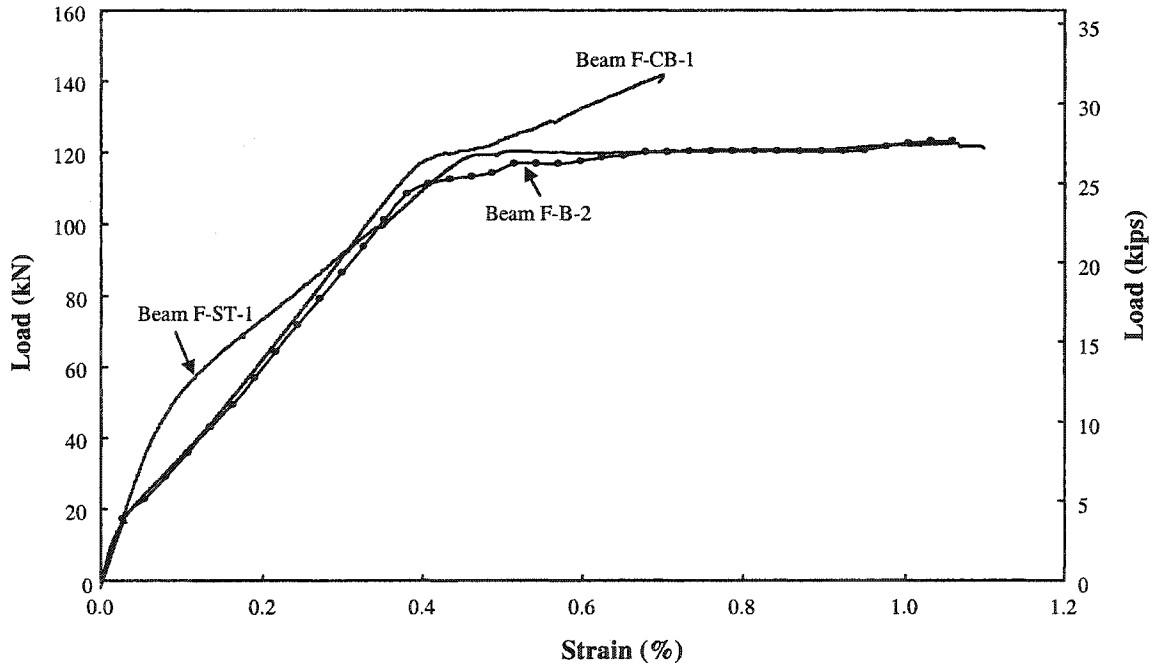

(b) Midspan FRP strain

Fig. 5.6 Behavior of group (C) beams strengthened at the bottom face only

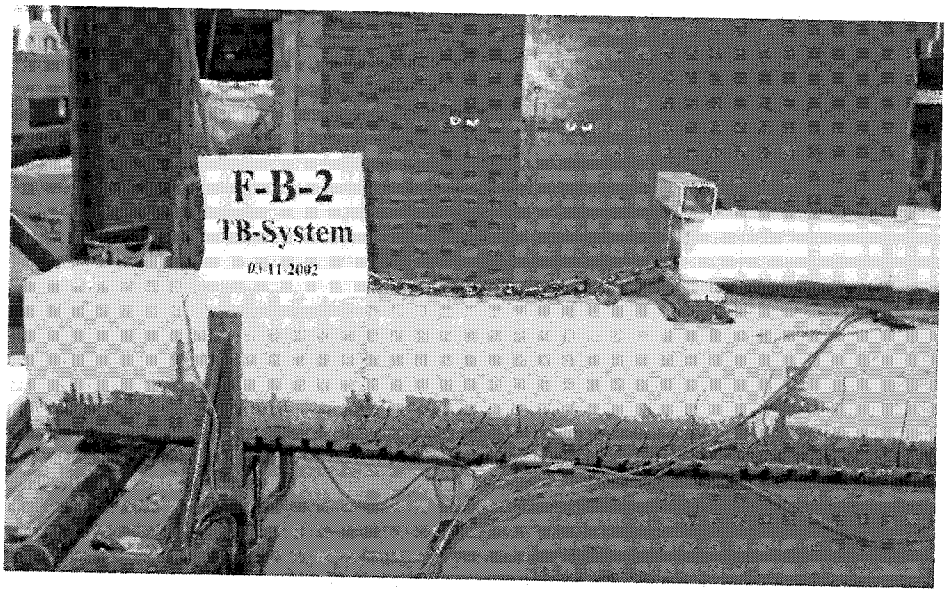

Fig. 5.7 Failure of beam F-B-2

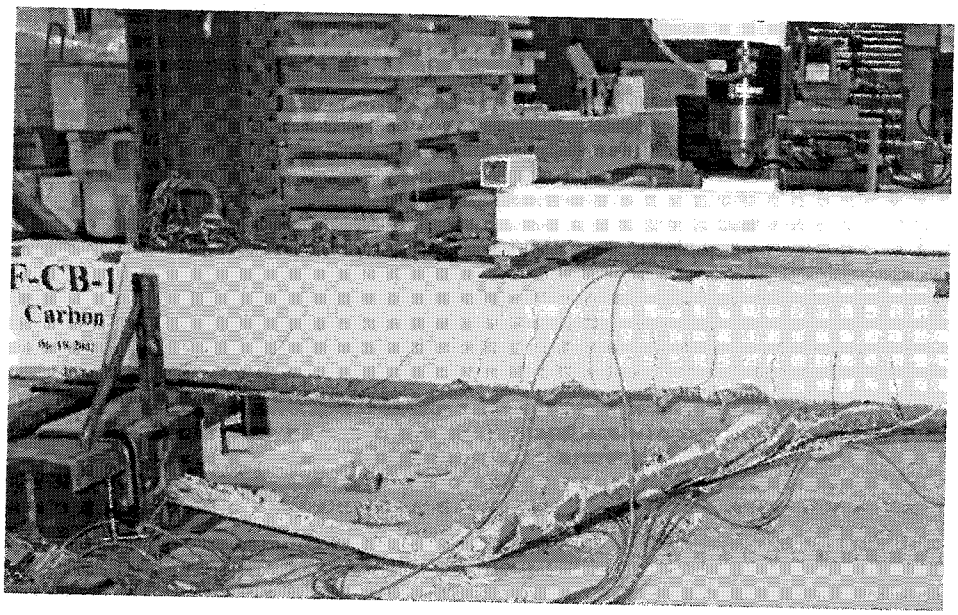

Fig. 5.8 Failure of beam F-CB-1

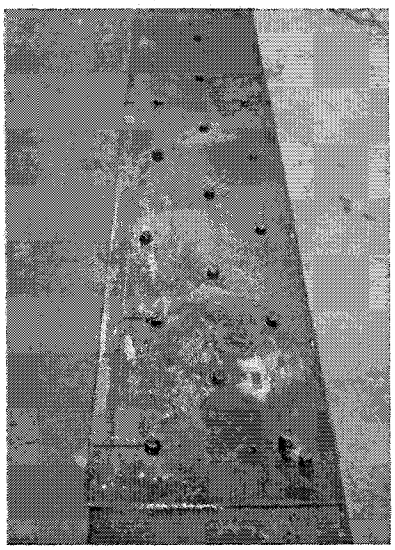

Fig. 5.9 Anchoring of the steel plate of beam F-ST-1 using steel screws

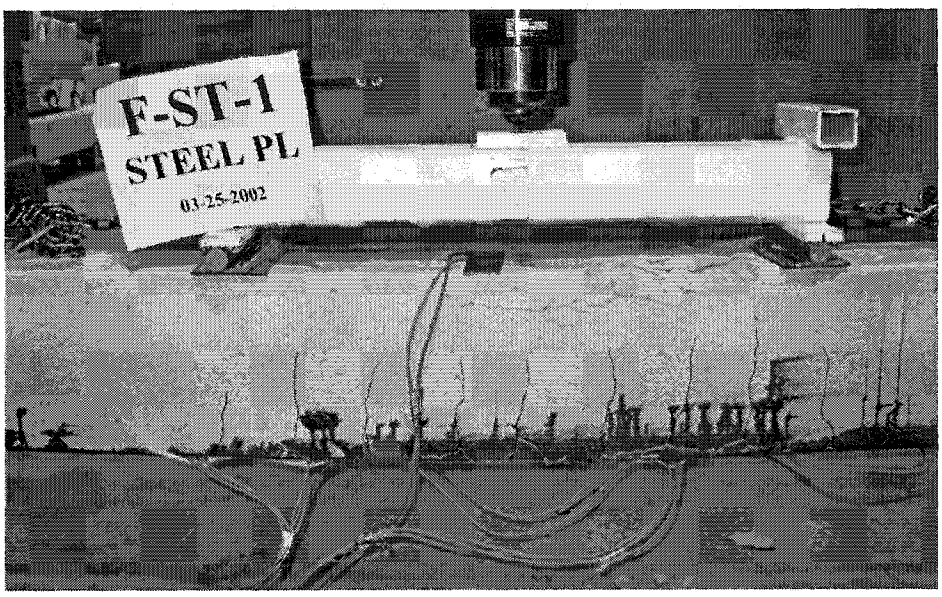

Fig. 5.10 Failure of beam F-ST-1

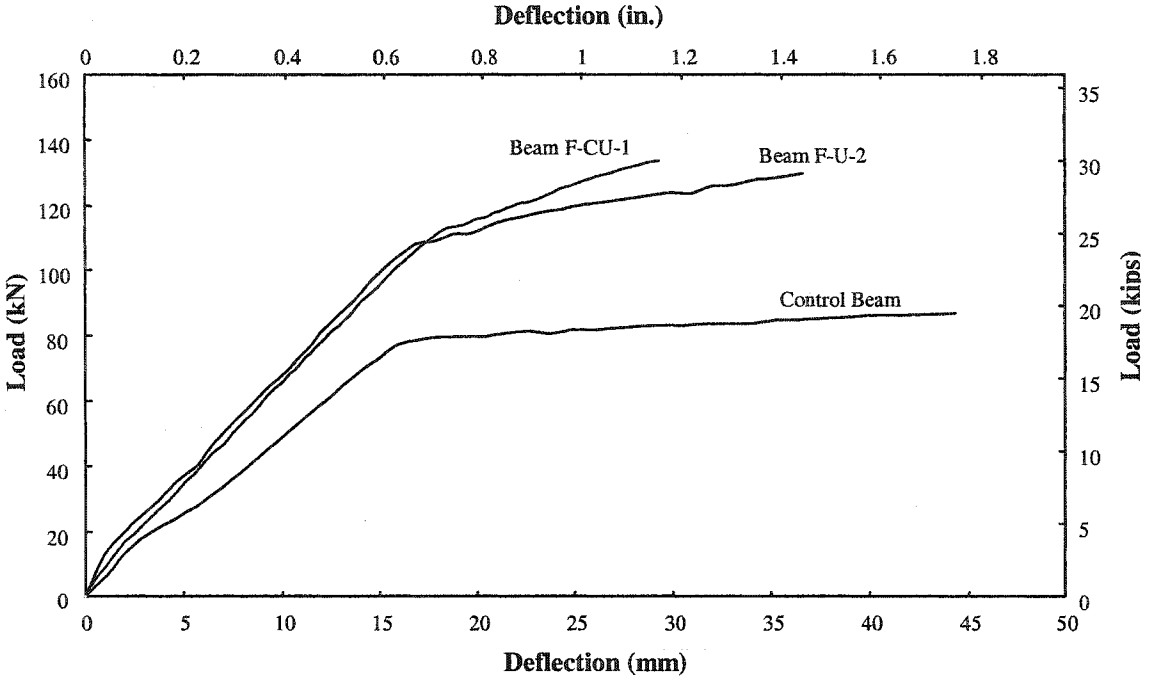

(a) Midspan deflection

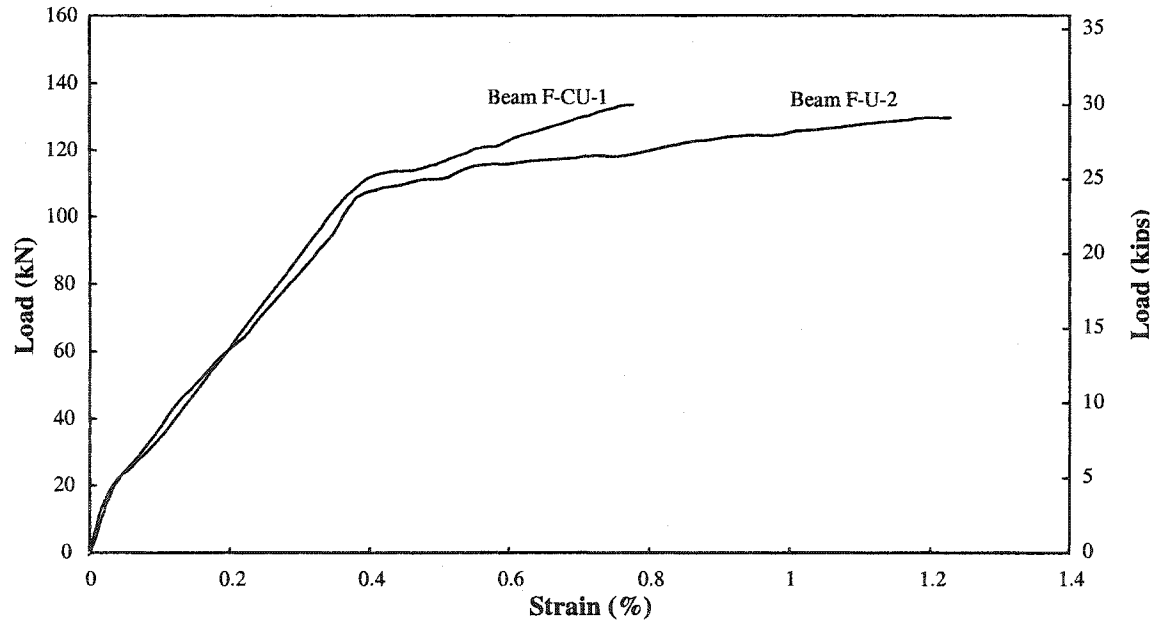

(b) Midspan FRP strain

Fig. 5.11 Behavior of group (C) beams with U-wrap scheme

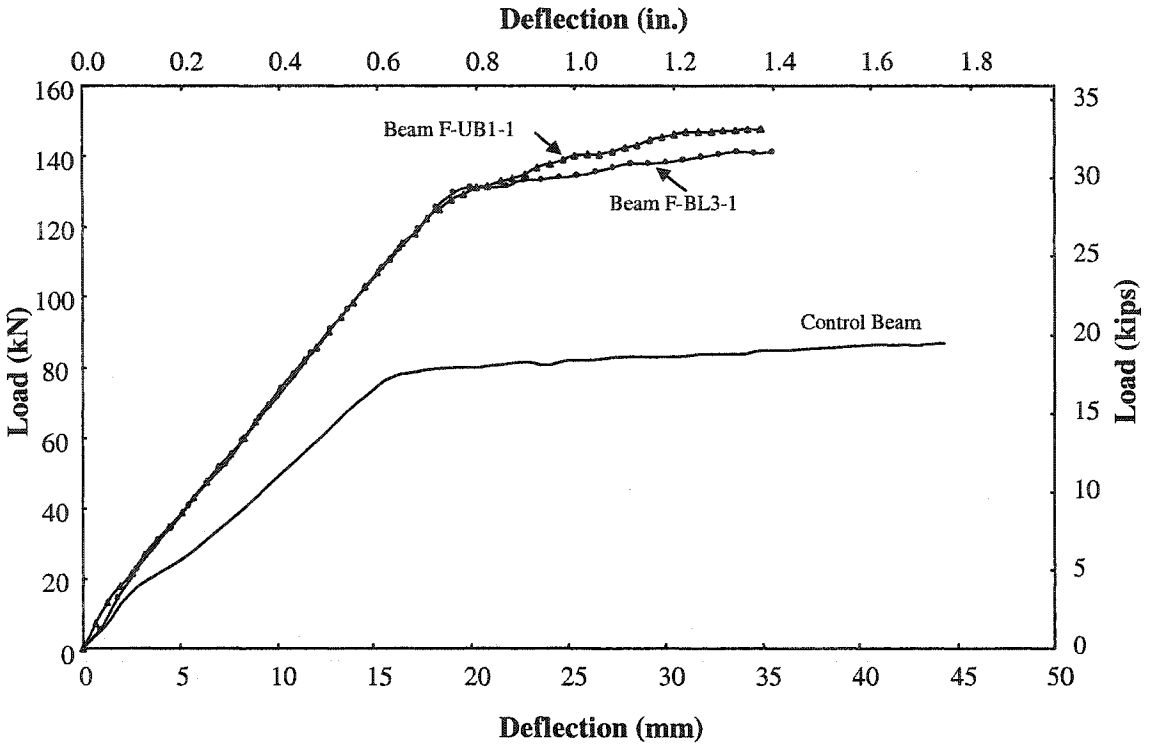

(a) Midspan deflection

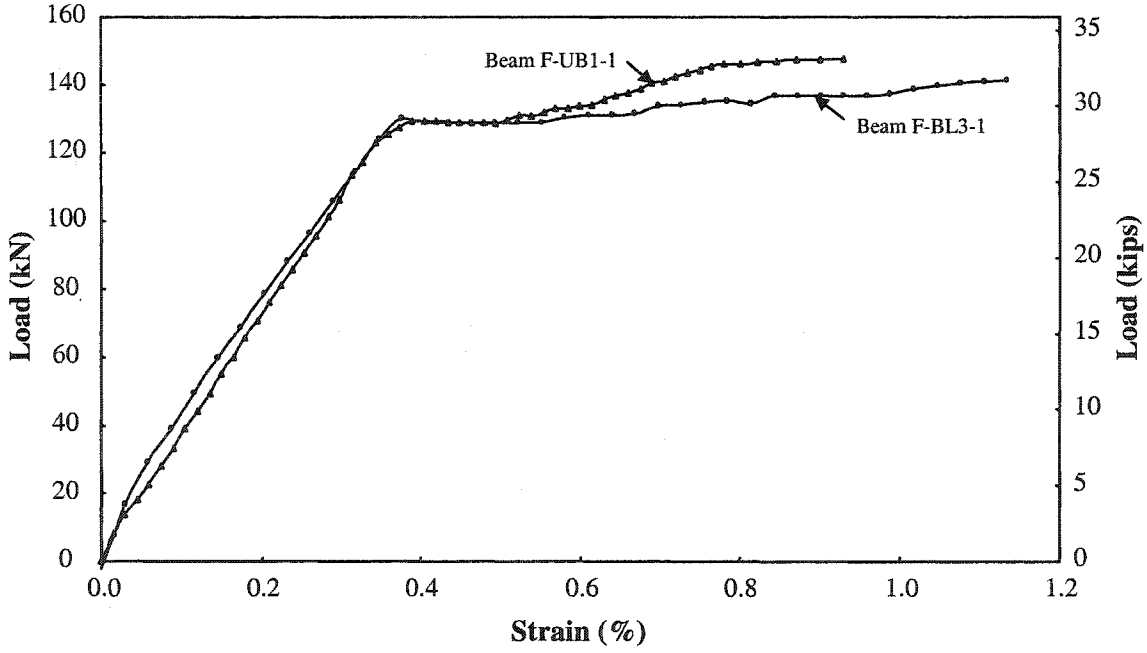

(b) Midspan FRP strain

Fig. 5.12 Behavior of Beam F-BL3-1 and Beam F-UB1-1

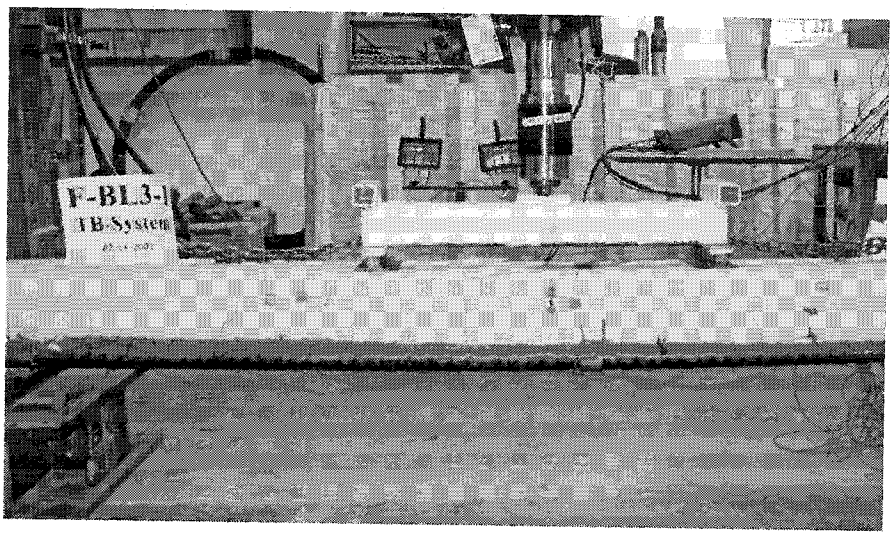

Fig. 5.13 Failure of beam F-BL3-1

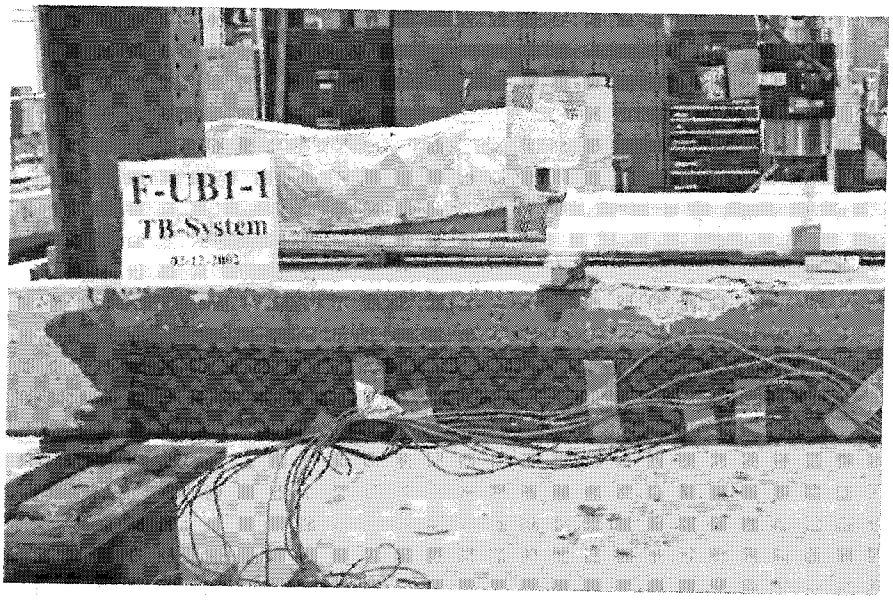

Fig. 5.14 Failure of beam F-UB1-1

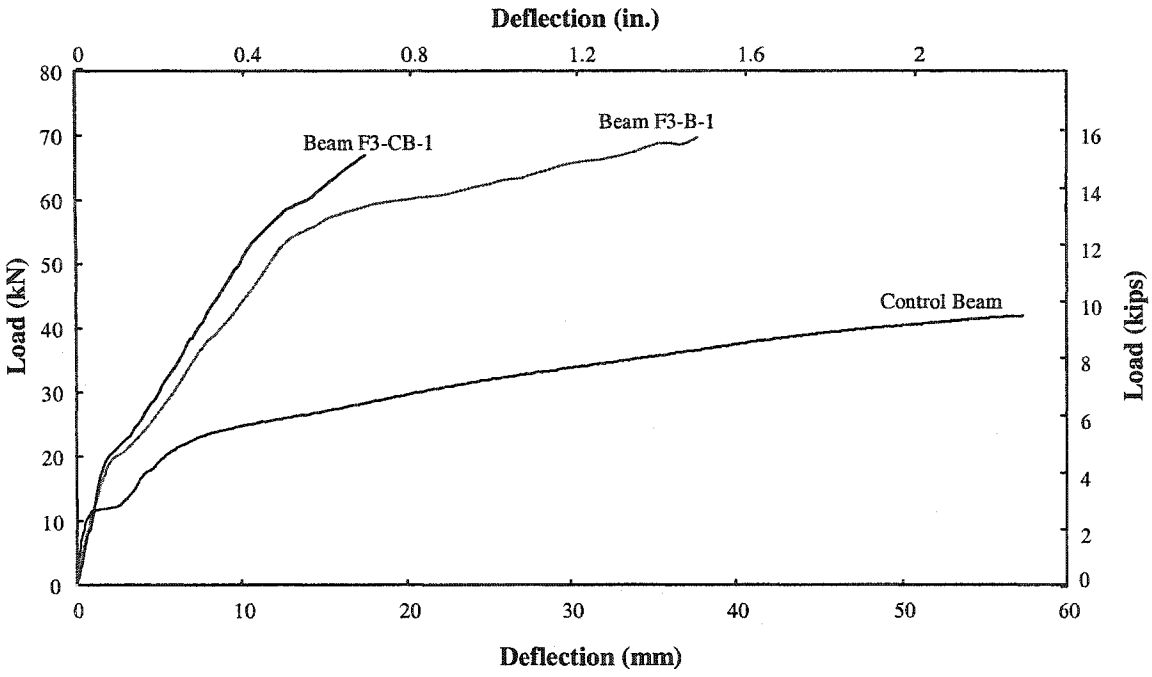

(a) Midspan deflection

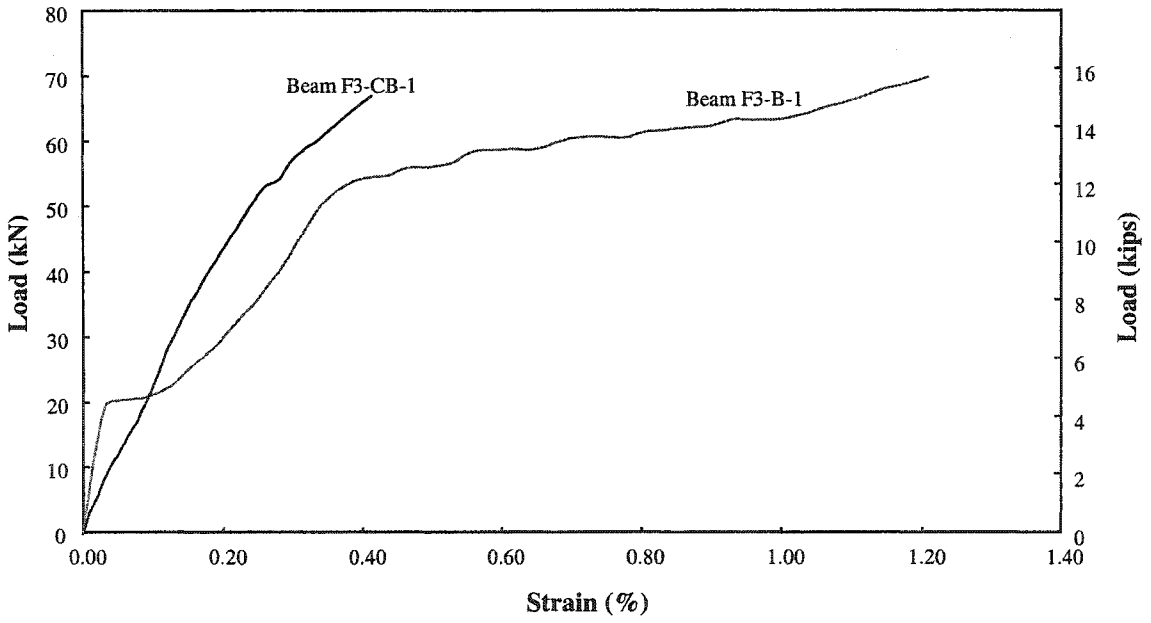

(b) Midspan FRP strain

Fig. 5.15 Behavior of group (D) beams strengthened at the bottom faces only

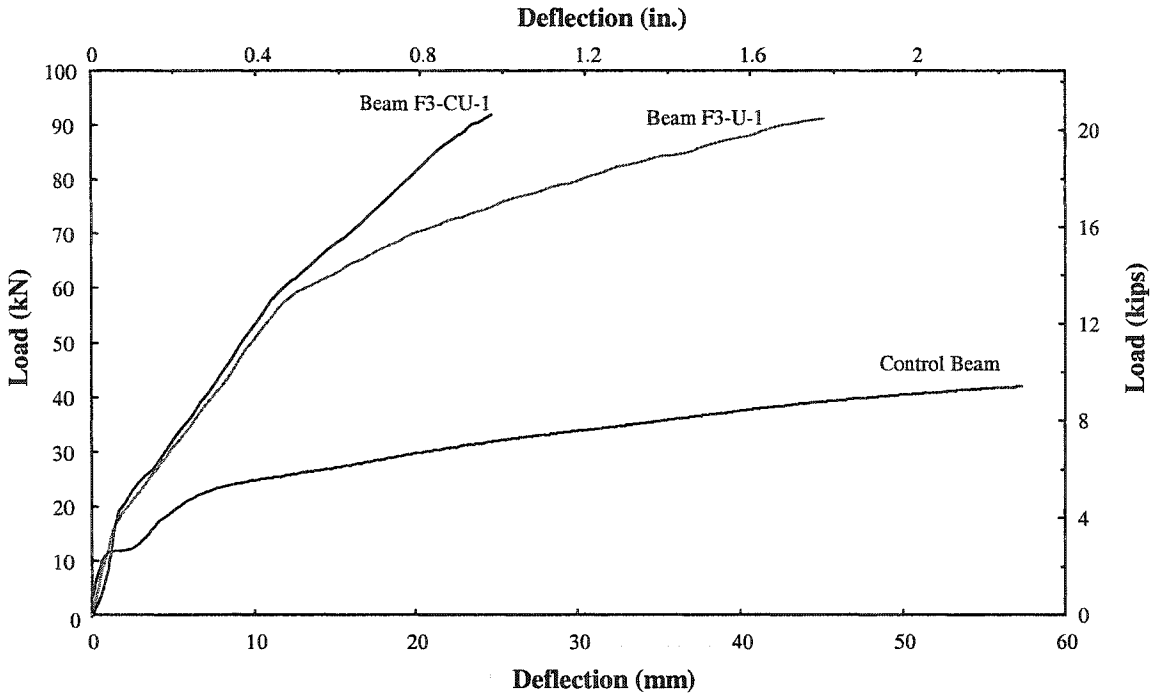

(a) Midspan deflection

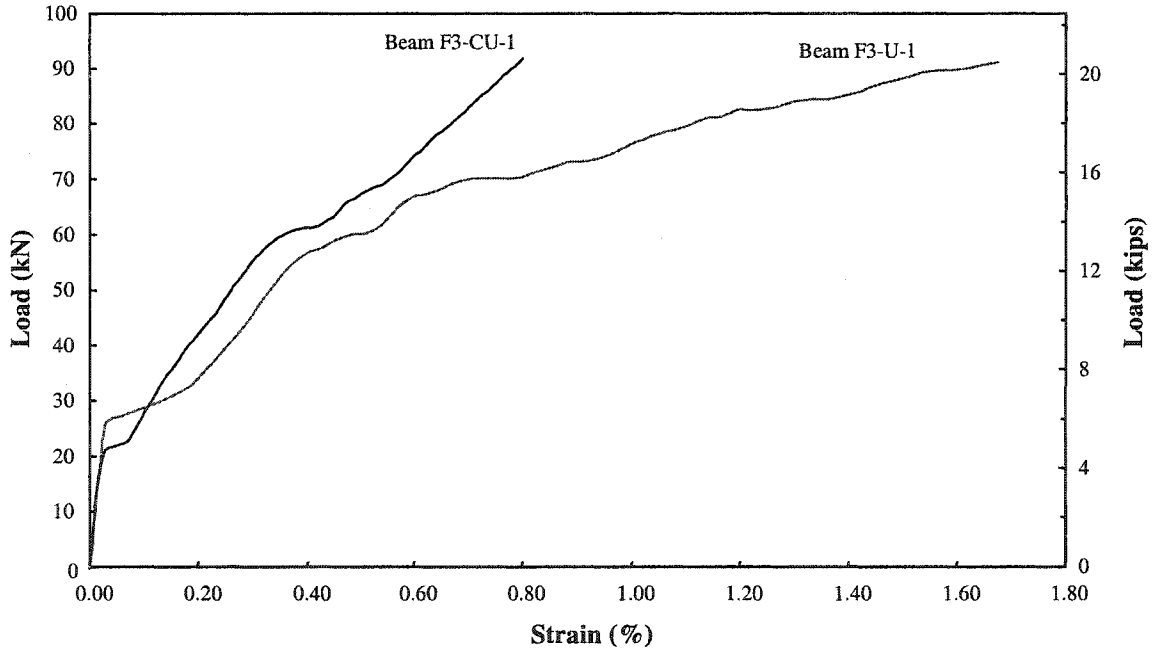

(b) Midspan FRP strain

Fig. 5.16 Behavior of group (D) beams with U-wrap scheme

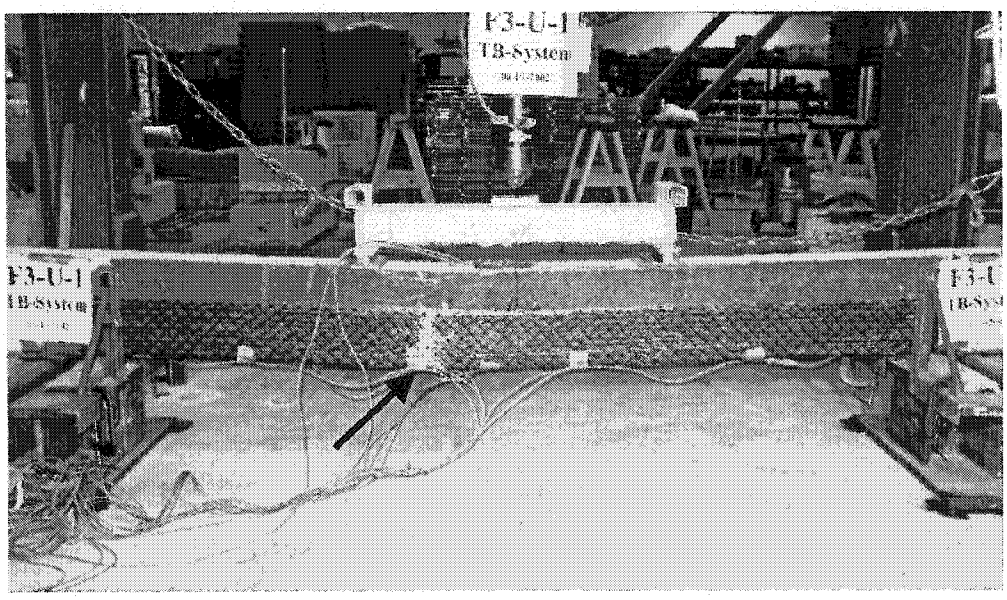

(a) Beam F3-U-1 (fabric rupture)

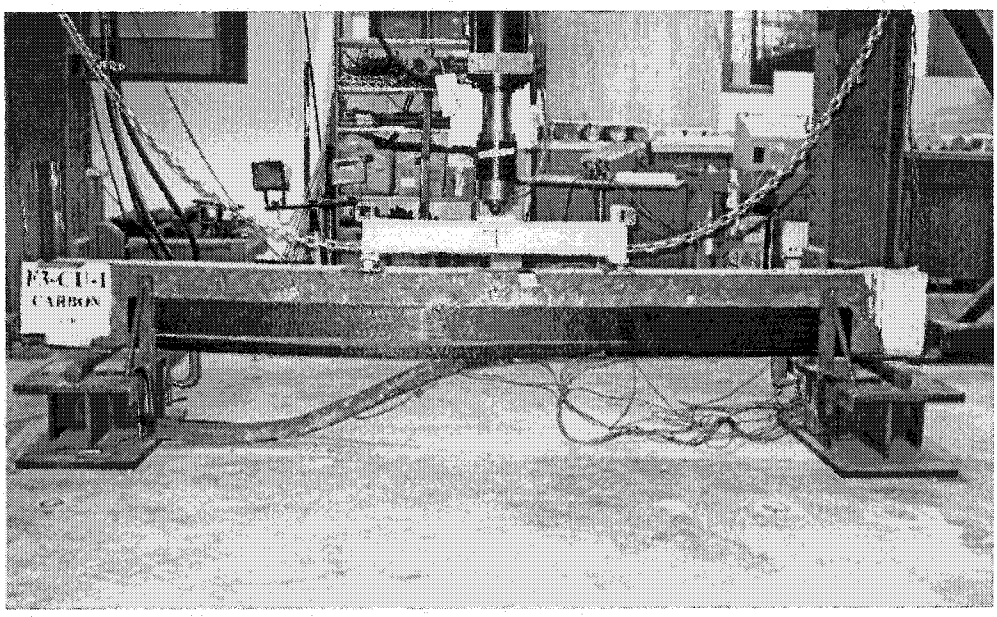

(b) Beam F3-CU-1 (sheet debonding)

Fig. 5.17 Beams F3-U-1 and F3-CU-1 at failure

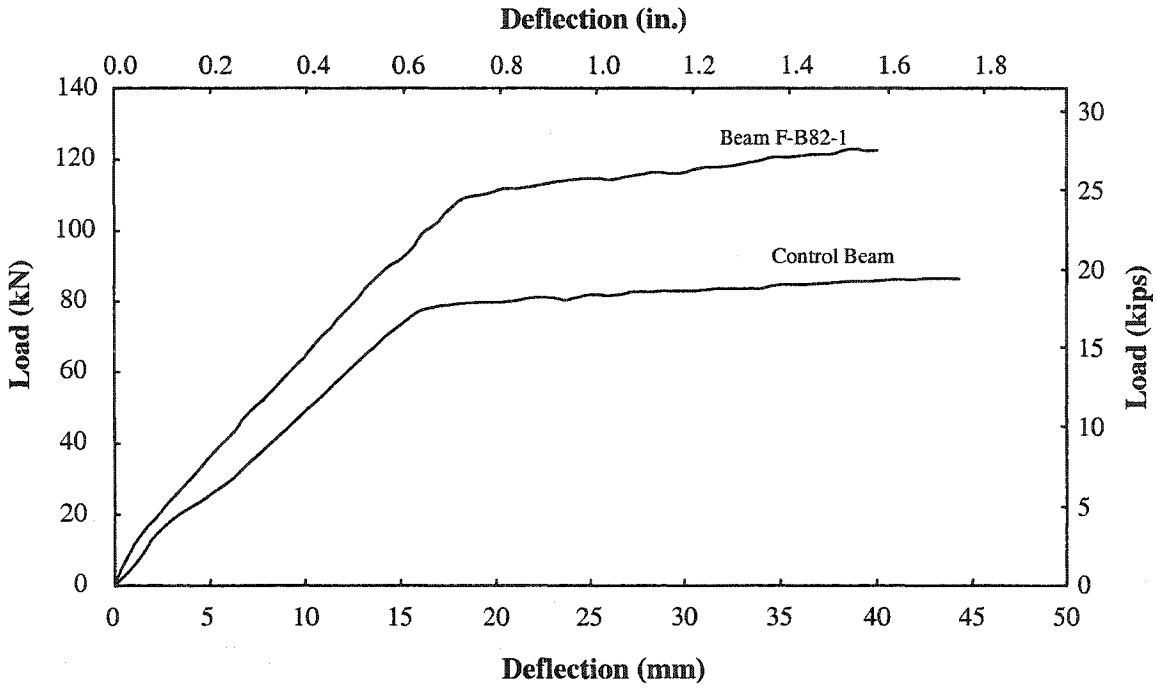

(a) Midspan deflection

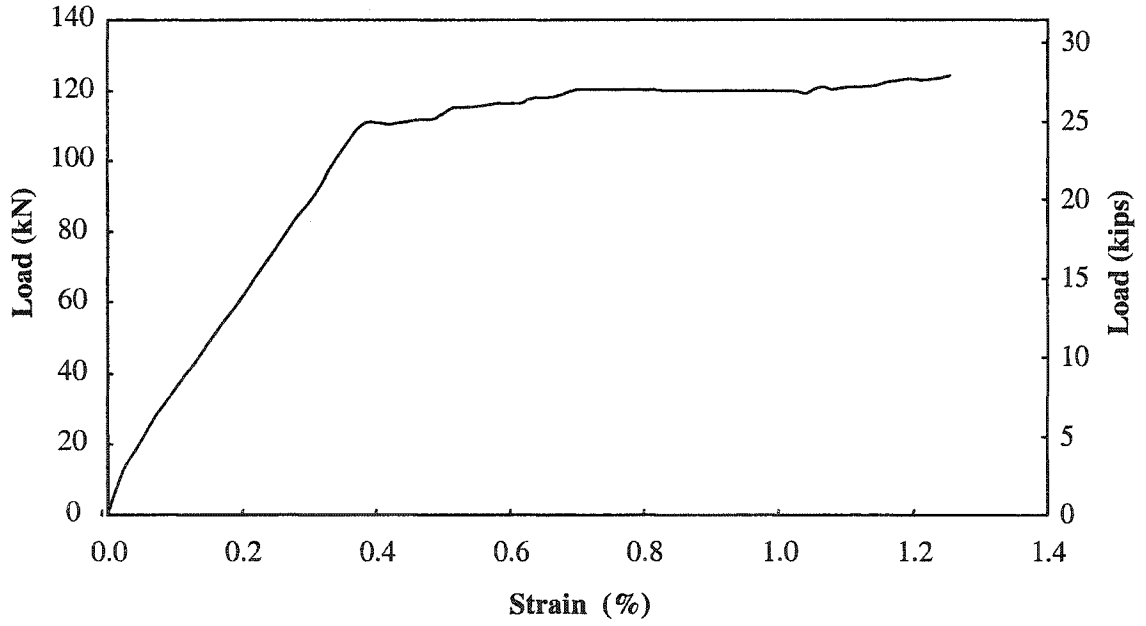

(b) Midspan FRP strain

Fig. 5.18 Behavior of beam F-B82-1

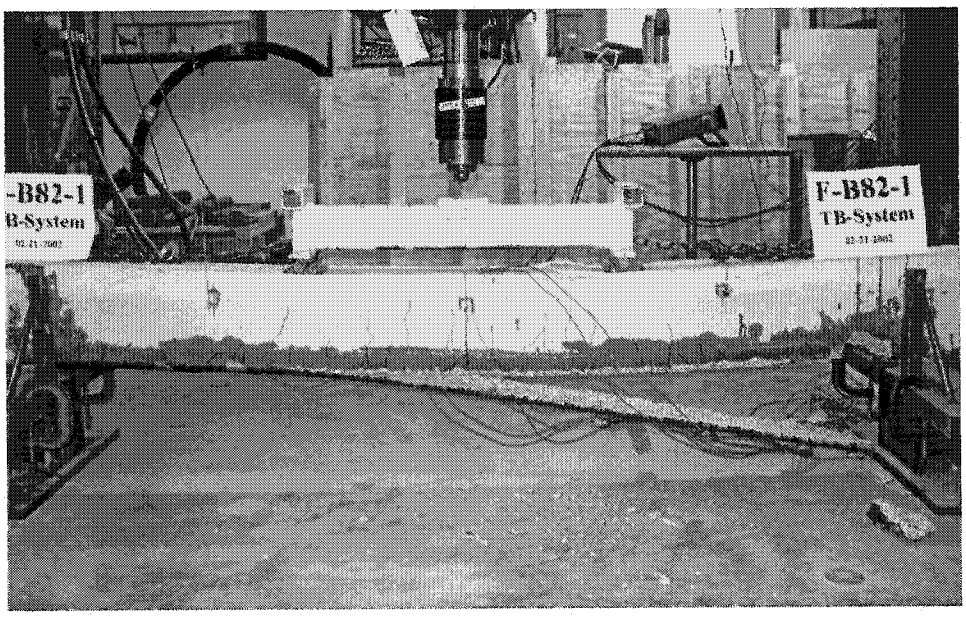

(a) Overall view of the beam

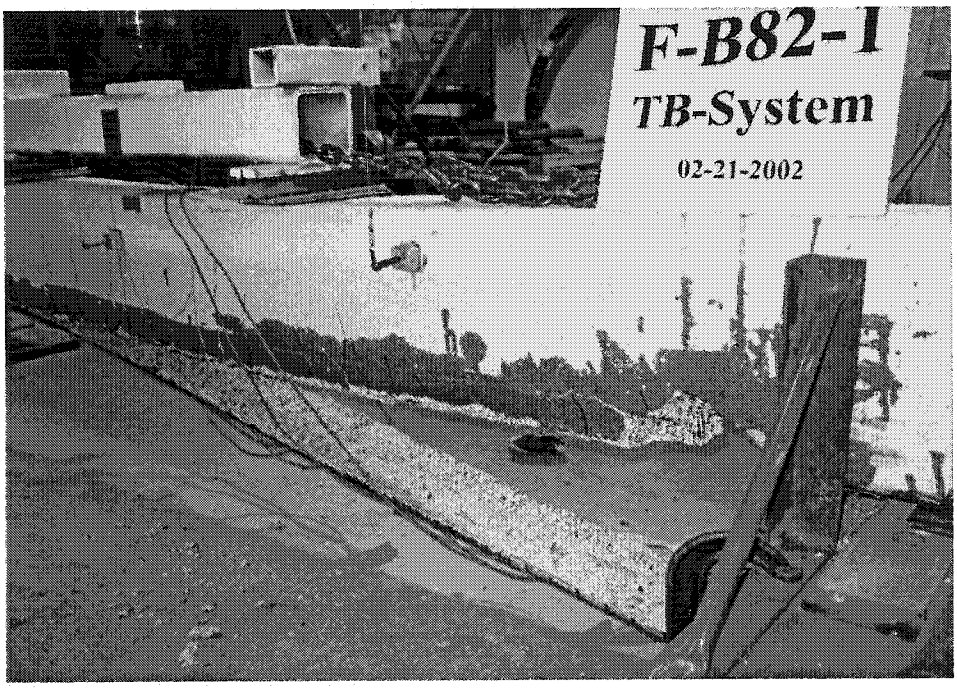

(b) Close up view of the debonded area

Fig. 5.19 Beam F-B82-1 at failure

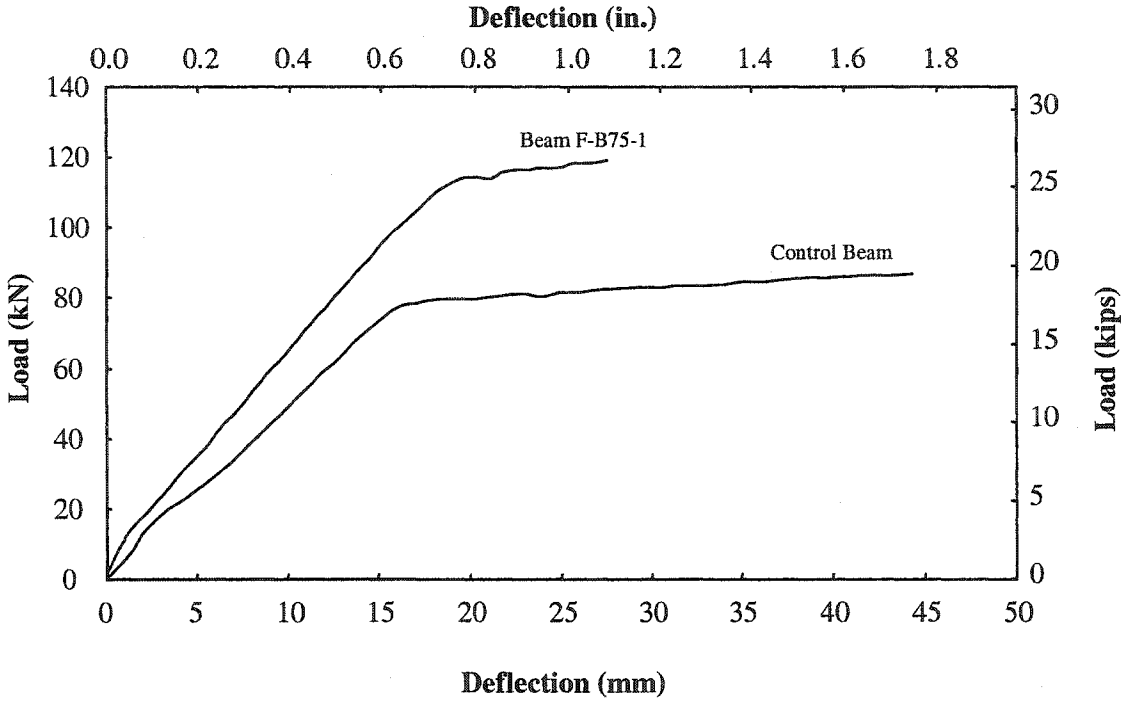

(a) Midspan deflection

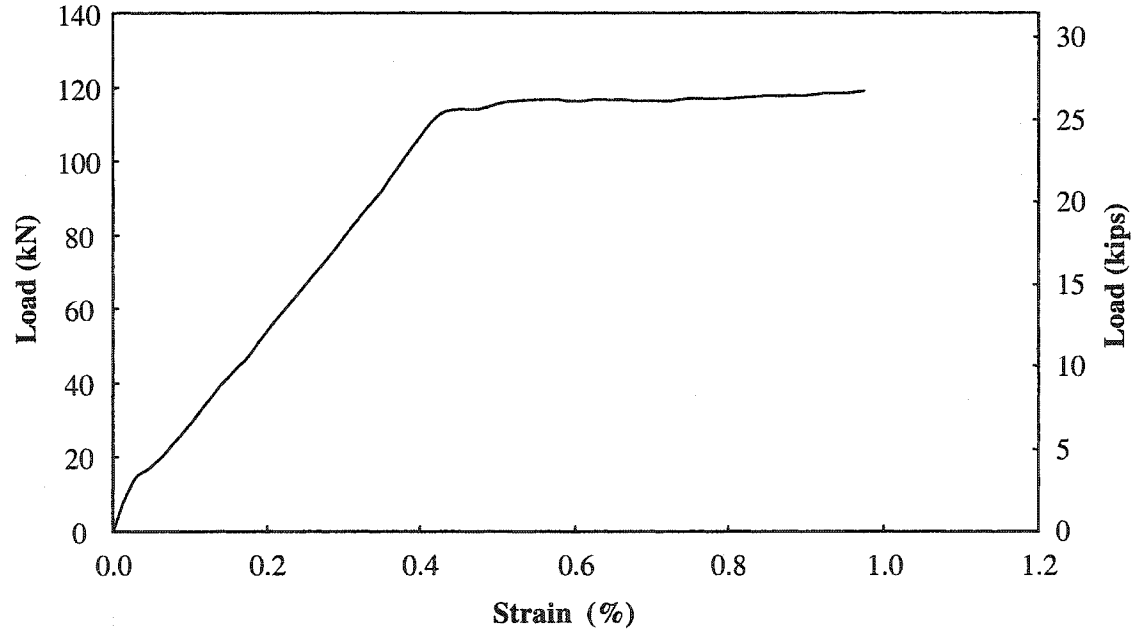

(b) Midspan FRP strain

Fig. 5.20 Behavior of beam F-B75-1

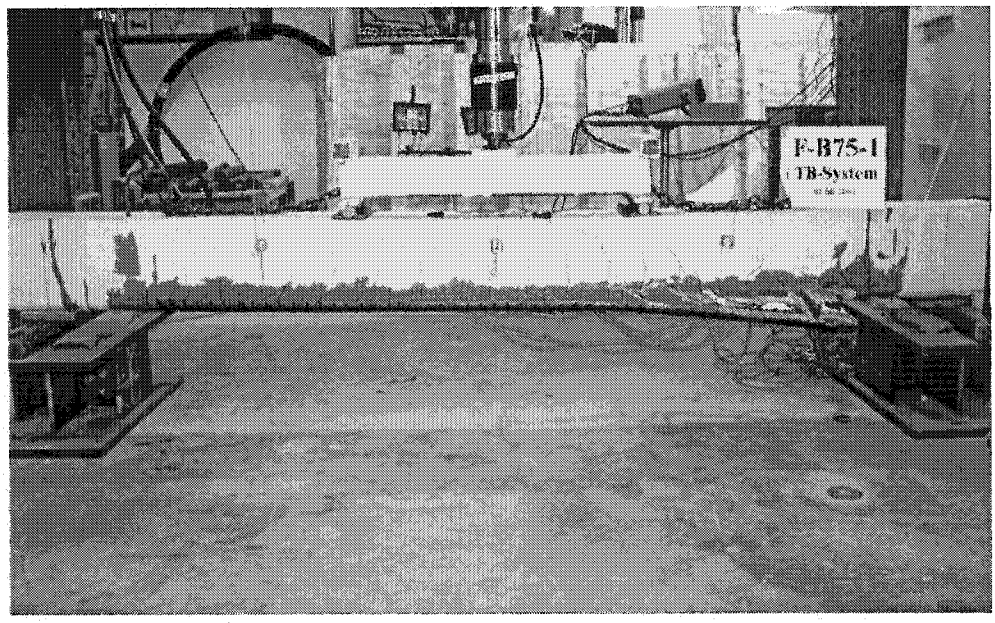

(a) Overall view of the beam

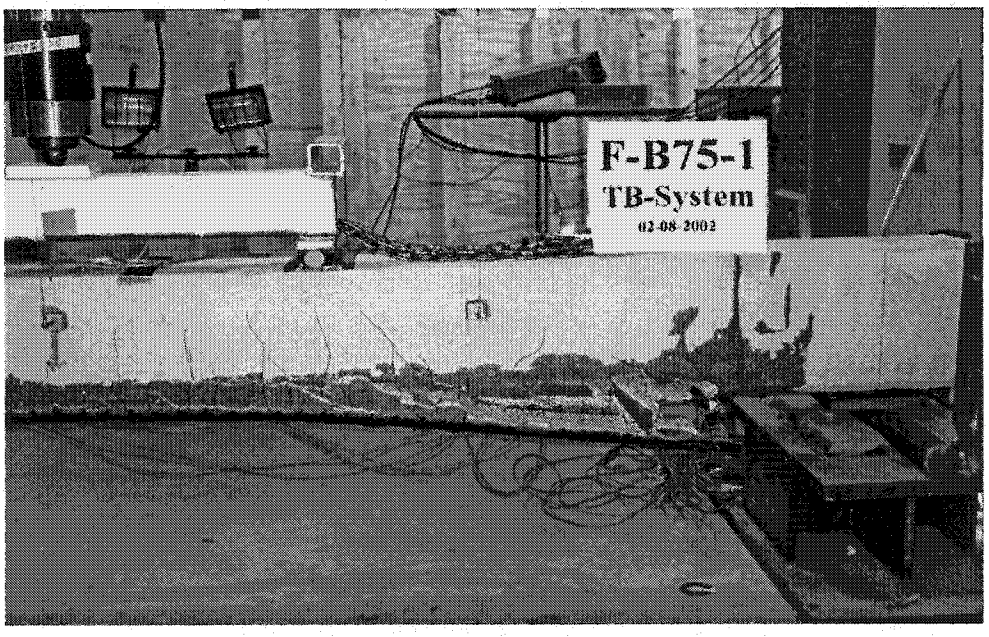

(b) Close up view of the failure

Fig. 5.21 Beam F-B75-1 at failure

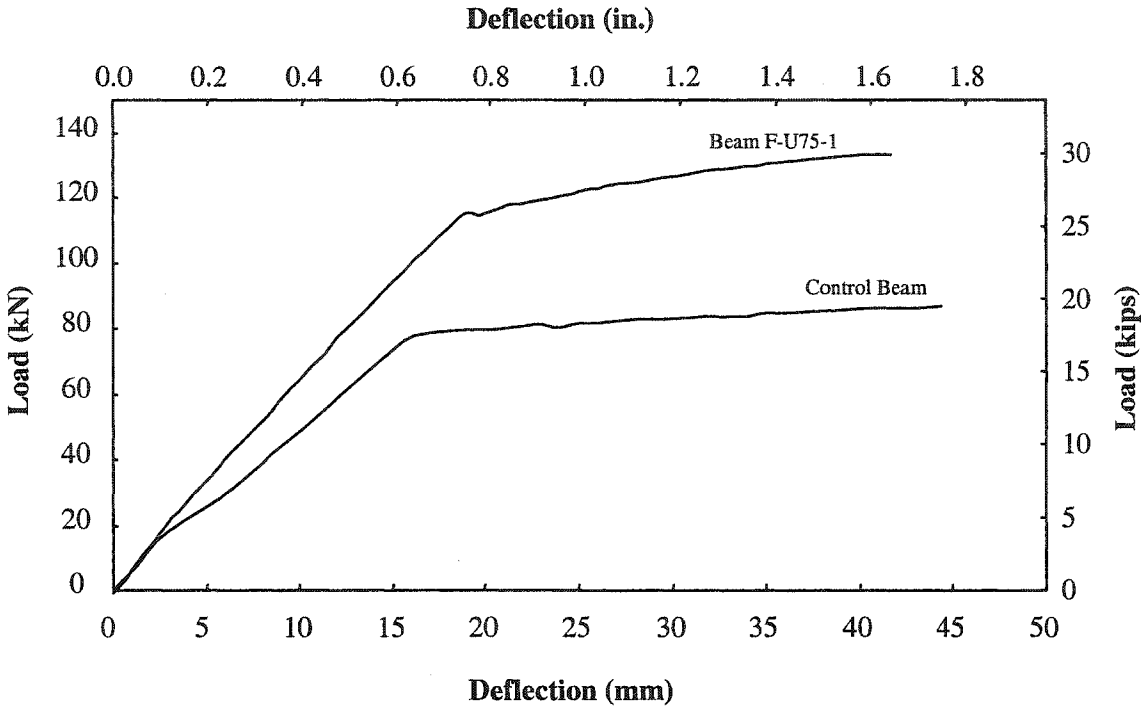

(a) Midspan deflection

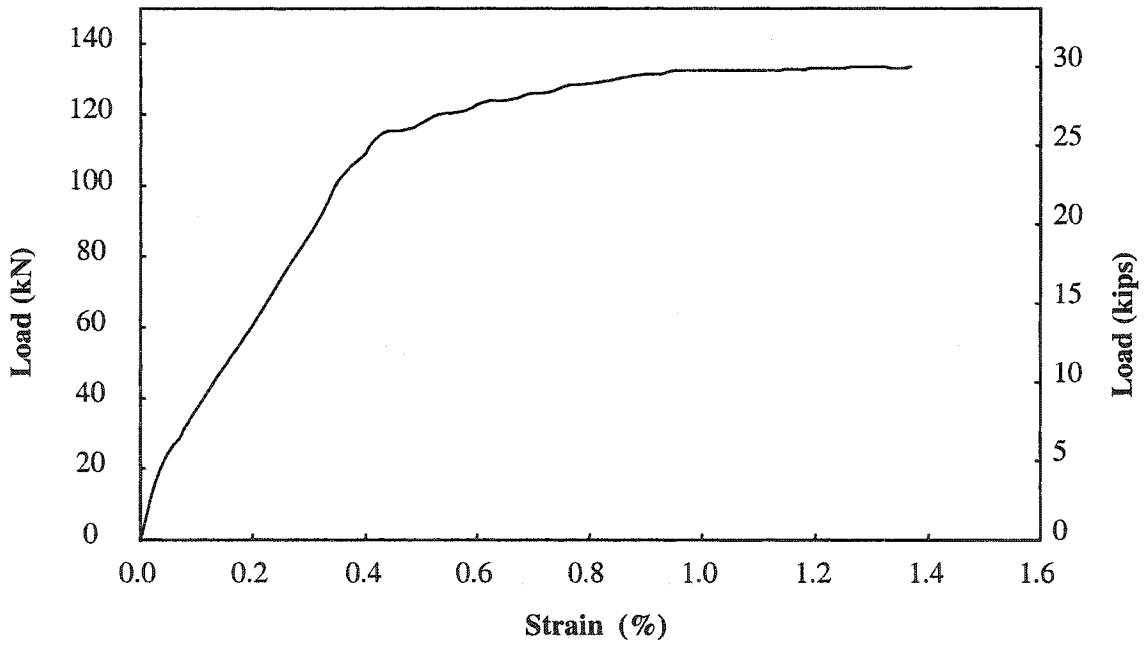

(b) Midspan FRP strain

Fig. 5.22 Behavior of beam F-U75-1

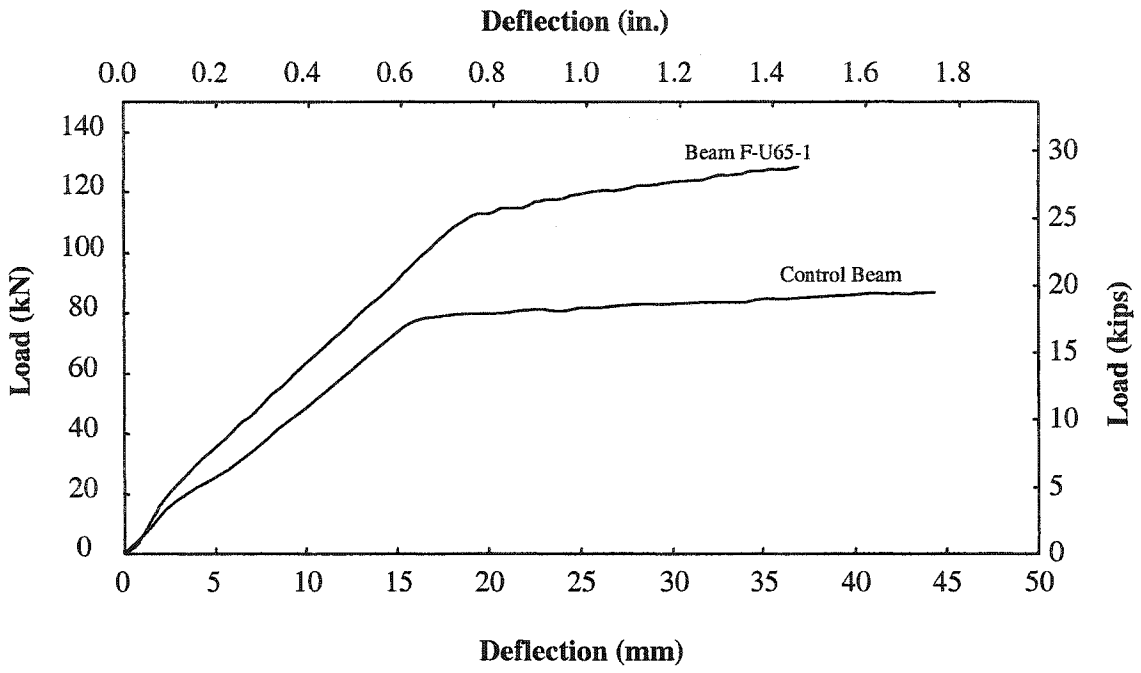

(a) Midspan deflection

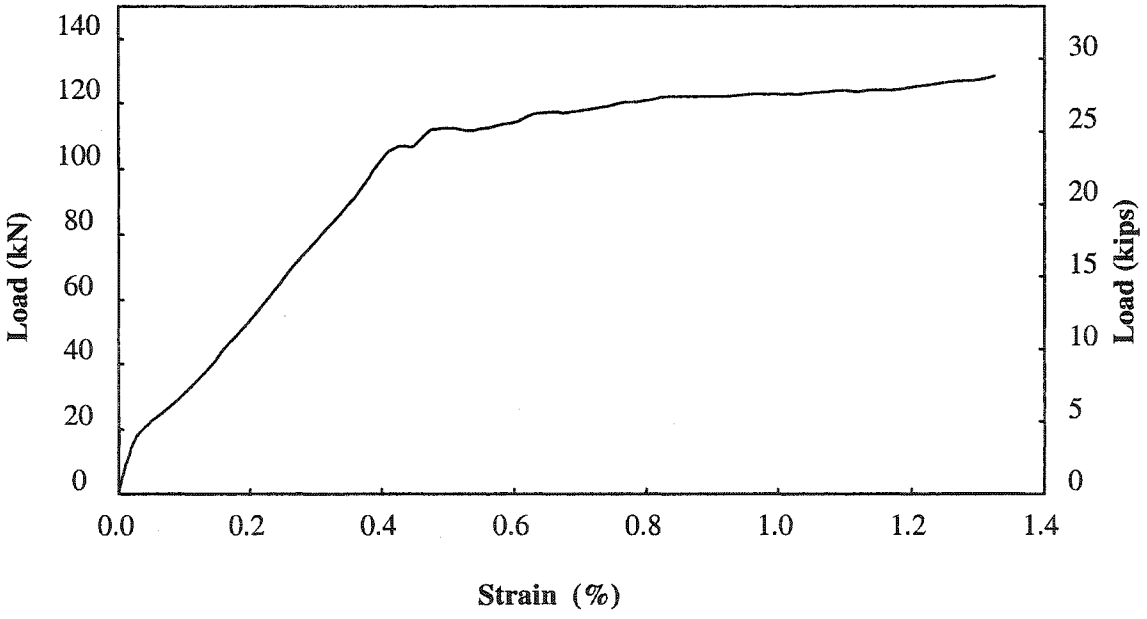

(b) Midspan FRP strain

Fig. 5.23 Behavior of beam F-U65-1

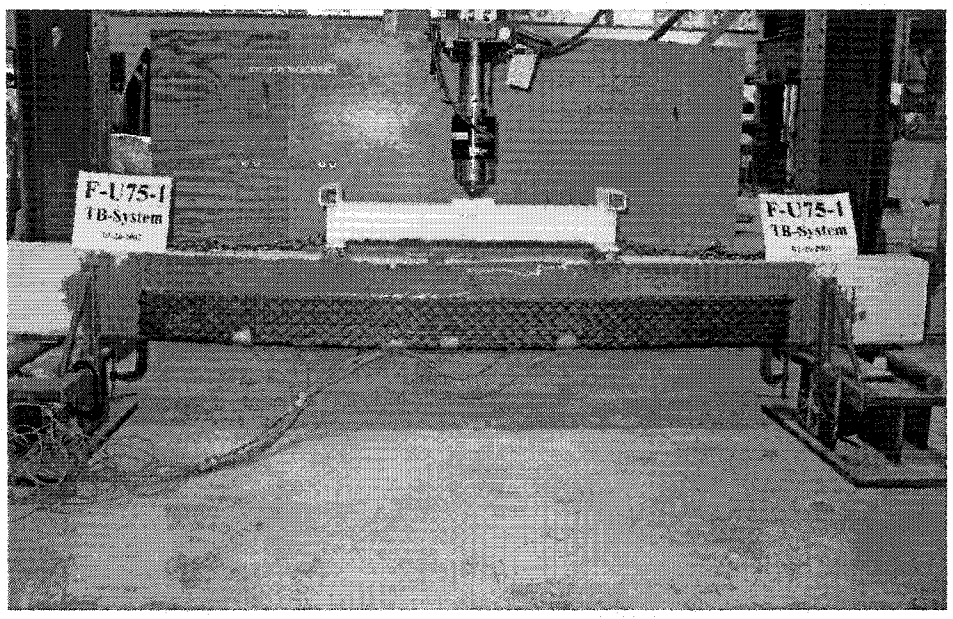

Fig. 5.24 Failure of beam F-U75-1

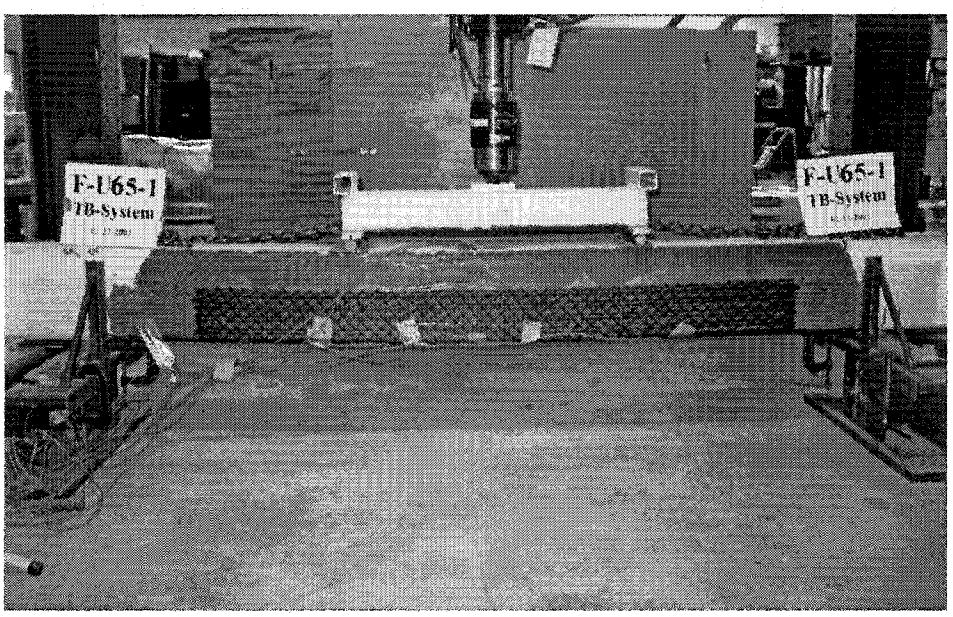

Fig. 5.25 Failure of beam F-U65-1

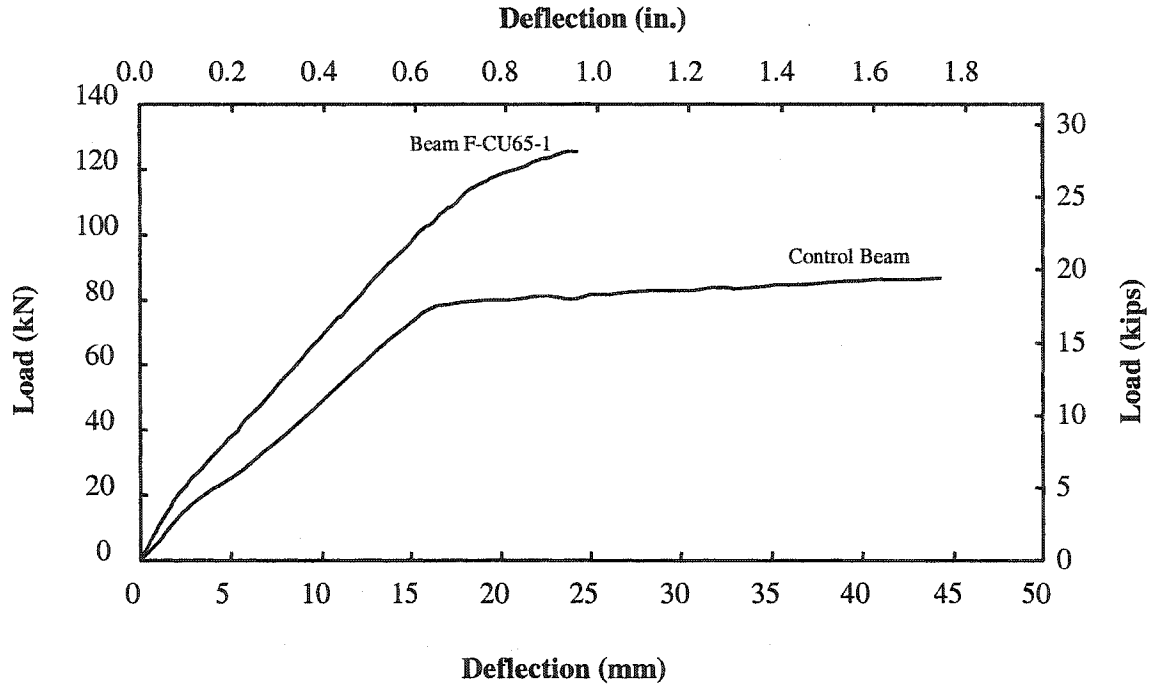

(a) Midspan deflection

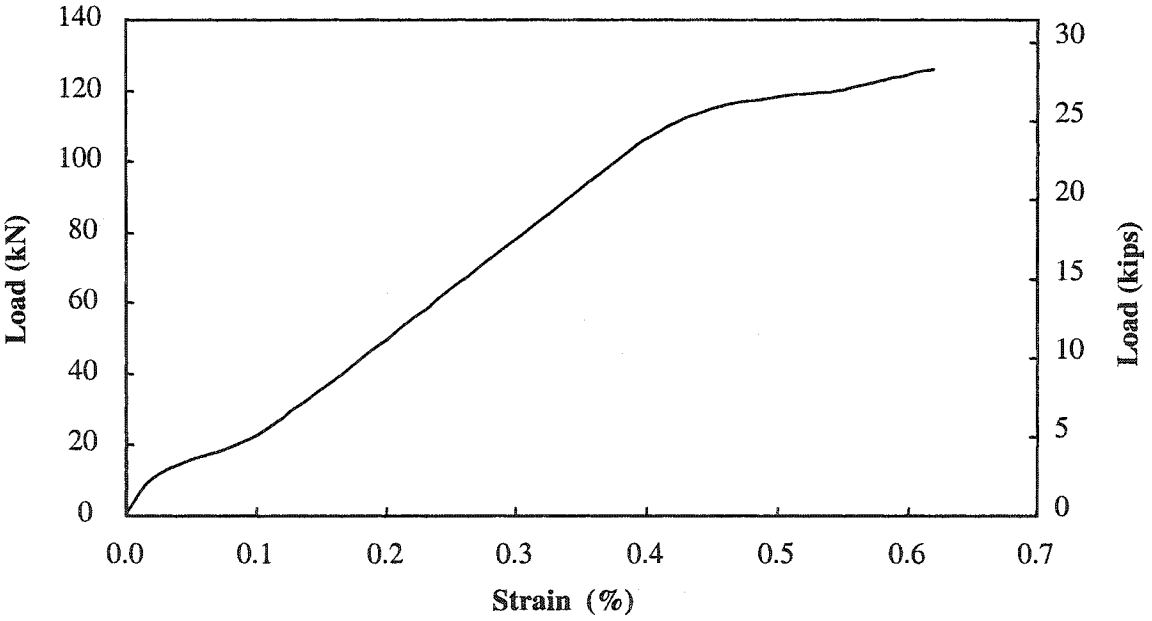

(b) Midspan FRP strain

Fig. 5.26 Behavior of beam F-CU65-1

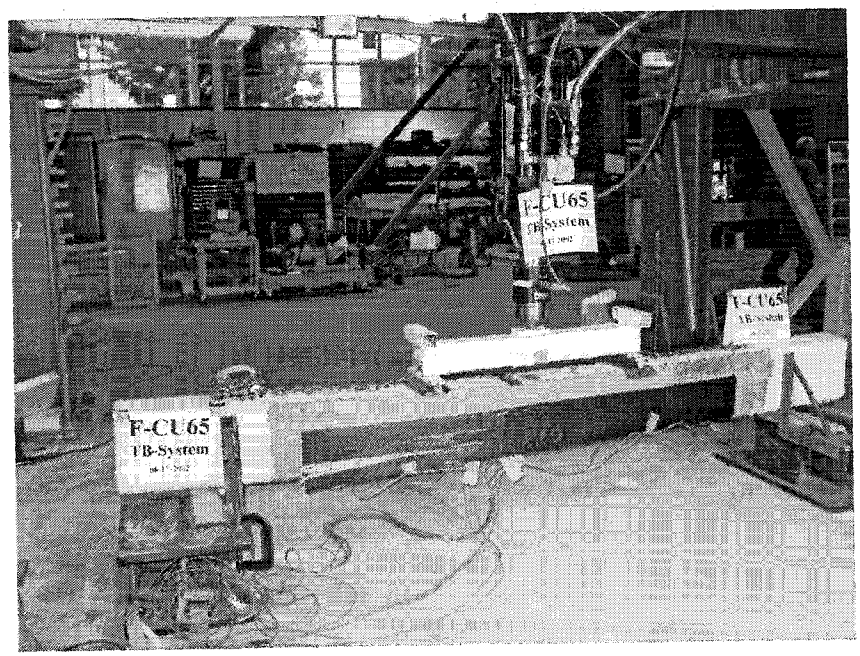

(a) Overall view of the beam

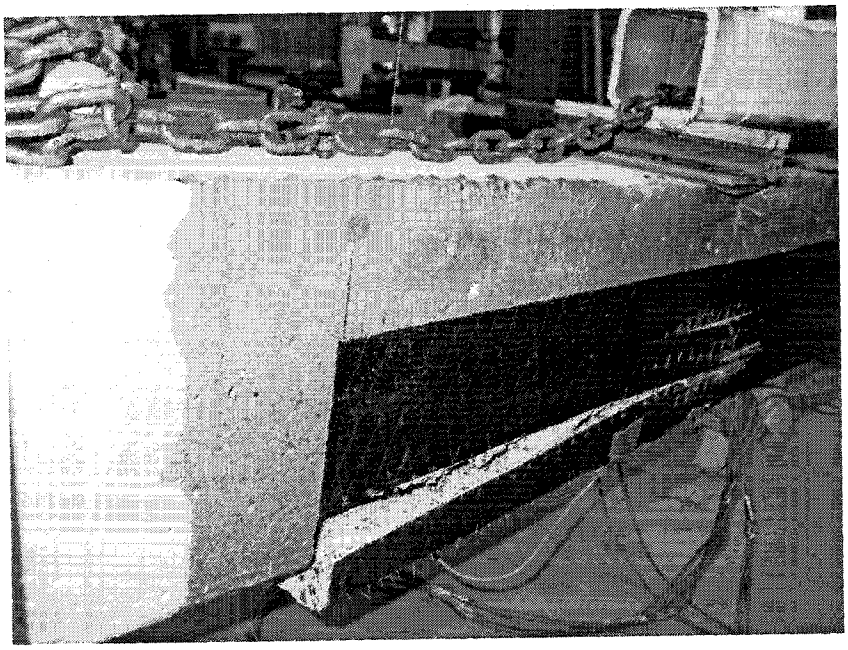

(b) Close up view of the shear-tension failure

Fig. 5.27 Failure of beam F-CU65-1

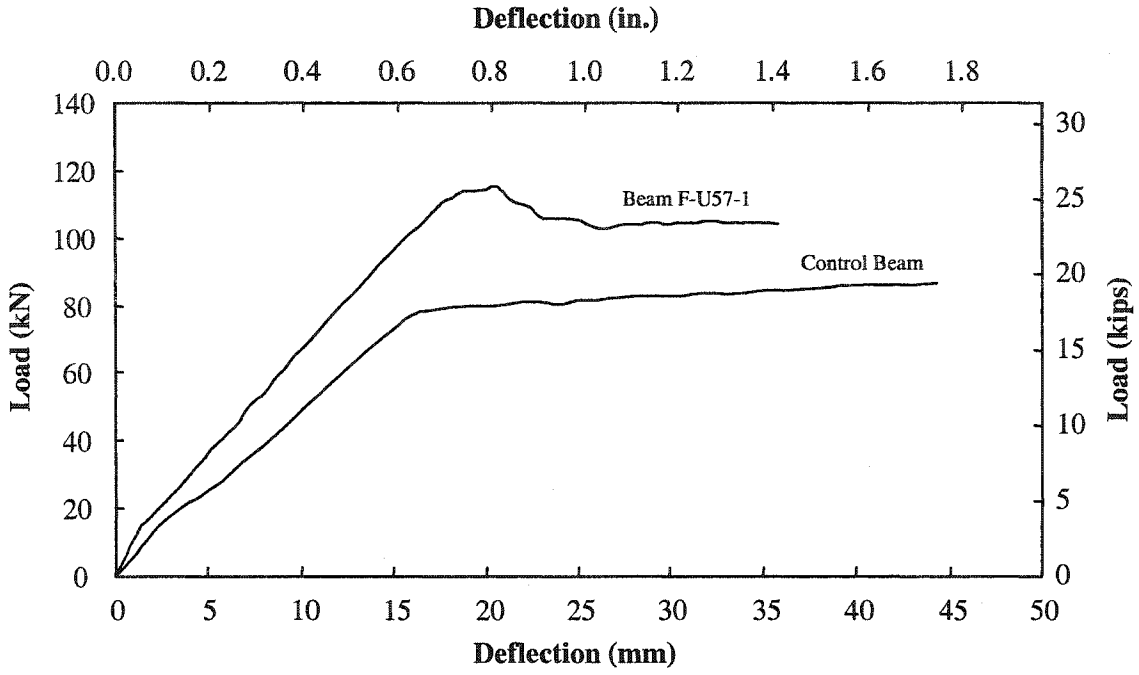

(a) Midspan deflection

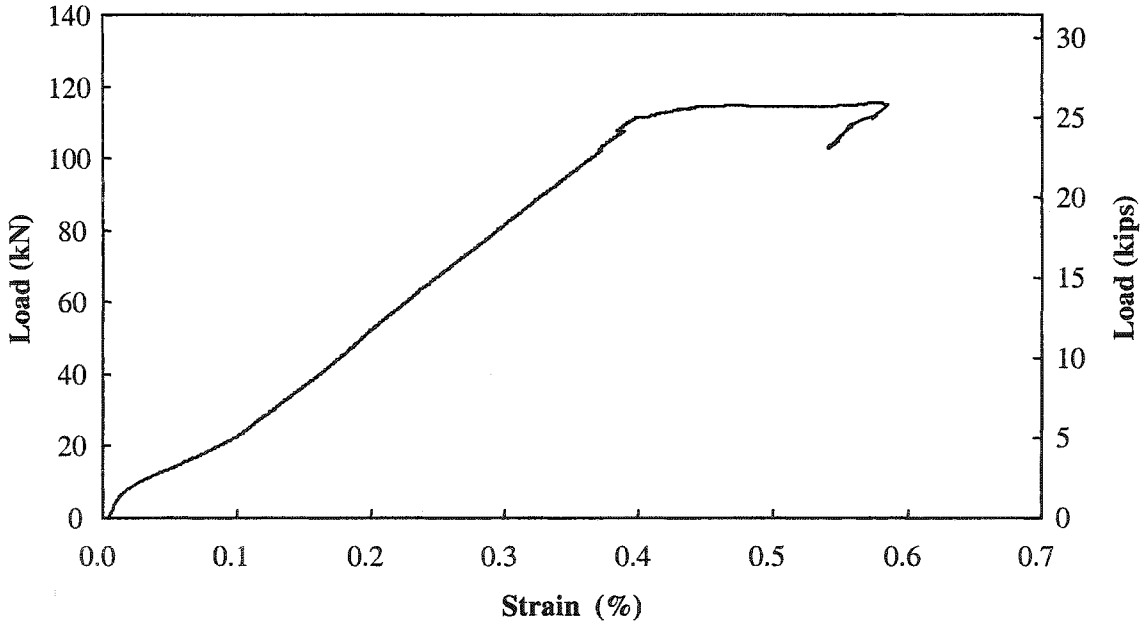

(b) Midspan FRP strain

Fig. 5.28 Behavior of beam F-U57-1

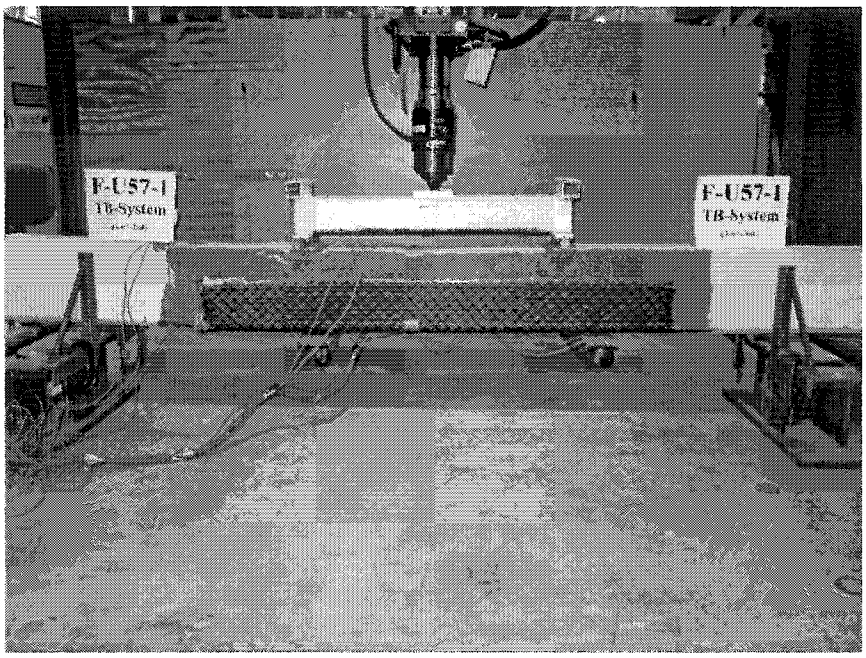

(b) Overall view of the beam

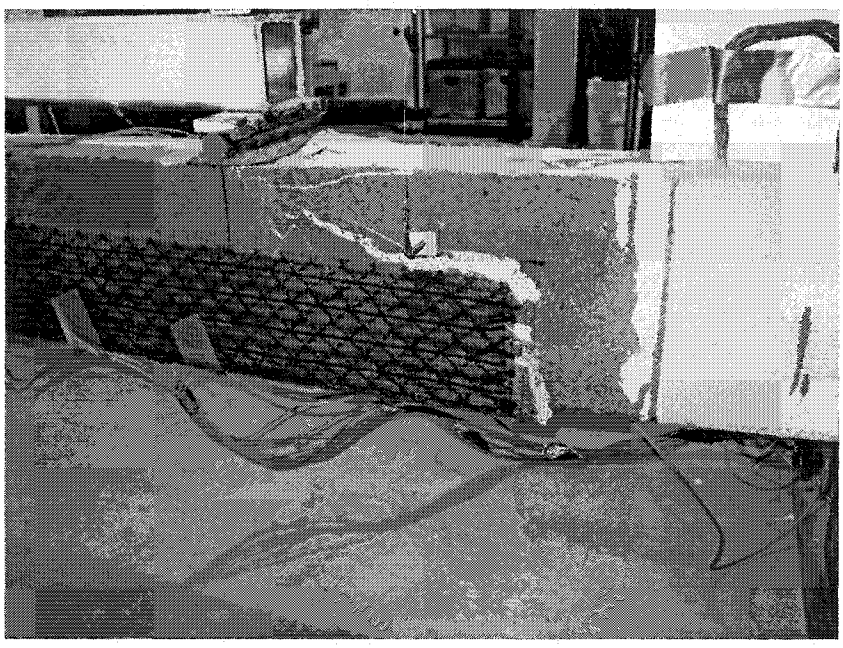

(b) Close up view of the failed section

Fig. 5.29 Failure of beam F-U57-1

CHAPTER 6

SHEAR STRENGTHENING OF RC BEAMS USING THE DEVELOPED TRIAXIALLY BRAIDED DUCTILE FABRIC

6.1 General

This chapter investigates the exploitability of the developed triaxially braided ductile FRP fabric in shear strengthening of reinforced concrete beams. Six simple beams have been strengthened in shear with the new triaxial fabric. A commercially available carbon fiber sheet was used to strengthen a similar beam in shear to compare its behavior with those strengthened with the triaxial fabric. The beams were loaded in four point bending until failure. The applicability of the approach of ACI committee 440 for estimating the fabric contribution to the shear strength of the tested beams was also examined.

6.2 Fabric Characteristics and Shear Strengthening

In many cases, strengthening of a reinforced concrete beam in flexure may be limited by its shear capacity. Therefore, increasing the flexural capacity of a beam may be accompanied by the need to strengthen it for shear. The recently reported experimental investigations reviewed in Chapter 2 showed that bonding FRP strips, fabrics, or sheets to the sides of beams improves their shear strength. These investigations showed that when the strengthened concrete beam reaches its shear capacity, the FRP stretches to a certain strain value known as the effective strain (ε_{fe}). This strain is usually a small fraction of the FRP ultimate strain and hence the full strength of the FRP is not fully exploited, and their use is not economical. In addition, the effectiveness of the FRP increases as the

fibers' direction becomes perpendicular to the diagonal crack. Therefore, installing the FRP with the fiber direction at 45° angle to the longitudinal axis of the beam increases the FRP effectiveness in beam shear strength. FRP materials are also highly orthotropic. They significantly strengthen only if loaded into the fiber direction. Therefore, for simultaneous flexure and shear strengthening of beams, more than one layer of these materials must be used.

As discussed in Chapter 3, the fabric was designed to avoid all these drawbacks. As the fabric contains bundles of fibers triaxially braided in three directions (+45°, 0°, -45°), it may strengthen simultaneously the beam for flexure and shear. The 0° fibers will act mainly for flexural strengthening, while the +45°, -45° fibers will act mainly for shear strengthening. Fig. 6.1 shows a lay-up for simultaneous shear and flexural strengthening of the beam. The fabric strength and load-strain behavior in its 45° directions were designed to obtain the optimum utilization of the fabric in beam shear strength. The +45°, -45° load-strain response in tension was designed so that the fabric has a linear load-strain response in these directions before the slope of the load strain curve decreases; that is, the fabric exhibits a yield plateau similar to that of the steel. The fabric then ruptures after stretching to a reasonably high strain value. The yield-equivalent load value (at the end of the linear response) was adjusted to match the peak point of the effective strain curve discussed earlier in Chapter 3 (see Fig. 3.1), and its corresponding strain value to come close to 0.5%. Since it is possible to install more than one layer of fabric on a beam, the yield- equivalent load of the fabric was designed to be equal to the peak load of the smallest practical beam width.

The average 45° load-strain responses of three fabric samples tested according to ASTM D 3039 specifications are shown in Fig. 6.2 along with the effective strain and

load curve for 125 mm wide beam case. It can be noted that the fabric yield-equivalent point almost coincided with peak point of the effective strain-load curve, which meets the design objectives. The load-strain behavior of the fabric in its 0° direction is shown in Fig. 6.3 in comparison with its behavior in the 45° direction.

6.3 Beam Experimental Program

6.3.1 Test beams

Three groups of reinforced concrete beams were cast. The beams had cross sectional dimensions of 152 mm × 280 mm (6 in. ×11 in.) and lengths of 2740 mm (108 in.). The flexural reinforcement of the beams of group F and group G consisted of two #10 (32 mm) tension bars near the bottom and two #5 (16 mm) compression bars near the top, while the flexural reinforcement of the beams of group H consisted of two #5 (16 mm) tension bars near the bottom and two #3 (9.5 mm) compression bars near the top. The beams were deficient in shear; they were reinforced with #3 (9.5 mm) closed stirrups spaced at 295 mm (11.63 in.). All beams were formed with rounded corners of 25 mm (1 in.) radius, in order to facilitate the installation of the strengthening material on their sides and bottom faces without stress concentrations. Fig. 6.4 shows the beam dimensions, reinforcement, and loading set up. The steel reinforcement that was used had a yield stress of 490 MPa (71,000 psi). The concrete compressive strength at the time of testing was 41.5 MPa (6,000 psi). The beams were loaded in four point loading with a span of 2440 mm (96 in.)

The beams were prepared by sandblasting to roughen their surfaces and then cleaned with an air nozzle and finally wiped to remove any dust. Three strengthening configurations were used: (i) strengthening on the beam sides only (Group F), (ii) strengthening on the bottom face of the beam with extension up on both sides as a U-

wrap (Group G), and (iii) strengthening the beam at the bottom only (Group H). Table 6.1 describes the test beams. The strengthening material was installed for 2.26 m (89 in.), centered along the length of the beam. All beams of group F and group G were tested at a shear span of 838 mm (33 in.) except for beam S-S-3, which was tested at a shear span of 736 mm (29 in.). All the beams in Group H where tested at a shear span of 736 mm (29 in.).

6.3.2 Strengthening materials

The developed triaxial fabric was used to strengthen six beams. An identical beam was strengthened with a carbon fiber sheet installed so that its fiber direction was 45° to the beam axis, perpendicular to potential shear cracks. The sheet was selected to exhibit a similar load-stain response to that initially exhibited by the fabric in its 45° direction (before yielding). The tensile load-strain behavior of the fabric in its 0° and 45° directions are shown in Fig. 6.3, along with that of the carbon fiber sheet. The tensile properties of the strengthening materials are listed in Table 6.2. An epoxy resin was used to impregnate the fibers and to serve as an adhesive between the strengthening material and the concrete surface. This epoxy has an ultimate tensile strength of 66.2 MPa (9.62 ksi) with an ultimate strain of 4.4% and a compressive strength of 109.2 MPa (15.84 ksi). The epoxy was allowed to cure for at least two weeks before the beams were tested.

6.3.3 Instrumentation

The concrete compression strain at midspan was measured using strain gages located on the top surface of the beam. The FRP strain at the beam sides was measured with rosette strain gages located at the expected locations of shear cracks. The deflection was measured at the midspan using a string potentiometer. The beams were loaded using

a hydraulic actuator. The load was measured by means of a load cell. All the sensors were connected to a data acquisition system to scan and record the readings.

6.4 Test Results

6.4.1 Control beam I

The beam initially exhibited some tension cracks in the constant moment region near the midspan. Then, large diagonal cracks were formed in the constant shear span, which led to shear failure of the beam at a shear force (V) of 101 kN (22.7 kips).

6.4.2 Group F

The beams in this group were strengthened with one layer of the triaxial fabric on both sides. Test results for these beams are shown in Fig. 6.5 through 6.18 and listed in Table 6.3.

6.4.2.1 Beam S-S-1

The midspan deflection diagram, shown in Fig. 6.5, indicates that the beam did not yield. The 45° fabric strain diagram, shown in Fig. 6.7, indicates that the fabric was not active before the beam experienced shear cracks, which occurred at a shear force of 84 kN (18.9 kips). After cracking, the fabric experienced an increase in strain up to failure at a shear force of 137 kN (30.8 kips). The failure started by concrete cover spalling in the constant shear zone near the loading point on the top of the beam. The beam failed in shear without rupture of the fabric (see Fig. 6.9). The 45° strain diagram shows that the fabric exhibited a maximum strain value of 0.34%.

6.4.2.2 Beam S-S-2

This beam had exhibited a similar deflection behavior to beam S-S-1. However, it failed by concrete damage in the constant moment zone near the midspan at a shear force of 137 kN (30.8 kips). This damage appears to be caused by buckling of the fabric in the compression zone, causing lateral tensile stresses in the concrete leading to premature failure. The concrete exhibited a compression strain of 0.23%, which is less than the concrete failure strain (0.3%). The fabric strain readings showed a 45° strain of 0.48% when the beam failed. The failed beam is shown in Fig. 6.13.

6.4.2.3 Beam S-S-3

This beam was tested at a shear span of 736 mm (29 in.), slightly less than that of the other two beams. The beam had a similar strengthening scheme to that of beam S-S-1 and beam S-S-2. However, in order to avoid damage of the concrete in the compression zone due to buckling of the fabric, as experienced by beam S-S-2, a 76 mm (3 in.) wide strip at the top of the beam in the constant moment zone was not covered with the fabric. The beam failed by debonding of the fabric (see Fig. 6.17) at a shear force of 141 kN (31.7 kips). The fabric strain readings showed a strain of 0.45% when the beam failed.

6.4.3 Group G

Three beams in this group are strengthened with one layer of the triaxial fabric on both sides in addition to two layers on the bottom face, as a U-wrap scheme. A similar beam was strengthened with one layer of carbon fiber sheet U-wrapped with its fibers 45° to the beam longitudinal axis. Test results for all beams are shown in Fig. 6.19 through 6.31 and listed in Table 6.3.

6.4.3.1 Beam S-U-1

Beam S-U-1 did not yield but failed due to damage of the concrete near the midspan, caused by buckling of the fabric at a shear force of 145 kN (32.6 kips). The midspan strain gages at the top surface of the beam showed that the concrete had a compression strain of 0.21%, which is less than the failure compression strain of the concrete (0.3%). The rosette strain gage readings showed that the fabric contributed to the shear capacity of the beam after it cracked. The maximum recorded 45° strain on the beam side before the beam failed was 0.32%. The failed beam is shown in Fig. 6.22.

6.4.3.2 Beam S-U-2

This beam showed a similar deflection behavior to that of beam S-U-1; however, it failed by debonding of the fabric, followed by shear failure in the constant shear zone at a shear force of 154 kN (34.6 kips). The rosette strain gages showed a 45° strain value of 0.41% before the beam failed. The failed beam is shown in Fig. 6.26.

6.4.3.3 Beam S-CU45-1

This beam was strengthened with one layer of the carbon fiber sheet. This layer has a similar load-strain response to that initially exhibited by the triaxial fabric in its 45° direction (see Fig. 6.3). The beam failed in flexure at a shear force of 146 kN (32.8 kips). The rosette strain gages showed that the sheet contributed to the shear strength of the beam after shear cracking. The maximum recorded 45° strain reading for the fabric was 0.40%, as compared to its ultimate strain (1.2%). The failed beam is shown in Fig. 6.30.

6.4.4 Group H

This group included two beams. The first beam was not strengthened and was tested as a control beam. The second beam was strengthened at the bottom face only with three layers of the triaxial fabric 5.33 in. (135 mm) wide. The midspan deflection and concrete compression strain diagrams are shown in Fig. 6.32.

6.4.4.1 Control Beam II

The beam initially exhibited some tension cracks in the constant moment region near the midspan. Then, large diagonal cracks were formed in the constant shear span at a shear force of 44 kN (9.9 kips), which led to shear failure of the beam at a shear force of 50 kN (11.2 kips). The failed beam is shown in Fig. 6.33.

6.4.4.2 Beam FS-B3-1

Beam FS-B3-1 experienced large diagonal cracks that were formed in the constant shear span at a shear force of 53 kN (11.3 kips). Later, the concrete cracked horizontally at the level of the bottom reinforcement propagating from the shear crack causing failure of the beam at a shear force of 72 kN (16.2 kips). The failed beam is shown in Fig. 6.34. Herein, it can be noted that the fabric layers at the bottom were able to increase the shear strength of the beam until failure occurred by shear-tension failure at the fabric end

6.5 Discussions and Analysis

The test results revealed that the fabric exhibited strain values that were close to the fabric yield-equivalent strain before failure of the beam. This indicates that the fabric strength was almost fully utilized, which meets its design objectives. The triaxial fabric

has fibers in the 0° direction, in addition to the +45 °, -45 ° ones that contribute to the flexural strength of the beam. The fabric demonstrated the capability of increasing the beam flexure and shear strength using the same layer. None of the beams strengthened with the fabric failed in flexure, while the beam strengthened with carbon fiber failed in flexure. This is because the U-wrapped carbon fibers were installed 45° to the longitudinal axes of the beam and hence did not contribute in an optimum manner to its flexural strength.

As expected, the U-wrapped beams showed higher ultimate loads than those strengthened on the sides. The existence of the fabric in zones of high compression may lead to premature failure due to damage of the concrete as a result of buckling of the fabric as experienced by beams S-S-2 and S-U-1. This may be solved by avoiding the installation of the fabric in high compression zones whenever possible, as was done for beam S-S-3.

The ACI 440 committee (2002) presented an approach to calculate the contribution of FRP to the shear strength of the beam. In this approach, the FRP shear contribution (V_{frp}) is expressed by the following relation:

$$V_{frp} = \frac{2\, n\, t_f\, w_f\, \varepsilon_{fe}\, E_f\, (\sin\beta + \cos\beta) d_f}{s_f}$$

where

d_f = effective FRP depth

E_f = FRP elastic modulus

n = number of FRP layers

s_f = spacing of FRP strips

t_f = FRP thickness

w_f = width of FRP strip

β = angle between FRP fiber direction and longitudinal axis of the beam

ε_{fe} = effective FRP strain and it is calculated using the following equation:

$$\varepsilon_{fe} = K_v \varepsilon_{fu} \leq 0.004$$

where (K_v) is a bond reduction coefficient calculated from the following equation:

$$K_v = \frac{k_1 k_2 L_e}{11900 \varepsilon_{fu}} \leq 0.75$$

where (k_1, k_2) are bond reduction factors calculated from the following equations:

$$k_1 = \left(\frac{f_c'}{27} \right)^{2/3}$$

$$k_2 = \begin{cases} \dfrac{d_f - L_e}{d_f} & \textit{For U- wraps} \\ \dfrac{d_f - 2L_e}{d_f} & \textit{For two sides bonded} \end{cases}$$

where (L_e) is an effective bond length calculated form the following equation:

$$L_e = \frac{23{,}000}{(n t_f E_f)^{0.58}}$$

This approach was used to estimate the fabric contribution and compare it with the test results. The approach was applied for two cases: (i) the fabric bonded on two sides only, as that of beam group F, represented by beam S-S-3 and (ii) the fabric U-wrapped, as the case of group G, represented by beam S-U-2. The calculations are shown

in Table 6.4. The approach gave very close values to the experimental results; hence, it is recommended that it is be used for design when using this fabric.

6.6 Conclusions

The mechanical properties of currently available FRP materials are not fully exploited when they are used as strengthening materials for reinforced concrete beams for shear. These materials are also orthotropic and hence single layer cannot be used for strengthening in both flexure and shear. As the triaxial fabric contains bundles of fibers braided in three different directions (+45°, 0°, -45°), it has fibers (0° fibers) that act mainly for flexural strengthening and at the same time it has fibers in the +45°, -45° directions that act mainly for shear strengthening. The fabric strength and its load-strain behavior in the 45° directions were designed to have the optimum utilization in beam shear strength. The fabric was used to strengthen reinforced concrete beams in shear. The fabric maximum recorded strains were very close to the fabric yield-equivalent strain; hence, its strength was almost fully exploited. The fabric should not be installed in zones of high compression stresses as it may buckle causing the damage of the strengthened beam. The fabric layers at the bottom were able to increase the shear strength of the beam. The ACI committee 440 approach was found acceptable in calculating the fabric contribution to beam shear strength.

Table 6.1 Summary of Test Beams

Beam Group	Beam Designation	Shear Span	Strengthening Scheme	Strengthening Material
N/A	Control I	838 mm (33 in.)	N/A	N/A
Group F	S-S-1	838 mm (33 in.)	Sides only	Triaxial fabric (1 layer)
	S-S-2			
	S-S-3	738 mm (29 in.)		
Group G	S-U-1	838 mm (33 in.)	U-wrap	Triaxial fabric (1 layer @ sides + 2 layers@ bottom)
	S-U-2			
	S-CU45-1			Carbon fiber sheet (1 layer)
Group H	Control II	738 mm (29 in.)	N/A	N/A
	FS-B3-1		Bottom only	Triaxial fabric (3 layer)

Table 6.2 Properties of Strengthening Materials

Material		Yield-Equivalent Load kN/mm (kips/in.)	Yield-equivalent Strain (%)	Ultimate Load kN/mm (kips/in.)	Ultimate Strain (%)	Thickness mm (in.)
Triaxial Fabric	(0°) Direction	0.19 (1.08)	0.35	0.33 (1.89)	2.10	1.0 (0.039)
	(45°) Direction	0.115 (0.66)	0.47	0.20 (1.15)	2.05	
Carbon Fiber Sheet		-	-	0.34 (1.95)	1.2	0.13 (0.005)

Table 6.3 Summary of Test Results

Beam Designation	Strengthening Scheme	Strengthening Material	Shear Strength kN (kips)	Max. 45° Strain at beam side (%)
Control I	N/A	N/A	101 (22.7)	N/A
S-S-1	Sides only	Triaxial fabric (1 layer)	137 (30.8)	0.34
S-S-2			137 (30.8)	0.48
S-S-3			141 (31.7)	0.45
S-U-1	U-wrap	Triaxial fabric (1 layer @ sides + 2 layers@ bottom)	145 (32.6)	0.32
S-U-2			154 (34.60	0.41
S-CU45-1		Carbon fiber sheet (1 layer)	146 (32.8)	0.40
Control II	N/A	N/A	50 (11.2)	N/A
FS-B3-1	Bottom only	Triaxial fabric (3 layer)	72 (16.2)	N/A

Table 6.4 Calculation of Beam Shear Capacity Using ACI 440 Approach

Beam	S-S-3	S-U-2
$n\ t_f\ E_f$ (MN/m)	24.5	24.5
L_e (mm)	65.5	65.5
k_1	1.33	1.33
k_2	0.41	0.70
K_v	0.64	0.75
ε_{fe}	0.30	0.35
V_{frp} (kN)	32.6	38.0
V_{cal} (kN)	133.6	139
V_{exp} (kN)	141	154
Difference (%)	5.2	9.7

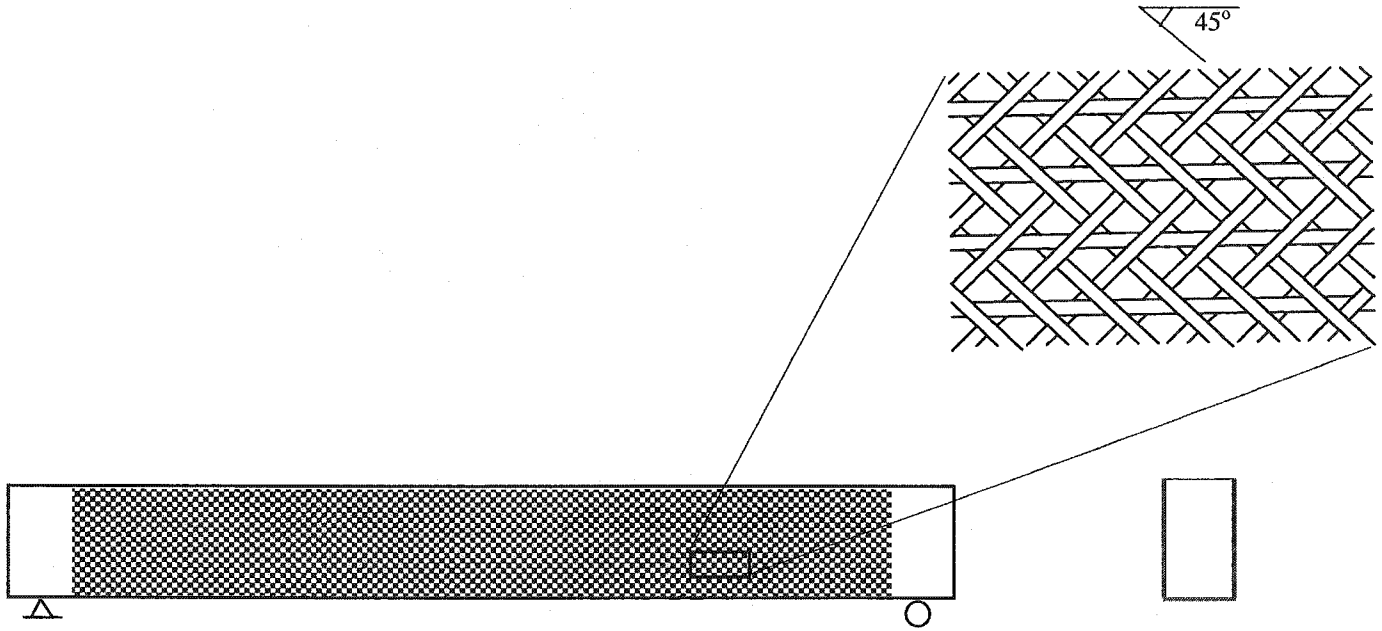

Fig. 6.1 Lay-up of triaxial fabric for simultaneous shear and flexural strengthening.

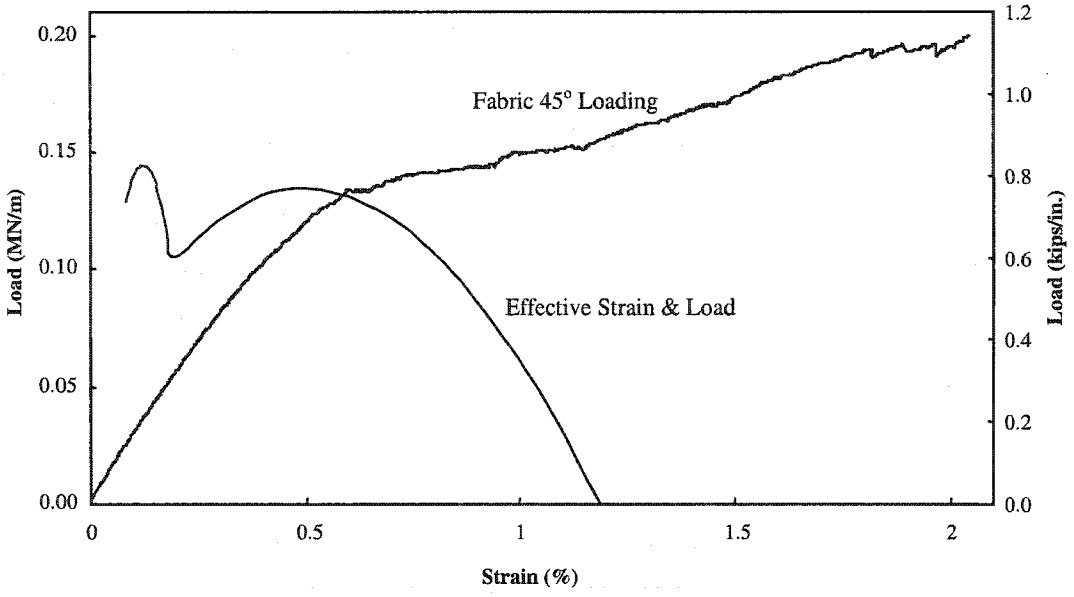

Fig. 6.2 Fabric 45° loading response and effective FRP strain & load curve of 125 mm wide beams

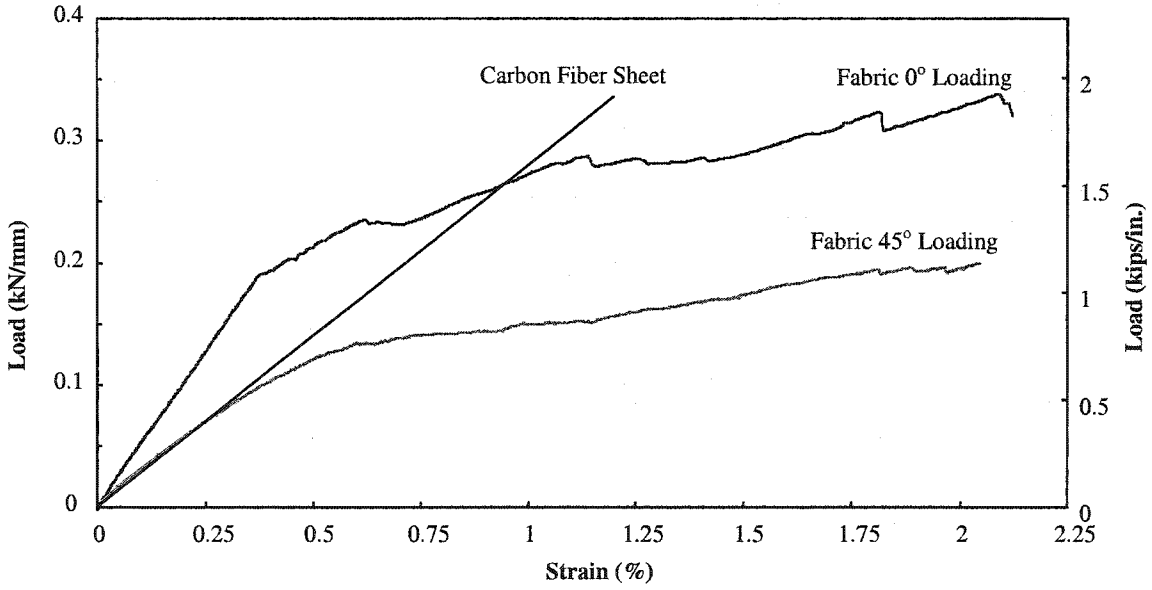

Fig. 6.3 Load-strain diagrams for triaxial fabric and commercially available carbon fiber sheet

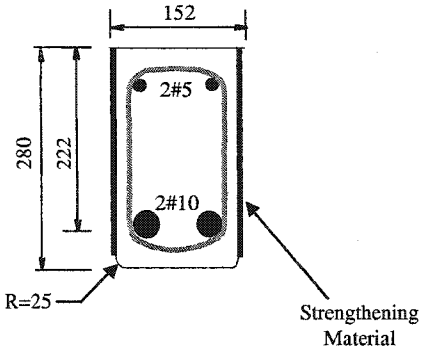

All dimensions in mm

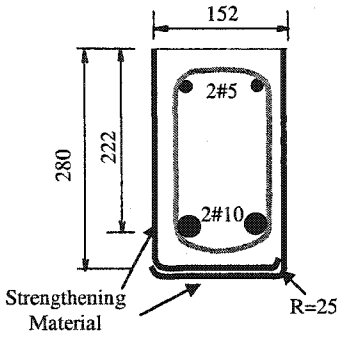

(a) Cross Section for Group F

(b) Cross Section for Group G

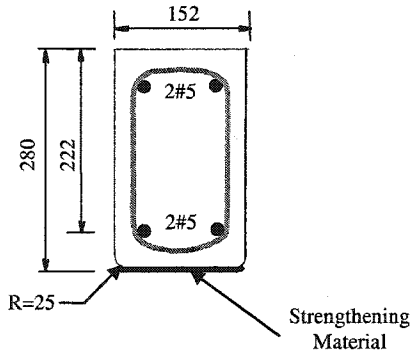

(a) Cross Section for Group H

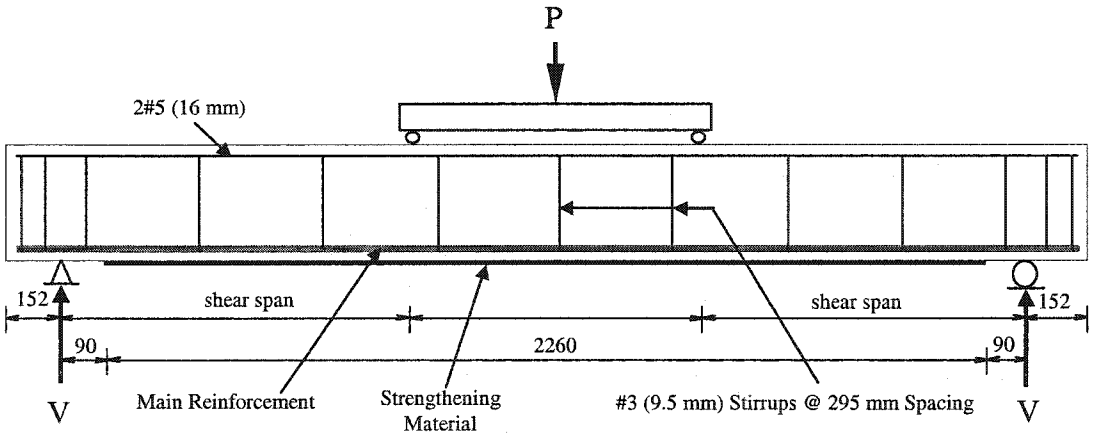

(s) Loading Set-up

Fig. 6.4 Details of test beam

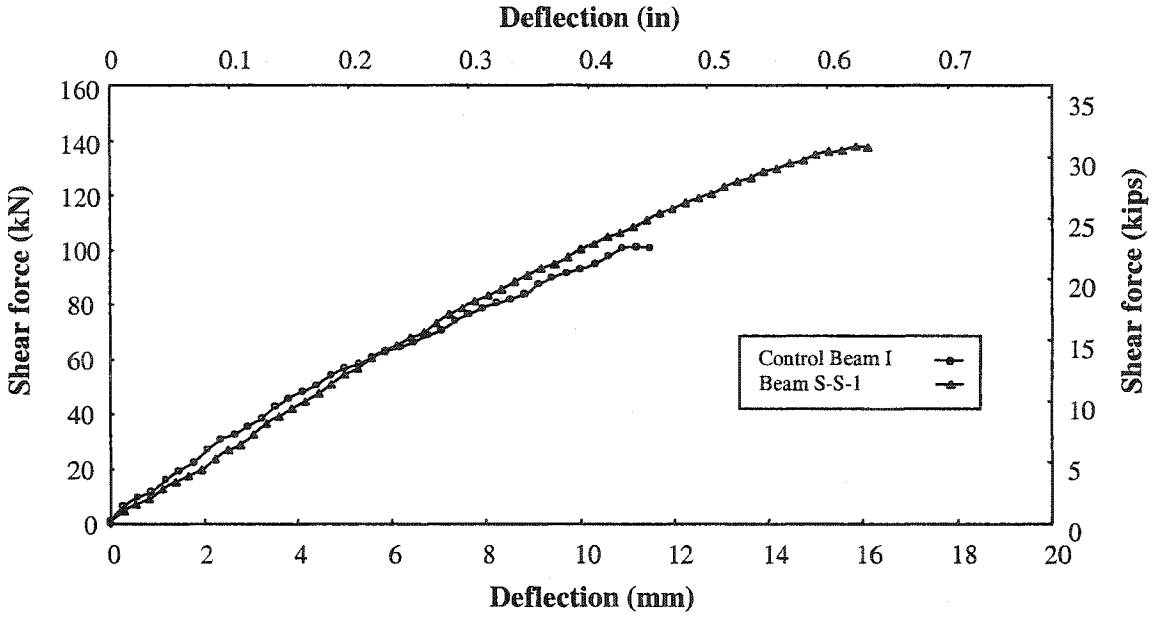

Fig. 6.5 Shear force-midspan deflection curve of control beam I and beam S-S-1

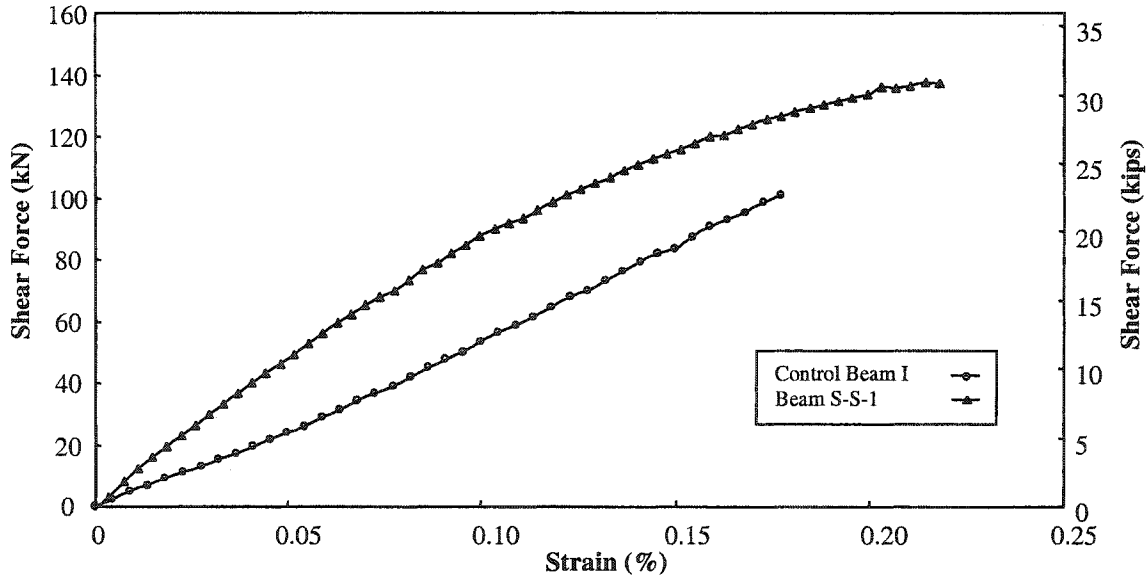

Fig. 6.6 Shear force-midspan concrete compression strain of control beam I and beam S-S-1

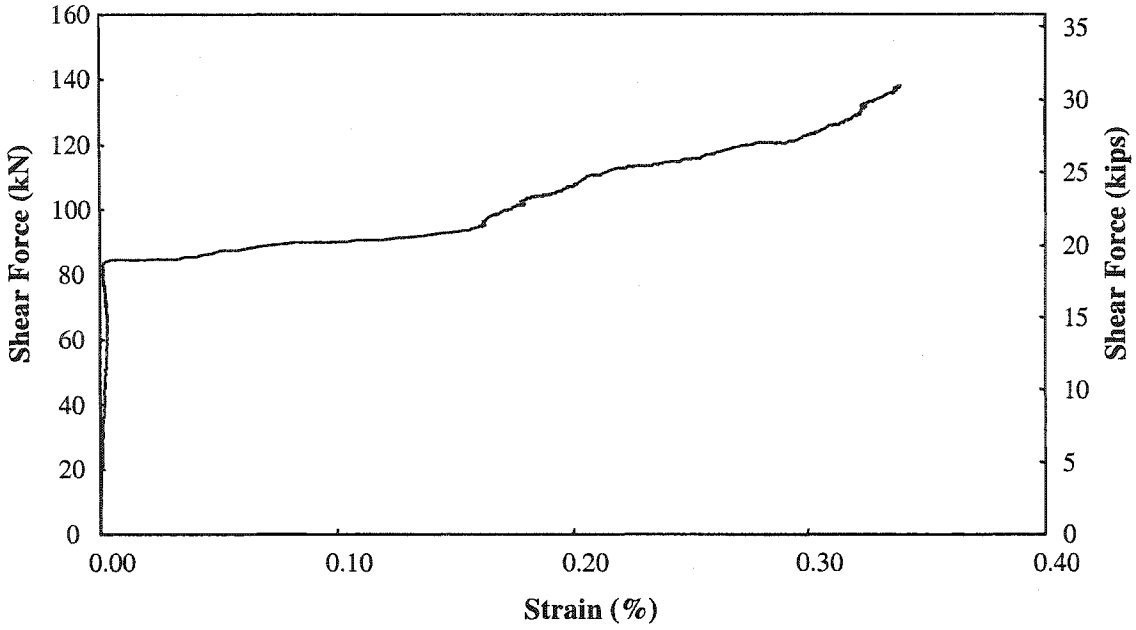

Fig. 6.7 Shear-45° strain at beam side of beam S-S-1

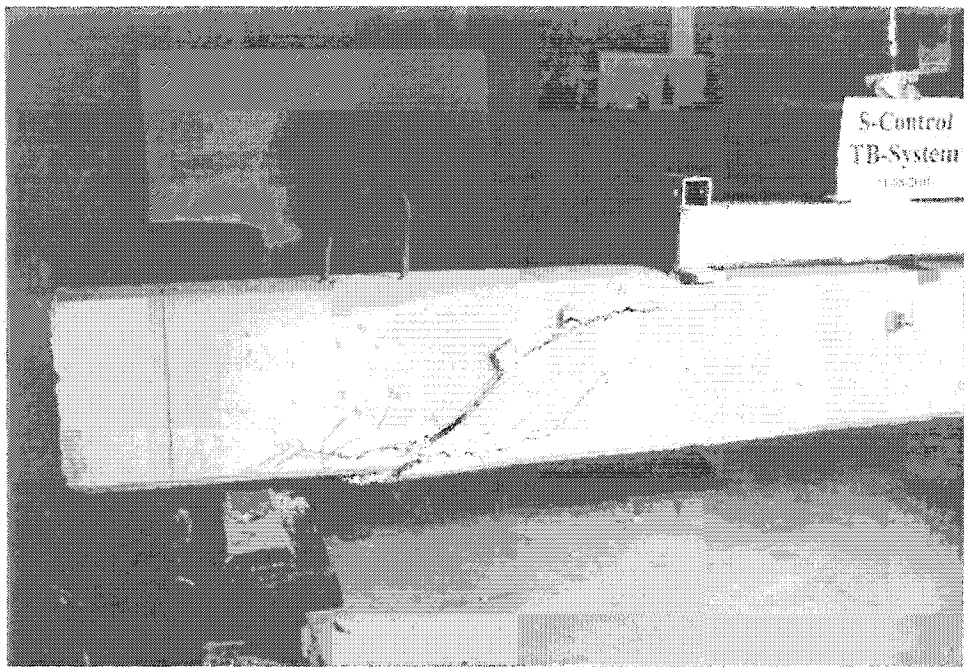

Fig. 6.8 Failure of control beam I

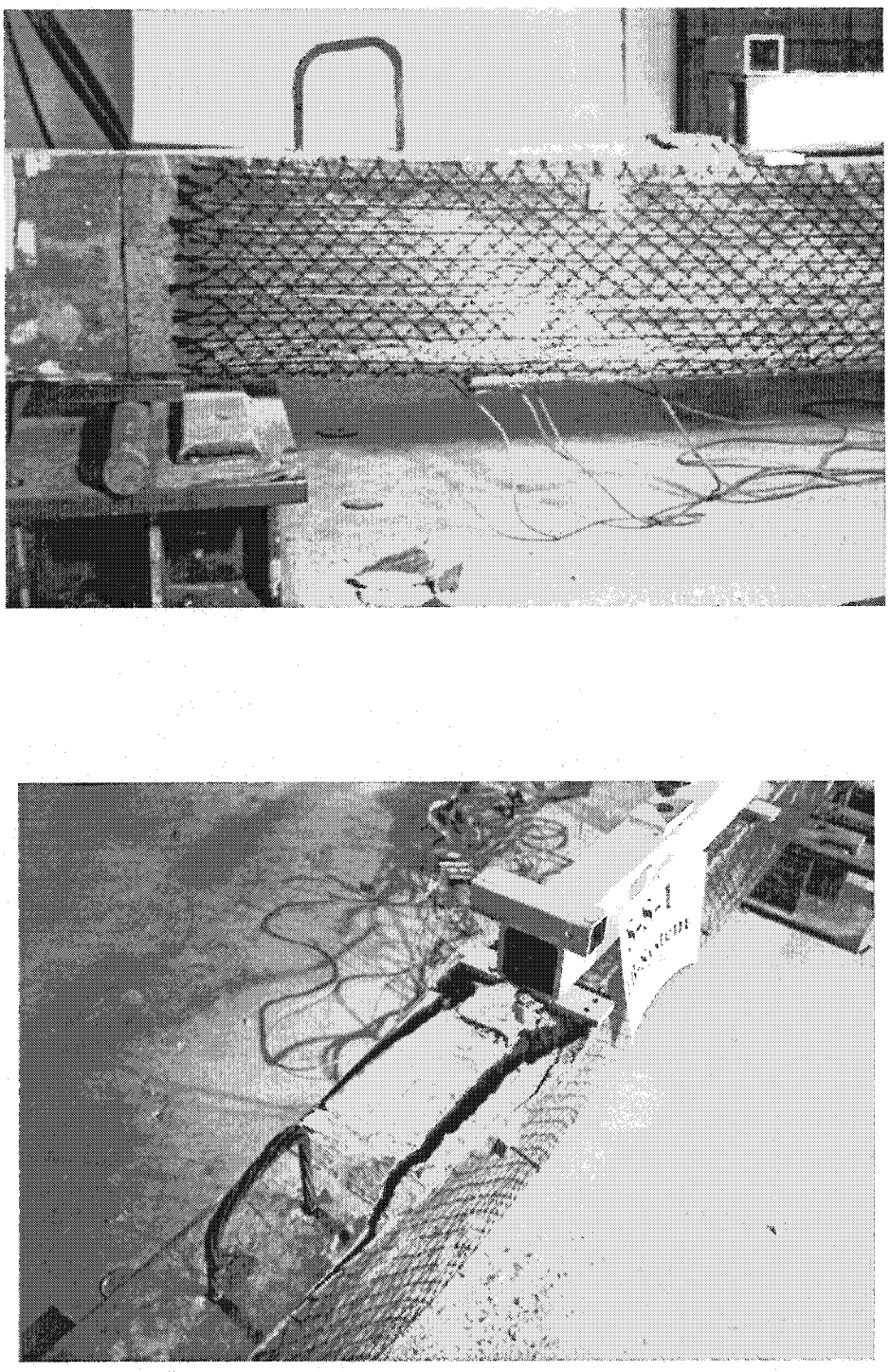

Fig. 6.9 Failure of beam S-S-1

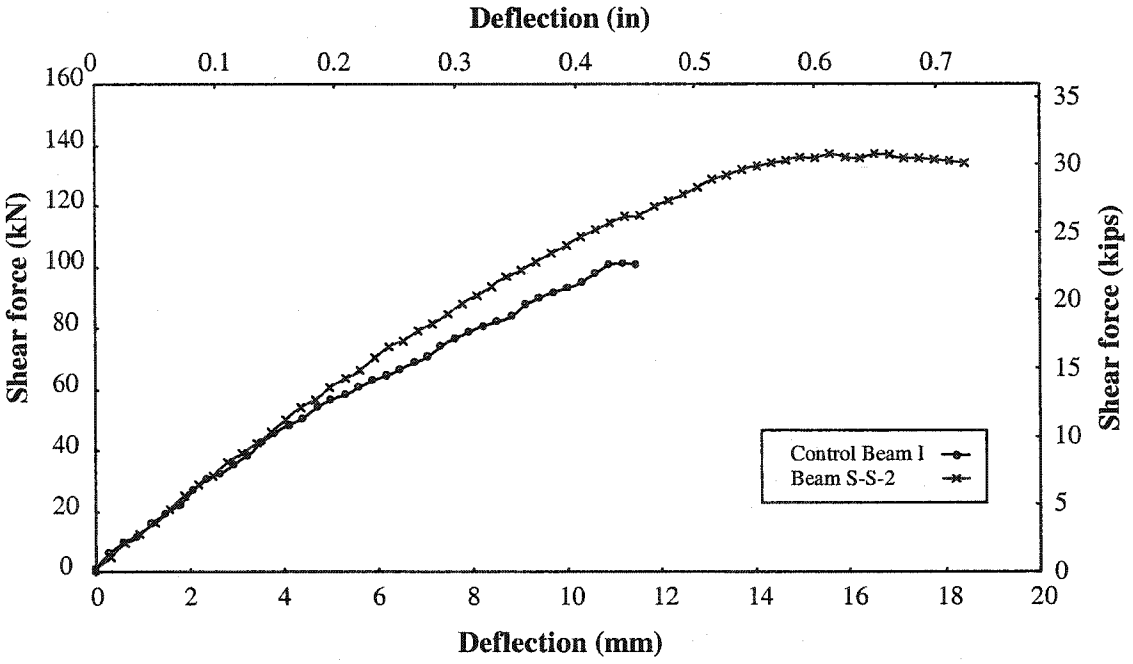

Fig. 6.10 Shear force-midspan deflection curve of control beam I and Beam S-S-2

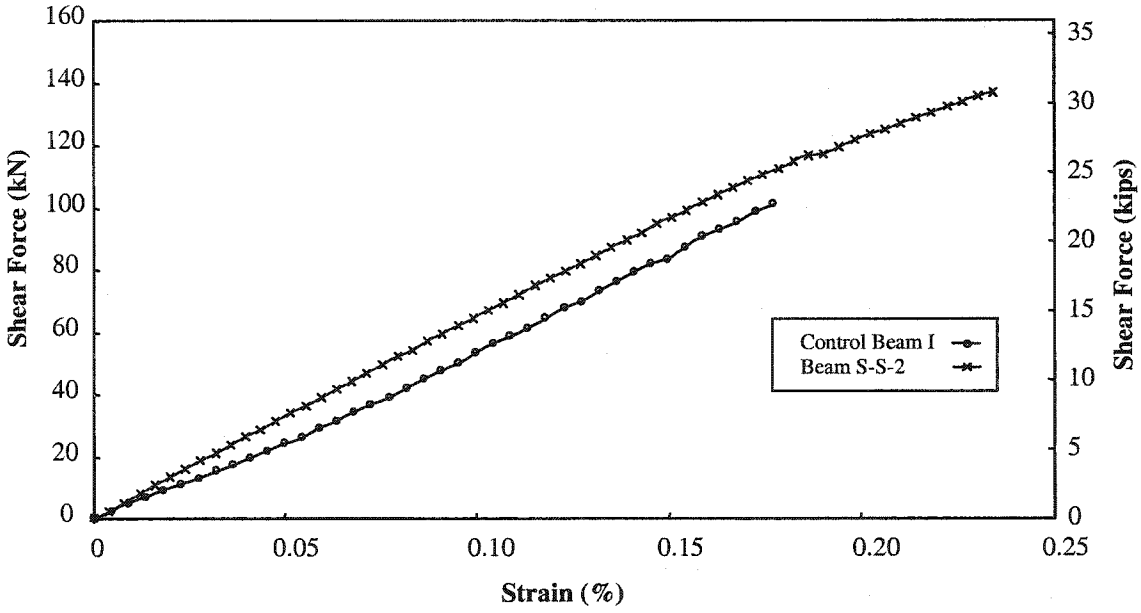

Fig. 6.11 Shear force-midspan concrete compression strain of control beam I and beam S-S-2

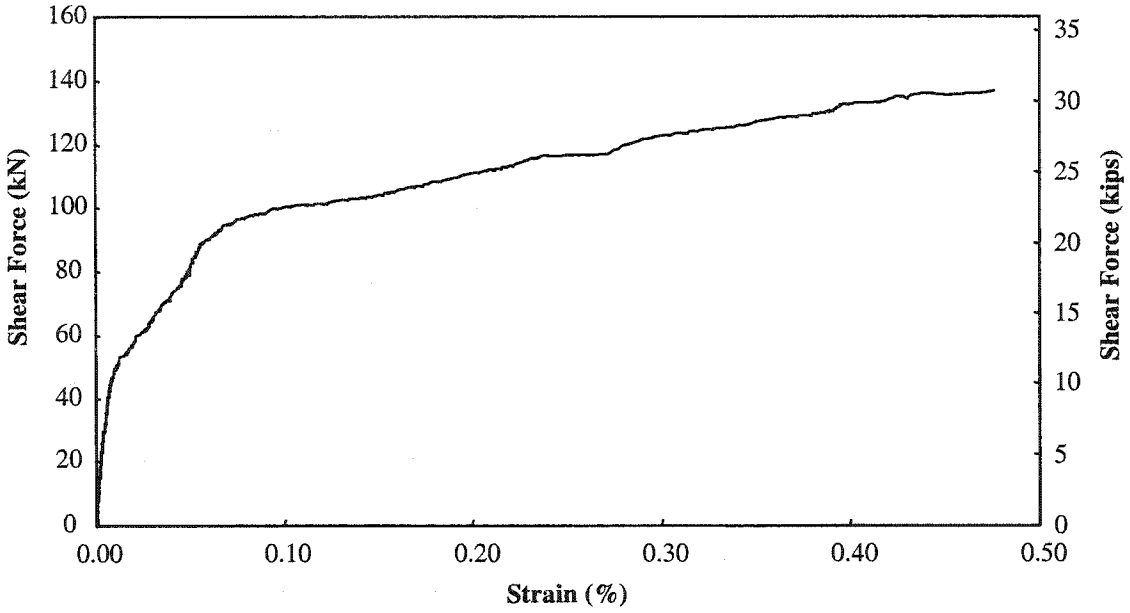

Fig. 6.12 Shear force-45° Strain at beam side of beam S-S-2

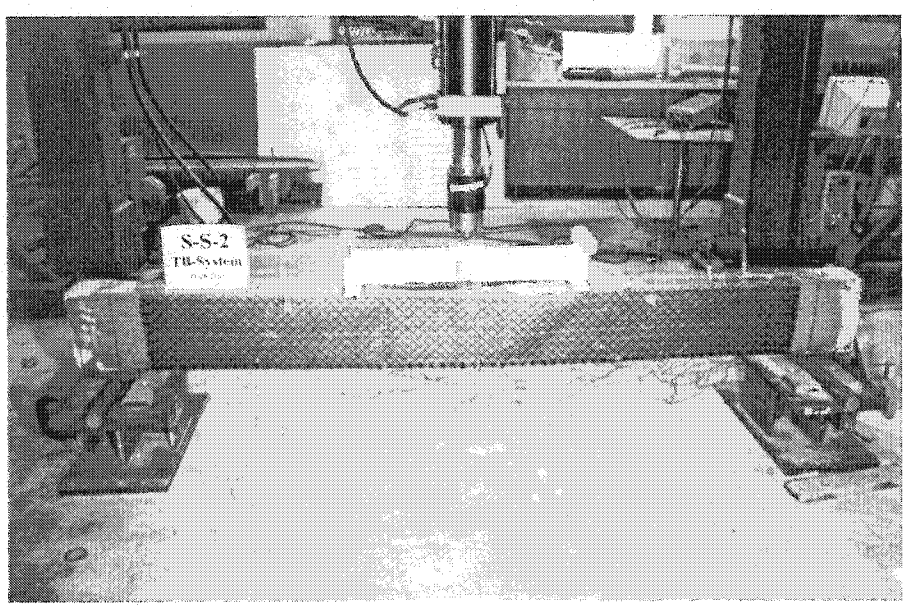

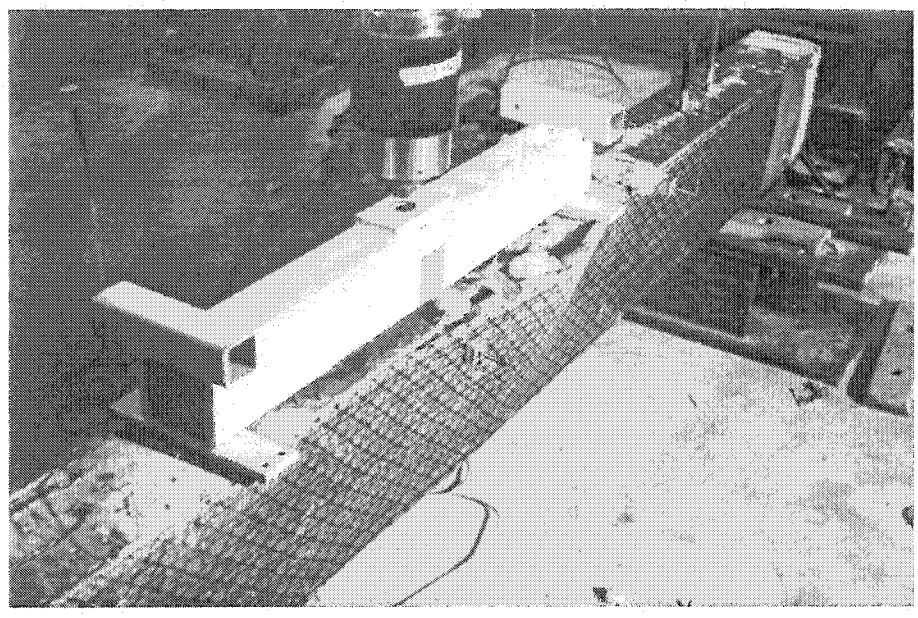

Fig. 6.13 Failure of beam S-S-2

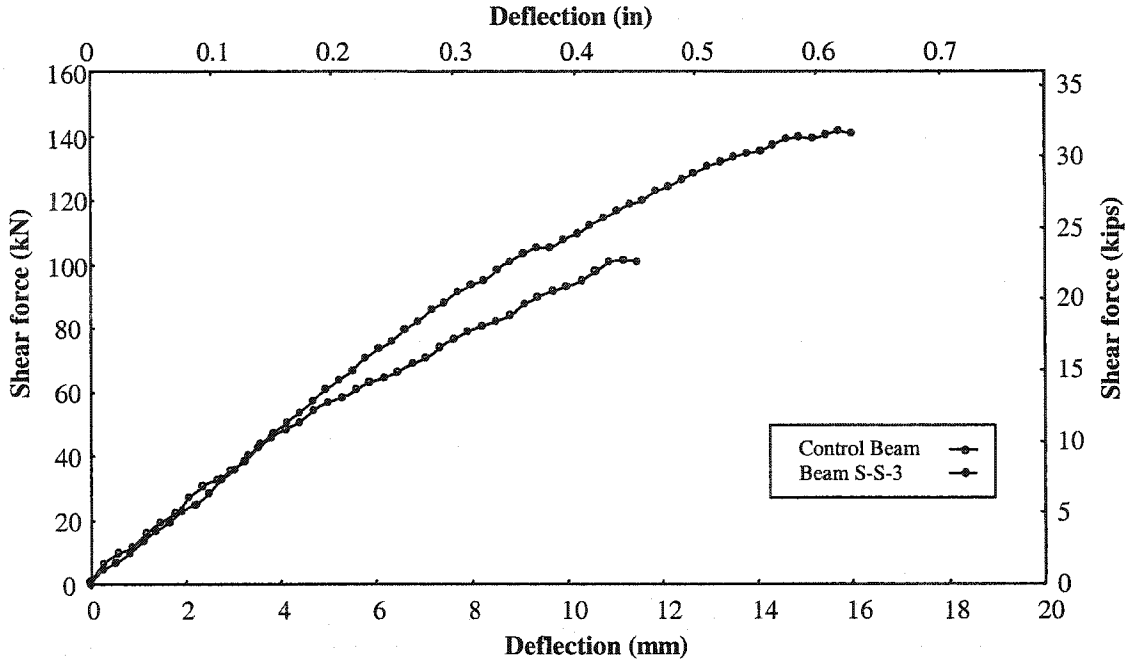

Fig. 6.14 Shear force-midspan deflection curve of control beam I and beam S-S-3

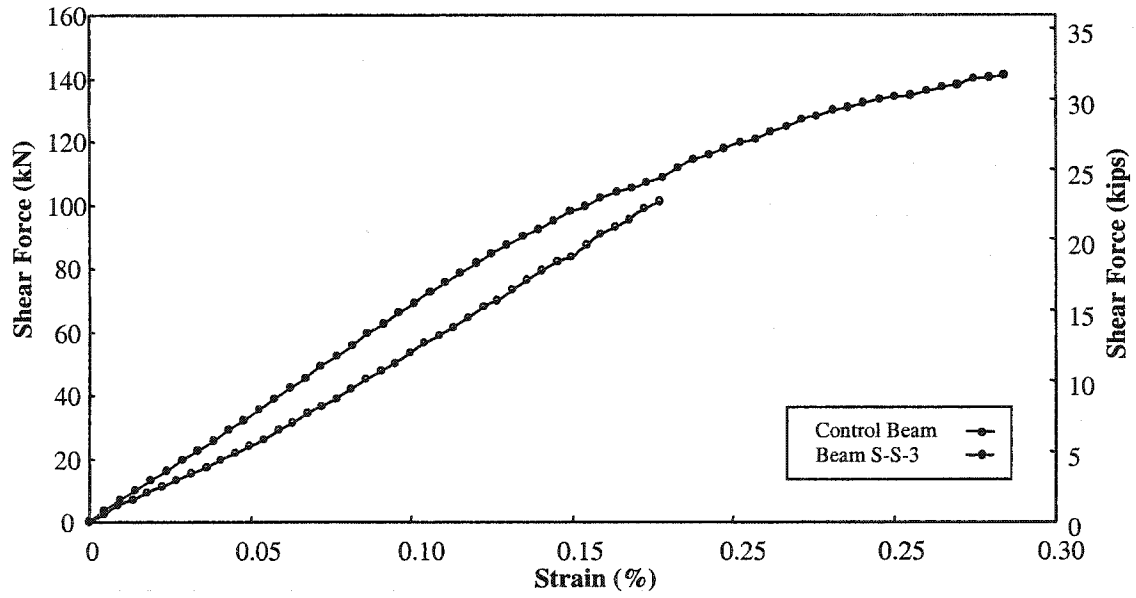

Fig. 6.15 Shear force-midspan concrete compression strain of control beam I and beam S-S-3

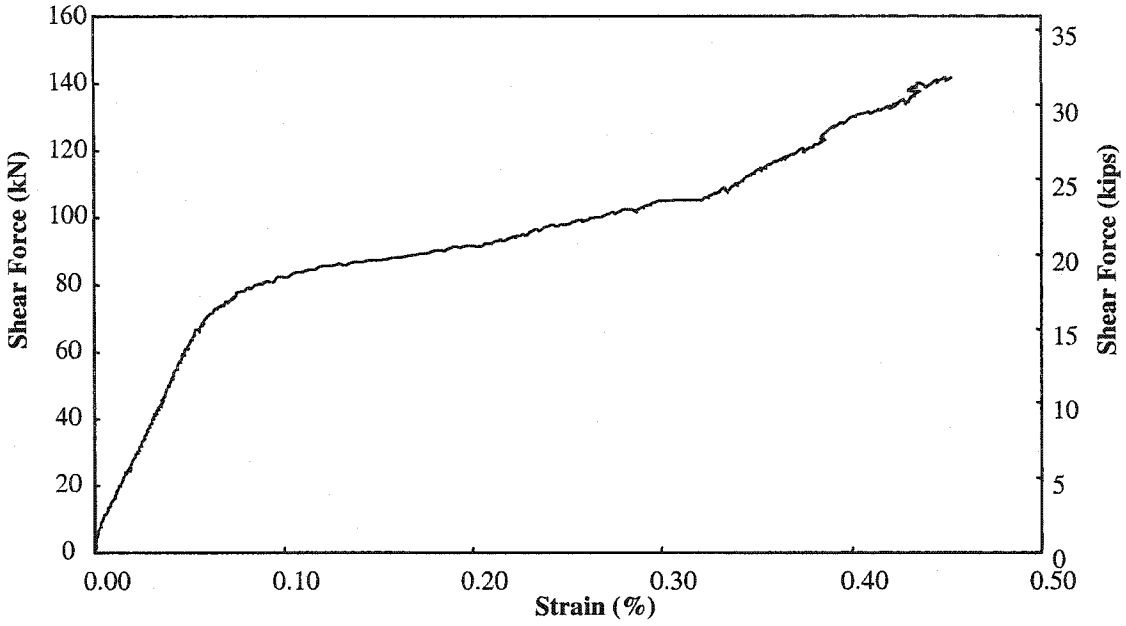

Fig. 6.16 Shear force-45° Strain at beam side of beam S-S-3

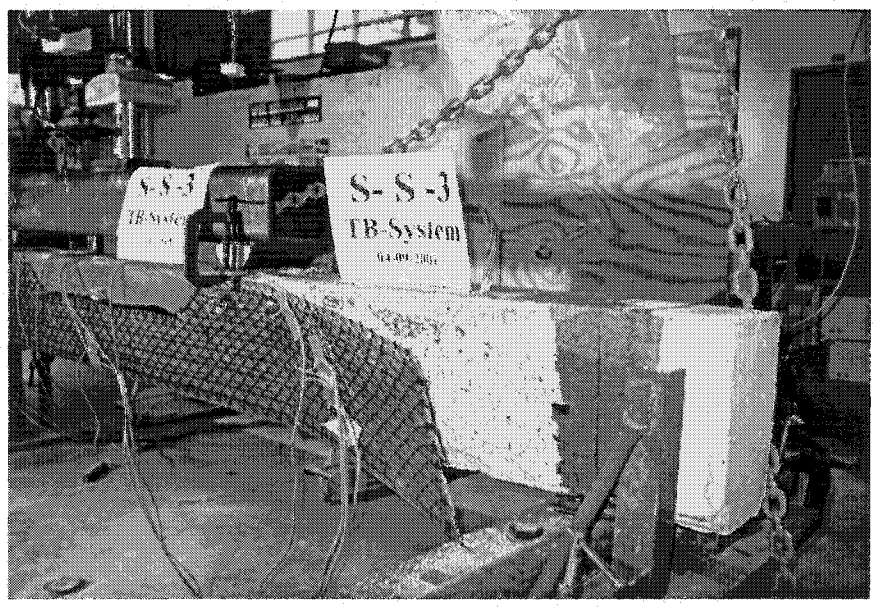

Fig. 6.17 Failure of beam S-S-3

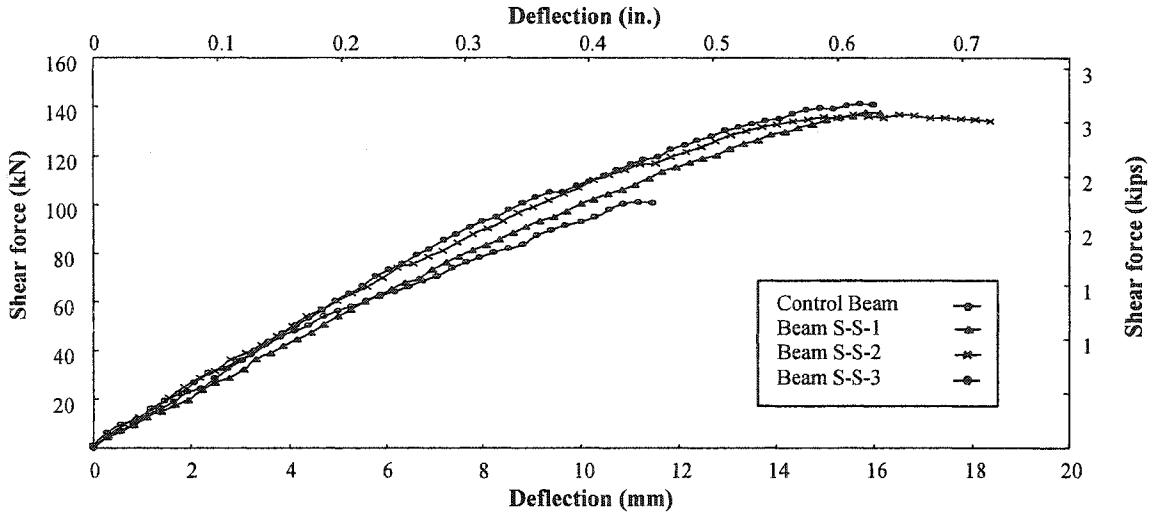

(a) Midspan deflection

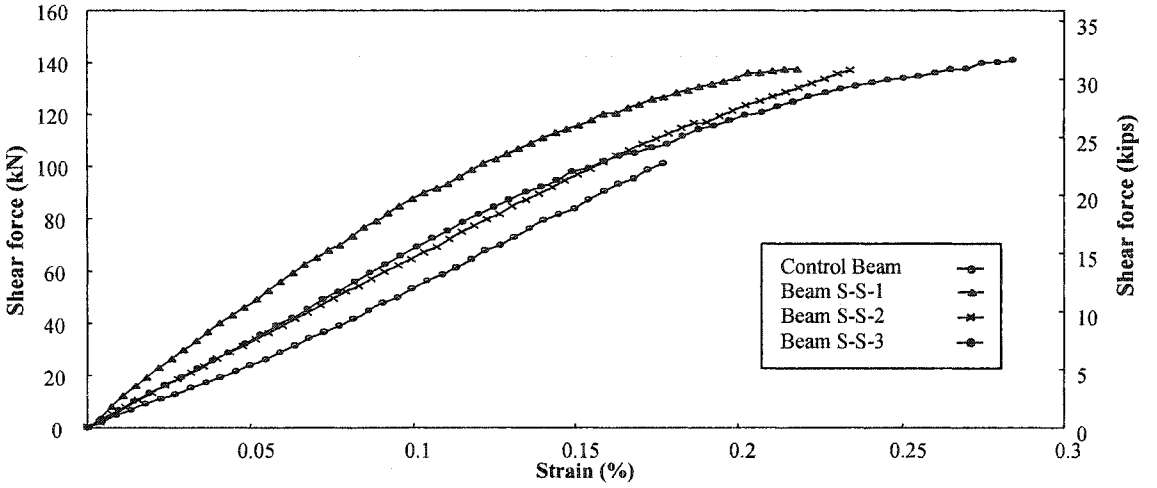

(b) Concrete compression strain at midspan

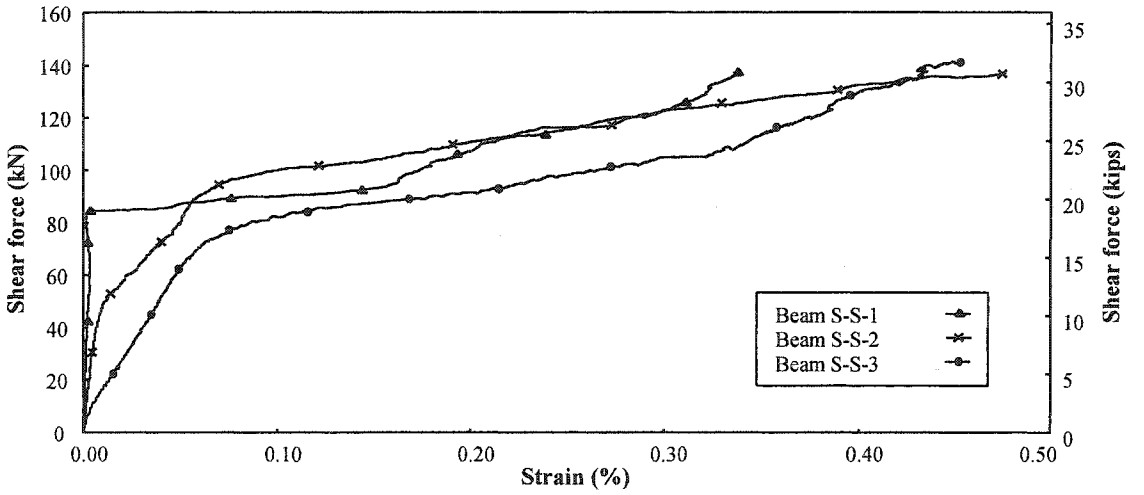

(c) 45° strain at sides

Fig. 6.18 Comparison between group F beams

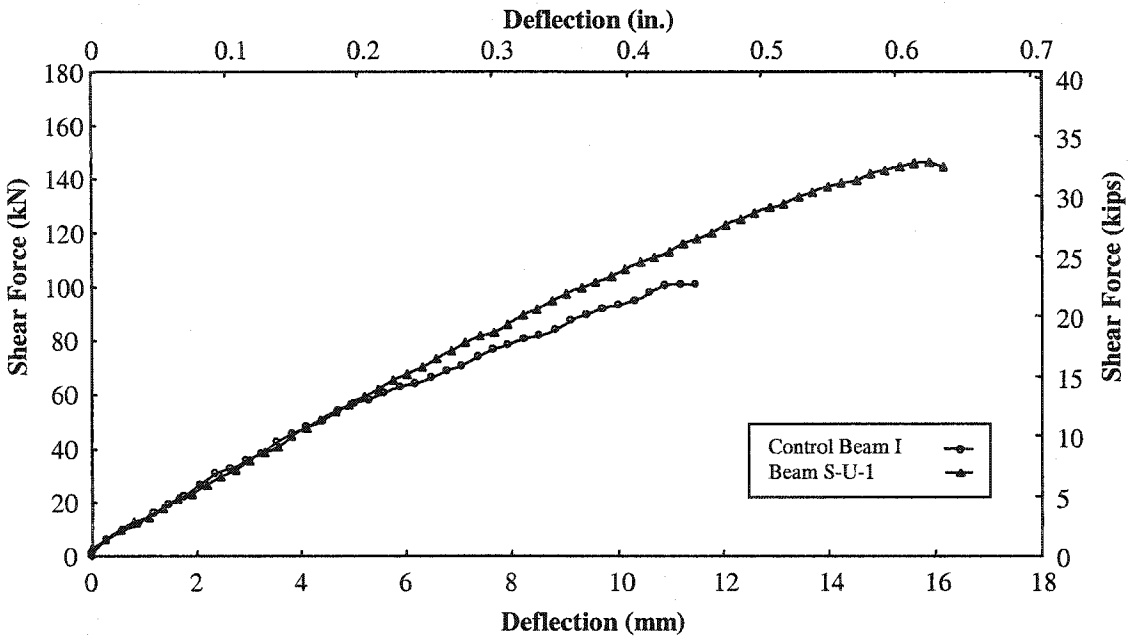

Fig. 6.19 Shear force-midspan deflection curve of control beam I and beam S-U-1

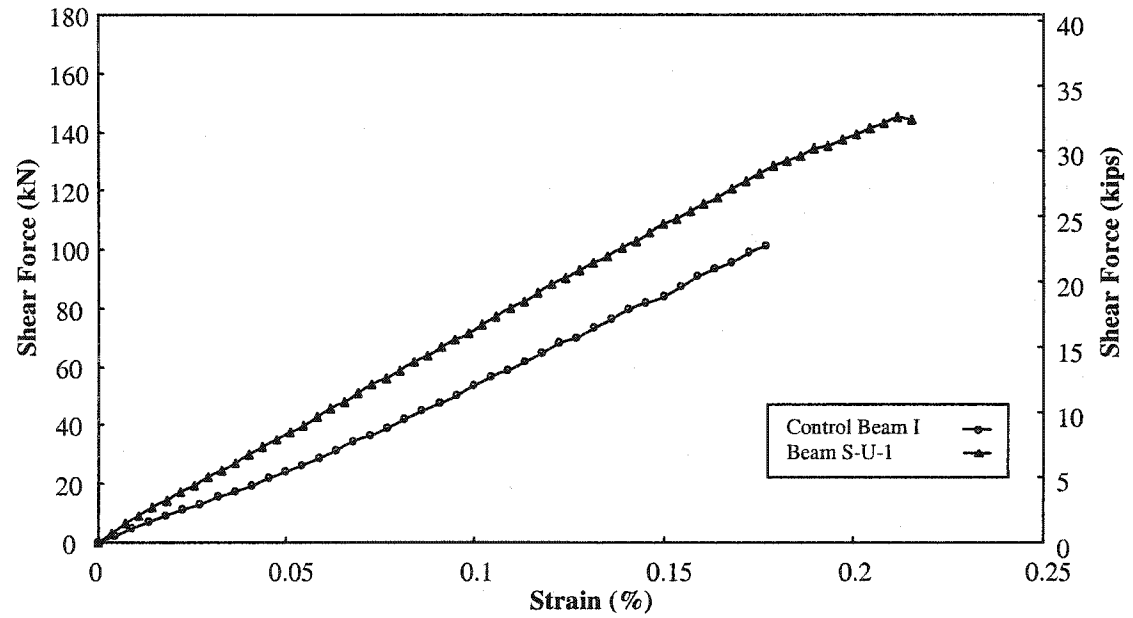

Fig. 6.20 Shear force-midspan concrete compression strain of control beam I and beam S-U-1

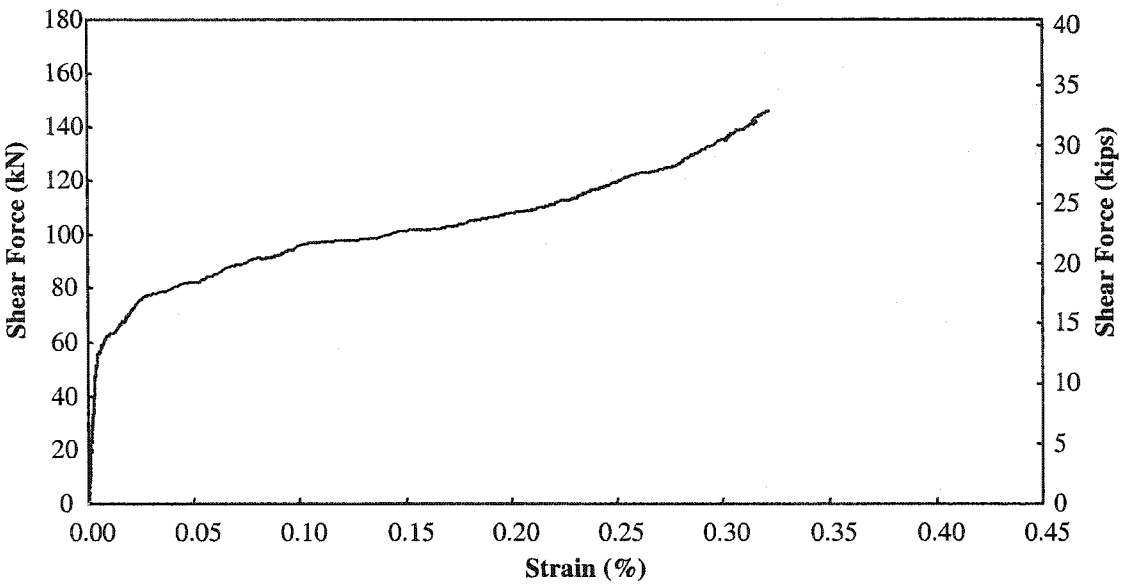

Fig. 6.21 Shear force-45° strain at beam side of beam S-U-1

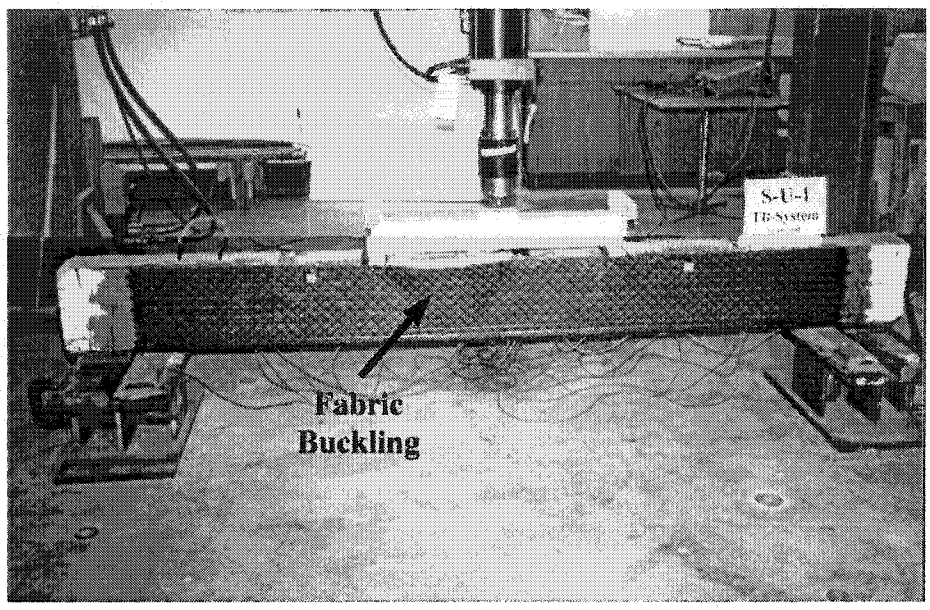

Fig. 6.22 Failure of beam S-U-1

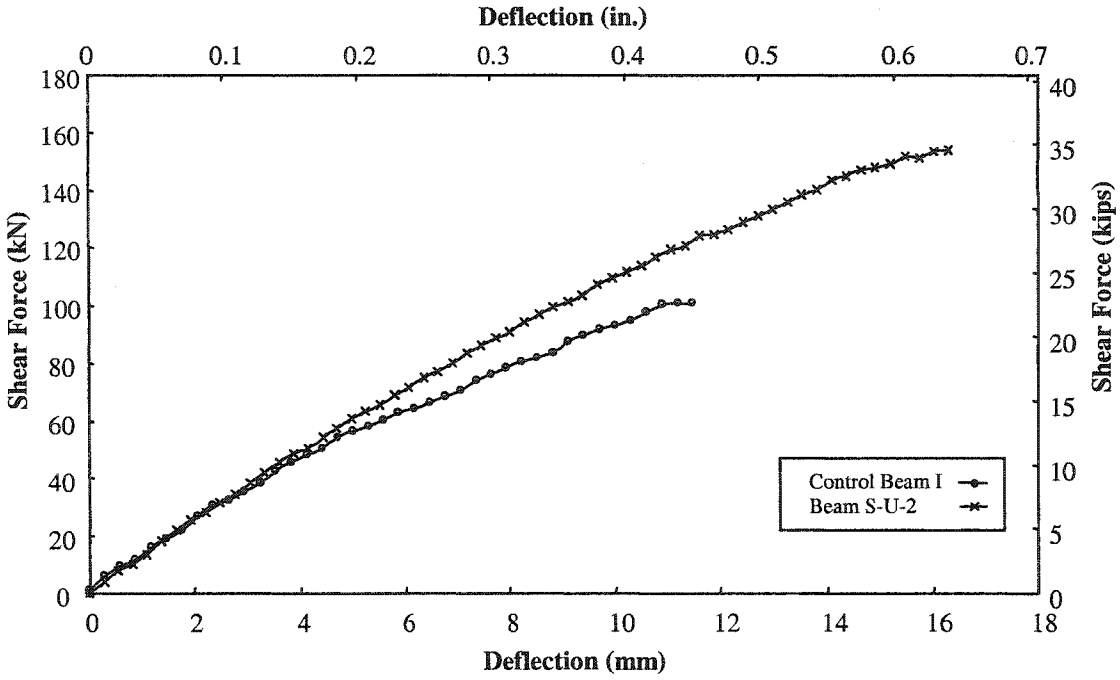

Fig. 6.23 Shear force-midspan deflection curve of control beam I and beam S-U-2

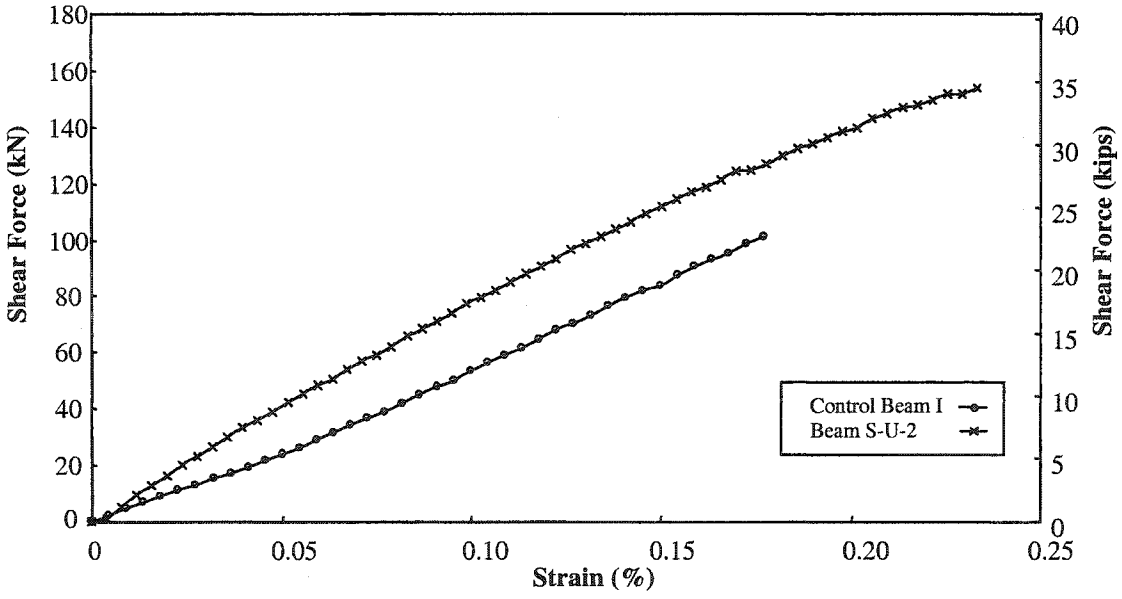

Fig. 6.24 Shear force-midspan concrete compression strain of control beam I and beam S-U-2

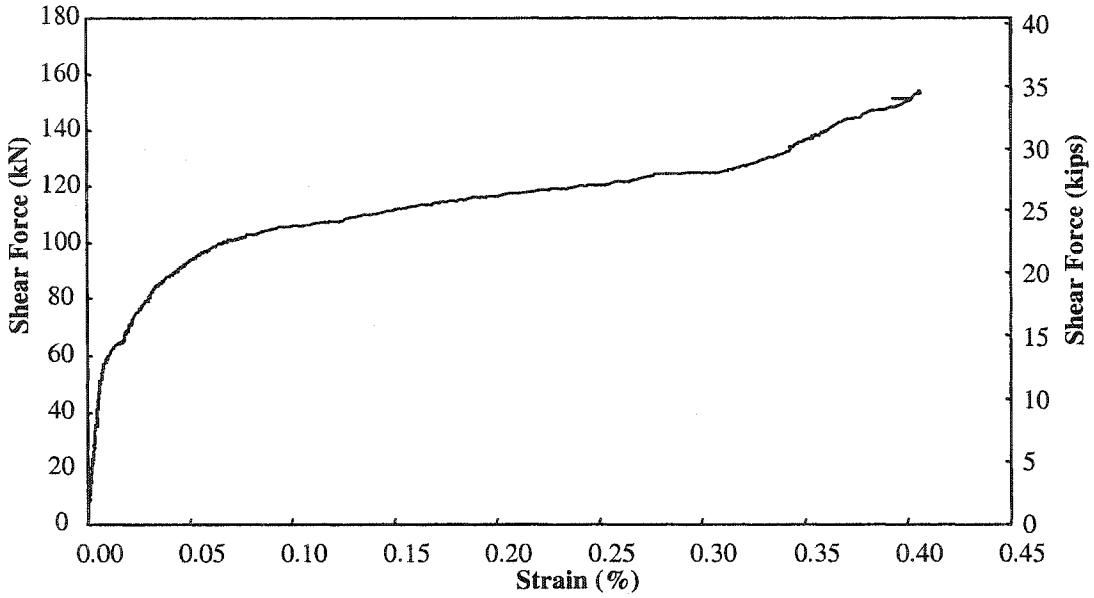

Fig. 6.25 Shear force-45° strain at beam side of beam S-U-2

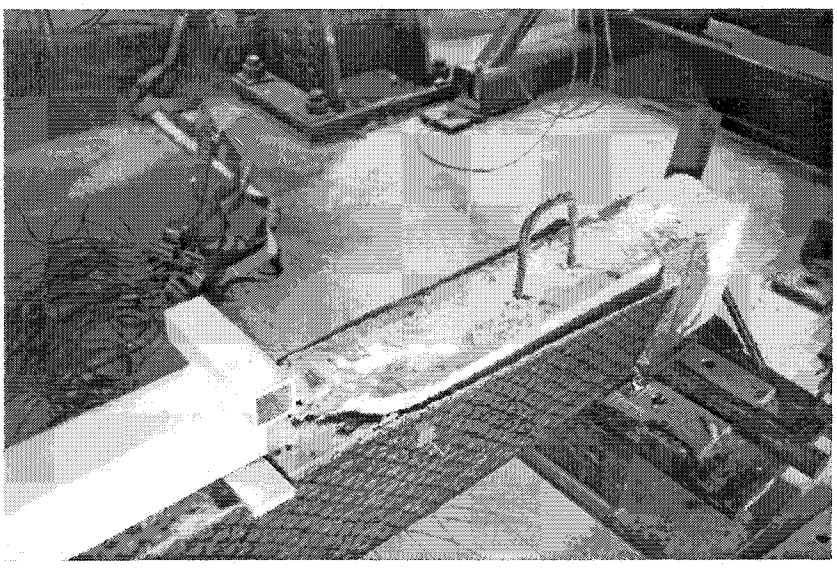

Fig. 6.26 Failure of beam S-U-2

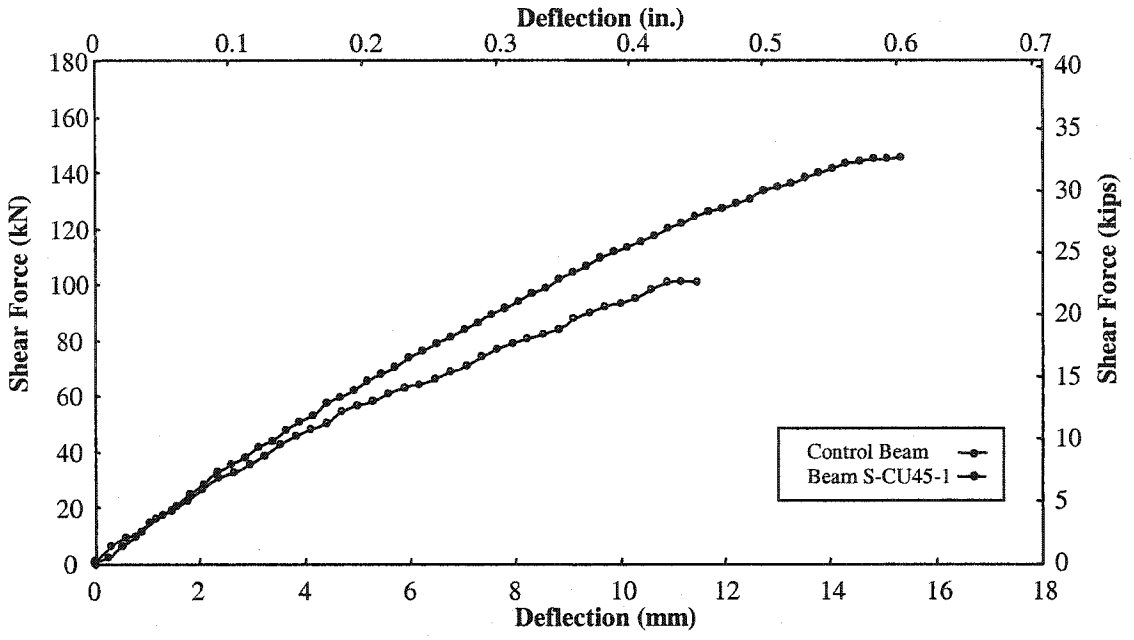

Fig. 6.27 Shear force-midspan deflection curve of control beam I and beam S-CU45-1

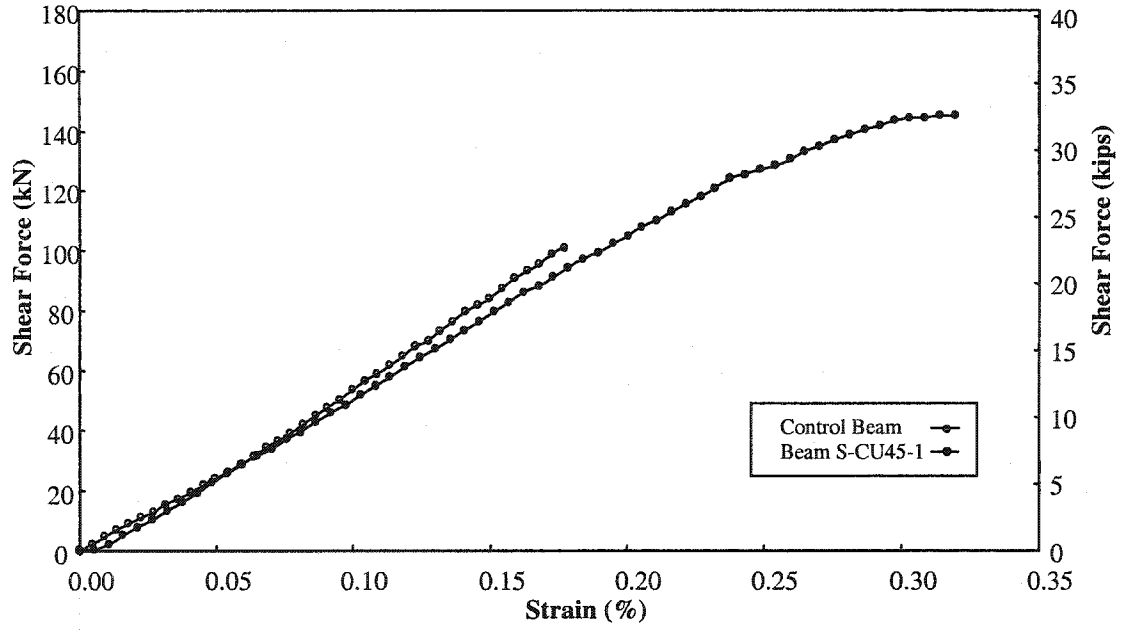

Fig. 6.28 Shear force-midspan concrete compression strain of control beam I and beam S-U-2

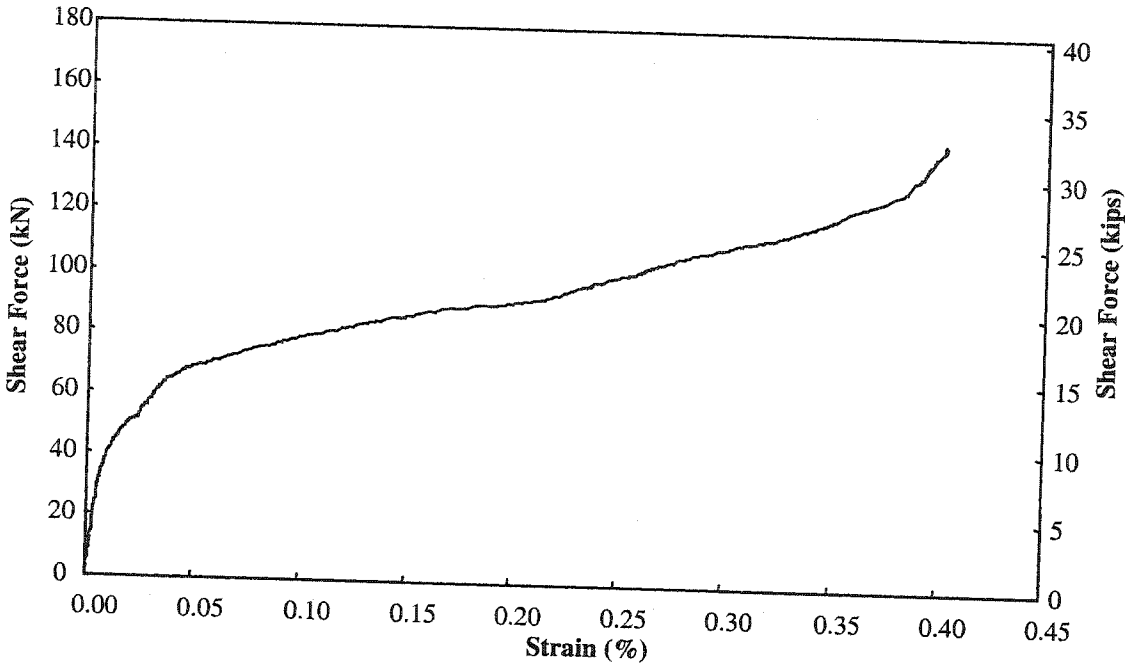

Fig. 6.29 Shear force-45° strain at beam side of beam S-CU45-1

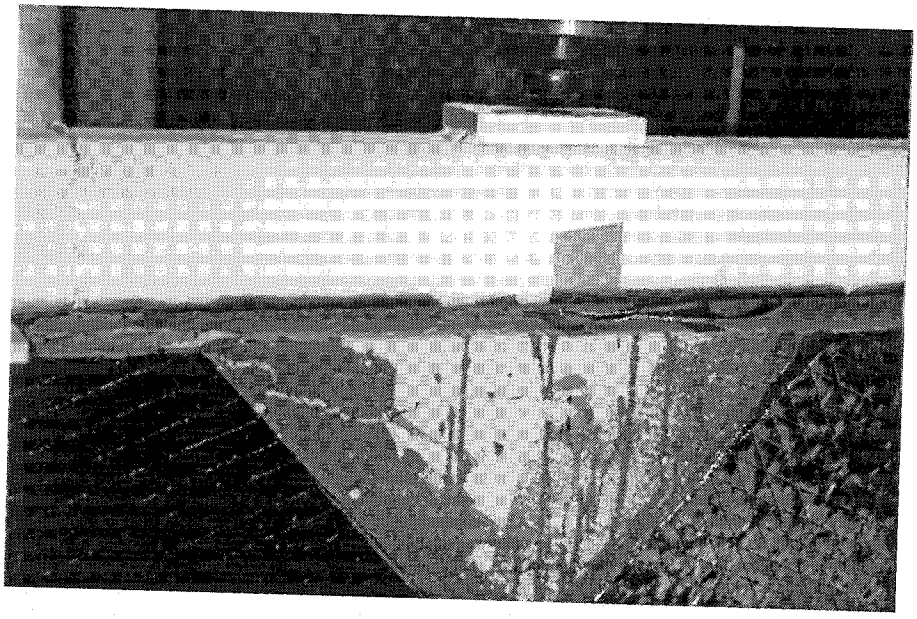

Fig. 6.30 Failure of beam S-CU45-1

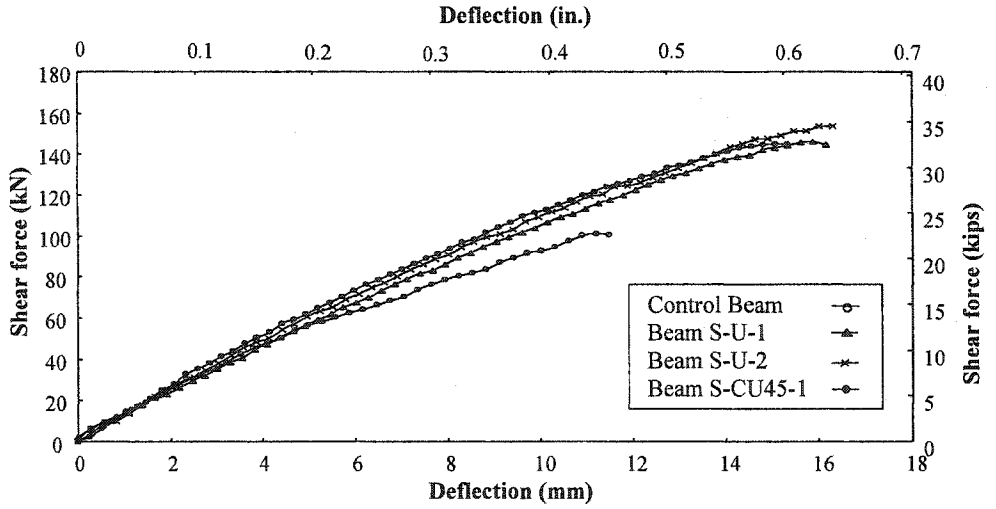

(a) Midspan deflection

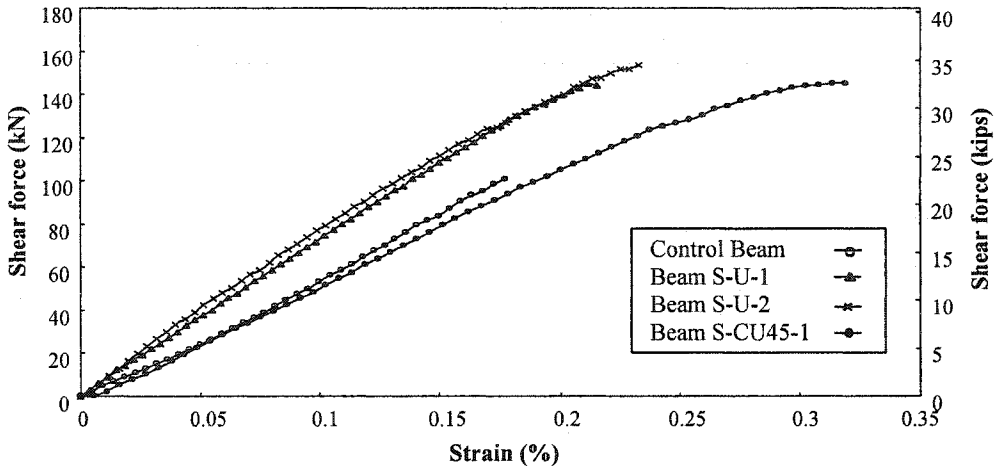

(b) Concrete compression strain at midspan

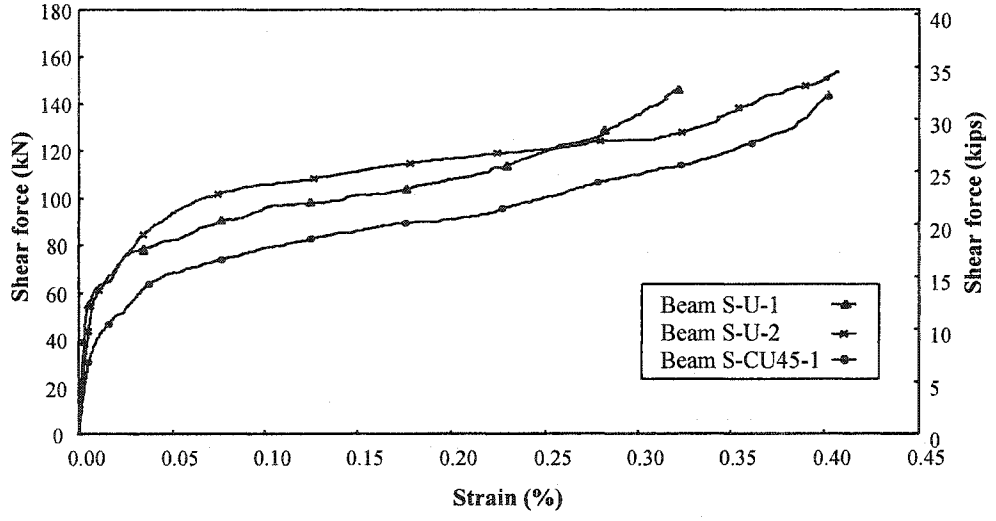

(c) 45° strain at sides

Fig. 6.31 Comparison between group G beams

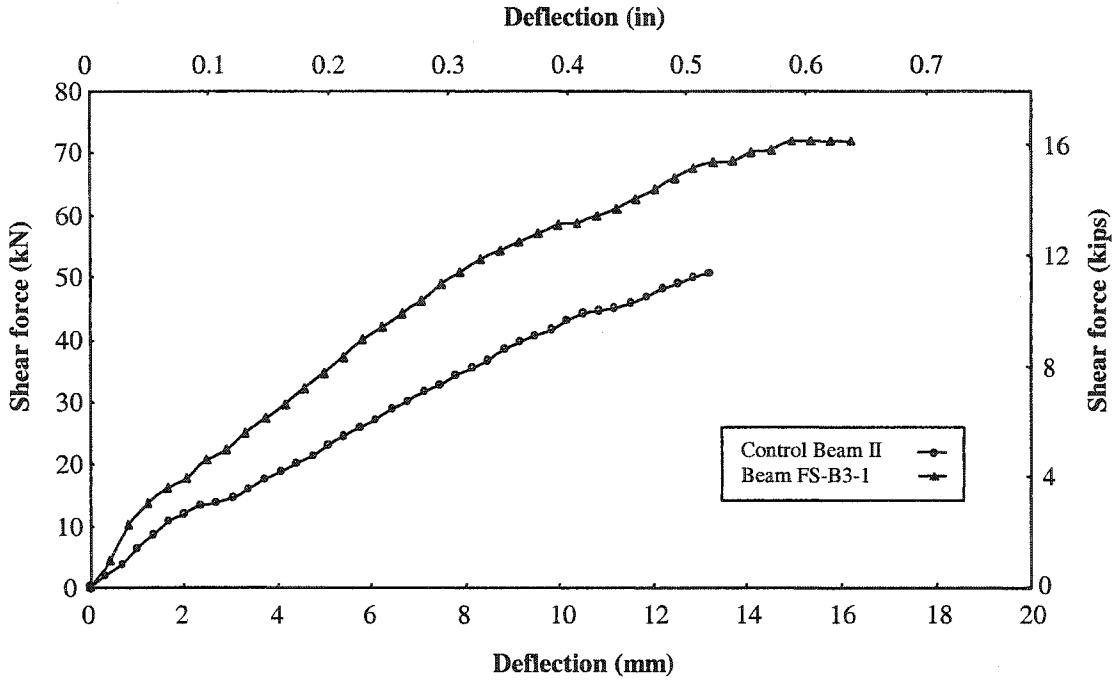

(a) Midspan deflection

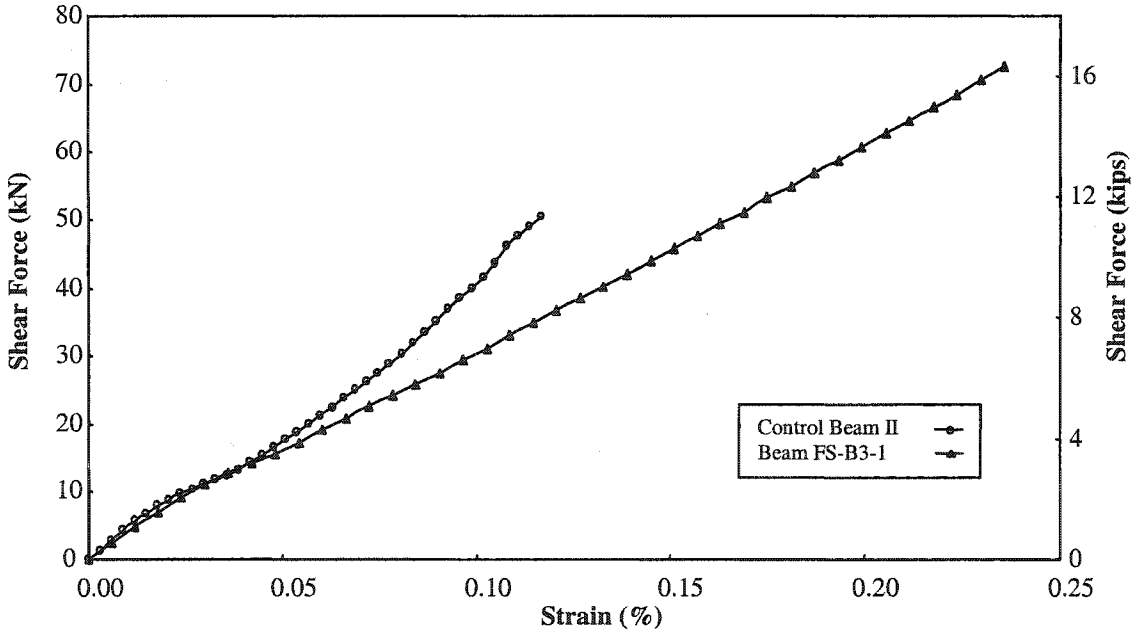

(b) Concrete compression strain at midspan

Fig. 6.32 Behavior of group H beams

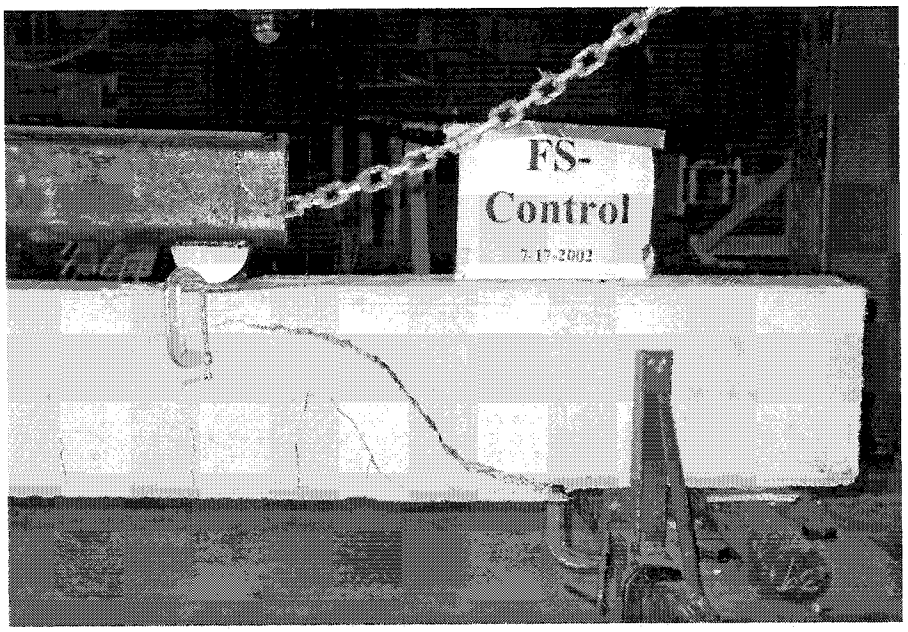

Fig. 6.33 Failure of beam control beam II

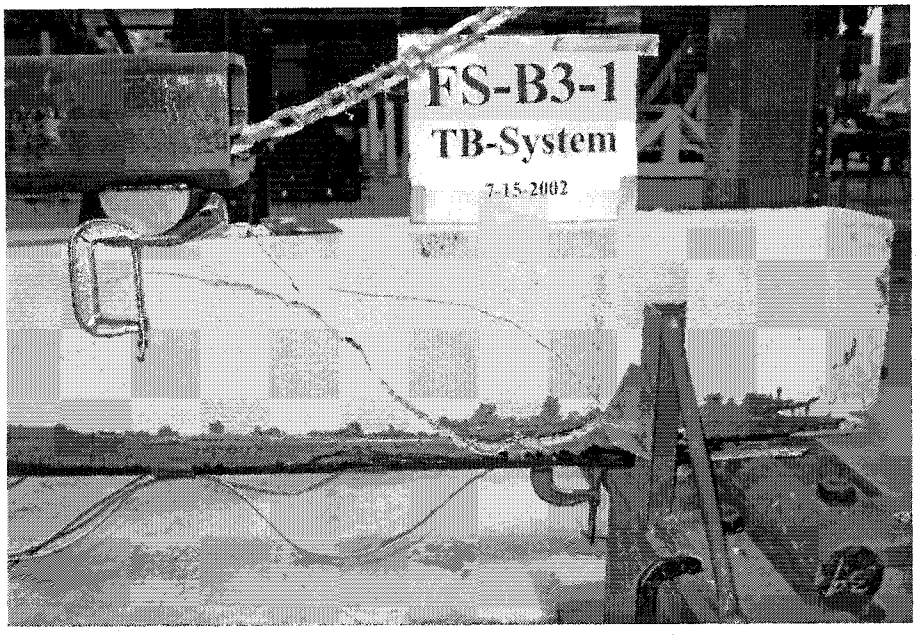

Fig. 6.34 Failure of beam FS-B3-1

CHAPTER 7

STRENGTHENING OF OVERHANGING AND CONTINUOUS BEAMS USING THE DEVELOPED TRIAXIALLY BRAIDED FABRIC

7.1 General

Ductility is a very important requirement in the design of any structural element. Ductile structures can exhibit large deformations before any potential failure and thus provide visual indicators that give the opportunity for remedial actions prior to failure. Ductility is even more important for statically indeterminate structures, such as continuous beams, as it allows for moment redistribution through the rotation of plastic hinges. Moment redistribution permits the utilization of the full capacity of more segments of the beam. A large loss in ductility is experienced when using currently available FRP materials for strengthening reinforced concrete beams for flexure. This chapter investigates the capability of the triaxially braided fabric to offer adequate ductility at the plastic hinge regions of strengthened reinforced concrete overhanging and continuous beams in flexure. Two groups of beams were experimentally investigated. The first group included beams with one overhanging cantilever strengthened in flexure and loaded with one concentrated load at the end of the cantilever. The second group included continuous beams with two spans strengthened in flexure along their positive and negative moment regions and loaded with a concentrated load at the middle of each span. One beam in each group was not strengthened and was tested as a control beam. The behavior of the beams strengthened with the new fabric were investigated and compared with the behavior of similar beams strengthened using a commercially available carbon fiber sheet. The responses of the beams were examined for deflections, strains, and failure modes.

7.2 Experimental Program

7.2.1 Test beams

The experimental program consisted of testing two beam groups with three beams each. All beams had identical cross sectional dimensions of 152 mm × 254 mm (6 in. × 10 in.) and lengths of 4270 mm (168 in.). The beams were symmetrically reinforced with two #5 (16 mm) rods at the top and the bottom. The beams were over-reinforced for shear with #3 (9.5 mm) closed stirrups spaced at 102 mm (4.0 in.). The beams of the first group, group I, were tested with one overhanging cantilever, while the beams of the second group, group J, were tested with two continuous spans. Fig. 7.1 through Fig. 7.4 show the beam dimensions, reinforcement details, and loading set up of group I and J. The beams were prepared by sandblasting their surfaces to roughen them, cleaned with an air nozzle, and finally wiped to remove any dust. The compressive strength of the concrete at the time the beams were tested was 41.5 MPa (6,000 psi). The steel reinforcement used had a yield stress of 490 MPa (71,000 psi).

7.2.2 Strengthening materials

In addition to the new triaxially braided ductile fabric, a commercially available carbon fiber sheet was used to strengthen identical beams in order to compare their behavior with those strengthened with the new fabric. In order to have an objective comparison, the carbon fiber sheet was selected to have a load-strain response similar to that initially (before yielding) exhibited by the triaxial ductile fabric. The experimental load-strain diagrams of the triaxial fabric and the carbon fiber sheet are shown in Fig. 7.5 and their properties are listed in Table 7.1. Herein, it can be noted that the new triaxial fabric has a yield-equivalent load of 0.19 kN/mm (1.08 kips/in.), while the carbon fiber sheet has an ultimate load of 0.34 kN/mm (1.95 kips/in). Using the tensile properties of

the materials, it was determined that two layers of the carbon fiber sheet would exhibit a load-strain response similar to that initially exhibited by one layer of the triaxial fabric. An epoxy resin was used to impregnate the fibers and to act as an adhesive between the strengthening material and the concrete surface. This epoxy has an ultimate tensile strength of 66.2 MPa (9.62 ksi) with an ultimate strain of 4.4% and a compressive strength of 109.2 MPa (15.84 ksi).

7.2.3 Strengthening and set up

7.2.3.1 Group I

Group I consisted of three beams with one overhanging cantilever each. Each beam had an inner span of 2440 mm (96 in.) and a cantilever span of 1070 mm (42 in.). One of these beams had no external strengthening and was tested as a control beam. The other two beams were strengthened on their top faces along 3350 mm (132 in.) of their length, as shown in Fig. 7.2. One of these two beams, beam F-NV, was strengthened using two layers of the new triaxial ductile fabric each 135 mm (5.33 in.) wide. The other beam, beam F-NVC, was strengthened using four layers of the carbon fiber sheet that 146 mm (5.75 in.) wide. The deflection of the cantilever was measured at the loading point and at its midspan, while the deflection of the inner span was measured at its mid and quarter points, using string potentiometers. The FRP strain was measured at different locations along the beam using electrical resistance strain gages, as shown in Fig. 7.1. The beams were loaded using a hydraulic actuator.

7.2.3.2 Group J

Group J contained three continuous beams. Each beam had two spans of 1980 mm (78 in.) each. The beams were loaded with a concentrated load at the middle of each

span. One of these beams had no external strengthening and was tested as a control beam. The other two beams were strengthened along their negative and positive moment regions around the top/bottom face extending 152 mm (6 in.) on both sides as a U-wrap at the locations shown in Fig. 7.3. The first beam, beam F-CT, was strengthened using one layer of the triaxial fabric that was 457 mm (18 in.) wide, U-wrapped around the tension faces and the sides, while the other beam, beam F-CTC, was strengthened using two layers of the carbon fiber sheet that were each 457 mm (18 in.) wide, with the same wrapping scheme. The deflection was measured at the middle and quarter of each span using string potentiometers. The FRP strain was measured at the beam tension face at the central support and at the middle of each span using electrical resistance strain gages. Two hydraulic actuators were used to load the beam, one for each span. Table 7.2 summarizes the test beams.

7.3 Test Results and Discussion

7.3.1 Group I

Test results for group I beams are shown Figures 7.6 through 7.9 and listed in Table 7.3. The failed beams are shown in Figures 7.10 through 7.12. The ductility of each beam was determined by calculating its ductility index; that is, the ratio between the ultimate deflection and the yield deflection of the cantilever end at the loading point.

7.3.1.1 Control beam I

The control beam had a yield load of 35 kN (7.9 kips) and an ultimate load of 38 kN (8.5 kips). The beam failed by yielding of steel followed by compression failure of concrete at the section of maximum bending moment. Fig. 7.6 indicates that the cantilever end exhibited excessive deflections after yielding with a considerable yield

plateau. The beam had a ductility index of 4.53. The failed beam is shown in Fig. 7.10. The deflection profile shown in Fig. 7.7 indicates that a considerable rotation of the beam occurred after the formation of the plastic hinge.

7.3.1.2 Beam F-NVC

Beam F-NVC yielded due to yielding of the steel reinforcement at a load of 48 kN (10.8 kips) and failed suddenly at a load of 54 kN (12.1 kips) due to debonding of the carbon fiber sheet from the concrete surface. The beam showed almost no yield plateau with a ductility index of 1.47. The maximum recorded carbon fiber strain at the section of the maximum bending moment was 0.70%, indicating that only 58% of the sheet strength was utilized. Fig. 7.9 shows that the strain distribution along the beam at failure was very similar to the distribution of the bending moment. Fig. 7.11 shows the failed beam.

7.3.1.3 Beam F-NV

Beam F-NV behaved similarly to beam F-NVC up to yield, which occurred at a load of 47 kN (10.6 kips) due to yielding of both the steel and the fabric. The fabric yielding was accompanied by the sounds of rupture of its low elongation fibers. Note from Fig. 7.6 and Fig. 7.7 that beam F-NV exhibited more deflection before failure than beam F-NVC. Failure in beam F-NV occurred at a load of 52 kN (11.7 kips) due to rupture of the fabric. A ductility index of 1.83 was exhibited. The fabric showed a considerable increase in strain after yield in comparison to the carbon fiber sheet, as shown in Fig. 7.8. The fabric strength was fully exploited; as its maximum recorded strain was 1.54%, which was more than its yield strain. The strain profile at failure, shown in Fig. 7.9, shows a noticeable increase in fabric strain at the section of the maximum bending moment. The failed beam is shown in Fig. 7.12.

Clearly, the difference between the failure modes of beam F-NV and F-NVC can be attributed to the difference in the tensile behavior between the triaxial ductile fabric and the carbon fiber sheet. While the carbon fiber sheet exhibits a linear stress-strain response up to failure, the triaxial fabric exhibits a linear stress-strain behavior up to a certain point, where the strain increases without a corresponding increase in load. Since the four layers of the carbon fiber sheet used in beam F-NVC had similar load-strain behavior to that initially provided by the two layers of the triaxial fabric used in beam F-NV, beam F-NVC behaved similarly to beam F-NV up to yield. After yield, the two beams behaved differently. The tension force in the carbon fiber sheet kept increasing after yielding of beam F-NVC, exceeding its anchorable limit and causing debonding of the sheet from the concrete surface. On the other hand, the force in the triaxial ductile fabric used in beam F-NV did not significantly increase after it yielded. Thus, it did not exceed its anchorable limit and debonding did not take place. In addition, the triaxial fabric exhibited an increase in strain after yield, which resulted in a higher ductility.

7.3.2 Group J

Test results for the beams of this group are shown Fig. 7.13 through 7.16, and listed in Table 7.3. The failed beams are shown in Fig. 7.17 through 7.20. Note that the load in Figures 7.13, 7.15, and 7.16 is the load at each span (P) and not the total load on the beam. The beam ductility index is calculated as the ratio between the ultimate midspan deflection and its deflection at first yield.

7.3.2.1 Control Beam J

The control beam exhibited a linear load-deflection behavior after cracking up to yielding of the tension steel at the section of the maximum negative bending moment

over the central support, which occurred at a load of 92 kN (20.7 kips). After this point, a gradual decrease in the slope of the load-deflection curve was observed. The tension steel at the sections of the maximum positive bending moment yielded later, causing a significant decrease in beam stiffness as the deflection then started to increase significantly without a corresponding increase in load, as shown in Fig. 7.13. The beam failed by compression failure of the concrete at the midspan at a load of 127 kN (28.5 kips). A ductility index of 3.12 was observed. The beam deflection profile, shown in Fig 7.14, indicates that deformation of the beam at failure was very localized at the sections of maximum positive and negative moments, at the midspan and the central support, respectively.

7.3.2.2 Beam F-CT

Beam F-CT yielded at a load of 126 kN (28.3 kips) due to yielding of both the tension steel and the fabric over the central support. Yielding of the fabric was accompanied by the sounds of rupture of the low elongation fibers of the fabric. A gradual decrease in beam stiffness was observed, which was revealed by the decrease in the slope of the load-deflection curve, as shown in Fig. 7.13. A significant decrease in beam stiffness was observed after yielding of the beam at the sections of maximum positive moment, which was caused by yielding of both the tension steel and the fabric. A yield plateau similar to that exhibited by the control beam was exhibited thereafter until failure at a load of 175 kN (39.2 kips). The beam failed by tensile rupture of the fabric over the central support, followed by rupture of the fabric at midspan (see Fig. 7.18). A ductility index of 2.65 was exhibited. The load-strain diagrams of the fabric at the midspan and over the central support are shown in Fig. 7.15 and 7.16, respectively. At first failure, the fabric exhibited strain values of 1.8% and 1.47% at the sections of

maximum negative and positive moments, respectively. The fact that these strain values were more than the yield strain of the fabric indicated that that fabric strength was exploited.

7.3.2.3 Beam F-CTC

Beam F-CTC yielded at a load of 136 kN (30.6 kips), where a slight decrease in the load-deflection curve slope was exhibited caused by yielding of the tension steel at the section of the maximum negative moment over the central support. The tension steel at the midspan yielded later causing further decrease in the slope of load-deflection curve. The beam failed suddenly at a load of 185 kN (41.6 kips) by shear-tension failure at one end of the negative moment strengthening carbon fiber sheet, as shown in the photo in Fig. 7.20, followed by debonding of the carbon fiber sheet of the positive moment, as shown in Fig. 7.19. A ductility index of 1.8 was observed. The load-deflection curve indicates a very brittle response as shown in Fig. 7.13. No significant yield plateau was experienced. The load-strain curves, shown in Fig. 7.15 and 7.16, indicate that the carbon fiber sheet exhibited noticeably less strain than the triaxial fabric used in beam F-CT. The maximum recorded strain values did not exceed 0.66%, which indicated that nearly half the strength of the carbon fiber sheet was not exploited.

The new triaxial fabric contains bundles of fibers in the $\pm 45^{o}$ directions. These fibers enable the fabric to have a self-anchorage along its length, when wrapped around the tension face and the vertical sides of the beam. As a result, anchorage failures similar to those experienced by beam F-CTC were not experienced in case of beam F-CT. On the other hand, the carbon fiber sheet used in beam F-CTC is uniaxial, and hence wrapping the beam did not enhance the anchorage. In addition, yielding of the fabric limited the increase in the tensile force developed in it. Therefore, the fabric needed less anchorage

than the carbon fiber sheet, whose tensile force kept increasing until a brittle failure took place. The increase in fabric strain after yield in beam F-CT resulted in a reasonable ductility in the plastic hinge regions and allowed for the redistribution of moment between negative and positive moment zones. Therefore, the full strength of the beam at the cross sections of maximum negative and positive bending moments was utilized.

7.4 Conclusions

1- The unique characteristics of the new triaxially braided ductile fabric helped to avoid the brittle failures associated with the use of conventional FRP materials in flexural strengthening of reinforced concrete beams. The beams strengthened with the new fabric exhibited more ductility than those strengthened with the carbon fiber sheet.

2- The new fabric was successful in providing adequate ductility at the plastic hinge regions. Therefore, the redistribution of the moment between the negative and positive moment zones of the continuous beam became possible. Redistribution of the moment allowed full utilization of the strength of the beam at the cross sections of maximum negative and positive bending moments.

3- Yielding of the fabric was accompanied by various noticeably audible sounds for a long period of time that are loud enough to warn of a potential failure.

4- The new fabric required less anchorage because its ability to yield limited the force that can be developed in it.

5- The existence of bundles of fibers in the $\pm 45^{\circ}$ directions enabled the new fabric to "self anchor" itself when wrapped around the tension face and the vertical sides of the beam along its length. Therefore, it was generally less vulnerable to anchorage failures than the uniaxial carbon fiber sheet.

6- The strength of the new fabric was fully exploited as its maximum recorded strains before beam failure were much more than its yield strain. In contrast, the maximum recorded strains of the carbon fiber sheet were noticeably less than its ultimate strain, which indicated that its strength was not fully exploited.

Table 7.1 Properties of the Strengthening Materials

Type	Yield-Equivalent Load kN/mm (kips/in.)	Yield-equivalent Strain (%)	Ultimate Load kN/mm (kips/in.)	Ultimate Strain (%)	Thickness mm (in.)
Carbon Fiber Sheet	-	-	0.34 (1.95)	1.2	0.13 (0.005)
Triaxial Ductile Fabric	0.19 (1.08)	0.35	0.33 (1.89)	2.10	1.0 (0.039)

Table 7.2 Summary of Test Beams

Beam Group	Beam Designation	Strengthening Scheme	Strengthening Material	Positive Moment Strengthening		Negative Moment Strengthening	
				Number of Layers	Strengthened Length	Number of Layers	Strengthened Length
Group I	Control I	N/A	N/A	None	None	None	None
	F-NV	Tension face only	Triaxial ductile fabric	None	None	2	3.35 m (11 ft)
	F-NVC		Carbon fiber sheet	None	None	4	
Group J	Control J	N/A	N/A	None	None	None	None
	F-CT	U-wrap around tension face and sides	Triaxial ductile fabric	1	1.63 m (5.33 ft)	1	1.42 m (4.67 ft)
	F-CTC		Carbon fiber sheet	2		2	

Table 7.3 Summary of Test Results

Beam Group (1)	Beam Designation (1)	Strengthening System (2)	Yield Load kN (kips) (3)	Deflection* at Yield mm (in.) (4)	Failure Load kN (kips) (5)	Deflection* at Failure mm (in.) (6)	Ductility Index (7) = Col. 6 / Col. 4	Type of Final Failure (8)
Group I	Control I	N/A	35 (7.9)	30.5 (1.20)	38 (8.5)	138.2 (5.44)	4.53	Steel yield followed by concrete failure
	F-NV	Triaxial ductile fabric	47 (10.6)	35.7 (1.41)	52 (11.7)	65.3 (2.57)	1.83	Steel & fabric yield followed by fabric rupture
	F-NVC	Carbon fiber sheet	48 (10.8)	37.8 (1.49)	54 (12.1)	55.6 (2.19)	1.47	Steel yield followed by sheet debonding
Group J	Control J	N/A	92 (20.7)	9.3 (0.37)	127 (28.5)	29.1 (1.15)	3.12	Steel yield followed by concrete failure
	F-CT	Triaxial ductile fabric	126 (28.3)	9.1 (0.36)	175 (39.3)	23.4 (0.92)	2.57	Steel & fabric yield followed by fabric rupture
	F-CTC	Carbon fiber sheet	136 (30.6)	8.9 (0.35)	185 (41.6)	16.1 (0.63)	1.81	Steel yield followed by shear-tension failure at sheet end

* Deflection at loading point(s)

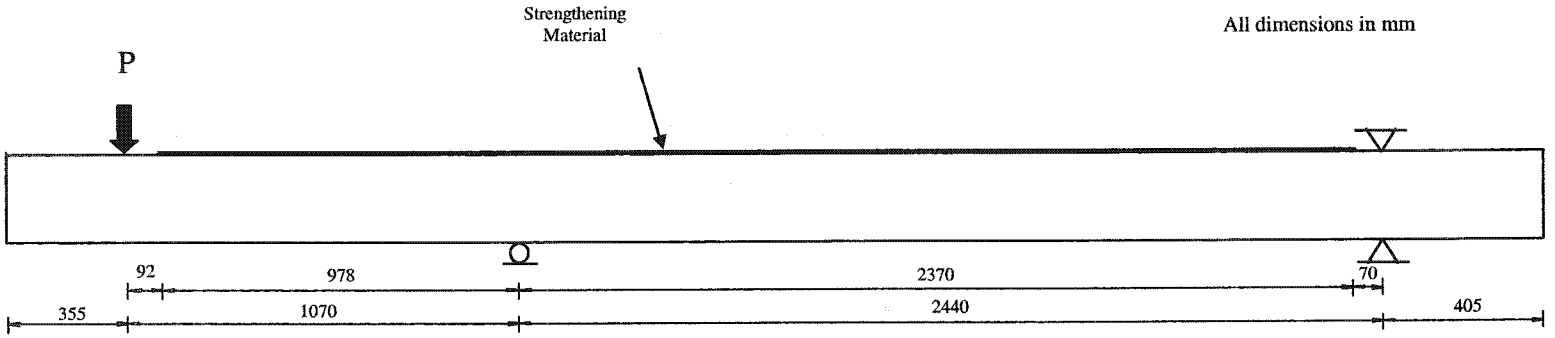

(a) Elevation

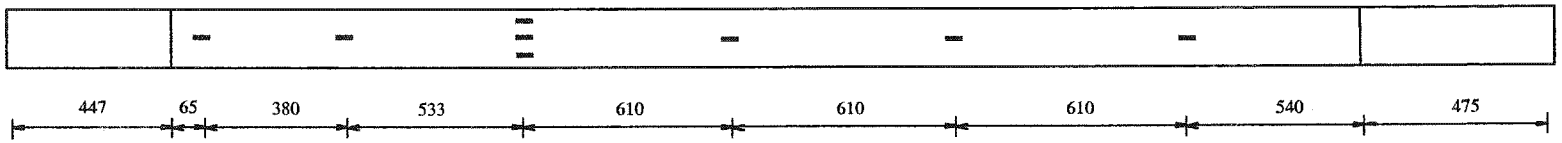

(b) Plan for strain gage locations

Fig. 7.1 Test beam of group I

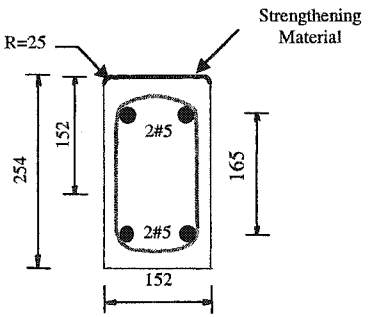

(a) Cross Section A-A

All dimensions in mm

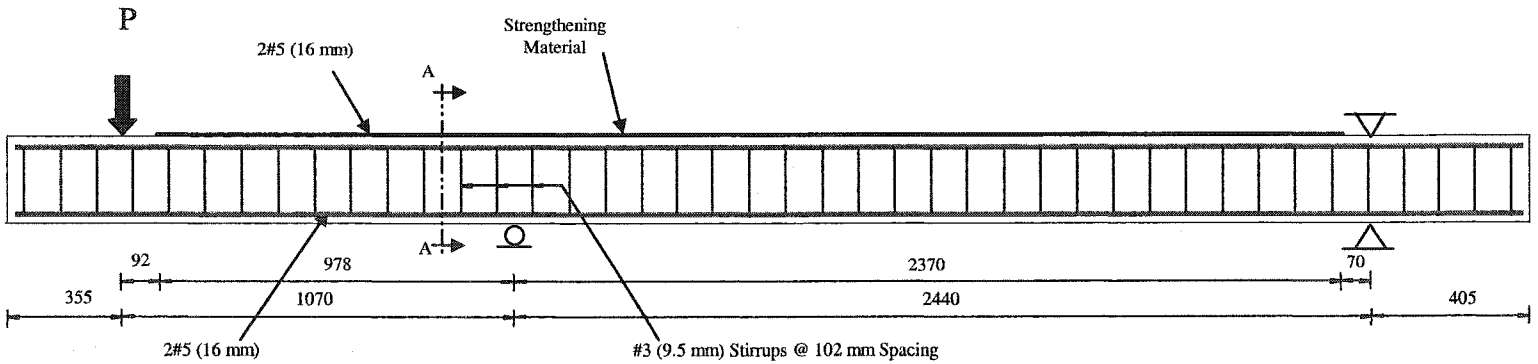

(b) Longitudinal Section

Fig. 7.2 Reinforcement details of test beam of group I

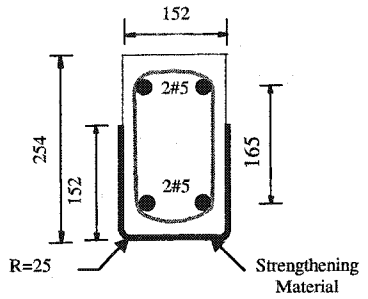

Cross Section A-A

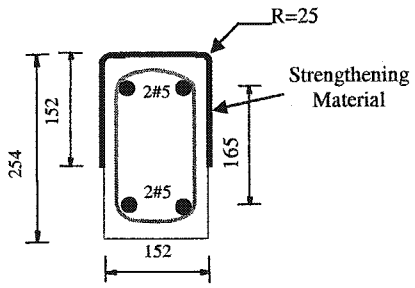

Cross Section B-B

All dimensions in mm

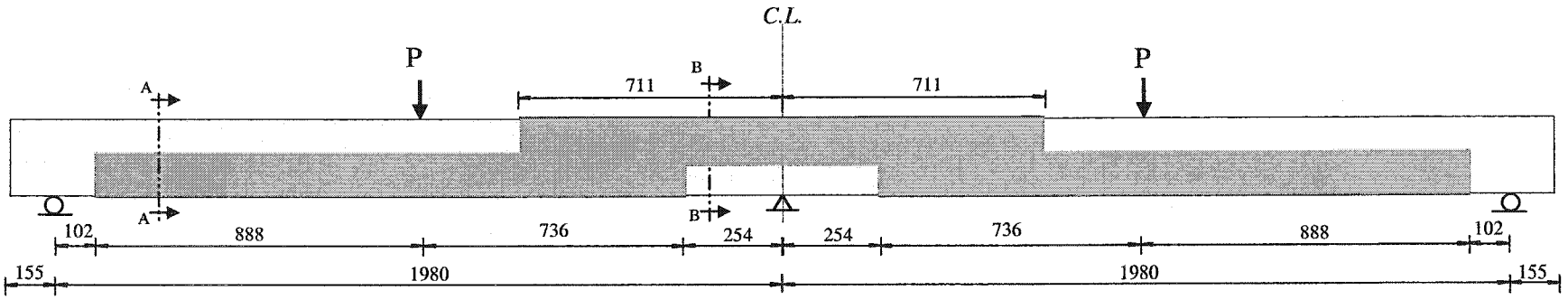

Elevation

Fig. 7.3 Test beam of group J

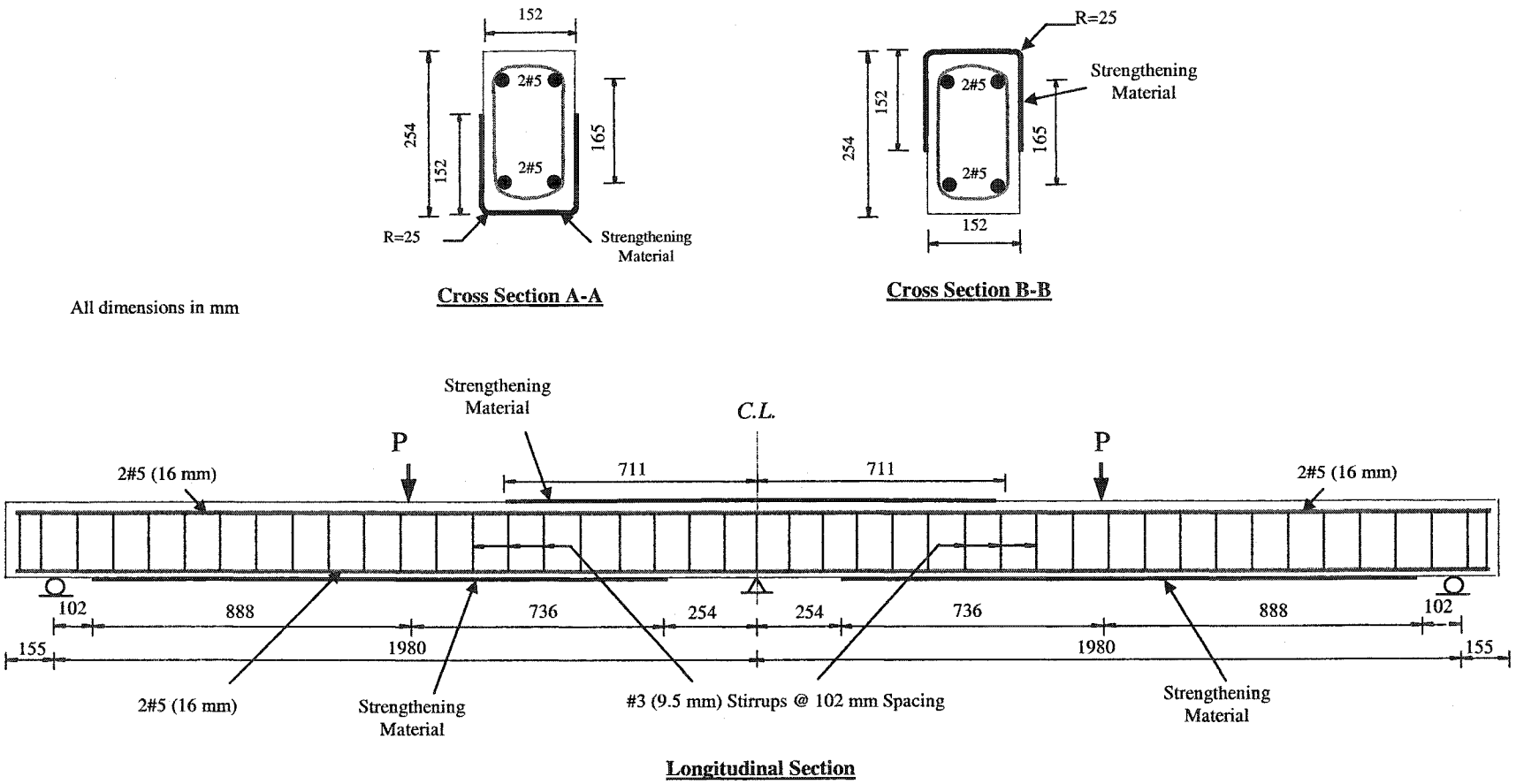

Fig. 7.4 Reinforcement details of test beam of group J

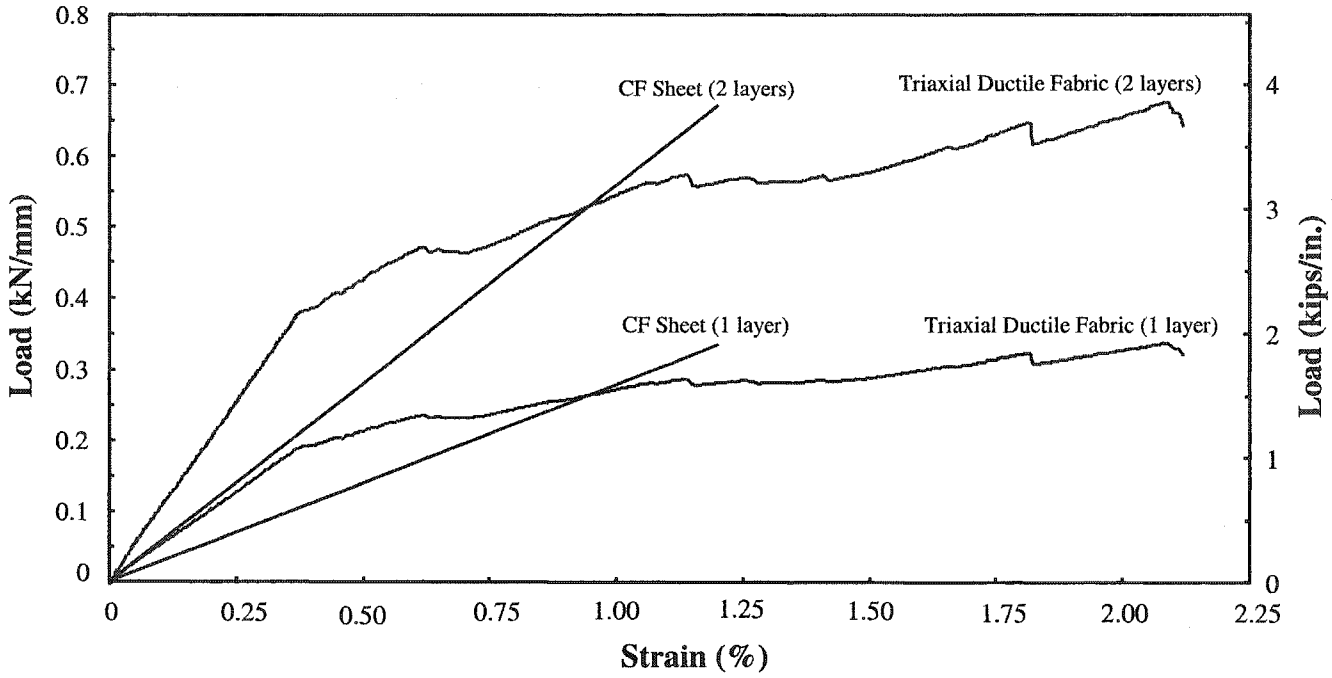

Fig. 7.5 Tensile properties of materials used

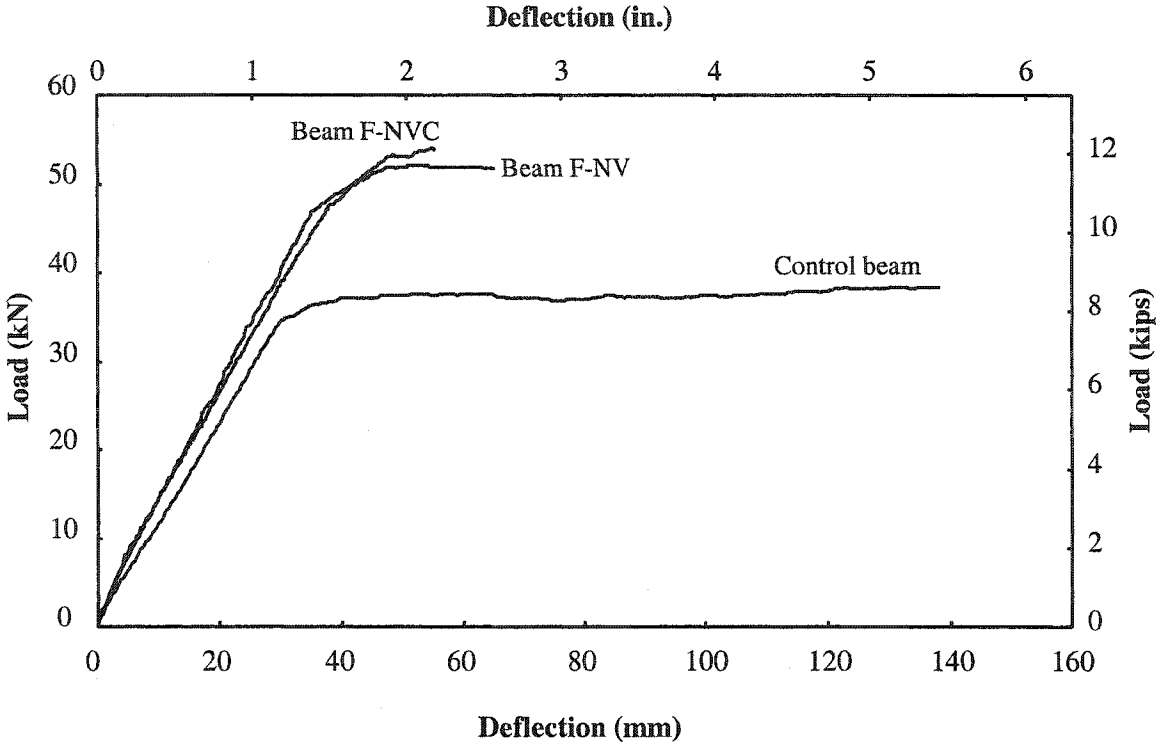

Fig. 7.6 Load-cantilever end deflection curves of group I beams

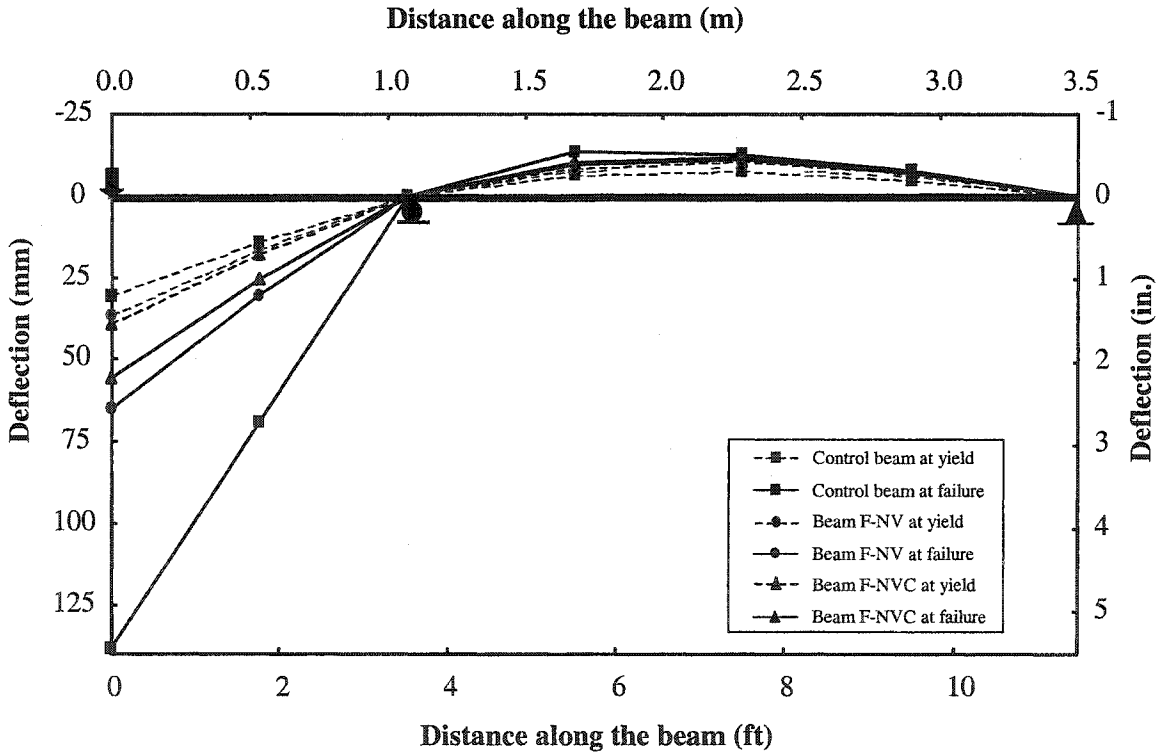

Fig. 7.7 Deflection profiles of group I beams

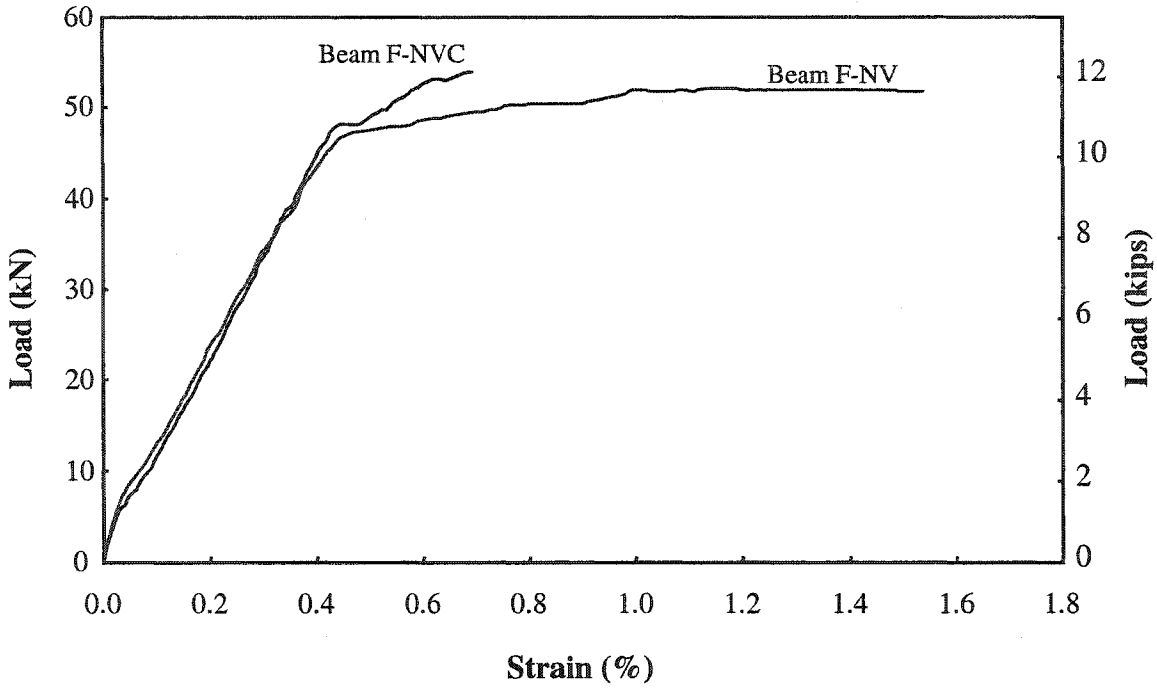

Fig. 7.8 Load-strain curves of group I beams

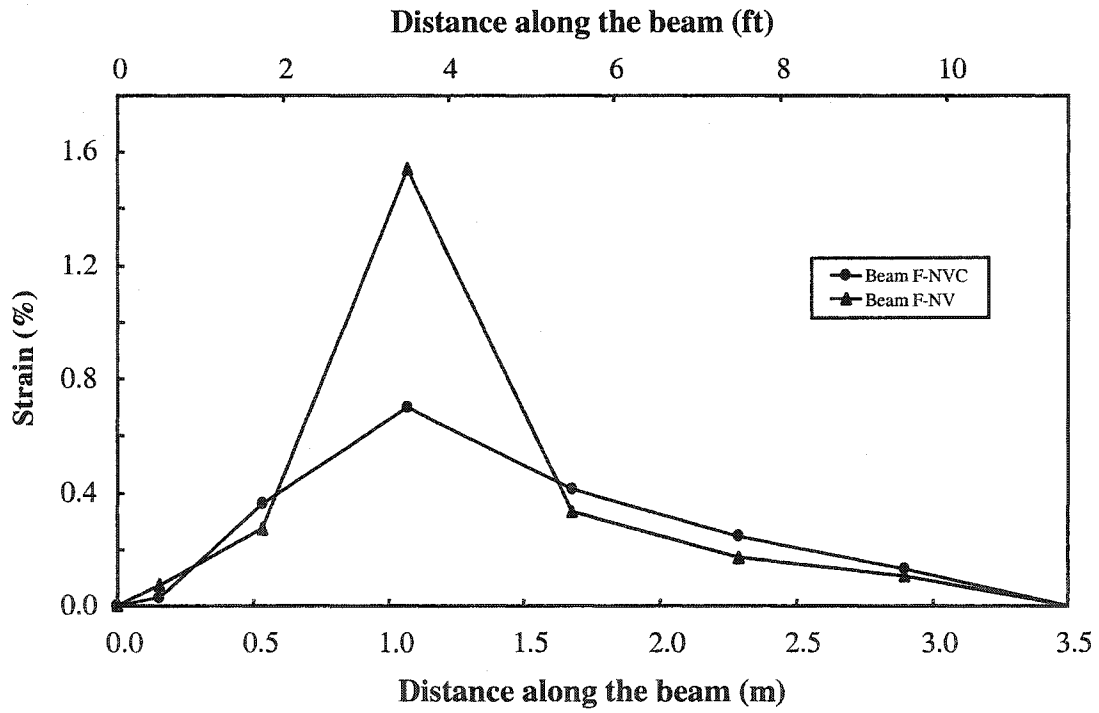

Fig. 7.9 FRP strain profiles at failure of group I beams

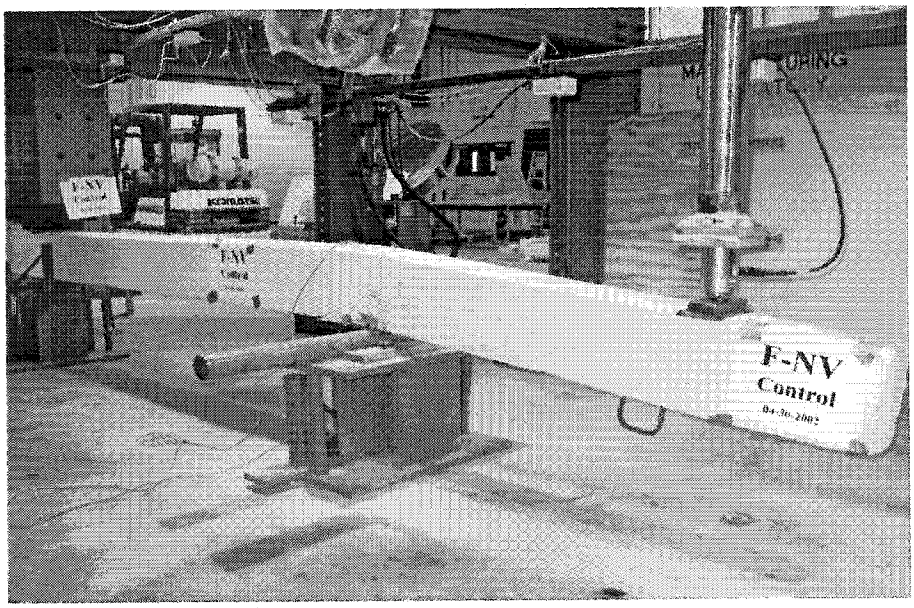

(a) Overall view of the beam

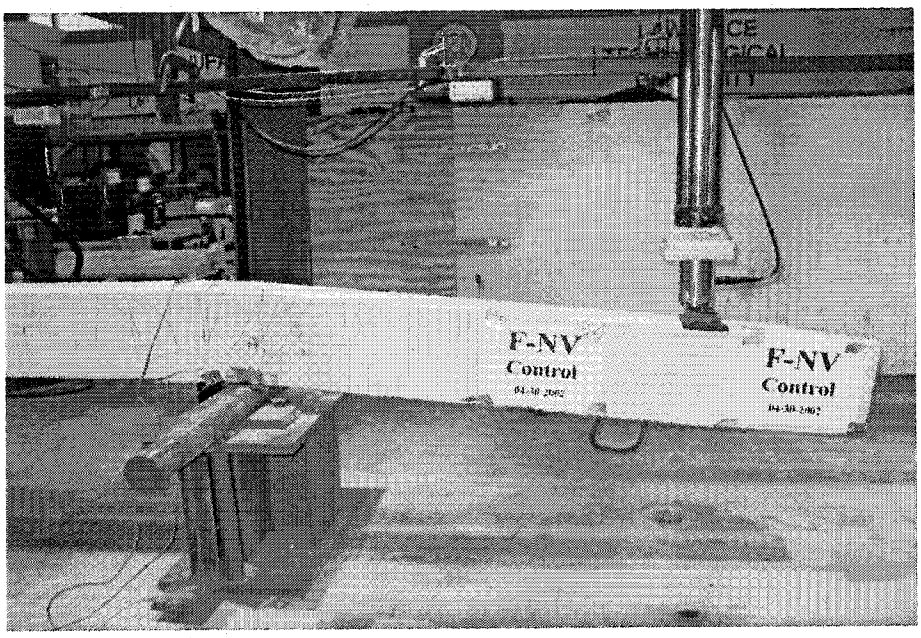

(b) Close-up view of the cantilever

Fig. 7.10 Failure of control beam of group I

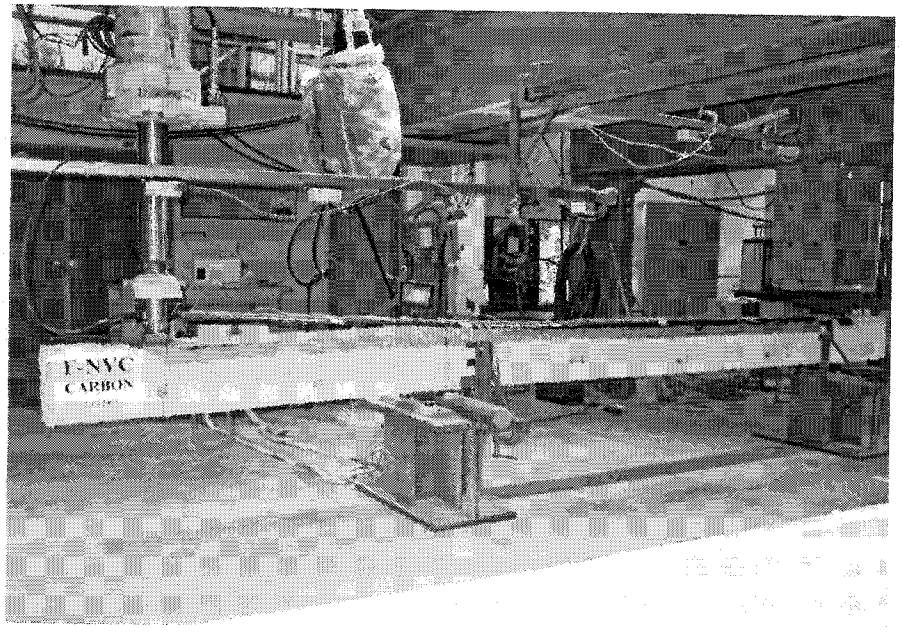

a) Overall view of the beam

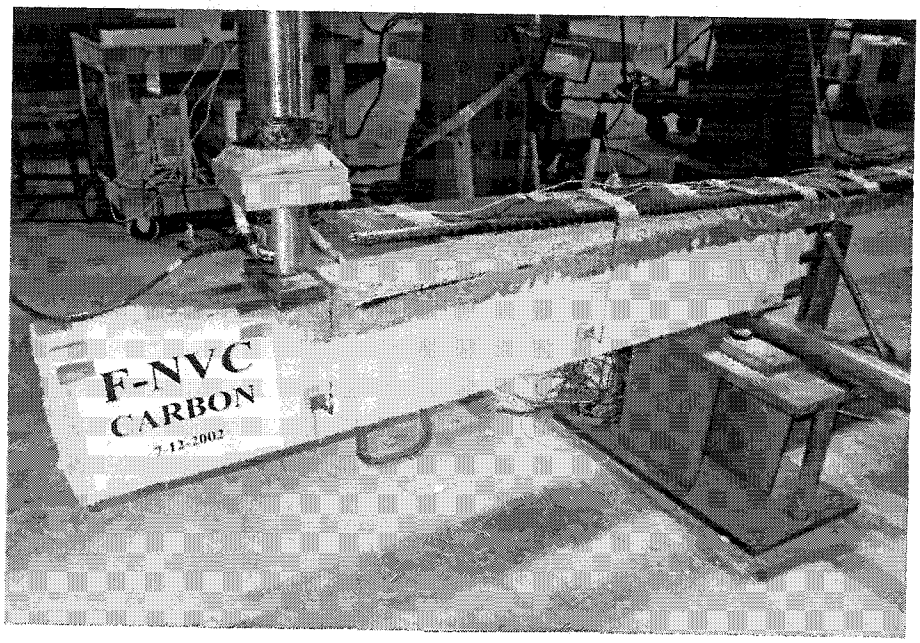

(b) Close-up view of the cantilever

Fig. 7.11 Failure of beam F-NVC

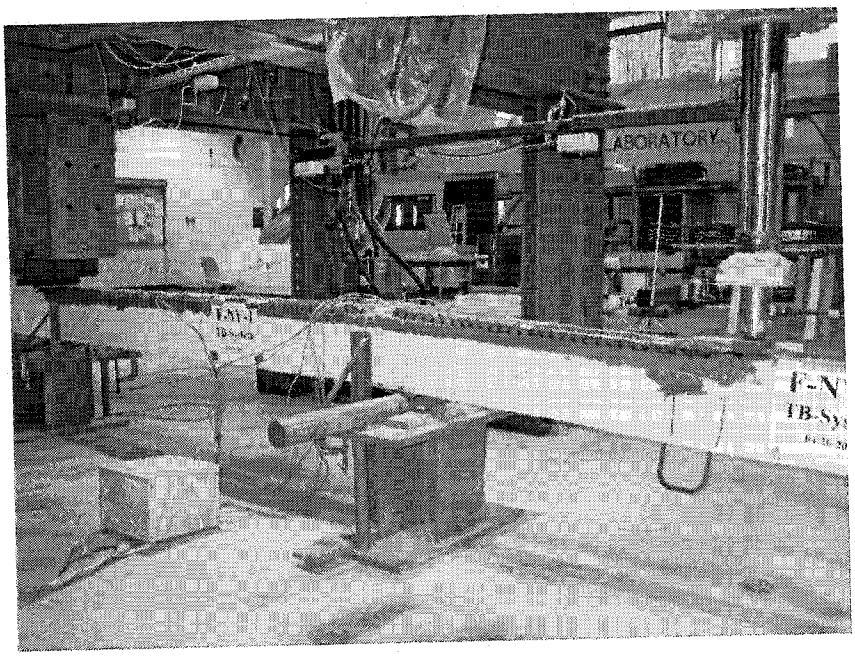

(a) Overall view of the beam

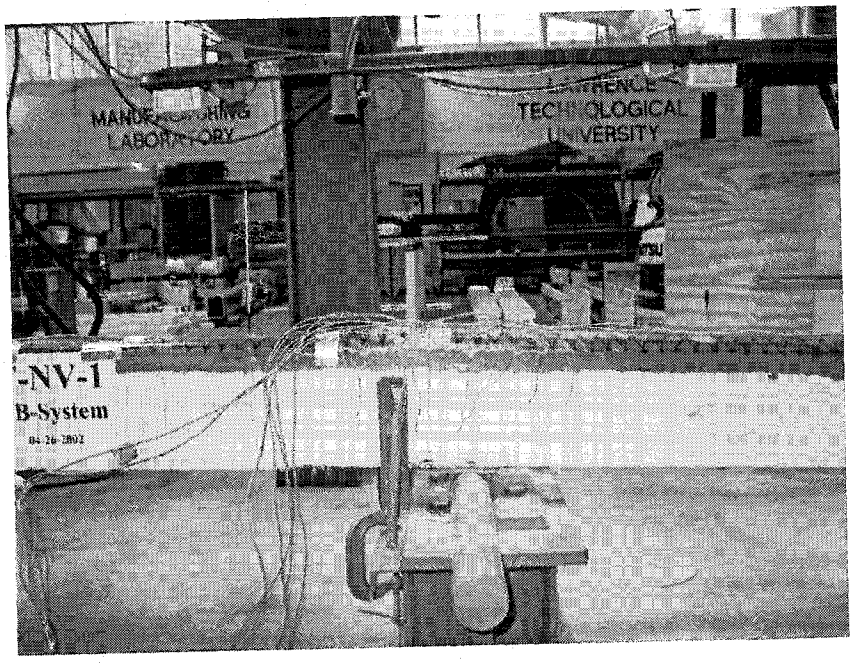

(b) Close-up view of the failed section

Fig. 7.12 Failure of beam F-NV

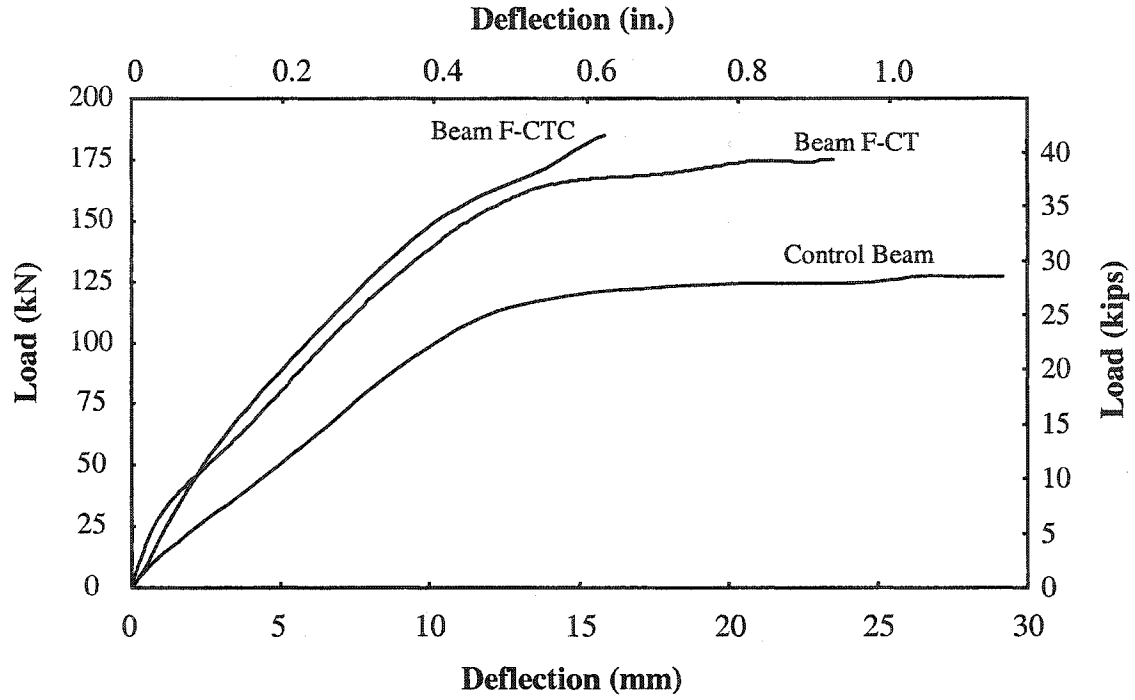

Fig. 7.13 Load-midspan deflection curves of group J beams

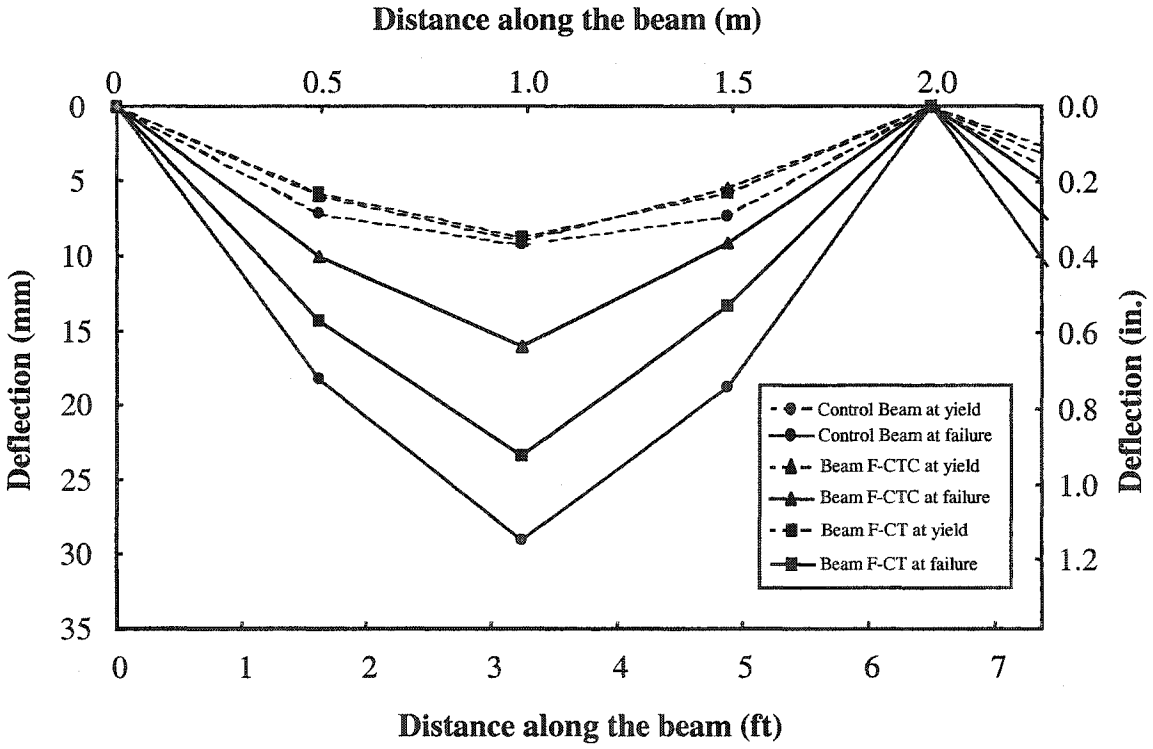

Fig. 7.14 Deflection profile of group J beams

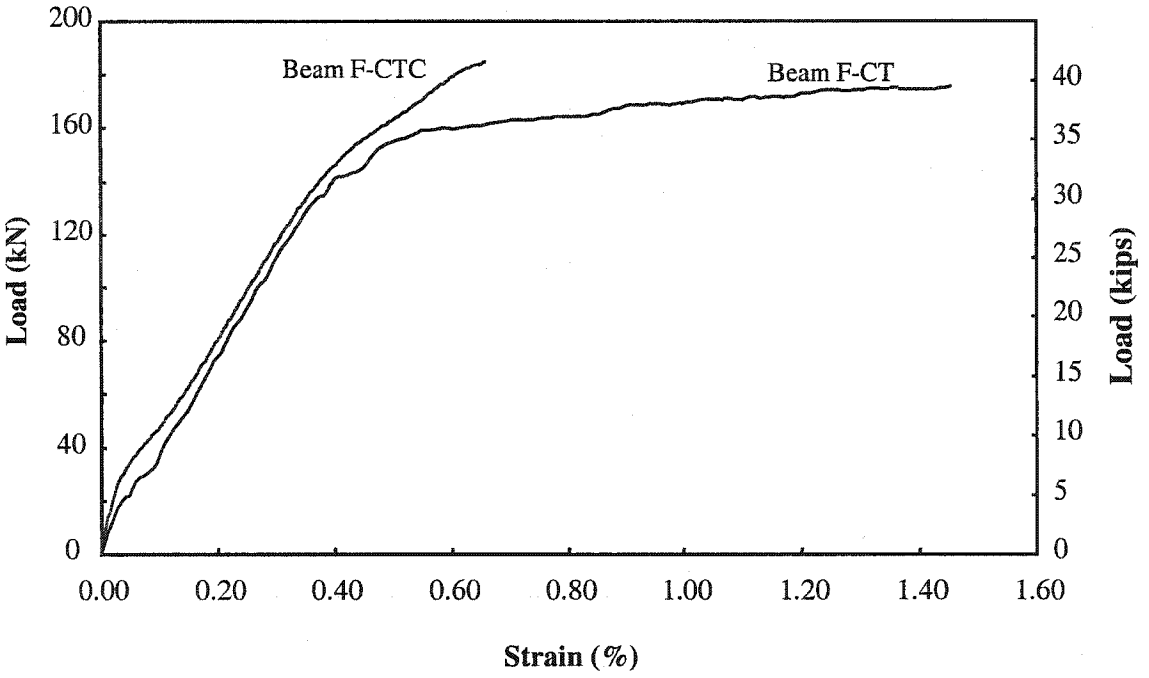

Fig. 7.15 FRP strain at midspan of group J beams

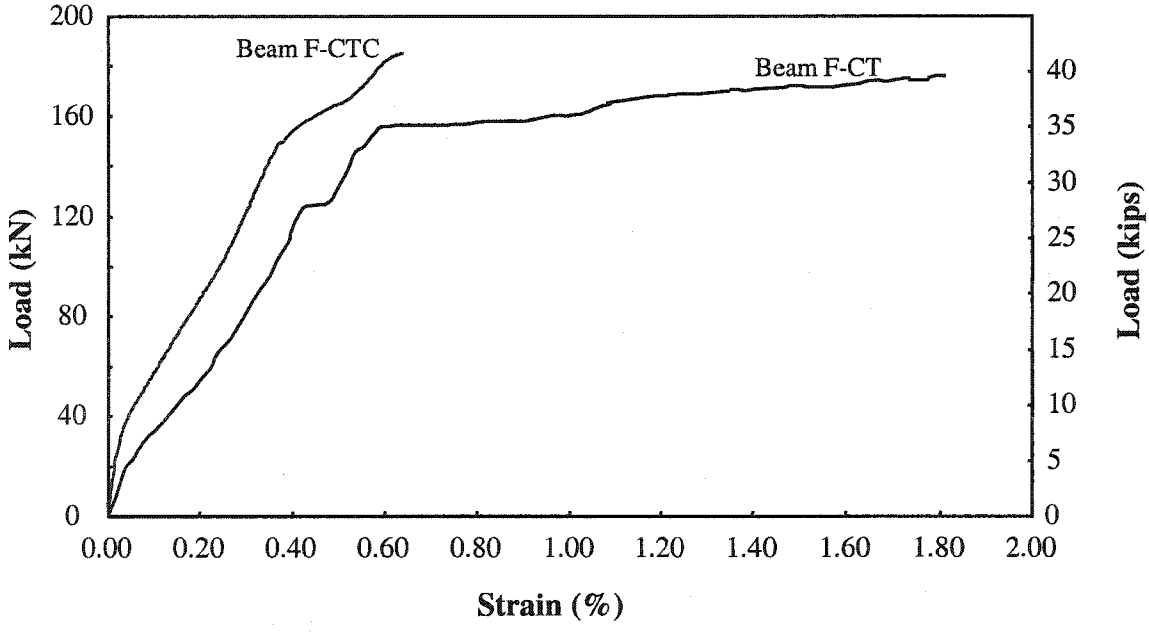

Fig. 7.16 FRP strain at middle support of group J beams

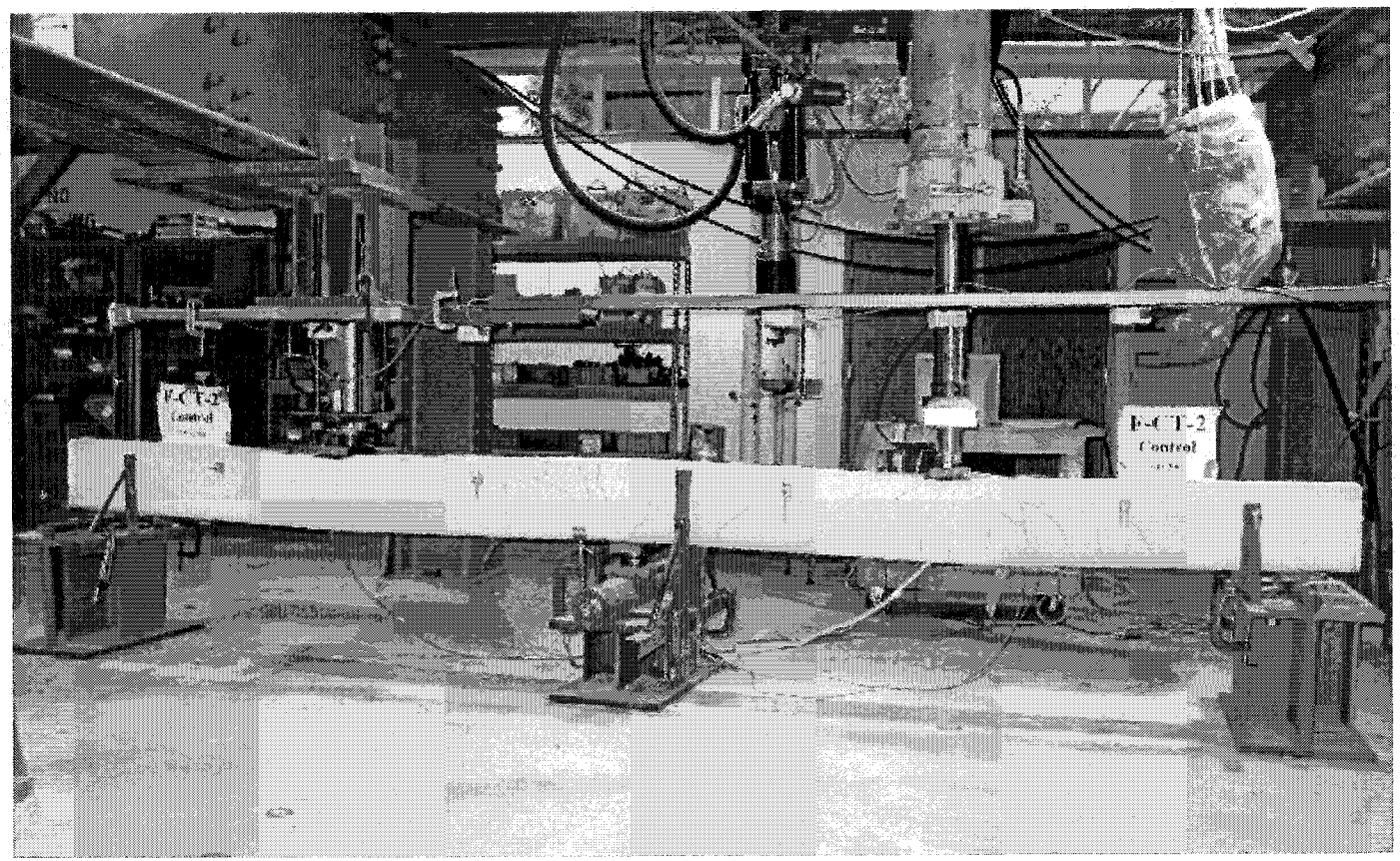

Fig. 7.17 Control beam J at failure

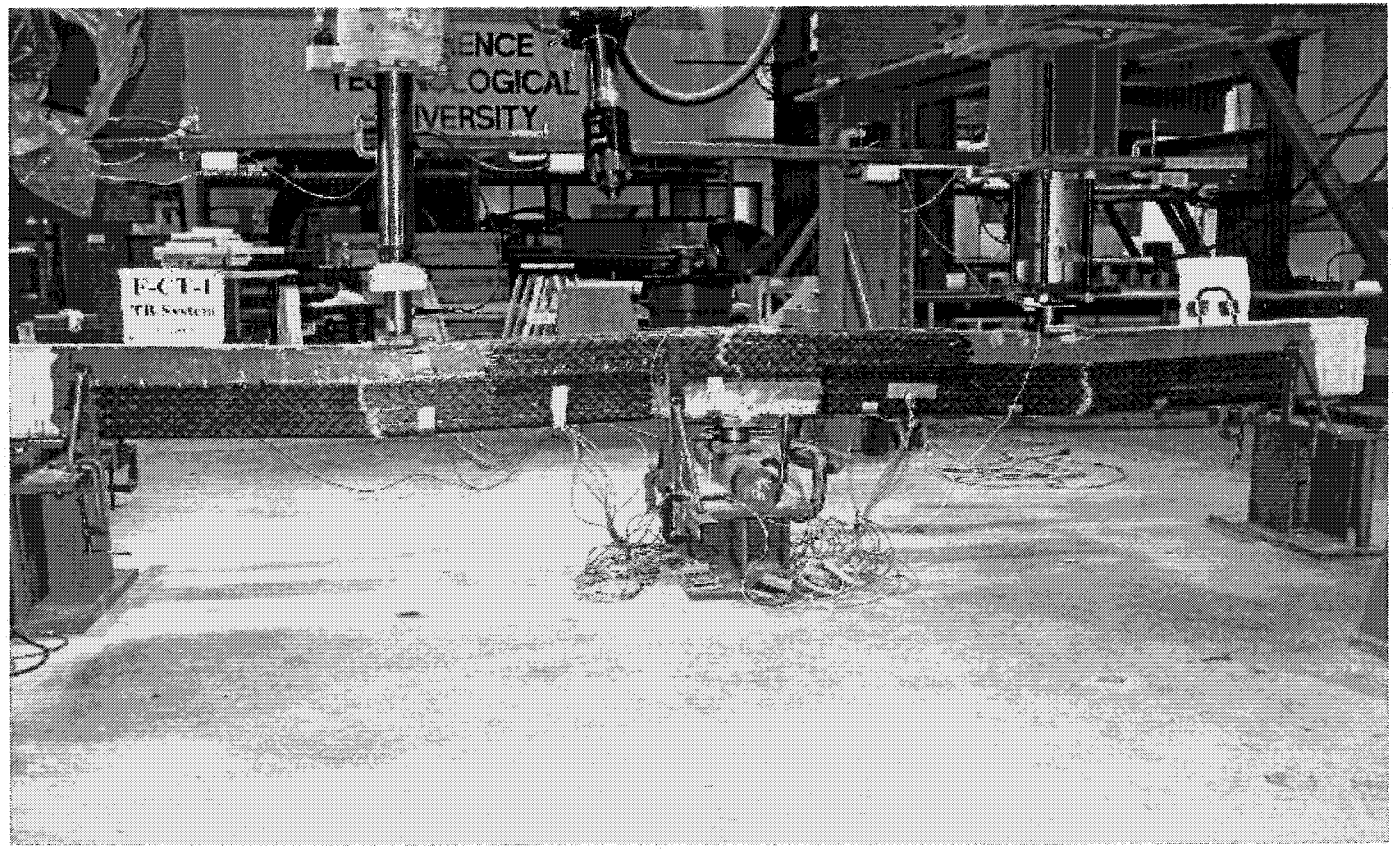

Fig. 7.18 Beam F-CT at failure

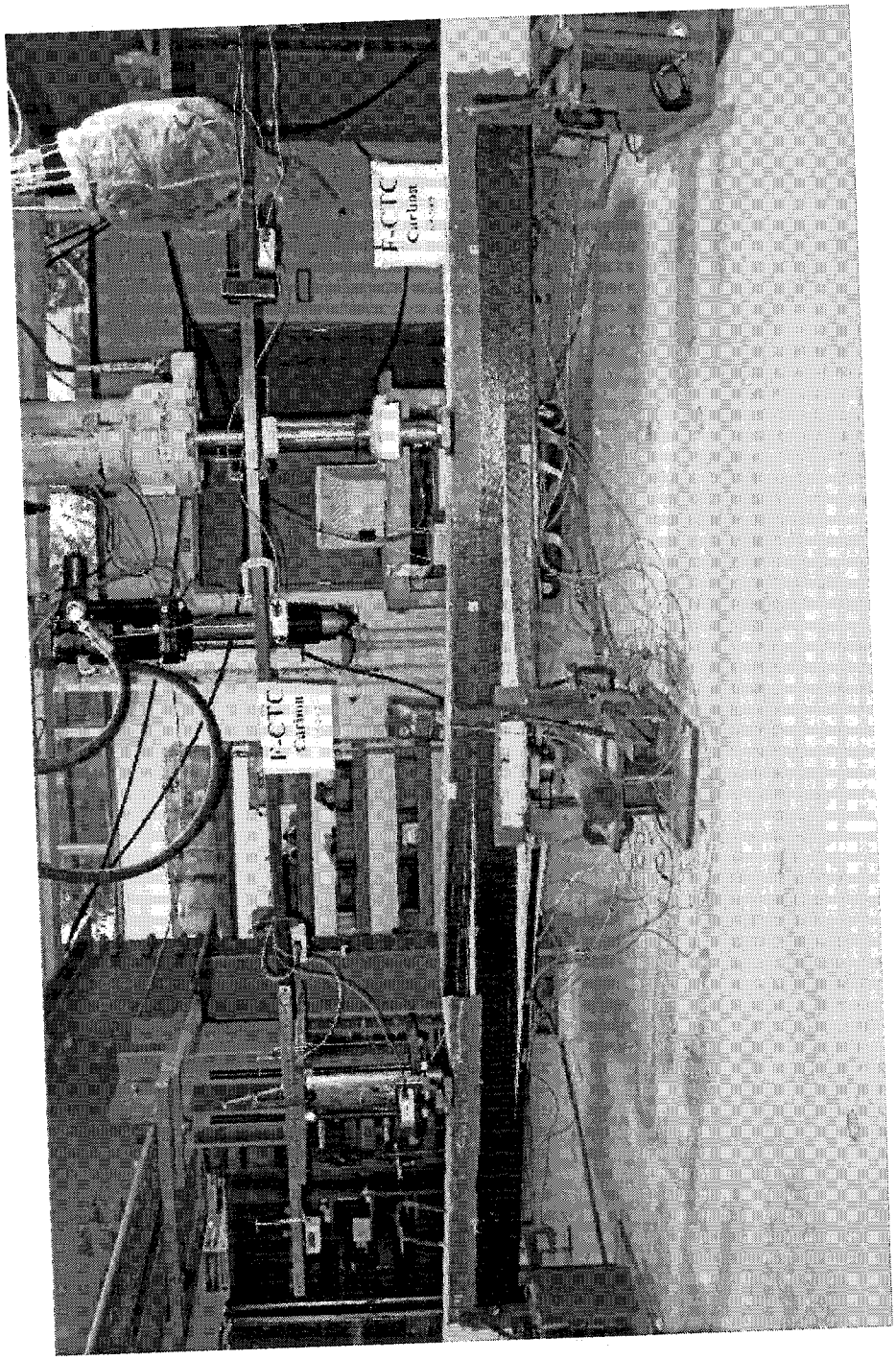

Fig. 7.19 Beam F-CTC at failure

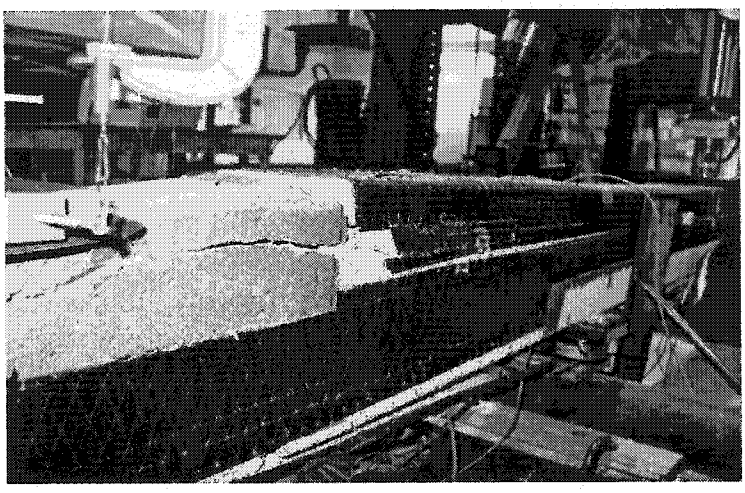

Fig. 7.20 Shear-tension failure at sheet end of beam CTC

CHAPTER 8

FLEXURAL AND SHEAR STRENGTHENING DESIGN USING THE DEVELOPED TRIAXIALLY BRAIDED FABRIC

8.1 General

This chapter presents guidelines for the design of the developed triaxial fabric for flexural and shear strengthening of reinforced concrete beams. Generally, the design follows the guidelines of ACI 440 committee (2002). Bilinear stress-strain relations were used to describe the fabric behavior. These behaviors were used to model the fabric for design. Numerical examples for reinforced concrete beams strengthened in flexure or shear are presented in order to clarify the design procedure.

8.2 Design Stress-Strain Behavior

8.2.1 Axial loading

The axial stress-strain behavior of the fabric can be approximated as a bilinear curve. Fig. 8.1 shows the tested fabric stress-strain behavior in the axial direction. The first linear relation represents the elastic zone, while the second one represents the behavior of fabric thereafter until rupture. The rupture strain of the fabric is suggested to be limited to 1.80%. The second linear part of the relation was defined by linear fitting the experimental stress-strain curve of the fabric from the yield equivalent point up to 1.80% strain value, which is shown in Fig. 8.1 as the "average curve". For the purpose of design, it is suggested to shift that line down by 10% to account for the difference between the normalized linear relation and the experimental curve, which is shown in Fig. 8.1 as the "Design curve". As will be explained later in detail, the maximum force in fabric should be compared to the maximum anchorable force in order to avoid debonding

failure. Using the "Design curve" to check the fabric force for debonding underestimates its real value, which is not safe. Therefore, a 10% up shift of the average curve is suggested to estimate the force in fabric for the purpose of bond check, which is shown in Fig. 8.1 as the "Bond check curve".

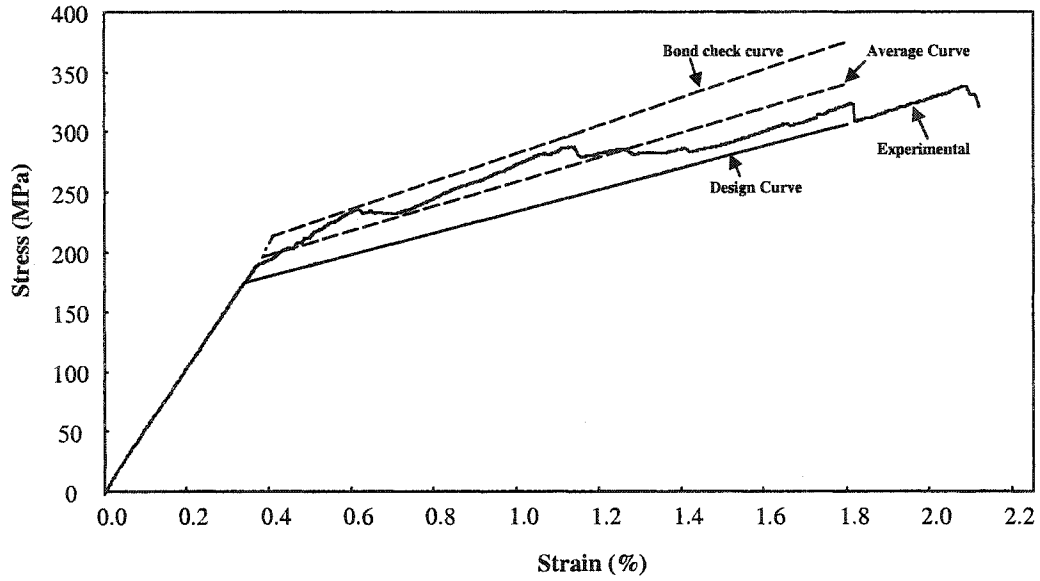

Fig. 8.1 Axial loading behavior of the triaxial fabric

Accordingly, the design curve shown in Fig. 8.1 will be used for design and the value of the stress from this curve multiplied by 1.22 will be used while checking the bond. Fig. 8.2 shows the design curve. Herein, the initial linear part of the curve ends at the yield equivalent point of the fabric, which corresponds to 175 MPa and 0.35% yield equivalent stress and strain, respectively with a modulus (E_{fa}) of 50 GPa. The second line starts from a strain value of 0.35% up to the failure strain of the fabric, which is taken to be 1.80%, with a modulus (E_{2fa}) of 9.0 GPa. The corresponding ultimate stress of the

fabric (f_{fua}) is equal to 305 MPa. Therefore, the stress-strain behavior of the fabric in the axial direction can be expressed by the following relation:

$$f_{fa} = \begin{cases} E_{fa} \times \varepsilon_{fa} & \text{for } \varepsilon_{fa} \leq 0.35\% \\ E_{fa} \times 0.0035 + E_{2fa} (\varepsilon_{fa} - 0.0035) & \text{for } 0.35\% < \varepsilon_{fa} \leq 1.80\% \end{cases} \quad (8.1)$$

where (f_{fa}) and (ε_{fa}) are the fabric axial stress and strain, respectively.

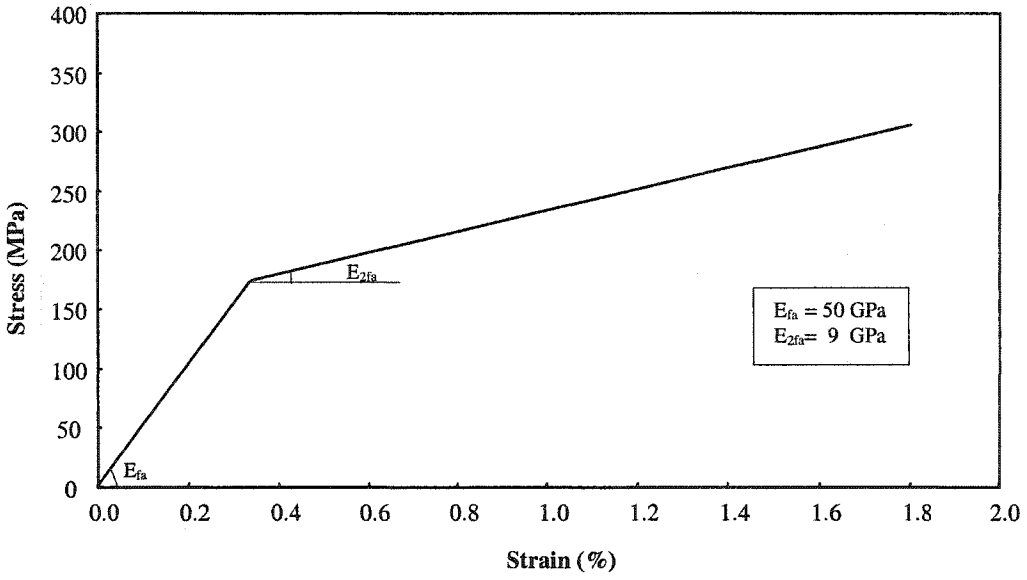

Fig. 8.2 Design stress-strain behavior of the triaxial fabric in the axial direction

8.2.2 Diagonal loading

The experimental stress-strain behavior of the fabric in the diagonal direction (45°), shown in Fig. 8.3, can be approximated as a bilinear relation, which is shown in the figure as the "average curve". The rupture strain of the fabric is suggested to be limited to 1.80%. For the purpose of design, a 10% down shift of the average curve is suggested as a "design curve", which is shown in figure. Fig. 8.4 shows the design curve. Herein, the

behavior is linear up to a stain value of 0.47%, which corresponds to a stress value of 115 MPa and a modulus (E_{fd}) of 24.5 GPa. The second line starts from a strain value of 0.47% up to the failure strain of the fabric, which is suggested as 1.80%, with a modulus (E_{2fd}) of 5.4 GPa. The corresponding ultimate stress (f_{fud}) is equal to 187 MPa. Therefore, the stress-strain behavior of the fabric in the diagonal direction can be expressed by the following relation:

$$f_{fd} = \begin{cases} E_{fd} \times \varepsilon_{fd} & \text{for } \varepsilon_{fd} \leq 0.47\% \\ E_{fd} \times 0.0047 + E_{2fd}(\varepsilon_{fd} - 0.0047) & \text{for } 0.47\% < \varepsilon_{fd} \leq 1.80\% \end{cases} \quad (8.2)$$

where (f_{fd}) and (ε_{fd}) are the diagonal stress and strain of the fabric, respectively. Table 8.1 lists the design properties of the fabric in both the axial and the diagonal directions.

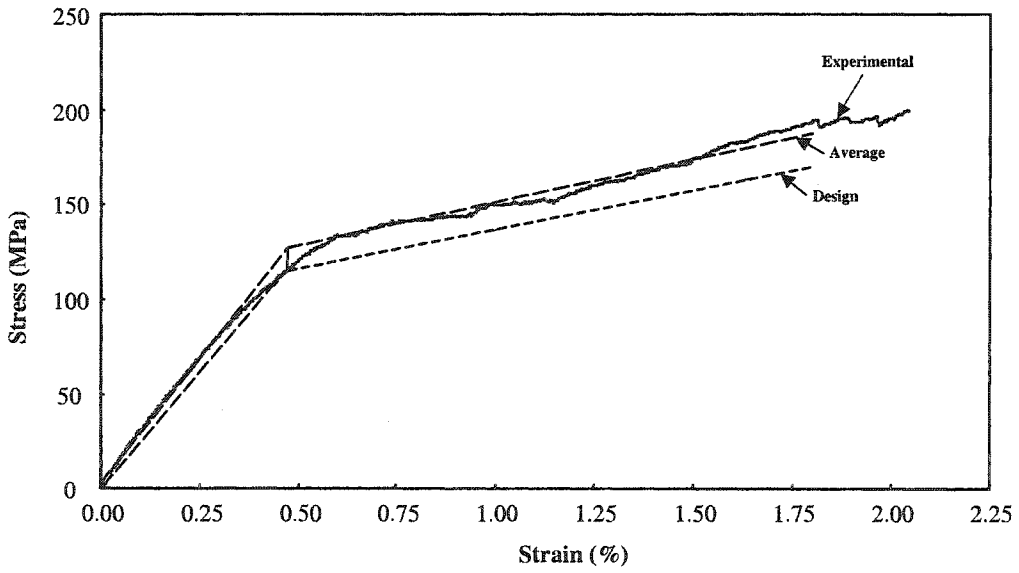

Fig. 8.3 Diagonal loading behavior of the triaxial fabric

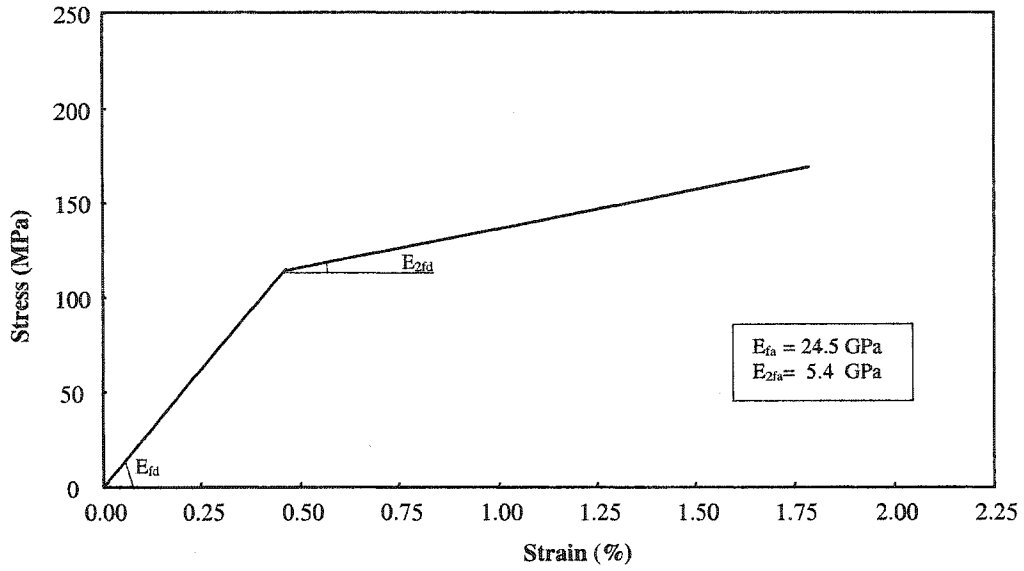

Fig. 8.4 Design stress-strain behavior of the triaxial fabric in the diagonal direction

Table 8.1 Design Characteristics of the Triaxial Fabric

Loading Direction	Yield Strength MPa	Yield Strain (%)	Initial Modulus GPa	Ultimate Load (%)	Ultimate Strain (%)	Thickness (mm)
Axial (0°)	175	0.35	50	305	1.8	1.0
Diagonal (45°)	115	0.47	24.5	187	1.8	

8.2.3 Creep rupture stress limit

ACI 440 committee guidelines (2002) recommended a maximum service load stress limit for the carbon and glass fibers to be 55% and 20%, respectively of the their ultimate stresses. For the fabric, a maximum limit of 55% of the yield equivalent stress will guarantee that none of the fibers used to manufacture the fabric will exceed these limits.

8.3 Flexural Strengthening Design

The design generally follows the guidelines of ACI 440 committee (2002) with slight differences to account for the different behavior of the fabric. The axial direction (0^{o} direction) of the fabric is responsible for strengthening the beam for flexure. The analysis is based on the principle of strain compatibility. The following assumptions are made:

1- The tensile strength of concrete is ignored.

2- The maximum usable compression strain of concrete is 0.003.

3- The strains in the reinforcement and concrete are directly proportional to the distance from the neutral axis.

8.3.1 Preliminary design

The existing flexural capacity of the beam (ϕM_n) is evaluated using ACI 318 code and compared with the desired moment capacity (M_u) to determine if additional strengthening is required. The area of the fabric needed is estimated based on the additional tensile force required to increase the moment capacity.

$$\phi M_{add} = M_u - \phi M_n$$

$$M_{add} = \phi M_{add} / 0.9$$

$$\text{Estimated additional force required (T)} = \frac{M_{add}}{0.80h} \qquad (8.3)$$

$$\text{Required area} = \frac{T}{f_{fya}} \qquad (8.4)$$

where f_{fya} is the fabric yield strength in its axial direction

$$\text{Number of layers needed (n)} = \frac{\text{Required area}}{\text{area of one layer}} \qquad (8.5)$$

8.3.2 Estimation of maximum usable strain

The maximum usable strain (ε_m) of the fabric is taken as the least of the following two values:

- The rupture strain of the fabric (1.8%).
- The strain value corresponding to the maximum anchorable strength (ε_b).

8.3.2.1 Calculation of ε_b

In order to account for the effect of debonding, the fabric maximum anchorable force should be calculated. FIB Bulletin 14 (2001) provided an expression for the maximum anchorable force in terms of the concrete and the FRP properties. This was expressed as follows:

$$\text{Maximum anchorable force } (T_m) = \eta_1 \eta_2 k_c k_b b_f \sqrt{n E_{fa} t_f f_{ct}} \quad \text{N} \qquad (8.6)$$

where:

b_f = fabric width (mm)

E_{fa} = fabric modulus of elasticity in the axial direction (MPa)

t_f = fabric thickness (mm)

n = number of layers

f_{ct} = tensile strength of the concrete (MPa) = $0.6\sqrt{f_c'}$ (ACI 318)

k_c = factor accounting for the state of compaction, generally taken as 1.0 for concrete faces with good compactions and 0.67 for concrete faces with low compaction

η_1 = factor obtained through calibration of test data, taken as 1.20

η_2 = reduction factor for the effect of inclined cracks, taken as 1.0 for beams with sufficient shear reinforcement and 0.9 for beams with low shear reinforcement

k_b = geometry factor equal to $1.06\sqrt{\frac{2-\frac{b_f}{b}}{1+\frac{b_f}{400}}} \geq 1.0$

b_f = fabric width (mm)

Accordingly, the maximum anchorable fabric stress (f_{fam}) can be calculated from the following relation:

$$f_{fam} = \frac{T_m}{n \psi t_f b_f} \qquad (8.7)$$

where ψ is a reduction factor to account from the difference between the fabric "bond check curve" and the "design curve" , as mention above, and can be taken as 1.22.

The fabric strain (ε_b) corresponding to the maximum anchorable stress (f_{fam}) can be defined from the design stress-strain diagram. In case of U-wrapped beams, this value can be taken as the rupture strain of the fabric (1.8%).

8.3.3 Calculation of existing strain

The existing strain is the strain due to the existing loads on the beam before strengthening. It is important to define this value to know the exact contribution of the fabric after strengthening. The initial strain can be calculated as follows considering the cracked section of the beam:

$$\varepsilon_o = \frac{M_o\,(h - kd)}{I_{cr}\,E_c} \qquad (8.8)$$

where

M_o = moment at the time of fabric installation (non-factored)

h = section height

k = ratio of the depth to the elastic neutral axis to the effective depth, d

d = effective depth

I_{cr} = moment of inertia of the cracked concrete section

E_c = modulus of elasticity of concrete

8.3.4 Estimation of failure mode and nominal moment

An estimation of the failure mode is required to select the method to determine the compressive stress distribution in the concrete. The modes of failures expected when strengthening a beam by bonding the fabric to its tension face are:

1- Compression failure in the concrete.

2- Tensile failure of the fabric by any of the following:

   a- Fabric rupture.

   b- Fabric debonding.

c- Shear-tension failure at fabric ends.

The mode of failure is estimated in an iterative manner by first assuming the location of the neutral axis and assuming the compression strain of the concrete to be 0.003. Based on this assumption, the fabric strain (ε_f) is calculated as follows:

$$\varepsilon_f = 0.003 \frac{c_2}{c_1} \qquad (8.9)$$

where

c_1 = Distance to the neutrals axis (initially assumed)

$c_2 = h - c_1$

Therefore, the mode of failure can be estimated as follows:

- Concrete compression failure when $\varepsilon_f < \varepsilon_m + \varepsilon_o$
- Fabric tensile failure when $\varepsilon_f > \varepsilon_m + \varepsilon_o$

In case of the first mode of failure, concrete compression failure, the equivalent rectangular stress block (Whitney stress block) method outlined in ACI 318 code can be used to calculate compressive strength of the concrete.

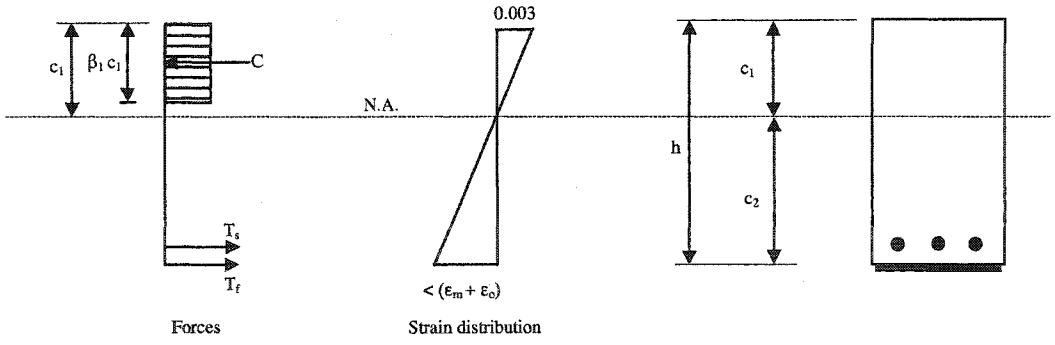

Fig. 8.5 Strain distribution and forces in case of concrete crushing

Section forces:

$$C = 0.85\ f_c^{'}\ b\ (\beta_1\ c_1)$$

$$T_s = A_s\ f_s$$

$$T_f = A_f\ f_{fa}$$

where

$f_c^{'}$ = Concrete compression strength

A_s = Area of tension steel reinforcement

A_f = Area of fabric

f_{fa} = Stress in fabric in its axial direction

T_f = Tension force in fabric

T_s = Tension force in steel reinforcement

f_s = Stress in steel

From equilibrium of forces, the value of (c_1) can be calculated from the relation:

$$c_1 = \frac{A_s\ f_s + A_f\ f_{fa}}{0.85 f_c^{'}\ b \beta_1} \qquad (8.10)$$

This value of c_1 is compared to the assumed value and iterated until the assumed value is equal to the calculated one.

The nominal moment capacity is calculated from the following relation:

$$M_n = A_s\ f_s\ (d - \frac{\beta_1\ c_1}{2}) + \psi A_f\ f_{fa}\ (h - \frac{\beta_1\ c_1}{2}) \qquad (8.11)$$

In case of the second mode of failure, fabric tensile failure, the equivalent rectangular stress block (Whitney stress block) method outlined in ACI 318 code cannot be used to calculate compressive strength of the concrete. Instead, stresses should be calculated directly from nonlinear stress-strain relationship for concrete in compression. The non-linear stress distribution based on the work of Todeschini et al. (1964) can be used in this case.

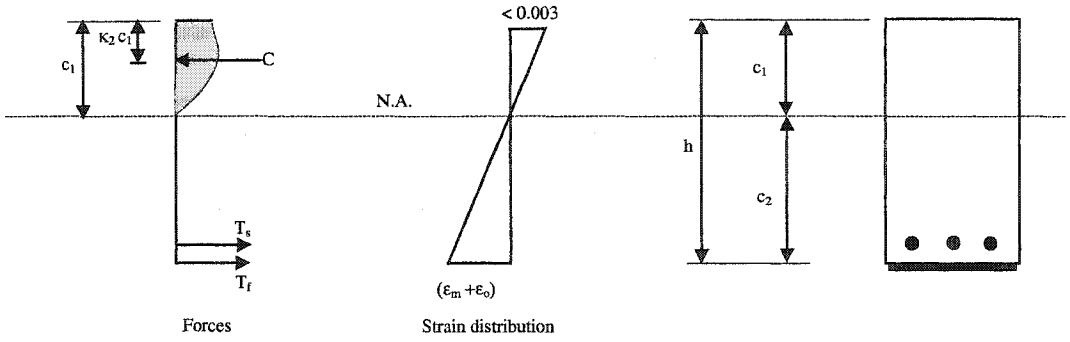

Fig. 8.6 Strain distribution and forces in case of fabric tensile failure

Section forces:

$$C = k_3 f_c' b(\beta_1 c_1)$$

$$T_s = A_s f_s$$

$$T_f = A_f f_{fa}$$

where

$$\beta_1 k_3 = k_3 \frac{\ln(1-x^2)}{x} = 0.9 \frac{\ln(1-x^2)}{x}$$

$$x = \frac{\varepsilon_c}{\varepsilon_c'}$$

$$\varepsilon_c' = \frac{1.71 f_c'}{E_c}$$

$$\varepsilon_c = (\varepsilon_m + \varepsilon_o)\frac{c_1}{c_2}$$

$$k_2 = 1 - \frac{2(x - \tan^{-1} x)}{x^2 \beta_1}$$

From equilibrium of forces, the value of (c_1) can be calculated from the relation:

$$c_1 = \frac{A_s f_s + A_f f_{fa}}{k_3 f_c' b \beta_1} \qquad (8.12)$$

This value of c_1 is compared to the assumed value and iterated until the assumed value is equal to the calculated one.

The nominal moment capacity is calculated from the following relation:

$$M_n = A_s f_s (d - k_2 c_1) + \psi A_f f_{fa} (h - k_2 c_1) \qquad (8.13)$$

8.3.5 Strength reduction factor

ACI 440 committee (2002) suggested the following strength reduction factor (ϕ):

$$\phi = \begin{cases} 0.9 & \text{for } \varepsilon_s \geq 0.5\% \\ 0.7 + \dfrac{0.2(\varepsilon_s + \varepsilon_{sy})}{0.005 - \varepsilon_{sy}} & \text{for } \varepsilon_{sy} < \varepsilon_s < 0.5\% \\ 0.7 & \text{for } \varepsilon_s \leq \varepsilon_{sy} \end{cases} \qquad (8.14)$$

where

ε_s = Strain in steel reinforcement

ε_{sy} = Yield strain of steel

8.3.6 Allowable service load stresses

The stresses in the concrete, steel, and fabric must be checked under the service loads. ACI 440 Committee (2002) suggested that the stress in the steel under service load should be limited by 80% of the yield strength in order to avoid inelastic deformation of the concrete beam after strengthening The stress level in the steel reinforcement (f_s) can be calculated based on cracked elastic analysis of the strengthened reinforced concrete section, as indicated in the following equation [ACI 440 Committee (2002)]:

$$f_s = \frac{\left[M_{service} + \varepsilon_o E_{fa} A_f (h - kd/3)\right](d - kd)E_s}{\left(E_s A_s (d - kd/3)(d - kd) + E_{fa} A_f (h - kd/3)(h - kd)\right)} \qquad (8.15)$$

In order to avoid creep-rupture of the fabric under sustained stresses or failure due to cyclic stresses and fatigue, the stress level in the fabric under the service loads should not exceed 55% of the yield stress of the fabric in its longitudinal direction. For the concrete, the service load stress should not exceed 45% of it compression strength. The stress in the concrete and the FRP can be calculated using the following equations:

$$\text{Concrete stress } (f_c) = f_s\left(\frac{E_c}{E_s}\right)\left(\frac{kd}{d - kd}\right) \qquad (8.16)$$

$$\text{Fabric stress } (f_{fa}) = f_s\left(\frac{E_{fa}}{E_s}\right)\left(\frac{h - kd}{d - kd}\right) - \varepsilon_o E_{fa} \qquad (8.17)$$

8.4 Shear Strengthening Design

The design generally follows the guidelines of ACI 440 committee (2002). However, it may be slightly different, due to the different behavior of the fabric. The diagonal directions ($\pm 45^{o}$ direction) of the fabric are responsible for strengthening the beam for shear.

8.4.1 Strengthening schemes

The fabric is to be installed so that the axial yarns are paralleled to the longitudinal axis of the beam on beam sides and maybe installed on the bottom face and sides as a U-wrap. The U-wrap is more effective than strengthening on beam sides only because it provides better anchorage. Fig. 8.7 shows the strengthening schemes.

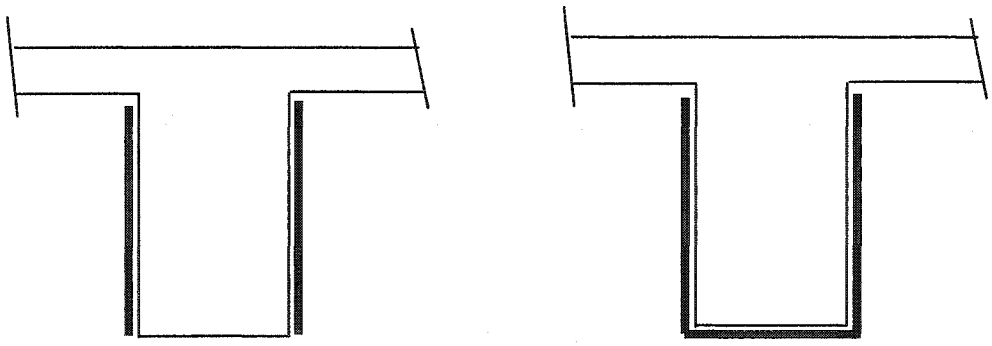

Fig. 8.7 Shear strengthening schemes

8.4.2 Calculation of shear strength

The nominal shear capacity of a reinforced concrete beam strengthened with the fabric can be calculated by adding the contribution of the fabric (V_{frp}) to the contribution of the concrete (V_c) and the steel reinforcement (V_s). An additional reduction factor of 0.70 is recommended by ACI committee 440 (2002) to be applied to the contribution of the fabric. The values of V_c and V_s can be calculated according to ACI 318 code. Therefore, the nominal shear capacity of the beam (ϕV_c) can be calculated using the following equation:

$$\phi V_n = 0.85(V_c + V_s) + 0.7\, V_{frp} \tag{8.18}$$

The shear strength provided by the fabric can be calculated by calculating the force resulting from the tensile stress in the fabric along the assumed crack. The usable tensile stress in the fabric is known as the effective stress and can be defined by calculating the effective strain (ε_{fe}). Therefore, the fabric contribution can be calculated using the following equation:

$$V_{frp} = \frac{2\, n\, t_f\, w_f\, \varepsilon_{fe}\, E_{fd}(\sin\beta + \cos\beta)d_f}{s_f}. \tag{8.19}$$

where

n = Number of fabric layers

t_f = Fabric thickness

w_f = Width of fabric strips

d_f = Effective depth of the fabric

s_f = Spacing of the fabric strips

w_f = Width of fabric strip

β = Angle between principle fiber orientation and longitudinal axis of the beam

E_{fd} = Modulus of elasticity of the fabric in the diagonal direction

Since the fabric is meant to be installed continuously and not as spaced strips, the fabric contribution can be calculated according to the following relation:

$$V_{frp} = 2\, n\, t_f\, \varepsilon_{fe}\, E_{fd}\, d_f \qquad (8.20)$$

8.4.2.1 Calculation of effective strain

ACI 440 committee (2002) presented an approach to calculate the FRP effective strain. This approach can be used to calculate the effective strain for the fabric case by considering only the initial stress-strain response of the fabric in its diagonal direction (up to its yield point). In this approach, the FRP shear contribution (ε_{fe}) is calculated using the following equation:

$$\varepsilon_{fe} = K_v \varepsilon_{fyd} \leq 0.004 \qquad (8.21)$$

where (ε_{fyd}) is the yield strain of the fabric in the diagonal direction and K_v is a bond reduction factor, which can be calculated from the following equation:

$$K_v = \frac{k_1 k_2 L_e}{11900 \varepsilon_{fyd}} \leq 0.75 \qquad (8.22)$$

where

$$k_1 = \left(\frac{f_c'}{27} \right)^{2/3}$$

$$k_2 = \begin{cases} \dfrac{d_f - L_e}{d_f} & \textit{For U- wraps} \\ \dfrac{d_f - 2L_e}{d_f} & \textit{For two sides bonded} \end{cases}$$

$$L_e = \frac{23{,}000}{(n\, t_f\, E_{fd})^{0.58}}$$

8.4.2.2 Reinforcement limit

The total shear reinforcement is limited by ACI 318 code to a maximum value. The total shear reinforcement in this case is the sum of the contribution of the fabric and the steel reinforcement. This limit is expressed by the following equation:

$$V_s + V_{frp} \leq \frac{2\sqrt{f_c'}\, b\, d}{3} \qquad (8.23)$$

8.5 Design Examples

8.5.1 Calculation of the ultimate capacity of a beam

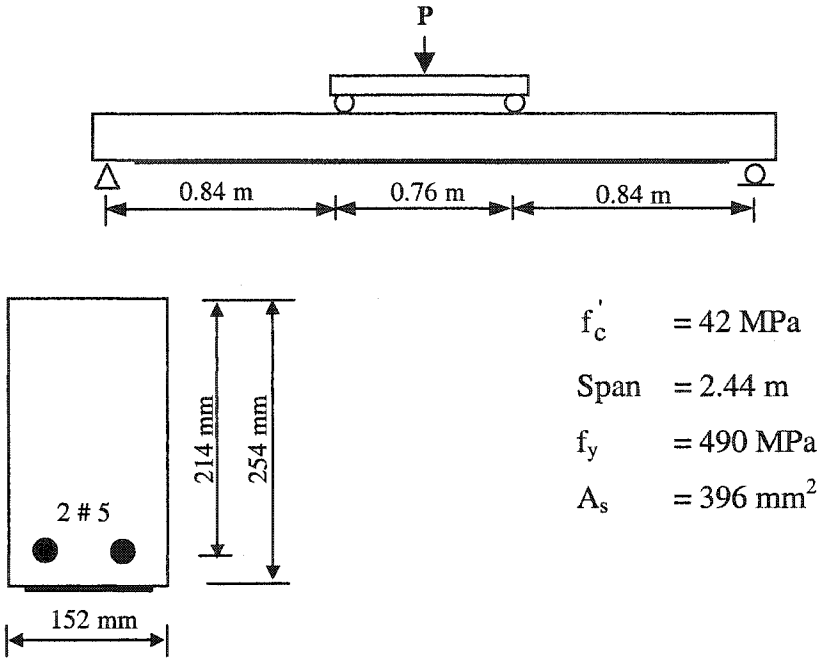

Fig. 8.8 Example for calculating ultimate load capacity

8.5.1.1 Statement of the problem

Calculate the ultimate load capacity (P) of beam F-B-2 reported earlier in Chapter 5 and compare it with the experimental value. The beam was strengthened with two layers of the triaxial fabric 135 mm wide installed on the bottom face of the beam.

8.5.1.2 Estimation of maximum usable strain

$$\text{Maximum anchorable force } (T_m) = \eta_1 \eta_2 k_c k_b b_f \sqrt{n E_{fa} t_f f_{ct}} \quad \text{N}$$

$$k_b = 1.06\sqrt{\frac{2-\frac{135}{152}}{1+\frac{135}{400}}} = 0.96 \longrightarrow 1.0$$

$$f_{ct} = 0.6\sqrt{42} = 3.89 \text{ MPa}$$

$$T_m = (1.2)\,(1.0)\,(1.0)\,(1.0)\,(135)\,\sqrt{(2)(50{,}000)(1.0)(3.89)} = 101{,}039 \text{ N}$$

From equation (8.7)

$$\text{The maximum anchorable stress } (f_{fam}) = \frac{T_m}{n\,\psi\,t_f\,b_f}$$

$$f_{fam} = \frac{101{,}039/1000000}{2\times1.22\times0.001\times0.135} = 306 \text{ MPa} > f_{fau} = 305 \text{ MPa}$$

Therefore, (ε_m) can be taken as the rupture strain of the fabric (ε_{fau})

8.5.1.3 Estimation of location of the N.A. and mode of failure

assume $c_1 = 64$ mm

$c_2 = h - c_1 = 254 - 64 = 190$ mm

$$\varepsilon_f = 0.3\left(\frac{190}{64}\right) = 0.90\%$$

$$\varepsilon_{fau} + \varepsilon_o = 1.8 + 0.00 = 1.80\% > 0.90\%$$

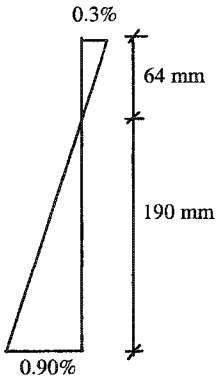

$\therefore$ The fabric will not rupture before crushing of the concrete

$$0\varepsilon_s = 0.90\left(\frac{214-64}{190}\right) = 0.71\% > \varepsilon_{sy}$$

Stress in fabric = $E_{fa}\times0.0035 + E_{2fa}\,(\varepsilon_{fa} - 0.0035)$

$$= 50000\times0.0035 + 9000(0.009 - 0.0035) = 225 \text{ MPa}$$

$$c_1 = \frac{A_s f_y + A_f f_{fa}}{0.85\beta_1 f_c' b} = \frac{(396)(490) + 2(135)(225)}{0.85(0.75)(42)(152)} = 63 \text{ mm} \cong 64 \text{ mm} \quad \text{OK}$$

8.5.1.4 Determination of nominal moment capacity of the section

$$M_n = A_s f_y (d - \beta_1 c_1 / 2) + A_f f_{fa} (h - \beta_1 c_1 / 2)$$

$$M_n = (396)\,(490)\,(214 - 0.75(64)/2) + 2(135)(225)(254 - 0.75(64)/2)$$
$$= 50.8 \text{ kN.m}$$

8.5.1.5 Determination of ultimate load of the beam

$M = (P/2)\,(0.84)$

$50.8 = 0.42\,P$

The ultimate load of the beam (P) = 121 kN

The experimental value of the ultimate load of beam F-B-2 was 123 kN, which is very close to the analytical results with a difference of 2.0%.

8.5.2 Increasing the flexural capacity of a beam

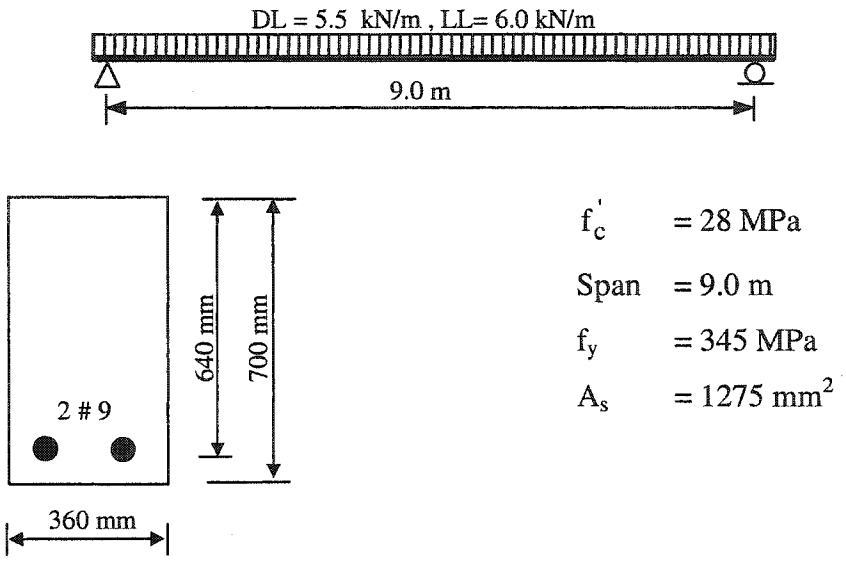

Fig. 8.9 Example for flexural strengthening

8.5.2.1 Statement of the problem

Determine the amount of triaxially braided fabric required to strengthen the simply supported beam shown in Fig. 8.8 to carry a superimposed dead load of 5.5 kN/m and a live load of 6.0 kN/m. The beam has enough shear reinforcement and the concrete is well compacted.

8.5.2.2 Calculation of existing flexural capacity

Total DL = DL + Own Wt = 5.5 + (0.70) (0.36) (1) (23.5) = 11.4 kN/m

LL = 6.0 kN/m

$M_{service}$ = (11.4 + 6.0) (9) (9) /8 = 176 kN.m

$$M_{factored} = [(1.40)(11.4) + (1.7)(6.0)](9)(9)/8 = 265 \text{ kN.m}$$

$$\beta_1 c_1 = \frac{A_s f_y}{0.85 f_c' b} = \frac{(1275)(345)}{0.85(28)(360)} = 51 \text{ mm}$$

$$\phi M_n = \phi A_s f_y (d - \beta_1 c_1 / 2)$$

$$\phi M_n = 0.9\,(1275)(345)(640 - 51/2) = 243 \text{ kN.m} < 265 \text{ kN.m}$$

$\therefore$ Strengthening is required

8.5.2.3 Estimation of amount of fabric needed

$$\phi M_{add} = M_u - \phi M_n$$

$$\phi M_{add} = 265 - 243 = 22 \text{ kN.m}$$

$$M_{add} = 22.0/0.9 = 24.4 \text{ kN.m}$$

$$\text{Estimated additional force required (T)} = \frac{M_{add}}{0.80h} = \frac{24.4}{(0.80)(0.70)} = 43.6 \text{ kN}$$

$$\text{Required area} = \frac{T}{f_{fya}} = \frac{43.6}{(175)(1000)} * 10^6 = 249.1 \text{ mm}^2$$

Area of fabric layer 340 mm wide = (340)(1) = 340 mm^2

$$\text{Number of layers needed} = \frac{249.1}{340} = 0.73 \text{ layer}$$ Try 1 layer

8.5.2.4 Estimation of maximum usable strain

Maximum anchorable force $(T_m) = \eta_1 \eta_2 k_c k_b b_f \sqrt{n E_{fa} t_f f_{ct}}$ N

$$k_b = 1.06\sqrt{\frac{2 - \frac{340}{360}}{1 + \frac{340}{400}}} = 0.8 \longrightarrow 1.0$$

$$f_{ct} = 0.6\sqrt{28} = 3.17 \text{ MPa}$$

$T_m = (1.2)\ (1.0)\ (1.0)\ (1.0)\ (340)\ \sqrt{(1)(50{,}000)(1.0)(3.17)} = 162{,}433$ N

From equation (8.7)

The maximum anchorable stress $(f_{fam}) = \dfrac{T_m}{n \psi t_f b_f}$

$$f_{fam} = \frac{162{,}433/1000000}{1 \times 1.22 \times 0.001 \times 0.34} = 391 \text{ MPa} > f_{fau} = 305 \text{ MPa}$$

Therefore, (ε_m) can be taken as the rupture strain of the fabric (ε_{fau})

8.5.2.5 Determination of existing strain along the tension face

$$M_o = \frac{(11.4)(9)^2}{8} = 115.4 \text{ kN.m}$$

$E_c = 24900$ MPa

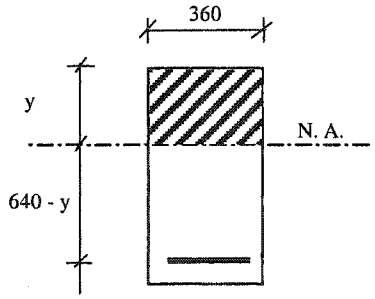

N.A.

$360\ y^2 = (1275)\ (200/24.9)(640\text{-}y)$

$y^2 = 28.44\ (640\text{-}y)$

$y^2 + 28.44 - 18206 = 0$

solving $y = 121$ mm

$$I_{cr} = 360 \times (121)^3/3 + (1275) \times (200/24.9)(640-121)^2 = 2.97 \times 10^9 \text{ mm}^4$$

$$\text{Estimating strain } (\varepsilon_o) = \frac{114{,}000{,}000\,(700-121)}{2.97\times10^9\times24900} = 0.0009 = 0.09\%$$

8.5.2.6 Estimation of location of the N.A. and mode of failure

assume c_1= 80 mm

$c_2 = h - c_1 = 700 - 80 = 620$ mm

$$\varepsilon_f = 0.3\left(\frac{620}{80}\right) = 2.32\%$$

$$\varepsilon_{fau} + \varepsilon_o = 1.8 + 0.09 = 1.89\% \;<\; 2.32\%$$

$\therefore$ The fabric will rupture before crushing of the concrete

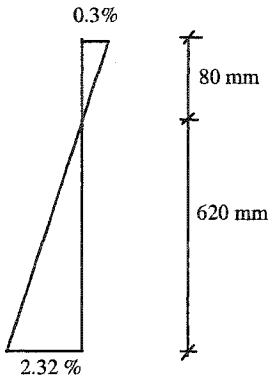

assume c_1= 80 mm

$c_2 = h - c_1 = 700 - 80 = 620$ mm

$\varepsilon_f = \varepsilon_{fau} = 1.8\%$

$$\varepsilon_c = (\varepsilon_{fau} + \varepsilon_o)\left(\frac{c_1}{c_2}\right) = 1.89\left(\frac{80}{620}\right) = 0.24\%$$

$$\varepsilon_s = (\varepsilon_{fau} + \varepsilon_o)\left(\frac{d - c_1}{c_2}\right) = 1.89\left(\frac{640-80}{620}\right) = 1.71\% > \varepsilon_{sy}$$

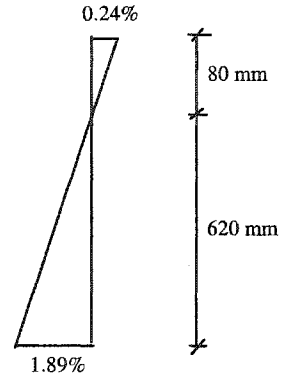

Modified stress block

$$\varepsilon_c' = \frac{1.71\,f_c'}{E_c} = \frac{1.71(28)}{24900} = 0.0019 = 0.19\%$$

$$x = \varepsilon_c / \varepsilon_c' = 0.24/0.19 = 1.26$$

$$x^2 = \left(\varepsilon_c / \varepsilon_c'\right)^2 = 1.60$$

$$\beta_1 k_3 = 0.9\,\frac{\ln(1+1.60)}{1.26} = 0.68$$

$$c_1 = \frac{A_s f_y + A_f f_{fa}}{(k_3\beta_1)\,f_c' b} = \frac{(1275)(345)+(340)(305)}{0.68(28)(360)} = 79.3 \text{ mm} \cong 80 \text{ mm}$$

8.5.2.7 Determination of nominal capacity of the section

$$k_2 = 1 - \frac{2(x - \tan^{-1} x)}{x^2 \beta_1} = 1 - \frac{2(1.26 - \tan^{-1}(1.26))}{1.26^2 (0.68/0.9)} = 0.40$$

$$M_n = A_s f_y (d - k_2 c_1) + \psi_f A_f f_{fa} (h - k_2 c_1)$$

$$M_n = (1275)(345)(640 - 0.4(80)) + 0.85(340)(305)(700 - 0.4(80))$$
$$= 326.3 \text{ kN.m}$$

since $\varepsilon_s > 0.5\%$ $\therefore \phi = 0.9$

$$\phi M_n = 0.9(326.3) = 294 \text{kN.m} > M_{factored} = 265 \text{ kN.m} \quad \text{OK}$$

8.5.2.8 Check of service load stress in concrete, steel, and fabric

Determine the depth to the neutral axis, kd, using the transformation areas for the steel and the fabric

Part	Area	y'	A y'
Concrete	360 kd	Kd/2	180 $(kd)^2$
Steel	$A_s n_s$ =0.5x2550x 8.04 =10251	kd - 640	10251(kd – 640)
Fabric	$A_f n_f$ =340x2 = 680	kd - 700	680 (kd – 700)

$$180 (kd)^2 + 10251 (kd - 640) + 680 (kd - 700) = 0$$

$$180 (kd)^2 + 10930 (kd) - 7036640 = 0$$

$$kd = 170 \text{ mm}$$

$$f_s = \frac{[M_{service} + \varepsilon_o E_f A_f (h - kd/3)](d - kd)E_s}{(E_s A_s (d - kd/3)(d - kd) + E_f A_f (h - kd/3)(h - kd))}$$

$$f_s = \frac{[176{,}000{,}000 + 0.0009(50000)(340)(700 - 170/3)](640 - 170)200{,}000{,}000}{(200{,}000{,}000(1275)(640 - 170/3)(640 - 170) + 50{,}000(340)(700 - 170/3)(700 - 170))}$$

$=250$ MPa $< 0.8 f_y = 276$ MPa OK

$$f_c = f_s\left(\frac{E_c}{E_s}\right)\left(\frac{kd}{d - kd}\right) = 250\left(\frac{24900}{200000}\right)\left(\frac{170}{640 - 170}\right)$$

$=11.26$ MPa $< 0.45 f_c' = 12.4$ MPa OK

$$f_f = f_s\left(\frac{E_f}{E_s}\right)\left(\frac{h - kd}{d - kd}\right) - \varepsilon_o E_f = 250\left(\frac{50000}{200000}\right)\left(\frac{700 - 170}{640 - 170}\right) - 0.0009(50000)$$

$= 25.5$ MPa $< 0.55 f_{fya} = 96.25$ MPa OK

Therefore, use one layer of the Triaxial Ductile Fabric 340 mm wide

8.5.3 Increasing the shear capacity of a beam

8.5.3.1 Statement of the problem

The beam shown in Fig. 8.9 was designed with # 3 shear stirrups spaced at 250 mm. The yield strength of the steel reinforcement is 275 MPa and the concrete strength is 27 MPa. It is required to strengthen the beam so that the cross section can sustain a factored shear force of 375 kN. Calculate the amount of externally bonded triaxially braided ductile fabric required to strengthen the beam.

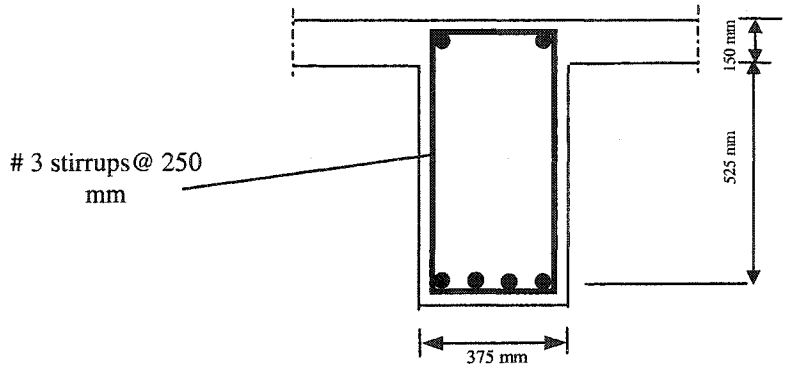

Fig. 8.10 Example for shear strengthening

8.5.3.2 Calculation of current shear strength of cross section

$$V_c = \frac{\sqrt{f_c'}\, b_w\, d}{6} = \frac{\sqrt{27}\,(0.375)(0.675)}{6} = 219.2 \text{ kN}$$

$$V_s = \frac{A_s F_y\, d}{s_s} = \frac{2(71)(275)(0.675)}{0.25\times 1000} = 105.4 \text{ kN}$$

$$\phi V_n = 0.85(219.2 + 105.4) = 275.9 \text{ kN}$$

$V_{factored} = 375\ kN > \phi V_n = 275.9\ kN$

$\therefore$ Strengthening is required

Try one layer of the Triaxial Fabric on both sides only

8.5.3.3 Determination of contribution of the fabric

$$V_{frp} = 2n\ t_f\ \varepsilon_{fe}\ E_{fd}\ d_f$$

$$L_e = \frac{23{,}000}{(n\,t_f\,E_f)^{0.58}} = \frac{23{,}000}{(1\times 0.001\times 24.5\times 10^6)^{0.58}} = 65.5\ mm$$

$$k_1 = \left(\frac{f_c'}{27}\right)^{2/3} = \left(\frac{27}{27}\right)^{2/3} = 1.0$$

$$k_2 = \frac{d_f - 2\times L_e}{d_f} = \frac{525 - 2\times 65.5}{525} = 0.75$$

$$K_v = \frac{k_1 k_2 L_e}{11900\,\varepsilon_{fyd}} \le 0.75$$

$$= \frac{(1.0)(0.75)(65.5)}{11900(0.0047)} = 0.88 \rightarrow 0.75$$

$$\varepsilon_{fe} = K_v \varepsilon_{fyd} \le 0.004$$

$$= 0.75(0.0047) = 0.0035 < 0.004$$

$$V_{frp} = 2n\ t_f\ \varepsilon_{fe}\ E_{fd}\ d_f$$

$$= 2\ (1)\ (0.001)(0.0035)\ (24.5\times 10^6)(0.525) = 90\ kN$$

8.5.3.4 Check of maximum shear reinforcement

$$V_s + V_{frp} \le \frac{2\sqrt{f_c'}\, b_w d}{3}$$

$$105.4 + 90 \le \frac{2\sqrt{27}\ (0.375)(0.675)}{3} = 876.9 \text{ kN} \quad \text{OK}$$

8.5.3.5 Calculation of shear capacity of the beam

$$\phi V_n = 0.85(V_c + V_s) + 0.7\, V_{frp}$$

$$\phi V_n = 0.85(219.2 + 105.4) + 0.7(90) = 338.9 \text{ kN} < V_{factored} = 375 \text{ kN} \quad \text{No Good}$$

Try two layers of the triaxial fabric

$$L_e = \frac{23{,}000}{(n\, t_f\, E_f)^{0.58}} = \frac{23{,}000}{(2 \times 0.001 \times 24.5 \times 10^6)^{0.58}} = 43.8 \text{ mm}$$

$$k_1 = \left(\frac{f_c'}{27}\right)^{2/3} = \left(\frac{27}{27}\right)^{2/3} = 1.0$$

$$k_2 = \frac{d_f - 2 \times L_e}{d_f} = \frac{525 - 2 \times 43.8}{525} = 0.83$$

$$K_v = \frac{k_1 k_2 L_e}{11900\, \varepsilon_{fyd}} \le 0.75$$

$$= \frac{(1.0)(0.83)(43.8)}{11900(0.0047)} = 0.65$$

$$\varepsilon_{fe} = K_v \varepsilon_{fyd} \le 0.004$$

$$= 0.65(0.0047) = 0.0031 < 0.004$$

$$V_{frp} = 2n\, t_f\, \varepsilon_{fe}\, E_{fd}\, d_f$$

$$= 2\,(2)\,(0.001)(0.0031)\,(24.5\times10^{6})(0.525) = 159.5 \text{ kN}$$

Check maximum shear reinforcement

$$V_s + V_{frp} \le \frac{2\sqrt{f'_c}\, b_w d}{3}$$

$$105.4 + 159.5 \le \frac{2\sqrt{27}\ (0.375)(0.675)}{3} = 876.9 \text{ KN} \quad \text{OK}$$

$$\phi V_n = 0.85(V_c + V_s) + 0.7\, V_{frp}$$

$$\phi V_n = 0.85(219.2 + 105.4) + 0.7\,(159.5) = 387.6 \text{ kN} > V_{factored} = 375 \text{ kN} \quad \text{OK}$$

Therefore, use two layers of the triaxial ductile fabric on each side

CHAPTER 9

CONCLUSIONS AND RECOMMENDATIONS

9.1 Conclusions

9.1.1 Development of systems

Two ductile FRP strengthening systems have been developed for reinforced concrete beams. The systems are hybrid of glass and carbon fibers. The first system is a uniaxial fabric and has been developed mainly for flexural strengthening of concrete beams. The second system is a triaxially braided fabric and has been developed mainly for shear and/or flexural strengthening of concrete beams. The fabric contains fibers braided in three different directions (0°, +45 °, and –45 °) and is designed to offer strength, stiffness, and ductility in all directions.

The ideal characteristics of a strengthening system for flexural and shear strengthening of reinforced concrete beams were discussed leading to the following conclusion:

1- The strengthening system should initially exhibit a linear stress-strain response up to a certain strain value, and then experience an increase in strain without a corresponding increase in stress, similar to the yield phenomenon experienced by steel.

2- The "yield strain" or "the yield-equivalent strain" should be slightly greater than the yield strain of steel.

3- The ultimate strain should be sufficient to guarantee adequate beam deformation before FRP rupture (more than 2%).

4- With respect to shear strengthening, the system should exhibit a certain value of yield strength at a strain value of 0.5% and should have fibers at 45° to the

longitudinal axis of the beam in order to get the optimum contribution to beam shear strength.

A parametric study was conducted on triaxially braided fabrics to study the contribution of the diagonal yarns to axial loading behavior and the effect of axial yarn size, axial yarn spacing, and diagonal yarn size on diagonal loading behavior. The following were concluded from this study:

1- The contribution of diagonal yarns to axial load carrying capacity is very little compared to the contribution of axial yarns.

2- Diagonal failure strain decreases with increasing diagonal and axial yarn sizes and increases with increasing axial yarn spacing.

3- Ultimate diagonal load generally increases with increasing diagonal yarn size and axial yarn spacing up to a certain limit where it starts to decrease and decreases with increasing axial yarn size.

4- Diagonal rigidity increases with increasing diagonal yarn size, decreases with increasing axial yarn spacing, and is slightly affected by axial yarn size.

In view of this parametric study, the fabric geometry was selected. Two fabrics were manufactured and their tensile behaviors were evaluated by tensile testing samples according to ASTM D 3039 specifications. The fabrics exhibited a linear behavior up a certain strain value, and followed by a yield plateau until rupture at strain values around 2.0%.

9.1.2 Flexural strengthening

An experimental investigation was conducted to evaluate the behavior of reinforced concrete simple and continuous beams strengthened in flexure using the new systems and compare it with the behavior of similar beams strengthened using some currently

available carbon fiber strengthening systems and steel plates. The following were concluded:

1- Currently available FRP materials used as flexural strengthening systems for concrete structures do not always provide yielding plateaus in the strengthened beams similar to those for unstrengthened beams. In some applications, the strengthening results in a brittle failure and/or insignificant increase in the yield load of the strengthened beam.

2- The beams strengthened using the systems developed in the present research generally show higher increase in yield load than those strengthened with the carbon fiber strengthening systems.

3- The beams strengthened with the new systems exhibited more ductility than those strengthened with the carbon fiber strengthening systems.

4- The beams strengthened using the new systems produced yield plateaus similar to those of unstrengthened beams and also similar to those produced by beams strengthened with steel plates.

5- Most of the beams strengthened with the carbon fiber sheets exhibited brittle failures due debonding of the carbon fiber sheet from the concrete surface. The beams strengthened with the new systems were less vulnerable to such failures due to the different load-strain response of the fabric. Yielding of the systems limits the force increase in them and as a result, they were less demanding for anchorage.

6- Although the beam strengthened with steel plate exhibited considerable ductility, the steel plate yielded at a lower load than the inner reinforcing steel, since the plate has both a lower yield strain than the steel bars and was installed on the outside surface of the beam that underwent more strains than the inner steel. In

contrast, as the triaxial fabric has a yield strain value that is slightly more than the yield strain inside steel, it has the potential to yield simultaneously with the inner steel reinforcement.

7- In case of U-wrapped beams, the triaxial fabric had an advantage over the uniaxial carbon fiber sheets as it contains yarns in the +45°, -45° directions. These yarns worked to self anchor the fabric to the beam surface and hence debonding failure was not experienced. On the other hand, because carbon fiber sheet is uniaxial, wrapping the beam did not significantly the anchoring of the fibers.

8- In case of U-wrapped beams, anchorage failures due to shear-tension failures at the fabric end are less likely to happen when the triaxial fabric is used.

9- When installed on the beam tension face only, insufficient strengthening lengths may result in debonding of the fabric from the concrete surface or shear-tension failure at fabric end. Such failures are catastrophic and therefore providing additional anchorage by U-wrapping the beam is important in these cases to maintain the beam ductility.

10- Yielding of new systems was accompanied by distinguishable sounds due to failure of the low and medium elongation fibers in these systems.

11- The strengths of the new systems were fully exploited as their maximum recorded strains before beam failure were much more than their yield strain values. In contrast, the maximum recorded strains of the carbon fiber systems were noticeably less than their ultimate strain values, which indicated that their strength was not fully exploited.

12- The triaxially braided fabric was successful in providing adequate ductility at the plastic hinge regions of a continuous beam. Therefore, the distribution of the moment between the negative and positive moment zones of the beam became

possible. Distribution of the moment allowed full utilization of the strength of the beam at the cross sections of maximum negative and positive bending moments.

9.1.3 Shear strengthening

An experimental investigation was conducted to evaluate effectiveness of the developed triaxially braided fabric for shear strengthening of reinforced concrete beams. The following were concluded from this investigation:

1- The fabric strength was almost fully exploited as its maximum recorded strains before beam failure were very close to its "yield-equivalent" strain.

2- The fabric was capable of simultaneously increasing the shear and flexural strength of beams.

3- The fabric should not be installed in zones of high compression stresses as it may buckle causing the damage of the strengthened beam.

4- The fabric layers at the bottom were able to contribute to the shear strength of the beam.

5- The ACI committee 440 approach was found applicable in calculating the fabric contribution to beam shear strength.

9.2 Recommendations for Future Studies

The experimental investigations reported herein confirmed that reinforced concrete beams strengthened with the developed systems exhibited ductile response and the catastrophic failures, traditionally experienced when using currently available FRP strengthening systems, were eliminated. However, structures are vulnerable to other catastrophic failures such as that caused by the effect of high temperature due to fires. Unfortunately, currently available FRP systems have limited fire resistance due to the

limited fire resistance of the polymers used with these systems. A research program conduced at Rutgers University [Foden et al. (1996)] resulted in the development of a new inorganic matrix that can resist very high temperatures, over 800 c^{o}. Using such matrix with the developed fabrics would result in an outstanding fire resistance/ductile system. Experimental investigations are required to verify the compatibility of this epoxy with developed fabrics. Furthermore, experimental and analytical investigations are needed to examine and verify the effectiveness and suitability of this system for use with various types of structural components.

REFERENCES

ACI committee 318 (1995). "Building code requirements for structural concrete and commentary." *ACI 318-95*, American Concrete Institute.

ACI Committee 440 (2002). "Guide for the design and construction of externally bonded FRP systems for strengthening concrete structures." *ACI 440.2R-02*, American Concrete Institute.

Araki, N., Matsuzaki, Y., Nakano, K., Kataoka, T., and Fukuyama, H. (1997). "Shear capacity of retrofitted RC members with continuous fiber sheets." *Non-Metallic (FRP) Reinforcement for Concrete Structures*, Japan Concrete Institute, Tokyo, 1, 515-522.

Arduini, M., Tommaso, A. D., and Nanni, A. (1997). "Brittle failure in FRP plate and sheet bonded beams." *ACI Structural Journal*, 94(4), 363-370.

ASTM. (2000). "Standard test method for tensile properties of polymer matrix composite materials." *Annual Book of ASTM Standards*, ASTM D 3039, 15.03, 106-118.

Belarbi, A., Chandrashekhara, K., and Watkins, S. E. (1999). "Performance evaluation of fiber reinforced polymer reinforcing bar featuring ductility and health monitoring capability." *Fourth International Symposium on Fiber Reinforced Polymer Reinforcement for Reinforced Concrete Structures*, ACI SP-188, Baltimore, Maryland, 647-657.

Bencardino, F., Spadea, G., and Swamy, N. (2002). "Strength and ductility of reinforced concrete beams externally reinforced with carbon fiber fabric." *ACI Structural Journal*, 99(2), 163-171.

Bunsell, A. R., and Harris B. (1974). "Hybrid carbon and glass fibre composites." *Composites*, 5, 157-164.

Chaallal, O., Nollet, M. j., and Perraton, D. (1998). "Shear strengthening of RC beams by externally bonded side CFRP strips." *Journal of Composites for Construction*, ASCE, 2(2), 111-113.

Chajes, M. J., Januszka, T. F., Mertz, D. R., Thomson, T. A., and Finch, W. W. (1995). "Shear strengthening of reinforced concrete beams using externally applied composite fabric." *ACI Structural Journal*, 92(3), 295-303.

FIB (2001). "Externally bonded FRP reinforcement for RC structures." *Technical report*, Bulletin 14, International Federation for Structural Concrete.

Foden, A., Lyon, R., Balaguru, P., and Davidovitz, J., (1996). "High temperature inorganic resin for use in fiber reinforced composites." *Proceedings, First International Conference on Composites in Infrastructures, ICCI'96*, Tucson, Arizona, 166-177.

Grace, N. F., Sayed, G. A., Soliman, A. K., and Saleh, K. R. (1999). "Strengthening reinforced concrete beams using fiber reinforced polymer (FRP) laminates." *ACI Structural Journal*, 96(5), 865-874.

Harris, H. G., Somboonsong, W., and Frank, K. K. (1998). "New ductile hybrid FRP reinforcement bar for concrete structures." *Journal of Composites for Construction*, ASCE, 2(1), 28-37.

Hayashi, T. (1972). "On the improvement of mechanical properties of composites by hybrid composition." *Proceedings, Eighth International Reinforced Plastics Conference*, Paper 22.

Khalifa, A., Gold W. J., Nanni, A., and Aziz. A. M. I. (1998). "Contribution of externally bonded FRP to shear capacity of RC flexural members." *Journal of Composites for Construction*, ASCE, 2(4), 195-202.

Maeda, T., Asano, Y., Sato, Y., Ueda, T., and Kakuta, Y. (1997). "A study on bond mechanism of carbon fiber sheet." *Non-Metallic (FRP) Reinforcement for Concrete Structures*, Japan Concrete Institute, Tokyo, 1, 279-286.

Manders, P. W., and Bader, M. G. (1981). "The strength of hybrid glass/carbon fibre composites: Part 1, failure strain enhancement and failure mode." *Journal of Materials Science*, 16, 2233-2245.

Naik, R. A. (1994a). "Analysis of woven and braided fabric reinforced composites." *NASA CR-194930*, National Aeronautics and Space Administration (NASA), Hampton, Virginia.

Naik, R. A. (1994b). "Failure analysis of woven and braided fabric reinforced composites." *NASA CR-194981*, National Aeronautics and Space Administration (NASA), Hampton, Virginia.

Naik, R. A. (1994c). "TEXCAD- Textile composite analysis for design." *NASA CR-4639*, National Aeronautics and Space Administration (NASA), Hampton, Virginia.

Nanni, A., Henneke, M. J., and Okamoto, T. (1994) "Tensile properties of hybrid rods for concrete reinforcement." *Construction and Building Materials*, 8(1), 27-34.

Norris, T., Saadatmanesh, H., and Ehsani, M. R. (1997). "Shear and flexure strengthening of R/C beams with carbon fiber sheets." *Journal of Structural Engineering*, ASCE, 123(7), 903-911.

Ritchie, P. A., Thomas, D. A., Lu, L., and Connelly, G. M. (1991). "External reinforcement of concrete beams using fiber reinforced plastics." *ACI Structural Journal*, 88(4), 490-500.

Saadatmanesh, H., and Ehsani, M. R. (1991). "RC beams strengthening with GFRP plates I: experimental study." *Journal of Structural Engineering*, ASCE, 117(11), 3417-3433.

Sato, Y., Ueda, T., Kakuta, Y., and Tanaka, T. (1996). "Shear reinforcing effect of carbon fiber sheet attached to side of reinforced concrete beams." *Advanced Composite Materials in Bridges and Structures*, M. M. El-Badry, Editor, The Canadian Society of Civil Engineering, 621-627.

Sato, Y., Katsumata, H., and Kobatake, Y. (1997). "Shear strengthening of existing reinforced concrete beams by CFRP sheet." *Non-Metallic (FRP) Reinforcement for Concrete Structures*, Japan Concrete Institute, Tokyo, 1, 507-514.

Somboonsong, W., Ko, F. K., and Harris, H. G., (1998). "Ductile hybrid fiber reinforced plastic reinforcing bar for concrete structures: design methodology." *ACI Materials Journal*, 95 (6), 655-666.

Spadea, G., Bencardino, F., and Swamy, N. (1997). "Strengthening and upgrading structures with bonded CFRP sheets design aspects for structural integrity." *Non-Metallic (FRP) Reinforcement for Concrete Structures*, Japan Concrete Institute, Tokyo, 1, 629-636.

Taerwe, L., Khalil, H., and Matthys, S. (1997). "Behavior of RC beams strengthened in shear by external CFRP sheets." *Non-Metallic (FRP) Reinforcement for Concrete Structures*, Vol. 1, Japan Concrete Institute, Tokyo, 483-490.

Takahashi, Y., Sato, Y., Ueda, t., Maeda, T., and Kobayashi, A. (1997). " Flexural behavior of RC beams with externally bonded carbon fiber sheet." *Non-Metallic (FRP) Reinforcement for Concrete Structures*, Japan Concrete Institute, Tokyo, 1, 327-334.

Todeschnini, C., Bianchini, A., and Kesler, C. (1964). "Behavior of concrete columns reinforced with high strength steels," *ACI Journal*, Proceedings, 61 (6), 701-716.

Triantafillou, T. C., and Plevris, N. (1992). "Strengthening of RC beams with epoxy-bonded-fiber-composite materials." *Materials and Structures*, 25, 201-211.

Triantafillou, T. C., (1998). "Shear strengthening of reinforced concrete beams using epoxy-bonded FRP composites." *ACI Structural Journal*, 95 (2), 107-115.

Triantafillou, T. C., and Antonopoulos, C. P. (2000). "Design of concrete flexural members strengthened in shear with FRP." *Journal of Composites for Construction*, ASCE, 4(4), 198-205.

Umezu, K., Fujita, M., Nakai, H., and Tamaki, K. (1997). "Shear behavior of RC beams with aramid fiber sheet." *Non-Metallic (FRP) Reinforcement for Concrete Structures*, Japan Concrete Institute, Tokyo, 1, 491-498.

PUBLICATIONS AND PRESENTATIONS FROM THIS WORK

PUBLICATIONS

1- Grace, N. F., Abdel-Sayed, G., and Ragheb, W. F. (2002). "Strengthening of concrete beams using innovative fiber-reinforced polymer fabric." *ACI Structural Journal*, 99(5), 692-700.

2- Grace, N. F., Abdel-Sayed, G., and Ragheb, W. F. (2002). "An innovative ductile composite fabric for strengthening concrete structures." *Proceedings, Third International Conference on Composites in Infrastructures, ICCI'02*, San Francisco, California, paper 60.

3- Grace, N. F., Abdel-Sayed, G., and Ragheb, W. F. (2002). "External strengthening of concrete beams using innovative ductile composite fabric." *The Third Middle East Symposium on Structural Composites for Infrastructures*, Aswan, Egypt.

4- Grace, N. F., Ragheb, W. F., and Abdel-Sayed, G. (2002). "New ductile FRP systems for strengthening concrete structures." Accepted for publication, *ASCE Journal of Composites for Construction.*

5- Grace, N. F., Ragheb, W. F., and Abdel-Sayed, G. (2002). "Strengthening of cantilever and continuous beams using new triaxially braided ductile fabric." Accepted for publication, *ACI Structural Journal.*

6- Grace, N. F., Ragheb, W. F., and Abdel-Sayed, G. (2003). "Flexural and shear strengthening of concrete beams using new triaxially braided ductile fabric." *ACI Structural Journal*, in press.

7- Grace, N. F., Ragheb, W. F., and Abdel-Sayed, G. (2003). "Development of new ductile FRP system for strengthening concrete beams." Submitted for publication, *ACI Concrete International.*

PRESENTATIONS

1- "Development of Hybrid Ductile Composite Systems for Strengthening Concrete Structures." ACI Spring 2002 Convention, Detroit, Michigan, April 22, 2002.

2- "Innovative Ductile Composite Fabric for Strengthening Concrete Structures." *Third International Conference on Composites in Infrastructures,* San Francisco, California, June 10, 2002.

VITA AUCTORIS

Wael Fathy Ragheb was born in 1971 in Egypt. He graduated in 1993 from Alexandria University, Alexandria, Egypt where he got his B.Sc. in Civil Engineering (with honor). He was the first rank graduate of the 1993 class. He obtained his M.Sc. in Civil Engineering in 1998 from Alexandria University, Alexandria, Egypt. He is currently a Ph.D. candidate in the Department of Civil and Environmental Engineering at the University of Windsor and hopes to graduate in Winter 2003.